DEVELOPMENT OF AN ACRYLONITRILE BUTADIENE STYRENE TONER FOR AN ELECTROPHOTOGRAPHY BASED ADDITIVE MANUFACTURING PROCESS

Rupesh A Chudasama

A Doctoral Thesis submitted in partial fulfilment of the requirements for the award of Doctor of Philosophy

Awarded by De Montfort University
Additive Manufacturing Technology Group
Faculty of Technology
March 2015

Abstract

Research in to utilising electrophotography for Additive Manufacturing has been under investigation for over a decade. However, the research has been primarily focused on resolving the height limitations caused by charge accumulation and also the development of toners from tough engineering polymers. The aim of this study is to develop a suitable negatively charging engineering polymer for the Selective Laser Printing process and a more efficient method of generating toners with a suitable particle range and to assess the mechanical properties of parts produced using the toner developed through this route.

The study is comprised for two parts; Chemical and Mechanical toner production. The chemical production method utilises a process, Evaporative Limited Coalescence, to produce an engineering toner in the desired 20-50μm range. It was found that during the chemical production process the negatively charging polymer was converted to charge positive. Analytical assessment of the toner was carried out to explain the change in polarity. Mechanical milling trials were also conducted under both ambient and cryogenic conditions, as well as a novel method to reduce the feed-stock material to the desired particle size range. The results suggest a significant increase in efficiency compared to prior research.

Printing trials were conducted using the mechanically milled toner to assess the mechanical properties for different heating, pressure and stand-off distance conditions. It was found that, due to insufficient heating and applied pressure the final samples suffered from high porosity and poor tensile strength.

Acknowledgements

First and foremost, I would like to thank Professor David Wimpenny and Dr Jason Jones for their unwavering support and guidance over the course of this PhD. I would also like to thank Dr Adam Moroz for his help with the statistical analysis.

The research would not be possible without the financial support from The UK Technology Strategy Board for funding the SPRINT project (project number: 100735; TP number: TP14IHVM/611IBD219A), to which I am grateful.

I would like to thank the project partners of SPRINT; MTT, Parker KV and Renishaw. A special thanks to Jake Ufton, Peter Nunn and Jeremy Pullin of Renishaw for their help and support throughout the course of the research.

CTG's Andreas Schoenberger, Stefan Wiese and Christian Hornickle for their technical assistance.

Beat Zobrist of Zobrist Engineering and Consulting (ZEAC) for his help in surface coating and technical discussions.

A big thank you to the technicians in the Engineering and Health and Life Sciences faculty who are too numerous to mention, for their help and support.

Dr Gibbons of Warwick University for making the facilities available to me at any time.

To my friends at the AMTG, both past and present for providing a great environment to learn and develop.

To the Bill Hutcheson, David Beckwith and Nii at Powdertech Inc. for the carrier they supplied and the technical discussions.

Last but by no means least, I would like to thank my family. My parents for their love and support throughout my research. My sister, Pooja, for her help with the images. A special thank you to my wife Poonam for being by my side and for the constant encouragement. To my daughter Tanvi, who finally has her dad back.

Research Output

J. B. Jones, D. I. Wimpenny, R. Chudasama, and G. J. Gibbons, "Printed Circuit Boards by Selective Deposition and Processing," in *22nd Solid Freeform Fabrication Symposium*, Austin, TX, USA, pp. 639-656. (2011),.

R. Chudasama, J. B. Jones, and D. I. Wimpenny, "Synthesis of an Electrophotographic Toner for Additive Manufacturing," in *Annals of DAAAM for 2012 & Proceedings of the 23rd International DAAAM Symposium, pp 0001 - 0004, Editor Branko Katalinic, Published by DAAAM International*, Vienna, Austria, 2012

J. B. Jones, D. Büttner, R. Chudasama, D. Wimpenny, and K. Krüger, "Laser Printing Circuit Boards and Electronics," *Journal of Imaging Science and Technology*, vol. 56, pp. 040503-1 – 040503-11, 2012.

Abbreviations

3D	Three Dimension/ Three Dimensional
ABS	Acrylonitrile Butadiene Styrene
AM	Additive Manufacturing
CAD	Computer Aided Design
CCA	Charge Control Agents
CMD	Conductive Magnetic Development
CGL	Charge Generation Layer
CTL	Charge Transportation Layer
DoE	Design of Experiment
DMA	Dynamic Mechanical Analysis
DPI	Dots per Inch
DSC	Differential Scanning Calorimetry
EDX	Energy Dispersive X ray
ELC	Evaporative Limited Coalescence
EMB	Electromagnetic Brush
FCA	Flow Control Agents
FDM	Fused Deposition Modelling
FT-IR	Fourier Transform Infrared
IMD	Insulative Magnetic Development
IR	Infrared
OPC	Organic Photoconductor
PC	Photoconductor
PSA	Particle Size Analysis/Analyser
PSD	Particle Size Distribution
Q/m	Charger to mass ratio
SEM	Scanning Electron Microscope
SLP	Selective Laser Printing
SLS	Selective Laser Sintering
T_g	Glass transition Temperature
T_m	Melt Temperature
TR	Transfer roller

Definition of terms

Back transfer	Adhesion of toner on to the photoconductor or transfer roller after a transfer.
Background	Toner that has transferred on to part of the photoconductor or transfer roller not intended.
Comminution	A process of reduction my mechanical methods.
Developer	A mixture of carrier and toner at a specific concentration.
Developer unit	A housing containing mixing blades to tribocharge the developer and produce a brush on the magnetic roller. The housing also acts as a reservoir containing additional toner.
Ghosting	Unwanted residual charge on the OPC leading to the previous image being deposited on to the substrate.
Mechanical milling	See Comminution.
Nip	The contact area between the transfer roller and substrate.
OPC	Organic Photoconductor – Almost exclusively used to produce photoconductors. Interchangeable with photoconductor and photoreceptor.
Photoconductor	A photosensitive drum onto which a latent image is formed. Previously made from amorphous selenium, now based on a variation of organic materials. Interchangeable with OPC and photoreceptor.
Photoreceptor	See photoconductor.
Q/m	The charge to mass ratio.
Tail end	The end of a PSD curve most closest to the D_{90} region
Transfix	Fusing printed sample off the rig.
Transfuse	See Transfix.

List of Figures

List of Tables

1 Introduction

Electrophotography, a method of precisely depositing fine polymeric powders typically onto a paper substrate using a combination of Van der Waals and electrostatic forces, was originally conceived as a rapid and accurate method of duplicating documents. The process was then adapted to enable direct printing from computers in the late 1970's [1]. Despite the significant strides made in inkjet printing technology, electrophotography still commands an advantage in terms of printing speed as well as an ability to provide "dry" printing onto surface unsuitable for "wet" printing. Moreover, the process is also highly flexible, able to print a wide range of dielectric materials [2–7]. The potential to apply electrophotography to the field of Additive Manufacturing has been appreciated [2, 4, 5, 8–14].

While the process of transporting and fixing toner in a conventional 2D application, such as document printing, is relatively straightforward and well developed, the transition from 2D printing to 3D Additive Manufacturing presents some important challenges. Indeed, to date, the production of a part by direct deposition using electrophotography has not been successfully achieved. Instead, electrophotography has been used indirectly to produce [13–15] the end product.

There are two key challenges that must be overcome to enable direct part printing by electrophotography. The first issue to address is the accumulation of charge as more layers are deposited which inhibits the deposition of material thus limits the height of parts, which can be produced to a few millimetres. This problem has been the subject of many years of research and although some progress has been made, at least in understanding the mechanisms that are at play, this still remains work in progress. Another issue is the difficulty in generating a suitable toner to yield engineering parts with acceptable

properties. Moreover, the process requires a sacrificial support material to enable complex parts with overhanging features to be produced. Conventional toners are typically manufactured from a brittle polymer by mechanical milling or chemical production to enable a 5-15µm particle to be produced. To date there has been little work to develop more effective toner materials [2, 4]. In order for the process to be successful, toners with good engineering properties are required.

Aims and objectives

Aim: To investigate an efficient method of production of toners from engineering polymers and to assess the performance on the part produced using an electrophotography based AM process.

Objectives:

1. Review a range of engineering polymers and select the most appropriate material for further development.
2. Evaluate methods for producing the powder with the required particle size/morphology from the selected polymer.
3. Develop and test toners produced from the polymeric powder.
4. Assess the mechanical properties of 3D samples produced by the SLP process from the new toner material.

Novelty & Anticipated Contribution to science:

The project builds on the previous work conducted in this field [2, 4, 5, 10] but will extend the capability of the SLP process through the development of novel toner formulations. The new toner will be based on a rigid engineering polymer and an integral part of the study will be to understand the relationship between processing parameters and final mechanical properties.

Structure of the thesis

The thesis is divided into nine chapters, including the introduction and references. The description of the chapter and its contents are described in Table 1:1.

Table 1:1: Thesis layout by chapter

Chapter	Subsection	Description
1	Introduction	
2,3,4	Additive Manufacturing	An overview of Additive Manufacturing (AM) process as well as some of the key technologies that are relevant to the study are presented.
	History of Electrophotography	A brief introduction to electrophotography is given, including the history and the key developmental steps made to commercialise the technology. This section will further describe the six steps of electrophotography.
	Toner and manufacturing methods	This section aims to provide the reader with an understanding of the composition and the mechanisms required to charge and transport the toner. Additionally, toner manufacturing methods are explained and discussed to understand the critical role that they play.
	Development systems	Development systems pertaining to dual component development are reviewed in this section, which also presents key improvements, made to develop images on the substrate.

	Additive Manufacturing for Electrophotography	A review of the state of the art related to the use of electrophotography, both directly and indirectly, in the production of parts by Additive Manufacturing is presented.
5	Methodology	In this section the aims and objectives of the study are presented. The novelty and contribution to science of the proposed work is described with reference to the current state of the art in this field. The methodology, which will be employed to undertake the experimental work in the study is explained and justified.
4	Experimental	The experimental procedures employed in the study are described encompassing methods, materials and the equipment employed. (Including the Selective Laser Printing (SLP) rig and its components).
6,7,8	Results and discussion	In this chapter the result of the experimental work are presented and the findings discussed.
9	Conclusions, recommendations and further work	The key conclusions of the work are listed and the achievements made in the study are presented to demonstrate the extent to which the original objectives, innovation and contribution to science have been met. Recommendations on the impact of the findings and further work that could be undertaken in the future are presented.
	References	

2 Additive Manufacturing

The aim of this section is to provide a brief overview of some of the key commercially available Additive Manufacturing (AM) techniques, which are used for the production of plastic parts. Additive Manufacturing (AM) refers to a process by which materials are joined from 3D Computer Aided Design (CAD) data in a layer wise additive manner as opposed to traditional subtractive methods[18]. Previously referred to as Rapid Prototyping, Solid Freeform Fabrication and 3D Printing. The process involves;

1. Obtaining a part from CAD file.
2. Slice the file into 2D layers.
3. Deposit the layer of powder, liquid or similar.
4. Fuse the material by means of laser, binder or other heat source producing a replica of the 2D CAD slice.
5. Deposit a new layer and repeat step 3 until the part is complete.

The first AM machine was introduced in 1987 by Chuck Hull, who invented and patented the Stereolithography process and founded 3D systems[19]. This marked a milestone in the AM industry. Within the next decade a number of new technologies were released and companies formed based on these technologies. Most notable of these technologies are Fused Deposition Modelling (Stratasys) and Selective Laser Sintering (formally DTM Corp).

Fused Deposition Modelling (FDM)

Fused deposition modelling FDM) was first patented in 1992 by Scott and Lisa Crump[20]. The same year Stratasys Inc. commercialised the process and is one of the most successful AM manufacturers.

Fused Deposition Modelling is an extrusion based process utilising two filaments, one for build and other for support material. The process is relatively simple compared to many AM systems. The material flows through a heated nozzle, which lays the semi molten material on the previous layer and is bonded. The build material has a number of choices ranging from ABS, polyphenylsulfones and polycarbonates. Stratasys was the first AM manufacturer to introduce ABS and still remains one of the very few manufacturers to have incorporated high impact engineering polymers. The process however, suffers from porosity due to its manufacturing method (see Figure 2:1), as the semi molten bead sits on the previous, relying on gravity to consolidate and reduce porosity[21–25]. Furthermore, models produced are good in compression but poor in tension, and have known to delaminate, making the build orientation a key factor[24, 26].

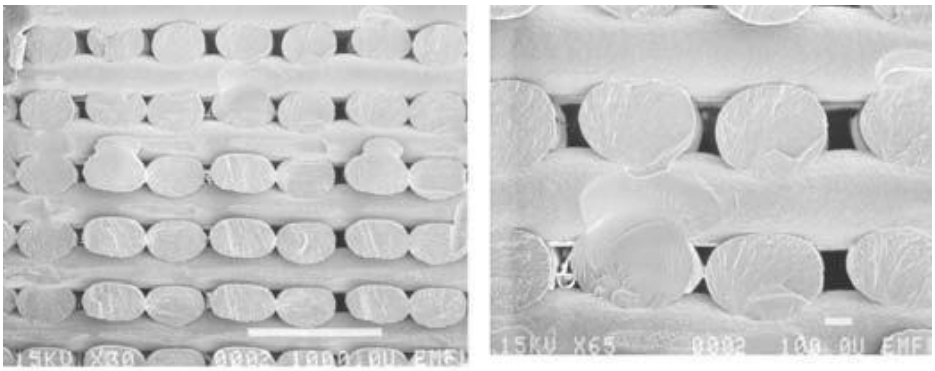

Figure 2:1: Cross section of ABS part built with a 0˚C and 90˚C raster[26]

Selective Laser sintering (SLS)

Laser sintering (LS) was developed in the late 1980's by Carl Deckard during his Masters at the University of Texas in Austin. The process was termed Selective Laser Sintering (SLS), which is a trade name of now 3D Systems.

The process begins with the powder feed cartridge rising. The powder feed roller rotating counter to the direction of travel spreads an even amount of powder across the powder bed. The layer is preheated before a laser scans the part bed of the sliced file sintering the powder to complete the first layer. The process is repeated until the part is complete. A schematic of the machine is presented in Figure 2:2 to give a clear understanding of the above description.

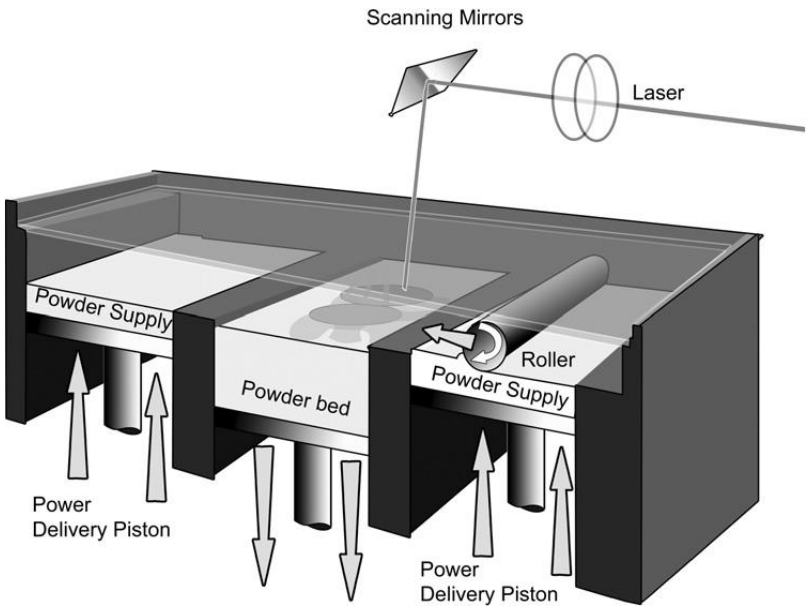

Figure 2:2: Laser Sintering schematic[27]

The post processing is very simple. The part bed is taken out of the machine and left to cool. Once cooled, the part is recovered by vibrating the loose powder surrounding the part and brushing away any powder that may compact between cavities and internal corners.

The LS process is capable of producing parts with densities approaching 95%[28, 29]. However, the process is limited to the polymers available and generally consists of variations of polyamides and styrene. In 2010[18] EOS released the EOSINT P800, a machine capable of processing PEEK for medical applications amongst others. The machine was able to process to temperatures up to 355˚C. 3D systems have similar machines capable of producing parts from polyamides, styrenes and composites for higher temperature models. In addition, 3D systems have an elastomeric material, Somos and Duraform Flex, for applications that require flexibility. The composite materials provide additional mechanical properties but not to the extent of the ABS from Stratasys.

Current polymer based AM systems mentioned above each have their advantages but also their drawbacks. The FDM process is able to process high temperature polymers such as ABS, but due to the internal architecture of the build, it is not ideally suited to the production of thin walled parts for functional testing, due to their propensity to delaminate.

The SLS process is able to produce close to full density parts and does not suffer from delamination. However, laser sintering has only a handful of polymers that can be processed due to the lack of materials available. In addition, the P800 from EOS, which is capable of sintering high performance polymer PEEK, requires a new machine at significant cost. Akin with many polymer based Additive Manufacturing process, the parts exhibit some degree of anisotropy in terms of their mechanical properties and they have much lower elongation to failure when compared to the bulk polymer properties. This opens up an area

where a process that is able to produce dense parts with a range of polymers would have a distinct advantage over the current systems.

3 Electrophotography

Electrophotography is a process primarily developed for the photocopying of documents. The process is dependent on dry polymeric powder that is precisely placed on a sheet of paper to develop an identical copy of the original document.

This chapter will provide a brief history of the electrophotography process and the key developmental steps used to improve the technology. The chapter will discuss the importance of the toner and its manufacturing methods as well as its development systems. The chapter will conclude with a review of the state of the art related to Additive Manufacturing employing electrophotography.

3.1 History of Electrophotography and the birth of Xerox

Electrophotography, also known as Xerography, was invented by Chester Carlson who filed a patent (No: 2,221,776) on 8th September 1938[30]. The patent, which was subsequently granted on 19th November 1940, describes a method of projecting an image of the document on to the surface of a photoconductor which is selectively discharged allowing a copy of the document to be formed by depositing a charged toner onto a sheet of paper – this is the basis of modern photocopiers.

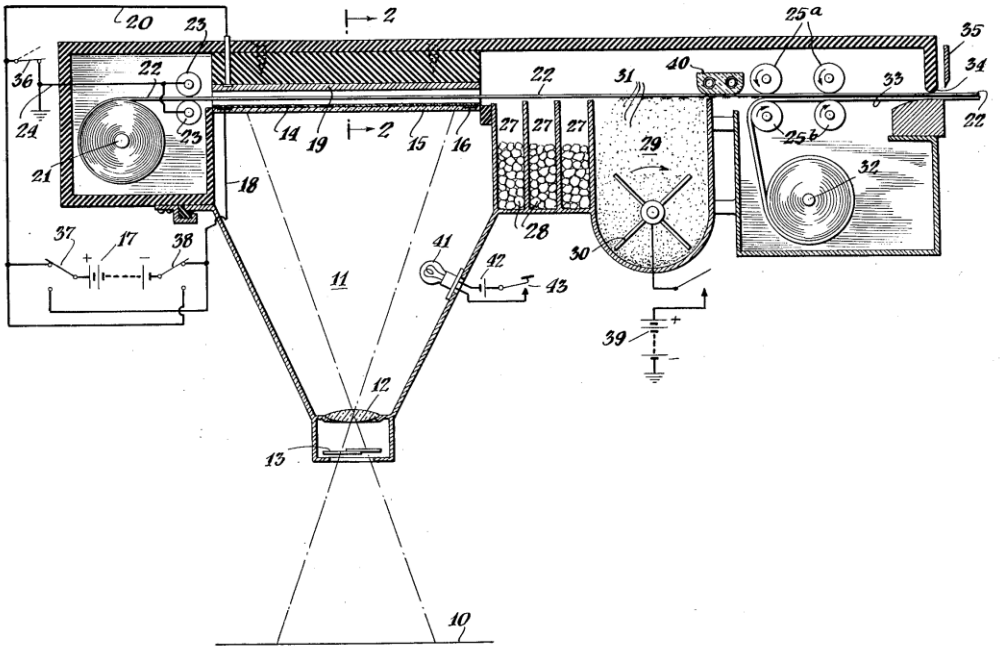

Figure 3:1: Chester Carlson's diagram of electrophotography [30]

A schematic of the process is shown in Figure 3:1. The image of the document (10) is "captured" by opening a shutter (13) and then focused by a lens (12) on to a charged photoconductor layer (14). The light areas of the image, corresponding to the blank areas of the document, result in a dissipation of the charge on the photoconductor. The latent (charged image) is transferred from the photoconductor onto the underside of an insulating belt (22). A fine powdered toner (29) which is also charged is attracted to the dark (charged) areas of the belt and the toner material is subsequently transferred to the paper (33) and fused in place by heating a thermosoftening adhesive. In addition to describing the process, the patent [30] also identifies the critical issue of humidity which is addressed in the patent through the use of a desiccant (27), positioned adjacent to the toner hopper, and also the potential to employ hydrophobic toner materials is proposed.

One of the major challenges Carlson faced was the development of a suitable photoconductor. In 1938 [31], Carlson enlisted the support of chemist, Otto Kornie. On 6th October 1938[31], Kornie successfully applied a thin, uniform zinc layer to form a photoconductor. A homogeneous electrostatic charge was formed by rubbing the photoconductor with a cotton napkin. Carlson proceeded to overlay a transparent ruler with a scale on top of the photoconductor and discharged it by shining a lamp over it forming a latent image. After removing the ruler, Carson sprinkled some lycopodium powder (rudimentary toner) over the photoconductor he could see that the powder adhered to the charged area to form a real image. The experiment was repeated again but this time India ink was used to write '10-22-38 ASTORIA' (date and street of the lab) on a glass slide from a microscope. The glass slide was placed on the charged photoreceptor and a light was shone to discharge the unmasked region. The light source was turned off and the latent image was turned into a real image by sprinkling some lycopodium powder over. This time however, the image was pressed against a wax paper and heated to adhere the image against it and the first electrophotographic image was created.

To commercialise the invention Carlson secured funding from Battelle Memorial Institute, a non-profit R&D organisation. Following Carlson's agreement with Battelle, a number of key developments were made, including improved charging of the photoconductor, better toner transfer and enhanced photoconductor materials [2]. These key developments are shown in Figure 3:2.

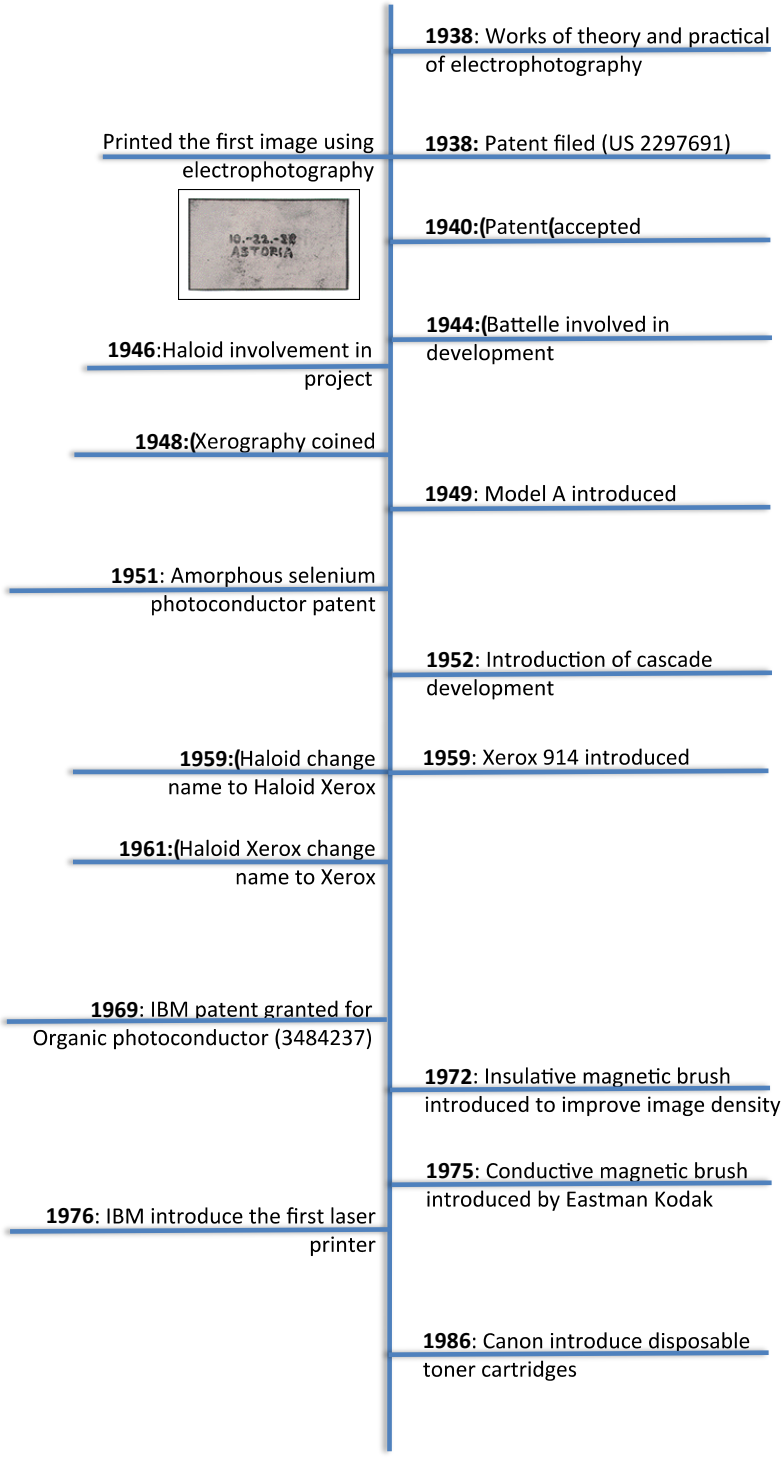

Figure 3:2: Timeline of key developments for the electrophotographic process

A corona device was designed to charge the photoconductor by showering it with ions (as described in Carlson's original patent). To improve the transfer of the toner from the photoconductor to the paper an opposite charge was applied to the underside of the paper attracting the toner onto it.

Another significant development was made by Edward Wise[32], who described the use of glass carrier beads to transport toner to the latent image. By using glass beads that are tribocharged (electrostatically charge by rubbing against an appropriate material - explained in Section 3.3.3) this provides a convenient and controlled method of transporting and transferring the toner onto the latent image. The toner is only stripped off the glass carrier beads if the attractive charge from the latent image is sufficiently strong. This results in a sharper image [31] with less background contamination of the printed sheet.

While the work at Battelle was progressing a commercial partner was sought to enable commercial exploitation. Following unsuccessful approaches to major corporations, including IBM and GE, Haloid, a small firm manufacturing photographic paper, expressed interested in the technology. In December 1946, Joe Wilson of Haloid signed an agreement with Battelle whereby both companies would work on the research to develop the machine to a saleable standard.

Between 1947 and 1949 many developments were made, including the use of an amorphous selenium and sulphur coating to generate a more effective photoconductor by William Bixby[33], which led to the very first fully commercially available photocopier, the Xerox Model A released in 1949 [34]. With the introduction of the Model A, Haloid incorporated Xerography in to the company name, to be named Haloid Xerox. By 1961,

Haloid Xerox had omitted Haloid from their company name, concentrating their efforts on Xerography.

Gary Stalkweather championed the idea of adapting the electrophotography technology for printing rather than photocopying [1, 35]. Despite initial scepticism by Xerox, laser printing became a significant aspect of work at the then recently established Palo Alto Research Centre (PARC). Research was also being carried out at IBM, and in 1975 IBM introduced the world's first laser printer [36]. Xerox followed suit two years later with the Xerox 9700.

The technology used in the laser printer was almost identical to Carlson's photocopier, with the major significance being the exposure system. IBM used a HeNe laser, to scan across the photoreceptor[37] to selectively discharge it based on the required text.

The electrophotography process has a number of components, which are expensive, and their life depends on the service cycle. In 1982 [37] Canon patented and introduced the first disposable print cartridge which, in addition to the toner, also housed the parts which required regular replacement [37]. This revolutionary step brought down the cost and increased the reliability of the laser printer.

3.2 Six steps of Electrophotography

Although there have been significant developments in laser printing hardware over the last four decades, the basic principles of Electrophotography still remains unchanged. Electrophotography is reliant on a six part process; 1) Charging, 2) Exposure, 3) Develop, 4) Transfer, 5) Fuse, 6) Clean and erase.

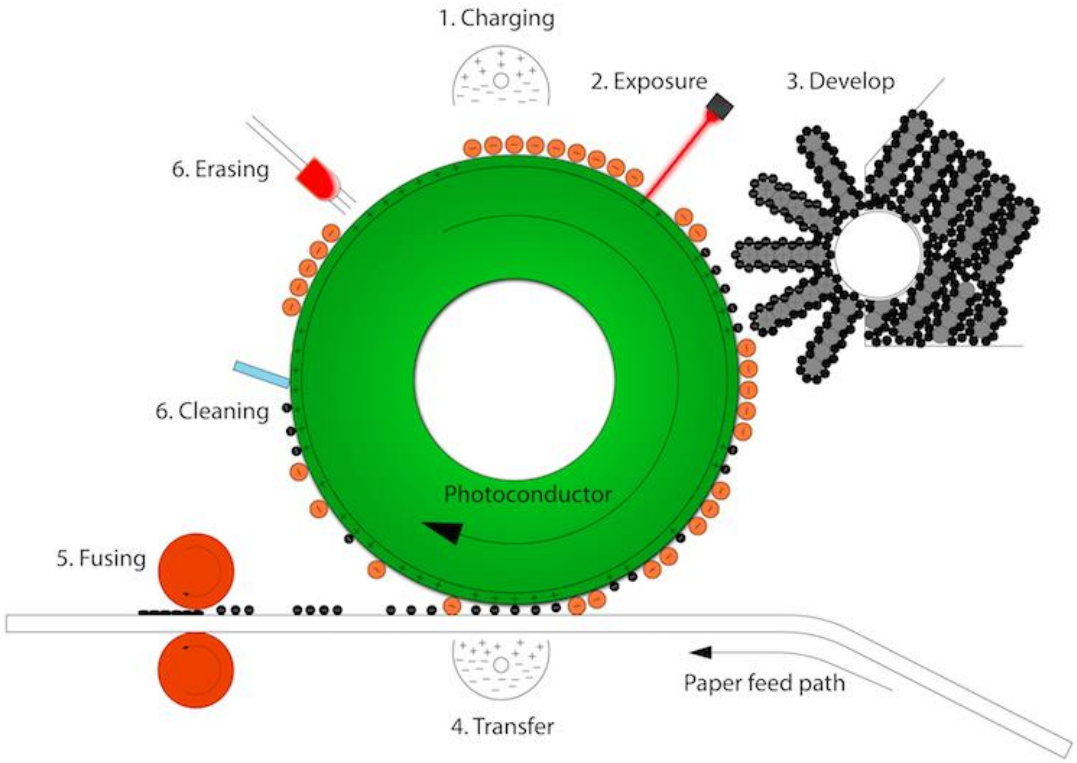

Figure 3:3: Process of electrophotography

A schematic showing the components within a laser printer are shown in Figure 3:3. The process is centred around the photoconductor (PC) which is usually a metallic cylindrical drum with a photoreceptive coating up to 30µm thick[37–40]. When the surface of the photoconductor is exposed to light it changes from an insulator to become conductive [3, 5, 30, 37–44].

Laser printing works by applying a charge on the photosensitive photoconductor. A laser is used to selectively discharge the region, changing the surface polarity of the drum creating a latent image. Next, the drum is brought to the vicinity of the developer unit where the charged toner is transferred electrostatically creating a real image. The toner remains on

the drum until it reaches the substrate. The substrate is travelling at the same linear velocity as the rotation of the drum. Using a charging device, opposite to the polarity of the toner, the toner is attracted to the substrate, again via electrostatic adhesion. The substrate is passed through the heated rollers, where the unfused toner is fused by heat and light pressure.

In the early to mid 1970's, to avoid patent infringement, IBM developed a new design of the photoconductor, which replaced the amorphous selenium with an organic coating. This Organic Photoconductor (OPC) consists of an aluminium drum with a thin coating, approximately 20µm thick of the photoconductive material. The coating material is selected based on the initial charge (polarity) applied to the drum.

3.2.1 Charging

There are three prominent charging methods; contact, induction and, the most notable of all, corona. A corona device, such as a corotron, consists of a fine diameter wire, partially surrounded by a grounded shield. The corona wire has a large voltage applied (typically in the order of thousands of volts). The high voltage applied across the wire releases free electrons due to ionization of the surrounding air. The voltage must be high enough to cause the breakdown of the air as described by Paschen's breakdown law. Paschen law dictates the voltage required to breakdown the air. It is reported[37] that a wire with a diameter of 50µm spaced 10mm from a grounded plate with a 8kV potential is sufficient to charge a photoconductor moving at 50mm/s.

The positive voltage of the corona wire repels the positively charged ions with the negatively charged ions remaining around the grounded shield. The positive ions are repelled at high velocity in the direction of the photoreceptor. As the photoreceptor is

rotating the charge is uniformly distributed over the surface. In the absence of light, the photoreceptor remains an insulator. A schematic of charging process is shown in Figure 3:4.

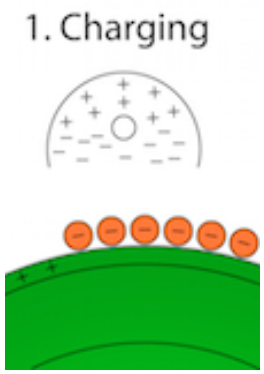

Figure 3:4: Step 1: Charging process depicting positive charge uniformly placed over photoreceptor

While the process of corona charging is one that has been well utilised, the process is not without its flaws. The corotron is used to generate a "strip" of ions close to the OPC. However, only 10%[5] of the ions actually make it to the surface of the photoconductor. Moreover, ozone is created as a by-product of the ionisation process which is hazardous to health[45–48].

The introduction of a contact charger solved the inefficiency problems associated with corona charging by using a charger roller to directly charge the photoconductor through contact. In addition to the improved efficiency, the lower voltage used reduces the level of ozone produced [43].

3.2.2 Exposure

Photoconductors are coated in a photoreceptive (light sensitive) material, which becomes conductive in the presence of light. Where the light hits the charged photoreceptor, the exposed region is discharged. The light source is usually a modulated laser or a linear LED array with the wavelength matched to the sensitivity of the coating[37, 38, 49]. The laser unit uses a laser with a rotating polygon mirror, writing on the photoconductor creating a latent image. While the LED array offers a cheaper and quieter option due to less moving parts the accuracy is limited to 2400dpi (dots per inch), whereas the laser can produce latent images with a resolution of up to 9600dpi[6]. An LED and laser discharging system are depicted in Figure 3:5.

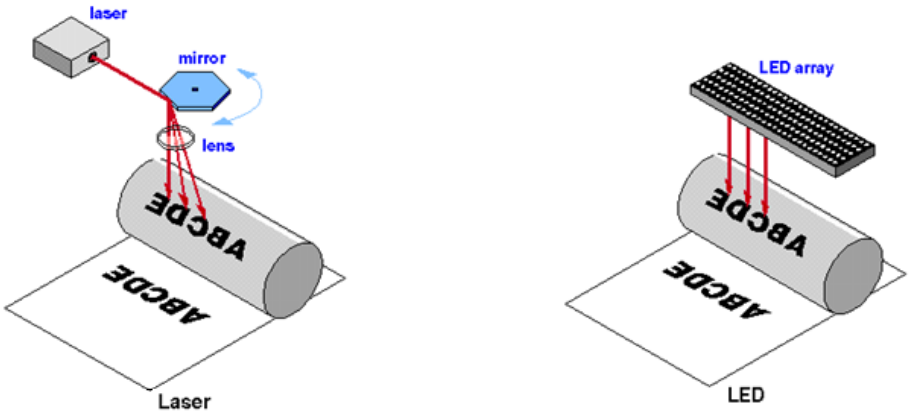

Figure 3:5: Step 2: Exposure of Laser (left) and LED (right) latent image forming[50]

3.2.2.1 Photoreceptor Technology

In the early days of electrophotography, the photoreceptor coating began as a thin film of sulphur and anthracene on zinc plates. The poor photogeneration of the sulphur and anthracene led to the development of photoconductors comprising of a metallic drum with a 10-50µm vapour deposited coating of selenium [40]. The volume of patents filed and publications is testament to the importance of photoconductor technology within electrophotography[39].

Today, Organic Photoconductors (OPCs) are almost exclusively used [14]. The OPC is a multi-layered coating consisting of a Charge Transportation Layer (CTL), Charge Generation Layer (CGL), a grounded electrode and the substrate. The surface of the CTL is uniformly charged with a negative ion shower. As the light hits the surface of the photoconductive layer, the electrons pass through the CTL and in to the CGL[44]. The electron Hole Transport Material (HTM) located in the CTL allows for the migration of the positive charge from the conductive substrate towards the surface of the photoconductor, while negative charges migrate to the metallic layer. The HTM is of significant importance as its function is to transport the positive charge through the layers. Inefficient transfer of charge and neutralisation can lead to ghosting (residual charge from a previous image). A schematic depicting the layers of the OPC and its principle of operation is shown in Figure 3:6[51].

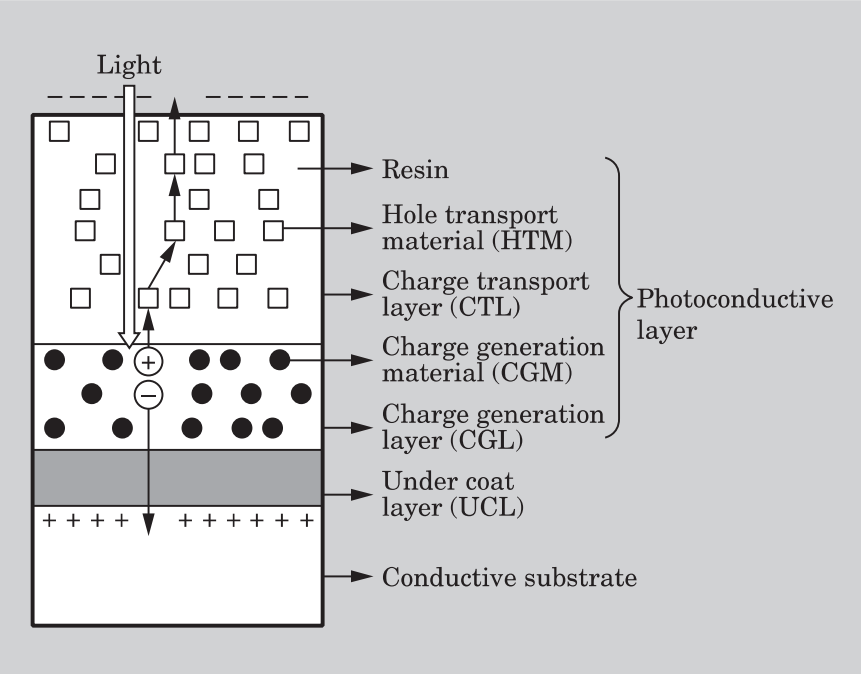

Figure 3:6: Schematic of a negatively charging OPC and its operation principles [51]

Organic photoconductors with multilayer photoreceptors are the most commonly used photoconductors[37, 38, 40]. A single photoreceptor layer system requires a higher quantum efficiency in photogeneration and charge mobility. Moreover, a multilayer configuration enables the photoconductor to have adequate mechanical strength to withstand contact with the substrate. For these reasons the multi layered system, with a negative charge, is most commonly employed[51, 52].

3.2.3 Development

It is at the development stage that the positive region of the OPC (latent image) is transformed into a visible or real image. The toner is located in a developer unit, which is effectively a reservoir, storing the toner powder and carrier beads. The developer unit

serves two purposes. Firstly, to agitate the developer (a toner and carrier mix) by reducing powder agglomeration and compaction. The second, and most important, is to induce a triboelectric charge between the toner and carrier. This will enable the carrier and toner to form a balanced, neutral charge [5]. Due to the charge accrued, the toner is attracted to the carrier and is held on by the Van der Waals forces and electrostatic attraction.

The charged toner (negatively charging polymer) and carrier (an iron core with a positively charging polymer shell), are transported by the magnetic roller in the developer roller. The rotation of the magnetic roller brings forward the developer to the vicinity of the latent image in the form of a brush. The difference in potential produces a field which overcomes the Van der Waals forces and electrostatic attraction, allowing the toner to transfer to the latent image on the OPC [38–40, 53], thus creating a real image (see Figure 3:7). The carrier, attracted by magnetic force is recycled in the developer unit where the toner is again tribocharged with the carrier. It is important to note that as the distance from the photoreceptor is increased, the field strength is reduced, compromising the quality of the image.

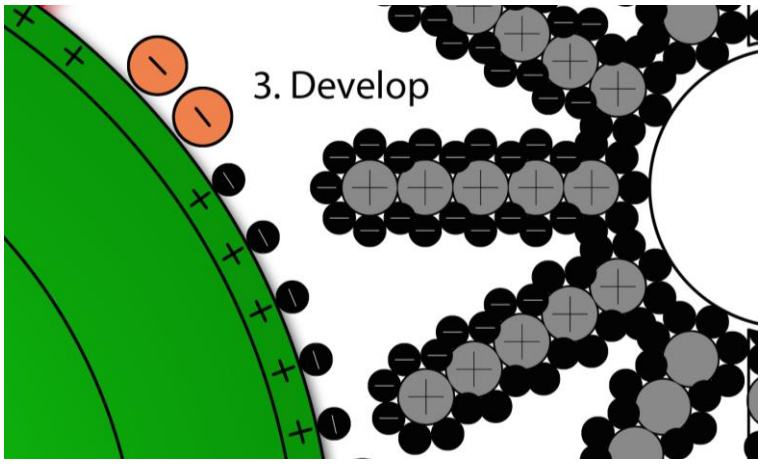

Figure 3:7: Step 3: Development of an image on the OPC

The former describes the transfer of toner by means of a magnetic brush, synonymous with dual component printing, however, there are numerous methods of image development (see sections 3.5.1 and 3.5.2).

3.2.4 Transfer

The toner, now adhered to the OPC drum by an electrostatic charge must be transferred to the substrate (normally a sheet of paper). As the substrate passes under the OPC a corona, or similar charging device, emits a positive charge from beneath the substrate to attract the toner. A schematic of the transfer process is shown in Figure 3:8.

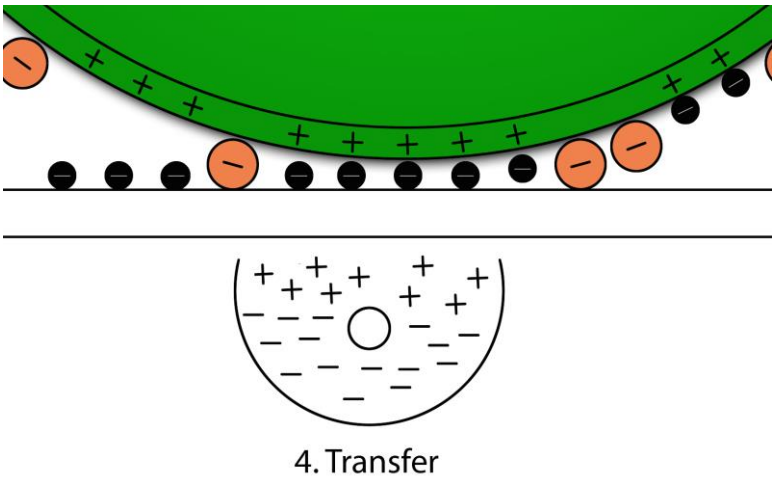

Figure 3:8: Step 4: Transfer step of electrophotography

3.2.5 Fusing

The toner is fused by applying heat and pressure to cause the toner to soften and adhere to the substrate (Figure 3:9). Fusing is generally accomplished using a roller which is rapidly heated from inside by halogen lamps. The substrate is subjected to heat from the bottom roller and pressure from the top via a non-stick roller to avoid toner sticking to it. In commercial printers, the surface of the fuser roller is lubricated with silicone oil to prevent toner from transferring on to it.

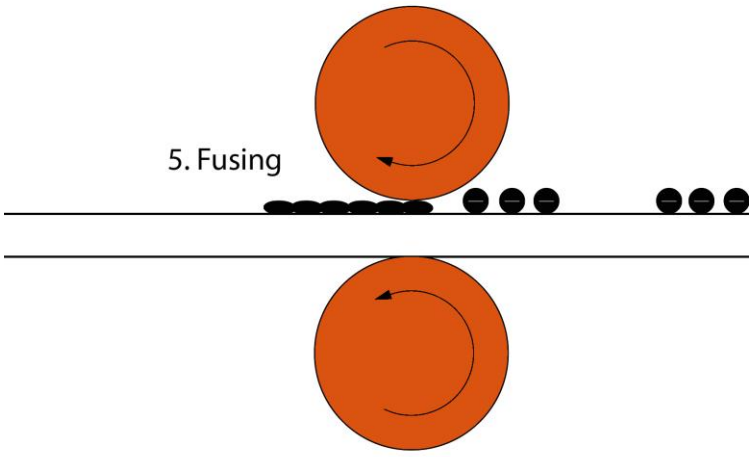

Figure 3:9: Step 5: Fusing toner to substrate

3.2.6 Clean and erase

In the cleaning stage, toner that has not transferred from the photoreceptor is removed mechanically. As the OPC is rotating, a cleaning tool, usually a brush or soft blade, is used to manually remove the toner off the OPC without damaging the photoreceptive coating. The residual toner is collected and stored in a waste toner bottle.

In order to remove any residual charge from the OPC, an additional light source is used to fully expose the OPC, as shown in Figure 3:10. This final step is essential to return the OPC to a suitable condition prior to the printing process being repeated.

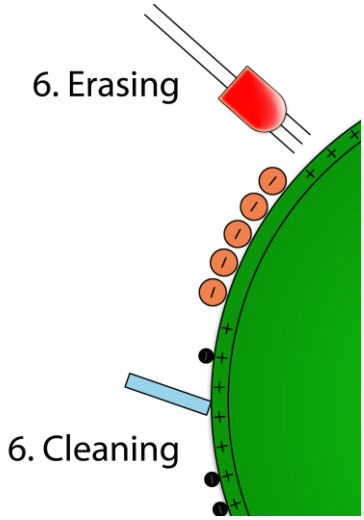

Figure 3:10: Step 6: Cleaning and erase process

3.3 Toner

Toner is typically a dry polymer powder of a given charge, shape and size, made up of various pigments and additives to give the toner its desired characteristics[3, 37, 39, 42, 54–61]. The first toner, lycopodium, was derived from spores of a plant[31]. Nowadays, the toner is a polymeric powder having a low melting point. To impart the required characteristics numerous additives are combined with the polymer (see Figure 3:11).

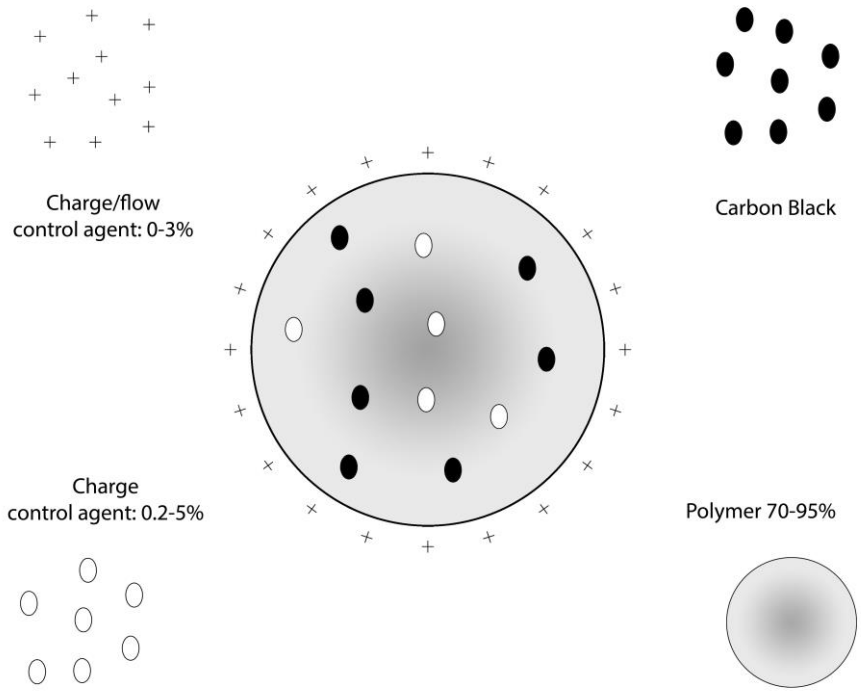

Figure 3:11: Typical composition for a dual component toner (after Banerjee[58])

Dual component toners are transferred using carriers and thus additives become necessary to impart a charge of the correct magnitude and in some cases polarity (positive or negative)

to ensure that the toner adheres and can be removed from the carrier at the appropriate point in the printing process.

The toner to carrier adhesion (for dual component systems) is via tribocharging (rubbing between the carrier and toner). The toner and carrier are attracted via two primary methods; electrostatic and electrodynamic. The effects of electrodynamic and electrostatic forces are still poorly understood and the relative significance which the two forces play on the toner are still contested [38, 62–64].

3.3.1 Electrodynamic

Van der Waals forces are cohesive intermolecular forces arising from spontaneous electric polarisation in charge neutral materials [65]. Van der Waals forces enable like charged particles to be attracted to each other (see Figure 3:12). This is due to subtle, localised, changes in charge through intermolecular rearrangement. The particles can be dominated by two Van der Waals forces; dipole-dipole or dispersion forces. Dipole to dipole forces occurs when the electron is unpaired in one of the particles, resulting in attraction with the second particle. In a Van der Waals dispersion force, nonpolar particles can attract. Although two particles may be of the same polarity and are balanced, the constant movement of the electrons can cause a redistribution resulting in dielectric polarisation causing one particle be more dominant than the other, thus allowing the two particles to attract. This is exaggerated in Figure 3:12 which shows the two particles with the same negative polarity. The internal excitation caused by the movement of electrons, shifts the positive and negative regions, attracting the particles together.

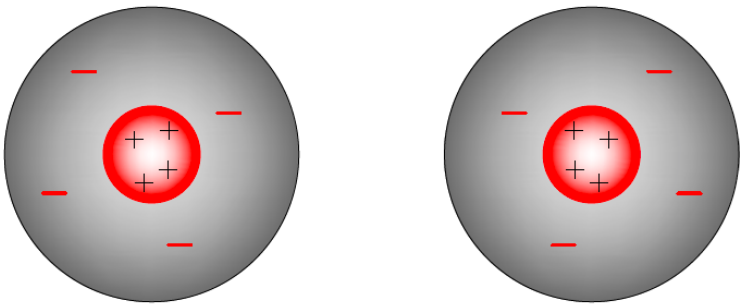

Two negatively charged particles with a repulsive force due to the negative charge around the nucleus.

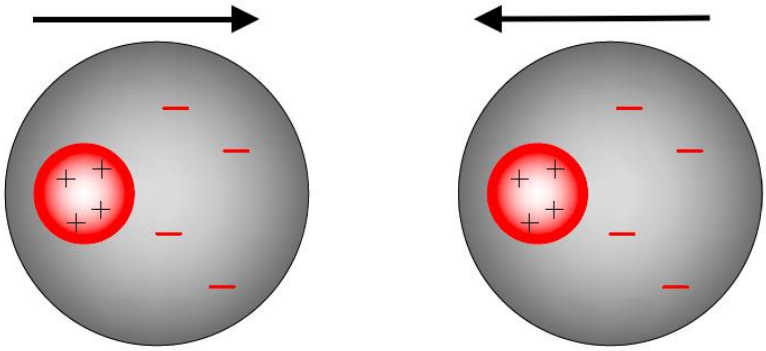

Intermolecular arrangement of electrons through excitation causes an artificial shift in polarity, causing an attractive force.

Figure 3:12: Van der Waals forces between two like sign particles. Top: Like sign particles spaced apart. Bottom: Effect on charge as particle brought together due to Van der Waals (after Owen)[66]

The force required to overcome the Van der Waals interaction can be solved using Equation 1[67].

$$\mathrm{F}_{vdW} = \frac{AR}{6h^2} \qquad \text{Equation 1}$$

Where;

A = Hamaker constant

h = Gap between the two particles

R= See Equation 2[67]

$$R = \frac{R_1 R_2}{R_1 + R_2} \qquad \text{Equation 2}$$

Where;

R= Reduced radius of the interacting particles (R_1 and R_2)

Van der Waals force is classed as a 'short range' and has been described by many as a weak force [65, 68, 69], contrary to the long range coulombic force. The attraction between the two particles becomes measurable at a proximity between 5-30nm[63, 65, 70]. It is debated by researchers whether Van der Waals forces is of greater or lesser significance than the electrostatic force between particles[64, 65, 71–76]. A study of the force required to remove one particle from another has been extensively carried out by Hays *et al*[62, 65, 71]. Feng and Hays concluded that a particle with a 10µm diameter predominantly has an electrostatic force acting on it, with a force ratio of 2:1 for electrostatic and cohesive, respectively[65]. However, as the size of the particle reduces, the cohesive force becomes more dominant. The progressive reduction of toner size means a particle below 10µm is not uncommon. To reduce the influence of Van der Waals forces on the toner, surface additives are used[65, 73–75, 77].

3.3.2 Electrostatic

The most notable of the forces between the toner and carrier is the electrostatic force or Coulombic force. Coulomb's Law or Coulomb's inverse law describes the relationship between two or more charged particles. Coulomb's law dictates that the magnitude of the electrostatic force (F_e) between the interactions of two charged points and is directly proportional to the scalar multiplication of the magnitudes of the charges and is inversely proportional to the square of the distance between them (see Equation 3[67]).

$$F_e = \frac{q_1 q_2}{4\pi\kappa\varepsilon_o r^2} \qquad \text{Equation 3}$$

Where;

F_e is the magnitude of electrical force, measured in Newton (N)

q_1 is the charge on particle 1, measured in Coulombs (C)

q_2 is the charge on particle 2, measured in Coulombs (C)

κ is the relative permittivity

ε_0 = the permittivity of free space in a vacuum (8.8542×10^{-12} F/m)

r = is the distance separating the two charged particles

Although the force decreases with the square of the distance, electrostatic forces, unlike Van der Waals forces, are regarded as long range forces. Electrostatic forces are able to attract and repel and hence are used in toner transportation within the EP process[37].

3.3.3 Tribocharging

In dual component printing, for the toner to adhere to the carrier an electrostatic charge between the two has to be established. The pairing between toner and carrier is initially reliant on a triboelectric series. A triboelectric series is a table, ranking the materials in charge magnitude (see Figure 3:13). Typically, the largest positive charge is positioned at the top of the table with the neutral change in the middle and the highly negative material at the bottom of the table. Unfortunately, although there are numerous tables in circulation no single table encompasses every material or even every polymer. Schein [37] explains that this is due to the potential to generate a tribocharge through a wide range of material interactions.

+ POSITIVE END OF SERIES
Asbestos glass
Silicone elastomer with silica filler
Borosilicate glass, fire polished
Window **glass**
Polymethylmethacrylate
Ethylcellulose
Polyamide 11
Polyamide 6-6
Rock Salt (NaCl)
Melamine formol
Wool, Knitted
Silica, fire polished
Silk, Woven
Polyethylene glycol succinate
Cellulose acetate
Polyethylene glycol adipate
Polydiallyl phthalate
Cellulose sponge
Cotton, woven
Polyurethane elastomer
Styrene-acrylonitrile copolymer
Styrene-Butadiene copolymer
Polystyrene
Polyurethane flexible sponge
Borosilicate glass, ground state
Polyethylene glycol terephthalate
Polyvinyl butyral
Formo phenolique, hardened
Epoxide resin
Polychlorobutadiene
Butadiene-acrylonitrile copolymer
Natural rubber
Sulphur
Polyethylene
Polyvinyl chloride without plasticizer
Polytriflurochloroethylene
Polytetrafluoroethylene (PTFE)
- NEGATIVE END

Figure 3:13: Triboelectric series with bold highlighting the most used for toner [5]

Dual component systems are reliant on tribocharging between the carrier and toner. When pairing a toner and carrier the correct Q/m is imperative. There are a number of methods used to determine this. The most notable is the cage blow off method outlined in ASTM F4125-06[78].

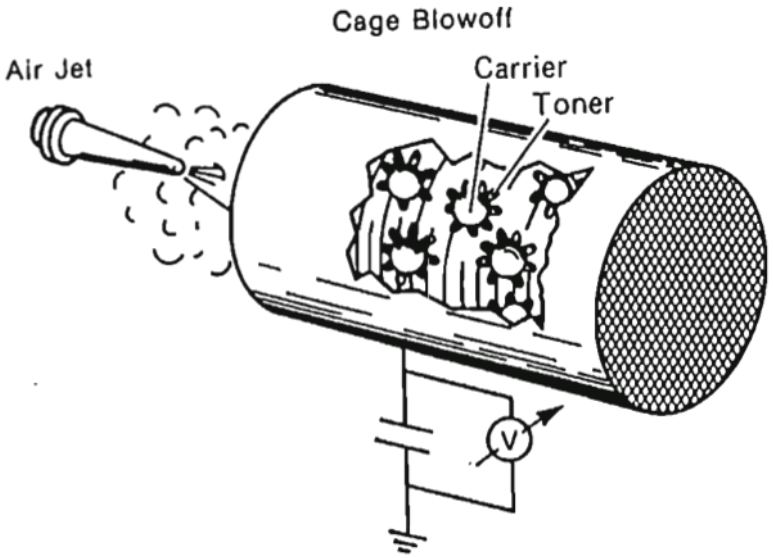

Figure 3:14: Cage blow off method used to determine charge magnitude between toner and carrier[67]

The blow off method relies on a stainless steel faraday cage with wire meshes on either side. The mesh is large enough for the toner to pass through but small enough to restrict the larger carrier. A known mass of developer is loaded and a jet of air is passed through the cage. By measuring the change in both the mass and charge, an average Q/m can be established. A diagram of the cage blow off method is shown in Figure 3:14.

Charging, is however, not always straightforward and requires certain conditions to be constrained in order to optimise the efficiency. During the development of the electrophotography process, Carlson and Kornie experienced varying results in their experiments. They found they were unable to replicate their results when the weather was colder. It was found that one of the most influential factors affecting tribocharging is humidity and temperature. The effects of both factors on charging have been extensively studied[38, 60, 63, 79–81]. It has been shown (Figure 3:15) that at elevated temperatures, the resistivity dramatically decreases with varying moisture content[82]. This has been corroborated by many researchers[63, 79, 80, 82]. This is because moisture has a tendency to decreases the resistivity of a material providing a path of lower resistivity along which charge can migrate.

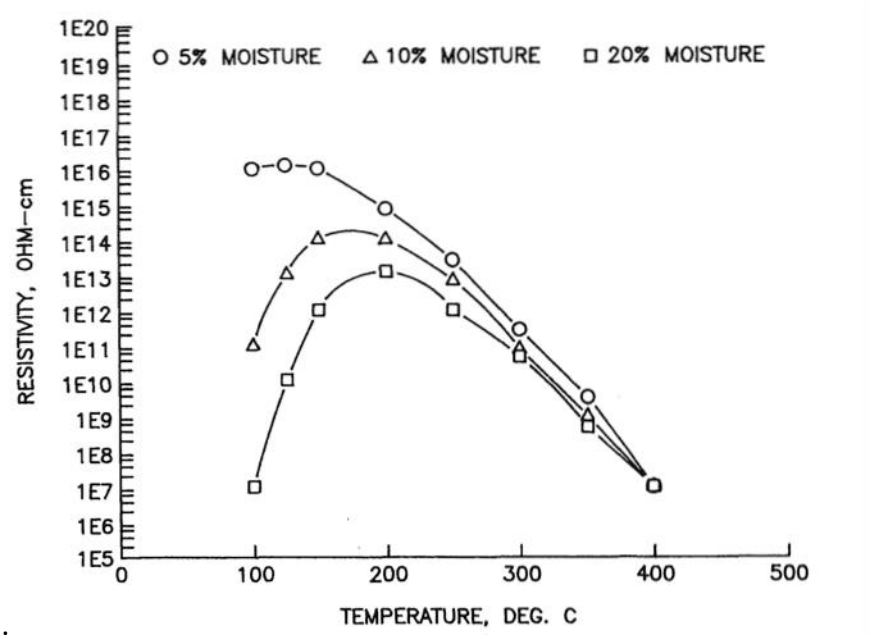

Figure 3:15: Resistivity of powders as a function of temperature at altering moisture content[82]

3.3.4 Toner development

During Carlson's development of the photocopier, he required a toner small enough to show the latent image, which he assumed, was created on the photoconductor. Carlson tried Lycopodium, an extremely fine spherical powder derived from the dry spores of the club moss plant to crystalline sulphur to dragons blood (a resin obtained from a number of plants)[31]. From this point onwards toner has been the subject of intense research, driven in part by the need to use finer particles.

3.3.5 Toner composition

Toner is an extremely complicated element of the electrophotographic process. The toner needs to be charged and moved around by electrostatics. The core material, or the polymer, is brittle with a low melt temperature. The low melting temperature of the polymer is advantageous in laser printing. The low melt polymer reduces fusing time, yielding greater productivity and reducing energy consumption. The base polymer used differs between manufacturers. For instance, Hewlett Packard uses a styrene acrylate, whereas Xerox and Ricoh both use a polyester blend[83–85].

The low melt polymer is however, only part of the component required to make up toner. While the polymer makes up the bulk of the toner (45-95% by weight) [86–88], additives are included to enhance specific properties of the toner. Additives such as Charge Control Agents (CCAs) and Flow Control Agents (FCAs) are used to improve the flow and charging characteristics of the toner. Wax is used to aid fusing and reduce sticking during the fusing stage. Pigments are used to impart colour to provide the required toner colour (black, yellow, cyan and magenta) [58, 86–88].

3.3.6 Polymer

The use of polymers as a constituent for a toner dates back to the development of the electrophotography process with Haloid and Battelle[32]. The toner is typically a polymer with a low melt temperature and brittle in nature. A typical polymer for a toner would be polyester, styrene copolymers or polymethylmethacrylate (PMMA) [37, 83–85, 88]. Another reason for choice in polymer is its dielectric properties. For toners the dielectric properties dictate the ability to polarise a material. By striking the right balance of dielectric constant with a low melt temperature, the toner is able to charge and transfer efficiently.

Toners are generally produced using two approaches – mechanical milling of coarse powder/granules to produce a fine powder (known as comminution) or production of the polymer powder directly during the polymerisation process (these techniques will be described in more detail in section 3.4.

3.3.6.1 Charge Control Agents

Charge control agents (CCAs) such as fluorinated PRO-TONER™ CCA 7 (negative charge) and quaternary ammonium salt of a sulphur containing acid (positive CCA) are extensively used in toner development [89, 90]. Their ability to increase the capability of the polymer to charge and even change the polarity of the polymer's natural charge has made it an important ingredient in toner manufacturing. The CCAs are added to the base toner polymer in quantities ranging from 1-3% by weight [89].

3.3.6.2 Flow Control Agents

Flow control agents (FCAs) are used primarily to aid the flow of the toner powder and reduce coalescing and agglomeration between toner particles. Fumed silica is the most prominent of negatively charging FCAs and is a low-density amorphous silica. Due to its hydrophilic properties, silica readily absorbs moisture and is also used to stabilise the triboelectric characteristics of the toner[58].

3.3.6.3 Wax and pigments

Toners are generally not the desired colour required for printing, it is for this reason a pigment is added to the toner for aesthetics. The pigment to produce a black toner is carbon black and is added in small quantities, between 3-7%[88] by weight, to provide the toner with a dense black colour. Wax is another material added to toner, although its use is not related to charge or aesthetics. Wax is added up to 2% by weight[91] to prevent the toner polymer sticking to the heat source during the fusing stage.

3.3.7 Toner size

The size of toner varies between manufacturers and printers; however, toner is typically between 5-20µm[37, 39, 53] in size. The need to reduce the size of toner particles has ultimately stemmed from image quality. The latent image developed on the photoreceptor has an extremely fine resolution. However, this image quality cannot be realised with the current toner size[38]. The printer image quality has improved over the years from a 600dpi to 2400 dpi resolution for home and commercial laser printers. The resolution of 600, 1200 and 2400 dpi printers equates to approximately 42µm, 20µm and 10µm resolution,

respectively. This progressive increase in resolution highlights the need for finer toner particles. For printers with a resolution greater than 2400dpi, toners are held in a liquid suspension due to the combustible nature of fine powders[5].

Although the resolution of a 2400dpi printer equates to approximately 10µm, the toner size will invariably have a particle range. Typically, chemically synthesised toners have a range of a few microns either side of the desired toner size (D_{50}). For mechanically milled toners the toner particle size is generally bigger due to the manufacturing process. This range can be extended by up to 10µm either side for older toners, resulting in lower resolution printers. Ideally, toner would be a single sized particle without a range. This would allow the Q/m to be unequivocally defined, minimising the amount of toner that is wasted, since the field strength required in overcoming the electrodynamic and electrostatic strength between the toner and carrier is the same. Moreover, a simpler setup of the printer could be achieved, which would save voltage set up time, carrier pairing, as well as additional surface/internal additives.

However, since the process of producing a single sized toner is commercially impractical, a suitable range is generally employed to produce a toner. It can be seen from the scatter plot (Figure 3:16) that the particle size of a toner sample has a large size distribution with each dot representing a particle from the sample. There is a large concentration of dots at a given size range. This dense distribution of dots is used to obtain the Q/m by calculating the average particle diameter and Q/m.

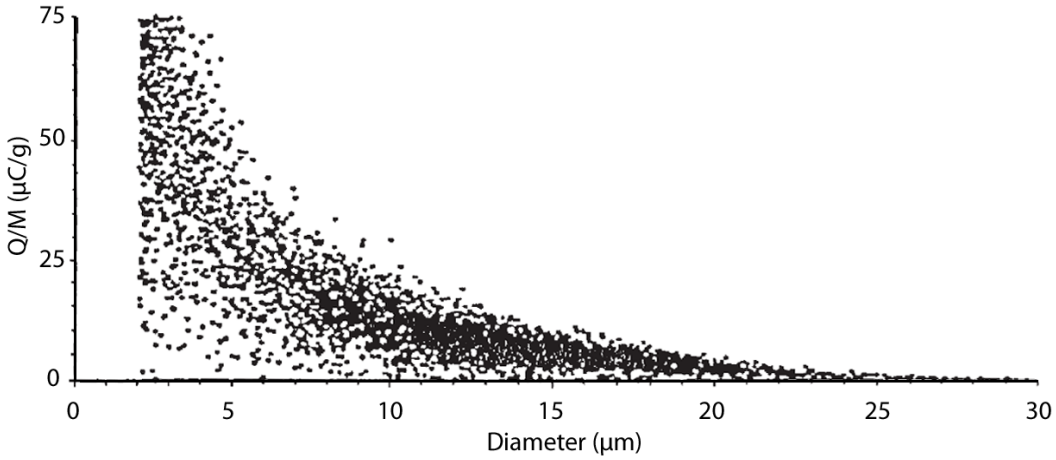

Figure 3:16: Scatter plot of 4000 dots showing particle size against Q/m[76]

Another important factor for toner is the shape. The charging between a toner and carrier is heavily influenced not only by the size of the toner, but also the shape. Toner manufactured via mechanical milling possesses an irregular shape. This requires additional CCAs and FCAs to compensate for the shape. Chemically produced toner (CPT) often do not require FCAs due to their spherical shape but lack the adequate charge to couple with the carrier.

3.3.8 Toner classification

Although particle size is of great significance, size distribution is of even greater importance. Particle size distribution can be expressed as a percentage of the entire sample size. For instance, the D_{50} also known as the median diameter is the value of the particle diameter at 50% of the cumulative distribution. Figure 3:17 shows a particle size distribution (PSD) of a material highlighting the divisions or cuts. The material is usually expressed in D_{10}, D_{50} or D_{90}, although D_{95} and D_{97} are not uncommon. It is imperative that the distribution of the toner is as narrow as possible to ensure consistent printing.

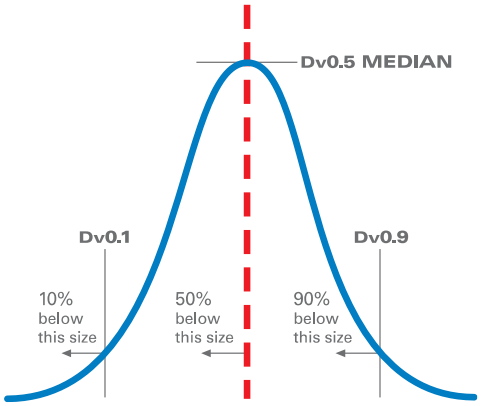

Figure 3:17: Particle size distribution showing the D_{10}, D_{50} and D_{90} of a given material[92]

For dual component systems the need for toner to tribocharge with the carrier is essential for efficient transfer. The size of the toner determines the Q/m (charge to mass) magnitude. The smaller the particle the larger the Q/m, this can result in a non-uniform transfer of toners and has a negative impact on image quality as well as causing heavy background contamination on the prints. On the contrary, toner particles, which are too large, can result in damage to the OPC.

The need to produce a fine polymeric toner with a tight distribution has become of such great importance that mechanical milling methods often incorporate sieves into the milling device to only allow material below a required particle size to pass. A secondary sieving process is employed to remove the fine (undersized) polymeric toner from the original sieved material to give a tight distribution. In chemical manufacturing particle size and distribution can be adjusted in situ, enabling a tighter particle size distribution at the source.

3.4 Manufacturing methods

The circularity factor (Figure 3:18) characterises the circularity of the toner and is a ratio between the circumference of the equivalent circle of projected area and the perimeter of the toner. For toners, the optimum circularity factor is between 0.96-0.98[4]. A toner, with a circularity ratio greater than 0.98, can cause the toner to act as a lubricant. Conversely, toner with a circularity factor less than 0.96 is deemed abrasive and can cause the toner to damage the photoconductor over time. A "potato shaped" toner [93] is often referred to as having the ideal circularity factor for toner material.

$$C_{factor} = \frac{2\sqrt{A}}{P^2}$$ Equation 4

Where;

A is the area of the particle

P is the perimeter of the particle

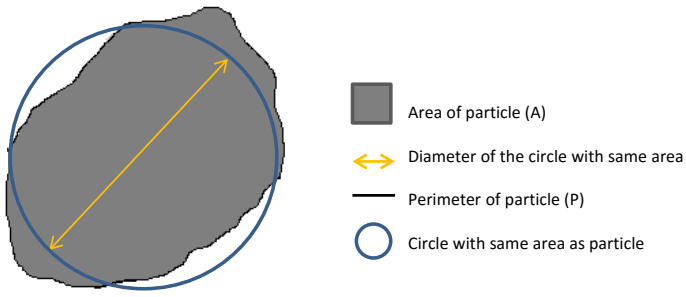

Figure 3:18: Circularity factor

Toner manufacturing is reliant on the ability to consistently produce fine polymeric powders. The method most synonymous with toner manufacturing is mechanical milling [4, 56, 57, 94, 95]. However, due to the need for finer particles, toners are now more commonly

produced by a chemical manufacturing process [7, 59, 74, 91, 95–100]. Figure 3:19 shows a schematic diagram of mechanical (left) and chemical (right) production methods.

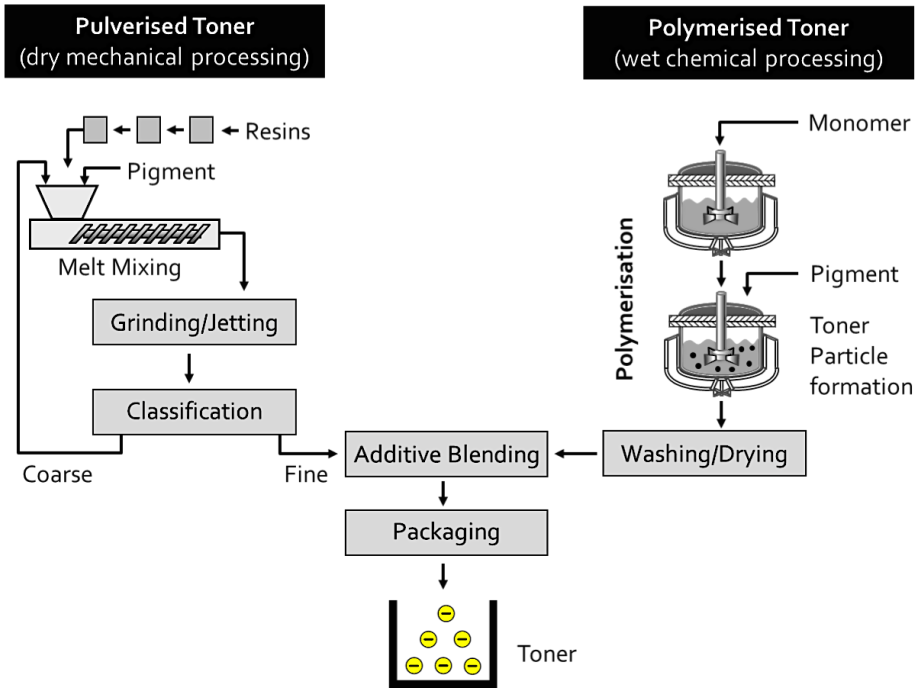

Figure 3:19: Chemical and mechanical manufacturing processed adopted in toner production[56]

The manufacturing process has a direct impact on the ability to charge the toner and the charge force. For instance, a mechanically milled toner does not possess the correct flow properties, however, the irregular, jagged edges allows the bulk of the charge to be concentrated at the tip of the point (see Figure 3:20 left). Conversely, a spherical toner shows the charge is evenly distributed along the surface area of the sphere (see Figure 3:20 right). While the mechanically milled toner is able to charge more readily than chemically produced toners, the need for finer toners with a much tighter size distribution favours chemically produced toners.

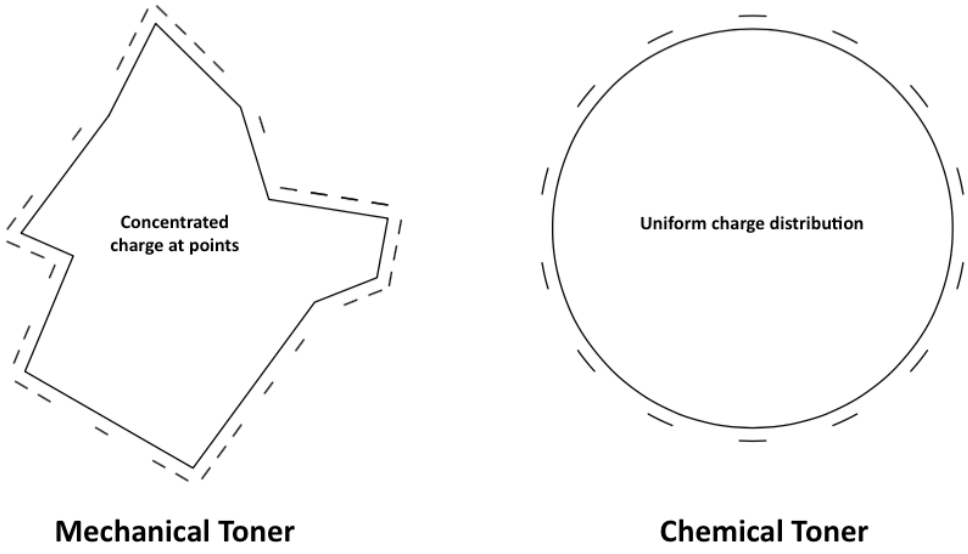

Figure 3:20: Charge concentration for mechanically milled (left) and chemically produced (right) toner

3.4.1 Mechanical methods

Described below are the mechanical methods employed to reduce polymers by the toner industry. The format is based on the natural progression the industry has taken in reducing the powder from the early large toner to the very fine based on the resolution of the printer.

3.4.1.1 Pulverisation

Comminution, or mechanical milling, as a means of particle reduction is employed in a wide range of fields from mining to pharmaceuticals[101–105]. Each sector employs a reduction technique particularly suited to producing the required size of toner for the specific application.

The traditional method of toner manufacturing relies on a brittle polymer combined with CCAs, FCAs, pigments and waxes as described in section 3.3.5. The ingredients are melt-mixed and reduced to the desired size by mechanical means. The mechanical methods utilised are of significant importance. Certain methods produce relatively coarse particles while other methods can generate extremely fine particles (particularly air milling and cryogenic techniques).

The fibrous and the viscoelastic nature of polymers, coupled with the ability to exhibit both elastic and plastic deformation (particularly for tough polymers), can mean that grinding is an extremely energy intensive process. It has been reported that the energy required to comminute tough engineering polymer can be two orders of magnitude greater than that for brittle materials[106, 107] – significantly increasing the processing time and cost. In the context of using electrophotography methods for AM, this presents a significant challenge as the requirement for a tough thermoplastic toner to generate engineering parts is counter to the production efficiency of the milling operation. Another key characteristic of comminution is that the particles produced in this manner are of irregular shape. This irregular shape can have a negative effect on the flow properties of the powder as well as the charging.

Toner particles generally fall in the range of 5-20µm. However, as the need for higher resolution arises, the demand for finer particles will increase [58, 91, 95, 108]. This section aims to give an overview of some of the mechanical methods for particle reduction employed specifically for polymer powders.

3.4.1.2 Hammer Mills

Hammer mills are implemented either in a fixed hammer or swinging hammer configuration, fracturing and breaking the polymer at impact and forcing the polymer against the outer plate, which are specifically designed to break the material on impact. A screen is placed below where the finer particles are able to pass through and the larger particles continue with the reduction process. This method is particularly suited to the production of course powders using brittle polymers [105, 109].

3.4.1.3 Pin mills

Pin mills (also known as stud, disc and impact mills) use a rotating disc on which numerous pins are mounted. The pin disc is rotated at high speed (10,000 RPM is not uncommon) and powder material is thrown by the pins onto the housing causing it to fracture [106].

Thermoplastics exhibiting either a low T_g (glass transition temperature) or T_m (melt point) tend to soften and flatten during prolonged impact, especially once the particle has been significantly reduced in size from the original feedstock[105]. This is due to heat stemming from the energy created via particle-to-particle interaction. The addition of forced air has a two-fold advantage; it cools the particles, which allows for a further reduction in particle size, and it aids the motion of particles thus reducing agglomeration. Pin milling can be used to grind powders to finer particles compared to hammer mills. Unfortunately, Pin mills tend to result in a wide particle size distribution and thus further classification is required to attain the desired distribution.

3.4.1.4 Air Jet milling

Air jet mills are used for the fracture of tougher polymers or when finer particles are required. In air jet milling multiple streams of compressed gases flow from the bottom of the mill. The feedstock is fed into the chamber and the velocity of the air stream causes the particles to impact each other and the impact plates. The classification of the powder is done via a free vortex. Large particles, on account of their higher mass, are projected onto the chamber wall, resulting in further size reduction. The smaller particles are able to exit the chamber via a sieve. The disadvantage of air jet milling is the need to control the quantity of feedstock, too much and the particles will not reduce efficiently. To counter this a higher air pressure is required, however, this results in higher energy consumption.

3.4.1.5 Cryogenic grinding

The use of cryogenics in grinding enables a substantial reduction of particle size at higher grinding efficiency, without the need to upgrade the original mill.

Cryogenic media such as liquid nitrogen are extensively used in grinding applications [101, 105, 107, 110–116]. The process of low temperature grinding enables higher efficiency in particle reduction and shorter processing time for thermoplastics. Moreover, it produces toner with a narrower particle size distribution [107].

In recent years, the process of pulverisation has been highly optimised to enable efficient grinding of tough thermoplastics at ambient grinding conditions. However, the use of such cryogenic materials has paved the way for much finer and efficient methods of production [106, 107].

A novel method of particle reduction has been developed by the Fraunhofer Group where the material is processed using air cooled by liquid nitrogen prior to comminution[107]. The process of comminution using liquid nitrogen is well established for toner manufacture but as the required size of particles decreases mechanical milling is reaching the limits of its cost effectiveness.

Additive Manufacturing requires the use of tough engineering polymeric powders for powder bed applications. The use of liquid nitrogen, together with other novel methods of particle reduction have helped to increase the ability of mechanical milling methods to generate finer toner. However the cost, energy consumption and processing time coupled with the relatively poor material efficiency of milling techniques ultimately means that a more flexible process is required to produce tough engineering thermoplastics.

3.4.2 Chemical production

For the last five years approximately 60% [5] of all colour toners were produced by chemical methods. The need for chemically produced tones has risen from the increased resolution of the image. Mechanical milling has the ability to reduce particles, however, the process lacks the efficiency of chemical produced toners for finer particles. Chemical toner production has a distinct advantage over mechanical reduction - most notably, the ability to produce particles with not only a tight particle distribution but also a homogenous shape and smaller overall particle size. Moreover, polymerisation enables the additives (described in section 3.3.6.1, 3.3.6.2 and 3.3.6.3) to be added in-process, resulting in a one step process for toner manufacturing.

A number of methods are available for chemically producing toners, however, only the most commonly employed methods are described here. The process of polymerisation was

categorised by William Hume Carothers in 1929 [117]. However, more recent terminology classifies polymerisation into Step and Chain polymerisation as classified by Remp and Merrill[117, 118]. The process of polymerisation can be split into two categories; Step growth and Chain growth, these are described in more detail below.

3.4.2.1 Step growth Polymerisation

Step growth polymerisation is the systematic build-up of molecular chains in a slow but stepwise manner. The monomers are combined with the each other resulting in dimers. Trimers are formed with the addition of a monomer and a dimer. Teramers are formed with the addition of two dimers, with the continual addition of these oligomers making up a polymer.

Table 3:1: Step wise growth mechanism of polymer molecules (after Odian)[117]

Monomer	+	Monomer	→	Dimer
Dimer	+	Monomer	→	Trimer
Dimer	+	Dimer	→	Teramer
Trimer	+	Monomer	→	Teramer
Trimer	+	Dimer	→	Pentamer
Trimer	+	Trimer	→	Hexamer
Teramer	+	Monomer	→	Pentamer
Teramer	+	Dimer	→	Hexamer
Teramer	+	Trimer	→	Heptamer
Teramer	+	Teramer	→	Octamer

The step growth mechanism, shown in Table 3:1 defines the sum of the rate of reaction, with the higher molecular weight polymer being produced towards the end of the polymerisation process [117–119]. However, the amount of monomer reduces as it is converted during the process to form the oligomer.

The process of step growth polymerisation is suited to polyimides, polyester as well as polycarbonates and polyurethanes. This is due to the collection of groups, such as acids glycols and amides, with H_20 being produced and evaporated during the endothermic reaction and then condensing. It is noteworthy that while the polymer has been formed the chain is open and not terminated[117].

3.4.2.2 Chain growth polymerisation

Chain growth polymerisation is characterised by relatively quick reaction rates, with monomer chains being formed at a much faster rate than for step growth polymerisation. This rapid increase in monomer chains enables the polymer to gain its molecular weight early on in the reaction phase. However, the monomer to polymer conversion rate increases. As the reaction progresses, the monomer concentration decreases. A chain end is open or active to receive the monomer one at a time. When the chain length is complete, the chain is ended, leaving a closed and complete chain. The section below describes a few methods of chain growth polymerisation.

3.4.2.2.1 Suspension polymerisation

Suspension polymerisation is a type of free radical polymerisation. The process utilises a two phase system, namely, the dispersion and continuous phase.

The dispersion phase consists of the monomer and the initiator for standard polymers. The process can be adapted to toners with the addition of CCAs, FCAs, waxes and pigments. The continuous phase is an aqueous solution in which surfactants and stabilisers are heated to enable the ingredients to dissolve. The function of the surfactants and stabilisers is to break

the surface tension of the aqueous solution and to assist the dispersion phase in producing the correct particle size.

The dispersion phase and the continuous phase are homogenised by blending the two phases using a propeller screw shaft or similar. The homogenising velocity is set according to the required size of the polymer particles, with an increased speed resulting in finer particles[120].

With the addition of heat, the free radicals are initiated and are formed into polymers by the addition process.

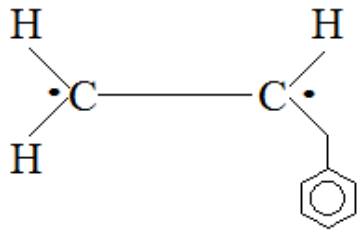

Figure 3:21: Initiation stage of polystyrene

Firstly, the initiator begins to decompose. The breakdown of the initiators releases the free radicals [117, 118, 121], signified by the "•" in the figure above (Figure 3:21). The free radical enables the addition, or propagation of another styrene monomer, forming the beginnings of a polymer chain length[56, 117]. It is worth noting that the chain length can be extended on both sides of the monomer simultaneously as seen in Figure 3:22.

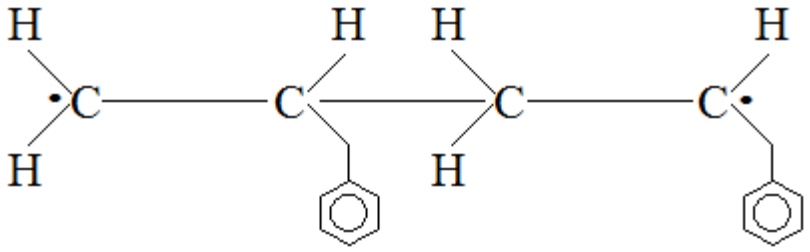

Figure 3:22: Propagation stage

The final step of the polymerisation process is termination (see Figure 3:23). The free radical, which allows for the linking of other monomers, is terminated by decomposition and the length of the polymer chain is dependent on the rate of decomposition[117, 118]. The process is terminated when the initiator is completely decomposed.

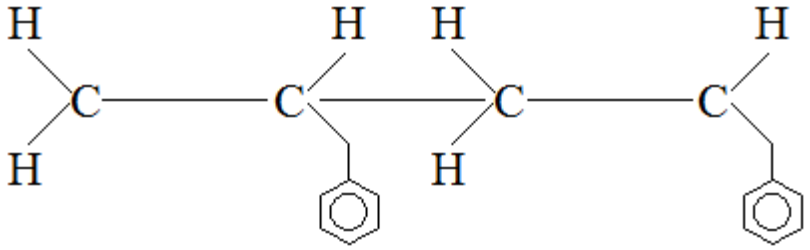

Figure 3:23: Termination stage

3.4.2.2.2 Emulsion polymerisation

Emulsion polymerisation takes place when a monomer is dispersed in a water solution containing surfactants. A surfactant molecule consists of a hydrophilic (polar) head and a hydrophobic (non-polar) tail [96]. The excess surfactant in the solution forms into spherical array or micelles - described as a "*colloidal particle formed by the reversible aggregation of*

dissolved molecules"[122]. Due to the electrically charged nature of the micelles, colloidal surfactants are used in emulsion polymerisation.

An initiator is dispersed in the aqueous solution, the monomer is added to the water and dispersed by a paddle mixer or similar. From the small amounts of monomer dispersed into the water, the (non-polar) monomer is absorbed into the centre (non-polar) region of the micelle. More of the monomer is dissolved into the water to replenish what has been absorbed into the micelle. The polymerisation process occurs in the "swollen" micelle when the water-soluble initiator is added to the water. The initiator interacts with the monomer located in the micelle, which begins to form a chain. Termination of the reaction is controlled by the supply of free radicals, which is dependent on the concentration of both the surfactant as well as the initiator. A diagram of the process is illustrated in Figure 3:24.

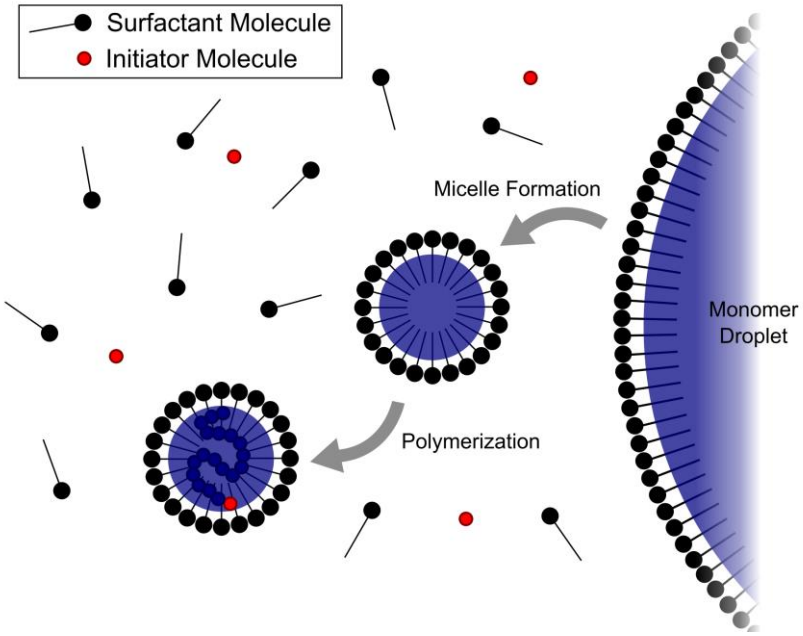

Figure 3:24: Emulsion polymerisation process[123]

3.4.2.3 Evaporative Limited Coalescence

Evaporative Limited Coalescence (ELC) is a process that has been employed in the toner manufacturing industry for over 20 years [124]. Toner manufacturers have their own variation of the ELC process and often use a proprietary method of shaping the toner to form the desired shape. It should be noted that the toner industry is extremely opposed in disclosing any more than the absolute minimum information in an effort to protect their toner recipe. As such, they publish a wide range for each ingredients used. For example, a toner base material can be represented as 70-90%, rather than the specific amount. [84].

The ELC process consists of two phases; an organic and aqueous phase. The organic phase typically consists of a carnauba wax, which is heated above 75˚C and cooled, forming micron-sized needle like precipitates. The carnauba wax is then homogenised with additives. A base polymer binder resin is added at a concentration usually above 90% by weight. Pigments are added at concentrations between 2-30% by weight. Charge control agents are added between 0-10% by weight. A solvent, usually, ethyl acetate or a similar, is used to dissolve the aforementioned ingredients [124].

An aqueous phase is produced consisting of a buffer solution. The buffer solution contains highly cross-linked latex particles and silicon oxides added at 3% by weight in the aqueous solution. The organic phase is added to the aqueous phase at concentrations 1:9 to 4:6 of organic to aqueous phase respectively. The two phases are subjected to an extremely high shear mixing followed by micro fluidising, creating a spherical shape. The aqueous phase is removed and the solvent is evaporated away leaving a fine precipitate with a non-spherical, regular shape. The precipitate is washed to remove the buffers and dried ready to coat the toner with surface additives.

3.5 Dual component development systems

A number of development systems have been created over time for improving the delivery of the toner and the toner density built up on the photoreceptor and consequently, the substrate. The most notable are Cascade, Insulative magnetic brush and Conductive magnetic brush.

The need for progression in the development steps arose from the poor image development for solid area printing. The introduction of cascade development was the most efficient method of toner transfer at the time. However, while text would print fine, solid areas would not print very well or not at all (See Figure 3:25a). This was especially prevalent during the early stages of electrophotography. The focus on image quality was always at the heart of electrophotography, however, the introduction of an alternative to cascade development would not come for another 20 years.

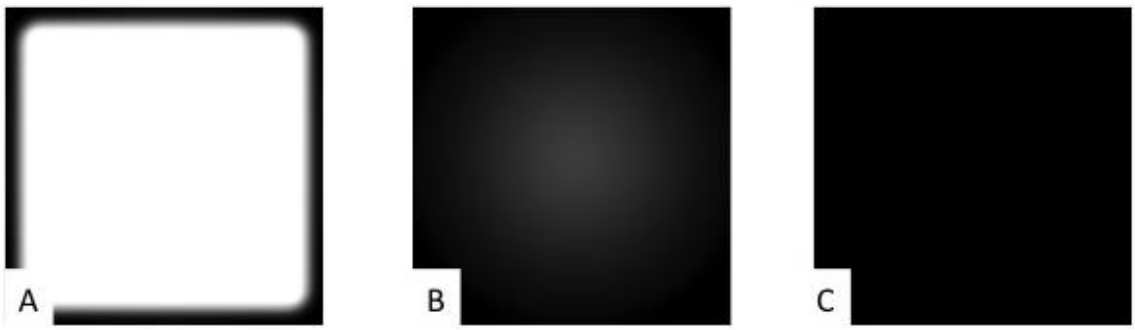

Figure 3:25: Images showing A) Cascade development, B) Insulative magnetic brush and C) Conductive magnetic brush (after Schein)[37]

3.5.1 Cascade development

Cascade development was a collaborative effort by Haloid and Battelle, developed in 1952 to resolve the issue of charging and development[31, 37]. In cascade development the toner is transported via a carrier bead. The developer mix is cascaded over the photoconductor that is set at an angle, hence the name. As the toner comes in contact with the latent image, the field generated on the photoconductor is used to electrostatically attract the toner off the carrier bead. The carrier beads continue to cascade due to gravity and are recycled back in to the toner mix.

The introduction of cascade development addressed the issues with toner transfer; however, it was not without its faults. Many factors influence the development of the image on the photoconductor. The speed and the direction at which the cascading beads fall off the photoconductor are critical to the development process. If the angle is incorrect the beads bounce preventing and image from forming and moreover, the errant beads can detach particles from the existing image thus reducing efficiency. By inclining the photoconductor at the optimum angle of 60° to the developer flow these problems are minimised [125].

Another fundamental issue with cascade development relates to solid area development. A line or letter can readily be developed and thus printed, however, this is not the case for large area development. Due to a phenomenon known as the fringe field effect, the outer edge of the image would develop whilst image quality of the interior deteriorates progressively towards the centre. This phenomenon is shown in Figure 3:26, which illustrates the original image with the field lines and the diminishing field strength closer to the centre.

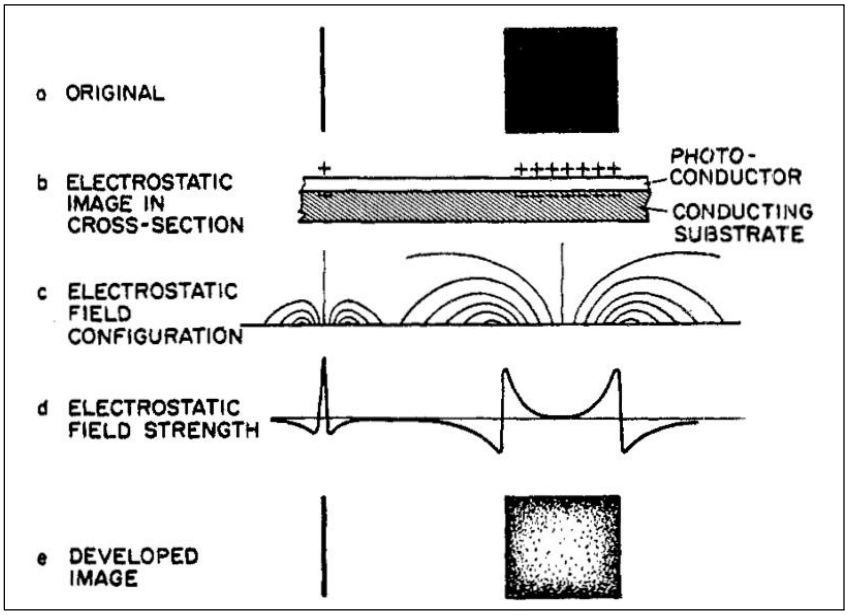

Figure 3:26: Fringe field effect on cascade development[37]

A method developed to overcome the fringe field effect is based on the introduction of an electrode at a given distance from the photoreceptor. A grounded or biased electrode is placed 2.4mm from the photoreceptor[126].

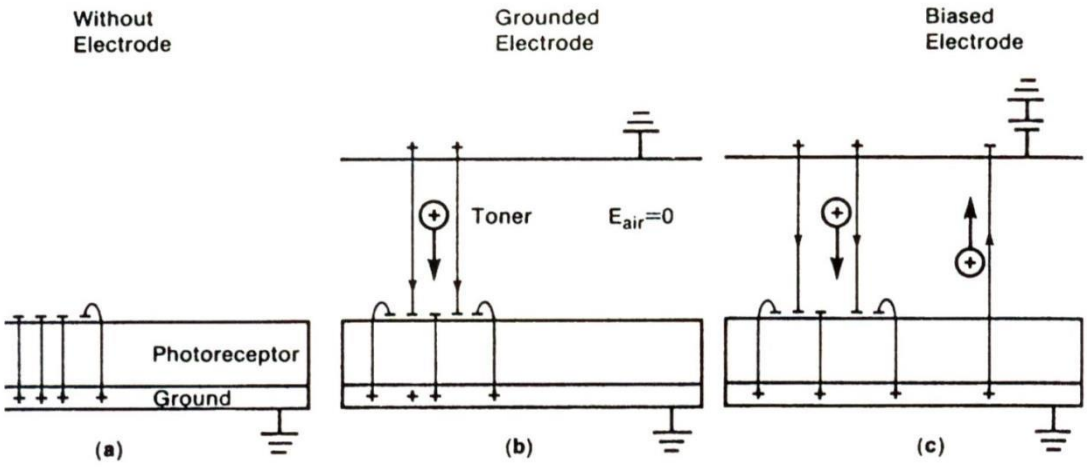

Figure 3:27: Influence of field line configuration with and without an electrode[126]

The electrode serves to manipulate the force lines from their natural field configuration resulting in even toner distribution over the entire area, rather than concentrated around the perimeter.

3.5.2 Magnetic brush development

It is well known that the electric conductivity of the developer has a considerable influence on the development[37, 127]. Should the conductivity be low, the field strength on the edge is greater than that at the centre of the latent image. The introduction of magnetic brush development addresses the issues associated with the fringe field effect. This section will discuss the introduction of the magnetic brush systems and describe the improvements in development for both insulative and conductive systems.

3.5.2.1 Insulative magnetic brush

Insulative magnetic brush (IMB) was invented by RCA towards the end of the 1950's but did not come to plain paper copying until 1972 when IBM introduced their Copier 2[37]. The introduction of the IMB development system was a vast improvement to the cascade development systems primarily due to improve solid area development, reduced background contamination and improve copying speeds. The insulative magnetic brush uses a carrier (magnetically soft) with toner attracted via tribocharging. The developer is introduced to the developer roller which has stationary magnets mounted inside. The magnetic flux lines create the carrier chain, which are transported around the developer roller via magnetism. The photoconductor is in close proximity to the developer roller allowing for the toner to transfer on to the photoconductor. However, it is the reduction in the resistivity of the carrier chain that enables greater toner density development on the photoconductor surface.

$$\frac{m}{A} = \frac{\varepsilon_{oV}}{\left\{\frac{d_s}{K_s}\right\} \cdot \left\{\frac{Q}{m}\right\}}$$ Equation 5

Where;

ε_o = Permittivity of free space (8.85×10^{-14} F/cm)

V = Applied Voltage

d_s = Photoreceptor thickness

K_s = Photoreceptor dielectric constant

Q = Charge

m = Mass

From Equation 5 is it evident that as the Q/m increases m/A is decreased resulting in a poorly developed solid area of the image, as shown in Figure 3-26. Due to the spherical carrier, the brush produced is insulative as the toner is encompassed around the entire surface area. As a result the resistivity is increased resulting in a reduced m/A.

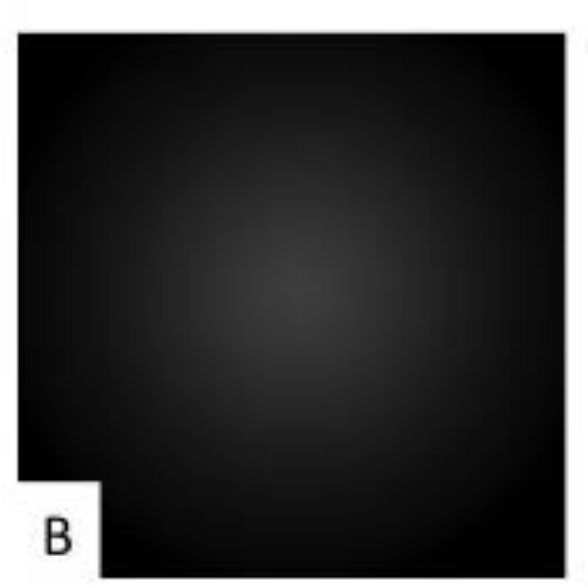

Figure 3:28: Insulative magnetic brush development with greater toner density but still lacking density in the centre of image. [37]

3.5.2.2 Conductive magnetic brush

Conductive magnetic brush development (CMD) was introduced in 1975 [37, 42] by Eastman Kodak to rival the insulative magnetic brush. The CMD system was developed to produce a more uniform and higher print density as well as limiting background printing (contamination of the printed page by “rogue” toner particles).

The process is identical to the insulative magnetic development, with the exception of the carrier, which is classed as a sponge carrier due to its porous structure and irregular shape (shown in Figure 3:29). Due to the organic shape of the carrier, a point of contact is maintained from the developer roller across the brush. Studying Figure 3:29 it is apparent that the organic shape of the carrier promotes a contact point between each carrier, enabling a path of least resistance.

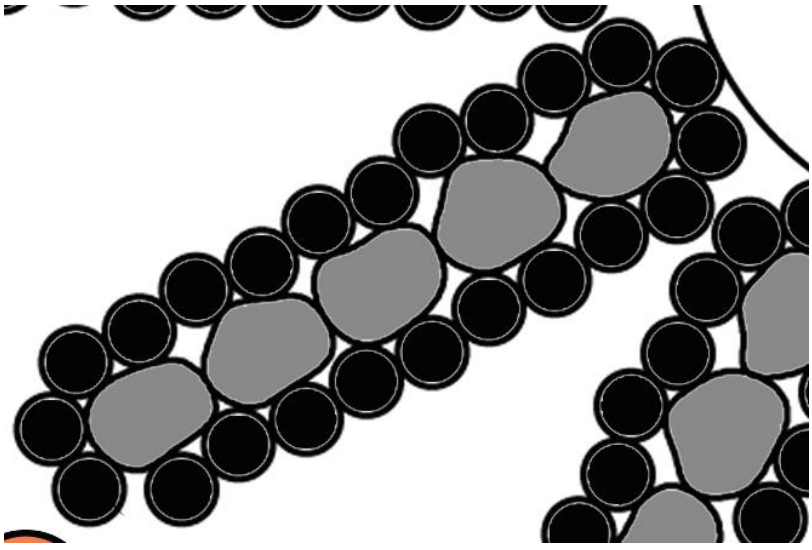

Figure 3:29: Sponge carrier for conductive magnetic brush development

Amendments to Equation 5 (see Equation 6) allow for the inclusion of the voltage across the carrier chain. It can be seen that if the Q/m is reduced the m/A is increased. This increase

in m/A resulted in a much deeper colour in solid area development as well as reducing the background.

$$\frac{m}{A} = \frac{\varepsilon_o(v_p - v_b)}{\frac{Q}{m}\left[\frac{t_p}{\kappa_p} + \frac{t_t}{\kappa_t} + \frac{(t_d - \delta)}{\kappa_d \nu}\right]}$$

Equation 6

where;

ε_0 = relative permittivity of the air

v_p = voltage on the surface of the photoreceptor

v_b = voltage on the magnetic carrier bead chains

Q/m = average charge on the toner

t_p = thickness of the photoconductive layer on the photoreceptor

κ_p = relative permittivity of the photoreceptor

t_t = thickness of the toner layer on the photoreceptor

κ_t = relative permittivity of the toner layer

t_d = thickness of the developer mix (i.e. the length of the bead chains)

κ_d = relative permittivity of the developer mix

$v = v_b/v_p$ or the potential difference between the brush and photoreceptor

3.6 Use of Electrophotography for Additive Manufacturing

A number of research institutes have also realised the potential of EP in an AM system. Figure 3:30 shows the previous and current research conducted from around the world. The research, while solely for the purpose of manufacturing, is based in a number of different sectors ranging from drug delivery to electronics to textiles.

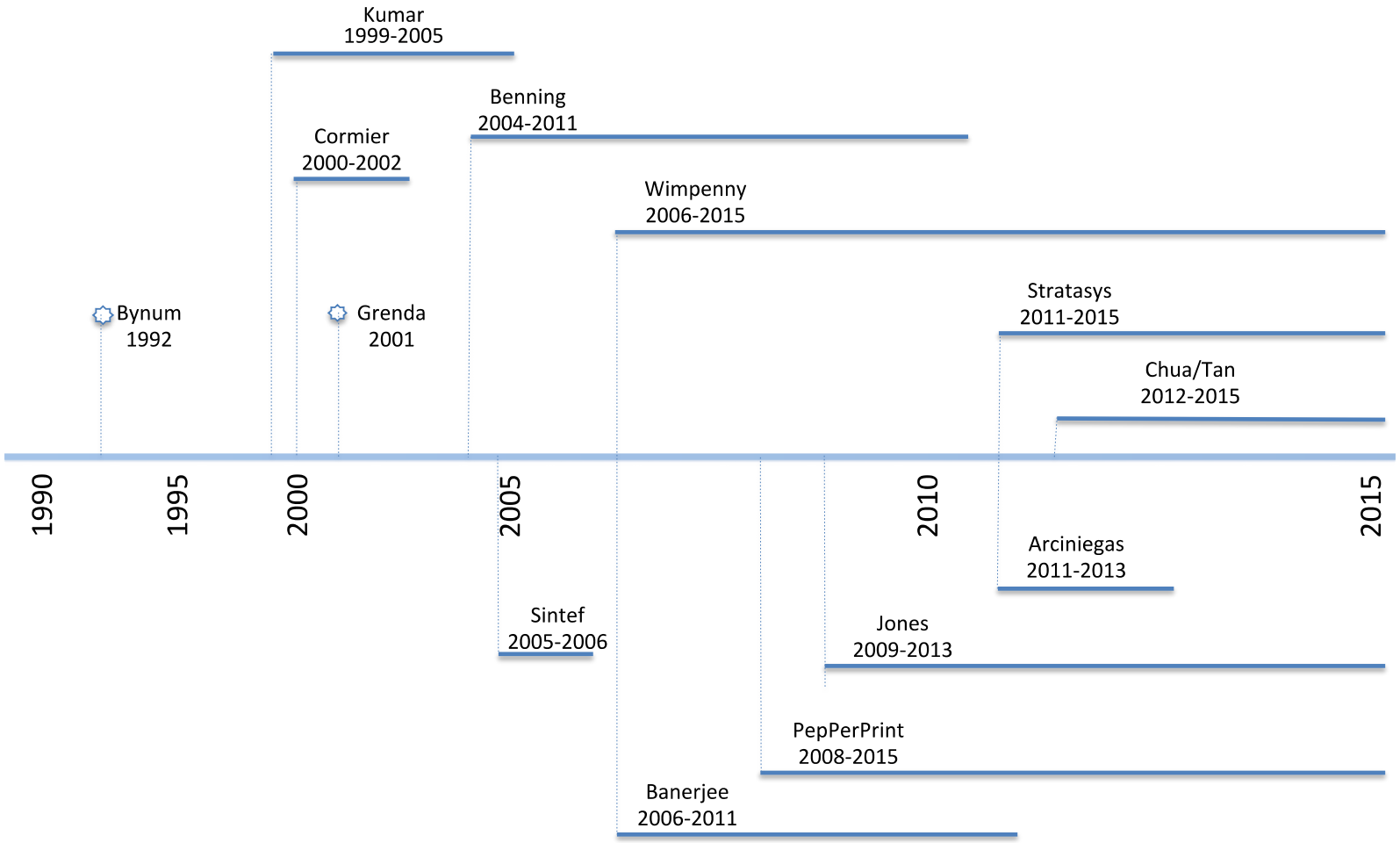

Figure 3:30: Research conducted in Additive Manufacturing using Electrophotography (after Jones)[5]

3.6.1 Automated manufacturing system using thin sections, Bynum (1999)

In 1992 Bynum was granted a patent entitled "*automated manufacturing system using thin sections*"[8]. It was the first time that electrophotography was proposed as a technology to be coupled with AM. The patent describes the use of a number of materials including metallic with alternative heating methods to compliment the toner, including solvent vapour and induction heat.

The method Bynum proposed was to print the material on to a transfer medium and to transfer it to the previous lamina (see Figure 3:31). A transfer belt (86) and a heat source (58) enabled the toner material to be brought up to the heat source and leave in a tackified (hot semi-molten) state. Bynum also proposed the transfer of the lamina to the stage lift (68) where it presses up against the back-up plate completing the adhesion to the previous laminate. The advantage of this proposed method lies in the ability to heat up the individual layer and deposit it with the use of pressure, loosely mimicking the process of injection moulding (heat and pressure). Bynum's patent has been at the core for researchers as a possible means of overcoming the electrostatic issues (discussed later in this thesis). However, Bynum does not appear to have undertaken any experimental work in this area and has not commercialised the proposed process.

Table 3:2: Bynum's abstract and primary from patent

Abstract
A method for automatically manufacturing objects directly from computer aided design, whereby the computer programming electronically sections the designed object into many thin planar sections, which are physically reproduced as lamina formed from sheet materials or powders by one of the embodiments of the invention. The thin planar this formed are bonded to the form a sandwich creating the object as designed.
Primary claim
A system for manufacturing three dimensional objects directly form design that comprises; a) means for receiving an electronic sectional data corresponding to an electronic representation of object to be manufactured. b) Means for exposing a charged electro-photographic element with an electromagnetic radiation pattern corresponding to the said electronic section to form an electrostatic latent image on said electrophotographic element. c) Means for applying a plurality of forming powders to said electrostatic latent image contained on said electrophotographic element to form a physical lamina. d) Means of transferring said physical lamina to an intermediate support. e) Means for causing said physical lamina to become tacky f) Means for transferring and bonding said physical lamina to previously formed lamina and building up a physical replication of said object in a step wise fashion whereby the three dimensional object is automatically formed from a composite of lamina.

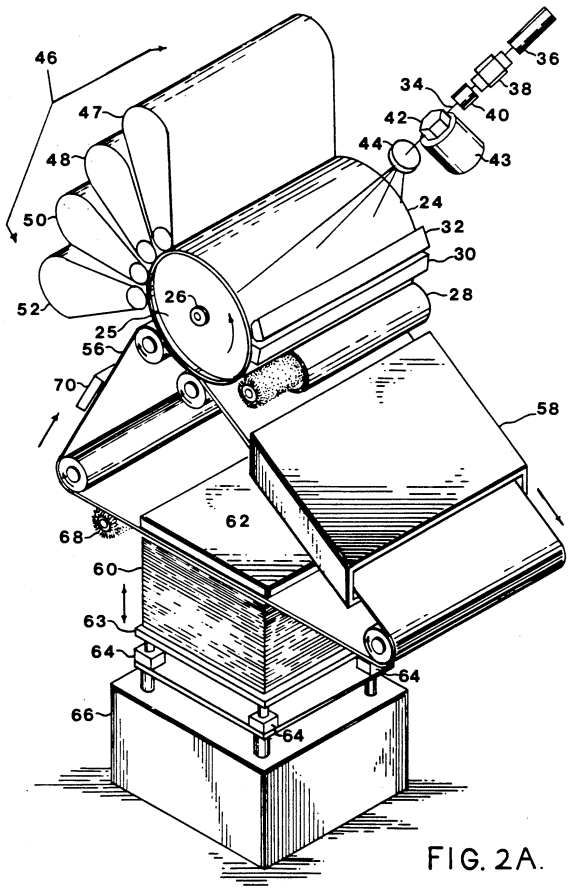

Figure 3:31: Bynum's method of manufacturing using EP[8]

3.6.2 Kumar, University of Florida (1999-2005)

Dr Ashok Kumar of Florida University, began investigating the use of electrophotography in Additive Manufacturing in 1998 after receiving a grant from the Office of Naval Research (Grant No: N00014-98-1-0694)[128]. Professor Kumar, the Principle Investigator, and his research team began work on developing the Electrophotographic Solid Freeform Fabrication (ESFF)/ Electrophotographic Rapid Prototyping (ERP) processes.

Kumar commissioned a test rig to be built which consists of a UV laser image projector, a 600dpi Canon electrophotography engine, a two-axis build platform, a compaction plate and a radiant heater, all mounted on an aluminium structural frame. In addition, the system has a digital motion controller and power supplies that drive the servomotors controlling the motion of the platform [10].

The ERP process is designed for magnetic powder (~ 5μm), ideal for single component print engines. The development roller is a metallic hollow cylinder rotating around a fixed magnetic core. Since the powder is magnetic, it adheres to the surface of the roller by magnetic force, with the doctor blade regulating the layer density. The build platform is supported on springs that are mounted on the Z-axis base plate, which is moved up against the compaction plate until the springs compress by the desired amount, detected by a proximity sensor mounted on the Z-axis (see Figure 3:32).

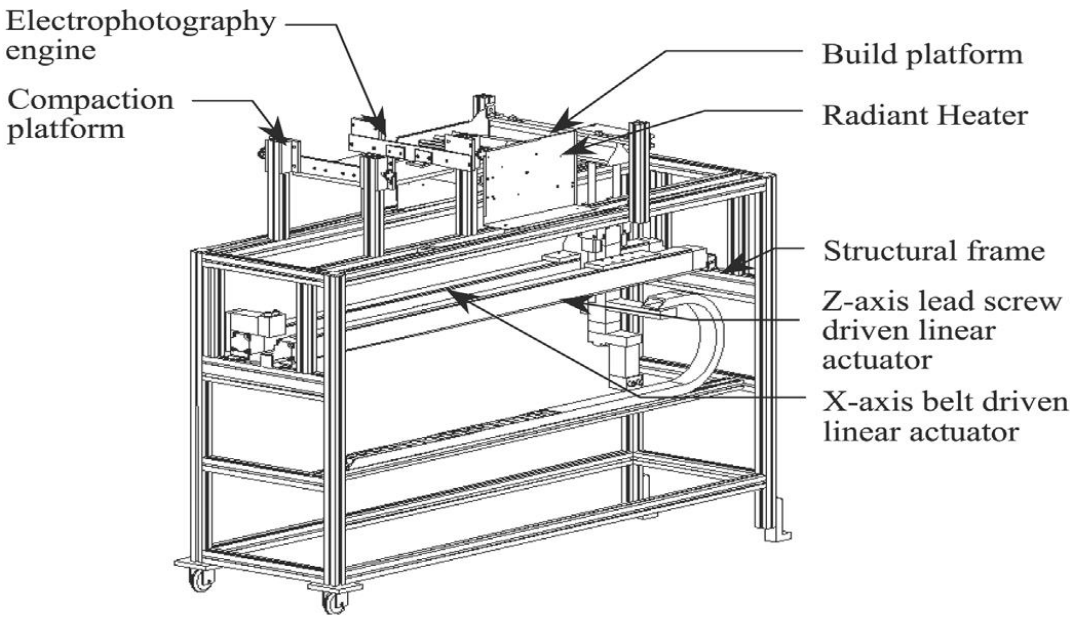

Figure 3:32: Electrophotographic Solid Freeform Fabrication rig [11]

As each layer is deposited, the amount of toner that is transferred on to the previous layer is reduced dramatically [11, 49, 129]. Using Gauss' law, Kumar *et al*. were able to model the field characteristic as shown in Figure 3:33. It can be seen as the layer increases in thickness the electrostatic field strength exhibits an exponential decay.

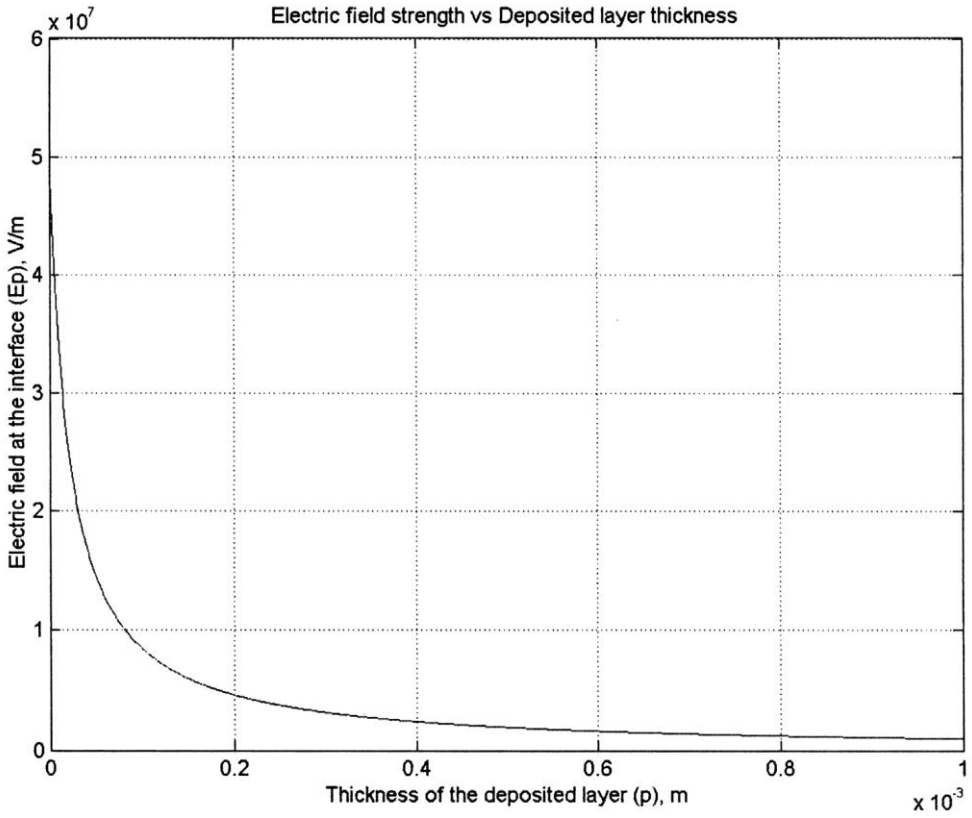

Figure 3:33: Electric field strength as a function of deposition [49]

In order to overcome this issue Kumar compensated for the decline in field strength by applying a 1kV DC voltage on the build platform. The application of a field on the build platform encourages the toner to be drawn to the field as per conventional toner transfer in standard printers. This method increased the efficiency of the deposition enabling the part height to increase for the first 20 – 30 layers although the deposition efficiency decreased thereafter[130]. At approximately 40 – 45 prints there is negligible toner deposition [10]. Kumar concluded that the efficiency drop in toner deposition is attributed to the highly resistive nature of the styrene rich polymer matrix. Further experiments were conducted attempting to apply a charge to the top layer of the deposited material. During the actual printing process the photoconductor comes in contact with the charging roller, as a result the photoconductor would obtain a +ve charge. When the photoconductor is

moved to the charging station, where it is uniformly charged –ve, this would result in neutralising the residual charge imparted from the charge roller. The neutralisation thus encourages the toner to stick to both the discharged regions and part of the neutral charge regions. This approach resulted in significant contamination of the printed “image” due to “background” transfer to the build platform.

Another method of part production investigated by Kumar was the use of a toner as a binder that is selectively printed onto a layer of ceramic powder, which is then fused by heating. To avoid the risk of contamination from the ceramic an intermediate transfer roller was employed. An alumina ceramic (part) powder was spread across the bed and compacted to increase the cohesion and reduce the risk of contamination of the printer (reverse printing). A polystyrene binder toner was printed onto the alumina bed. Figure 3:34 show a printed image – which although demonstrated proof of principle also highlights the issues associated with this approach (there is clear evidence of reverse printing).

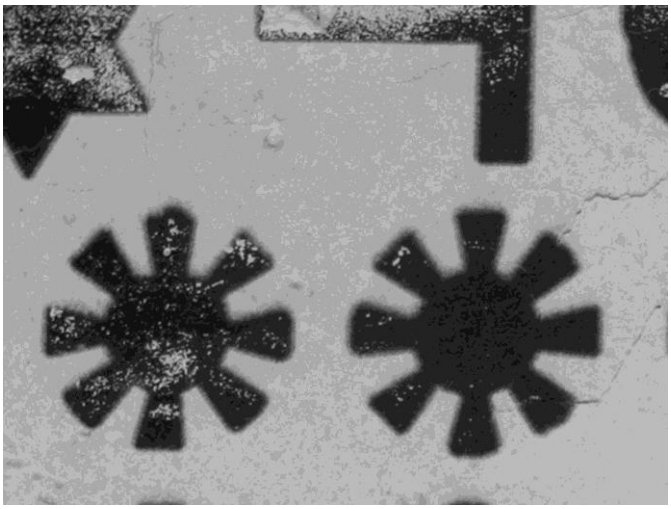

Figure 3:34: Parts printed on an alumina bed with a polystyrene binder toner[11]

Kumar identified a number of issues with printing a binder. Firstly, the issue of reverse printing, whereby the unbonded part material is picked up by the photoconductor. Secondly, Kumar identified the viscosity of the binder toner as an issue. If the binder is too viscous during the fusing stage, there is the potential for the binder not to penetrate deep enough to bond to the previous layer.

Kumar concluded that while the process of printing binder, compared to conventional binder jetting, has potential there are significant issues to be resolved. Moreover, the use of a transfer roller to prevent direct contact of the binder and photoconductor, thus reducing the potential for damage, this approach cannot totally eliminate reverse printing. Kumar concluded that direct printing of the part material would be more advantageous than printing just a binder.

Kumar had one final attempt at printing with the ERP rig using a toner comprising of a sub-micron silicon carbide ceramic core (SiC) with a polymeric shell [131]. The polymers trialled were polystyrene (PS), polybutadiene (PB) and LP1. The polymer is heated with a solvent until dissolved. A CCA is added to the dissolved solution to impart the desired charge [131].

Kumar carried out a number of trials on deposition using an electrode to transfer the toner. It was concluded from the trials that LP1 and PS, with the optimised solid loading and CCA quantities, would be better suited to making liquid toners with a favourable optical densities. Polybutadiene was dismissed due to the poor transfer efficiency

3.6.3 Cormier, North Carolina State University (2000-2002)

Professor Dennis Cormier while at North Carolina State University along with his students explored the use of EP for the production of polymer parts. The process utilised a HP LaserJet 4500 colour printer whereby colour build and support materials could be printed simultaneously[2, 132]. The fusing process employs a fusing plate where heat and pressure, similar to Bynum's approach, is employed. Interestingly, Cormier's patent was rejected on the basis of the close similarity to Bynum's patents [4].

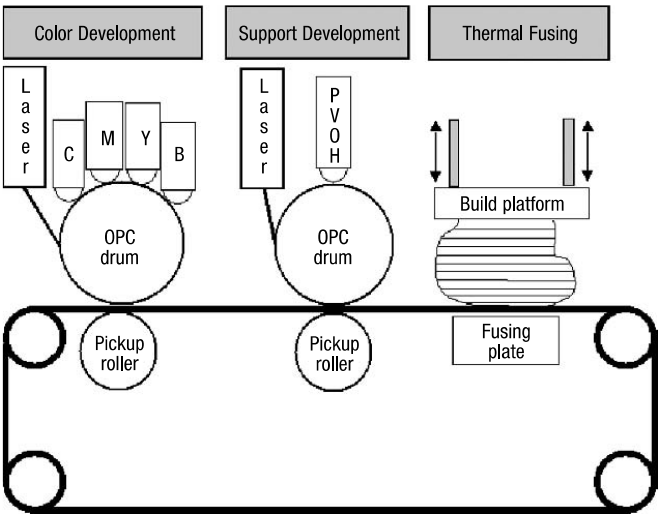

Figure 3:35: Cormier's approach to colour 3D printing via EP[132]

Cormier looked at printing conventional toners as well as high density polyethylene (HDPE) powders with varying colours. In addition to colour experimentation, Cormier also pursued support development, in particular, soluble toners. Cormier printed a varying coloured bulls eye using HDPE as shown in Figure 3:36 [2] This was the first time a coloured part had been printed using EP even thought it had been mooted several years earlier [8, 9].

Figure 3:36: Coloured part produced using HPDE[2]

In addition to build materials, Cormier has discussed the possibility of printing PVOH (Polyvinyl Alcohol) support material. Cormier was well versed in EP, he recognised the difficulties of obtaining a toner in the correct size and shape and also noted the problem of conventional transfer of toners. It is possibly for this reason that he opted for a mechanical transfer method, as opposed to an electrostatic transfer, in his trials.

3.6.4 Apparatus of fabricating 3 Dimensional objects be means of electrophotography, ionography or a similar process, Grenda (2001)

Grenda's research follows on from the patent of Bynum, where Grenda defines a key element of his claim although this is believed to be licensed [5, 8, 9]. Grenda's patent uses heat and pressure to make the printed material "substantially tacky" to enable transfer. The transfer belt positions the printed layer under a heat source (22) to be made tacky. Grenda has also noted methods using solvents, radiation as methods of tackifying the printed layer. Pressure is applied by means of solenoids (31) lifting the part bed (33) against a backup plate (32) thus transferring the tackified layer to the platform. The key difference between the work of Grenda and Bynum lies in the fact that Grenda explicitly details electrophotography as a means of part production.

Table 3:3: Abstract and primary claim from Grenda's patent

Abstract	Primary claim
Freeform fabrication apparatus for rapid prototyping. In one embodiment, the apparatus incudes ion-generating equipment for sequentially creating latent ion images of layers of an object to be fabricated. Developing apparatus is provided for adhering at least one object building substance to the sequential latent ion image to create a series of lamina. Thereafter, the series of lamina are assembled to fabricate the object.	A freeform fabrication apparatus comprising; Ion-generating apparatus for sequentially creating latent ion images of layers of an object to be fabricated; developing apparatus for adhering at least one object building substance to the sequential latent ion images to crease a series of lamina; and apparatus for assembling the series of lamina to fabricate the object.

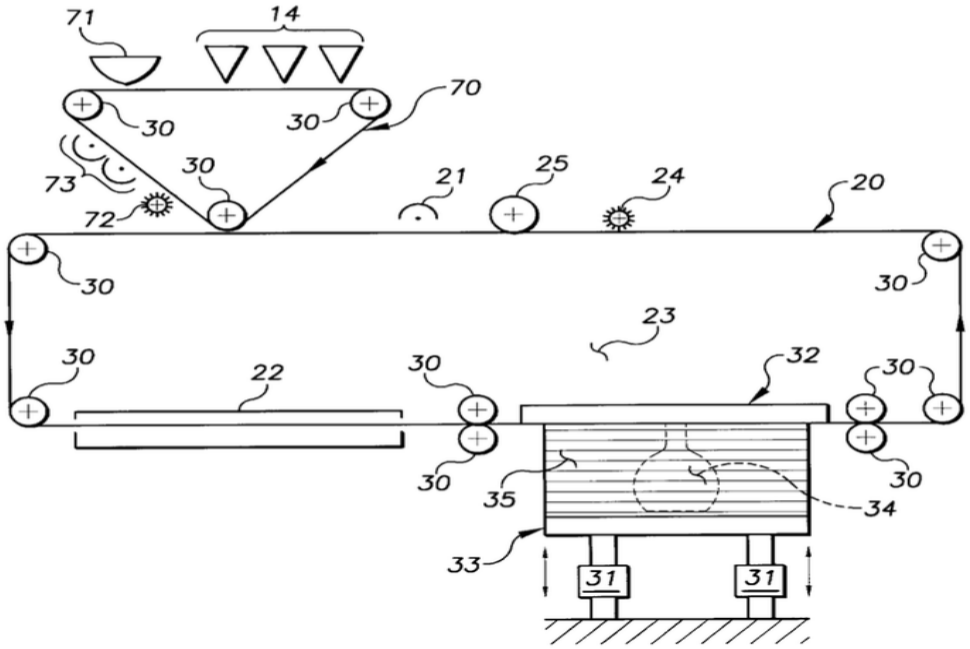

Figure 3:37: Grenda's proposed method of using laser printing technology for AM

3.6.5 Selective Mask Sintering (SMS), Sintermask GmBH (2003-2009)

Sintermask GmBH (formally Speed Part AB, Sweden) has produced a system indirectly based on EP [16, 133]. The Selective Mask Sintering (SMS) process involves using a mask printed by EP. The mask is used to control the fusing of a thermoplastic powder bed by selectively blocking out the radiation from a radiant IR heater unit so that only the portions of the part are fused (see Figure 3:38).

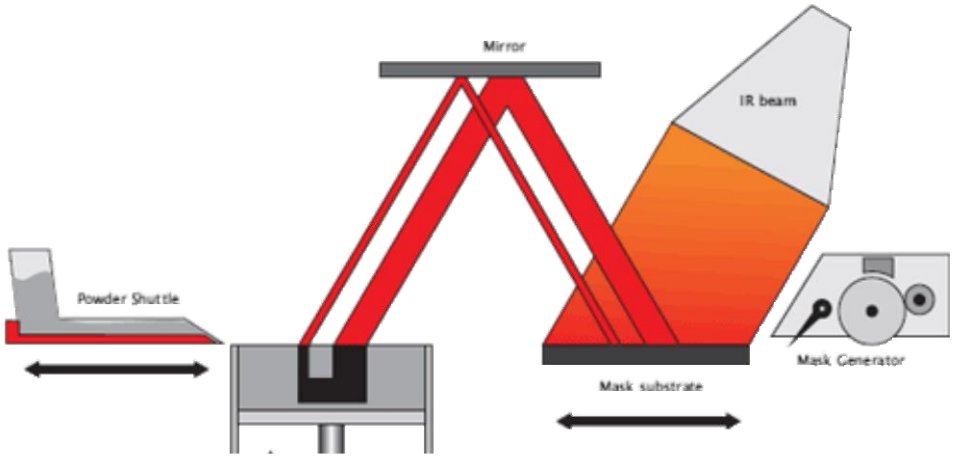

Figure 3:38: Selective Mask Sintering process [134]

A ceramic toner material was developed to act as a mask to prevent the toner from fusing on to the mask substrate (see Figure 2-37). Using an IR radiant heater lamp rather than a laser provides a lower cost heat source, which is able to process the entire layer simultaneously, resulting in relatively high deposition. Moreover, the high deposition speed of 20-30mm/ hour is independent of the part geometry and number of parts being build.

The SMS system (Pollux 32) has a resolution of between 50µm-120µm and a build area measuring 210x300x500mm[16, 19]. A drawback of this system is the availability of suitable

materials, with only polyamide (nylon) materials being offered. However, it has been suggested that other high temperature thermoplastics such as Polyethylene terephthalate (PET) and Polyetheretherketone (PEEK) could be processed [134].

3.6.6 Professor Dalgarno & Dr Benning, Newcastle University (2005-2011)

Matthew Benning undertook his PhD to develop an AM machine based on EP under the guidance of Professor Dalgarno at Newcastle University. Though a PhD has been completed there is very little information in the public domain on their process. [135]. The status of his PhD is still under restriction.

3.6.7 Metal Printing Process (MPP), Sintef (2006-2006)

The Metal Printing Process (MPP) was developed by SINTEF based in Norway. The technique employs ionography and xerography to build solid metal objects by depositing layers (typically 100µm thick) [110]–[112]. A patent for the Metal Printing Process was filed in 2004[136].

The MPP uses a scorotron to induce a charge to the photoreceptor. The photoreceptor is exposed using an LED print head creating a latent electrostatic image of the part slice. The photoreceptor is passed over the powder reservoir where the latent image is turned into a real image by means of electrostatic attraction. The real image is in turn transferred from the photoconductor onto the die by ionography, where it is heated to 900˚C with pressures of 200MPa. The process is depicted in the figure below (Figure 3:39).

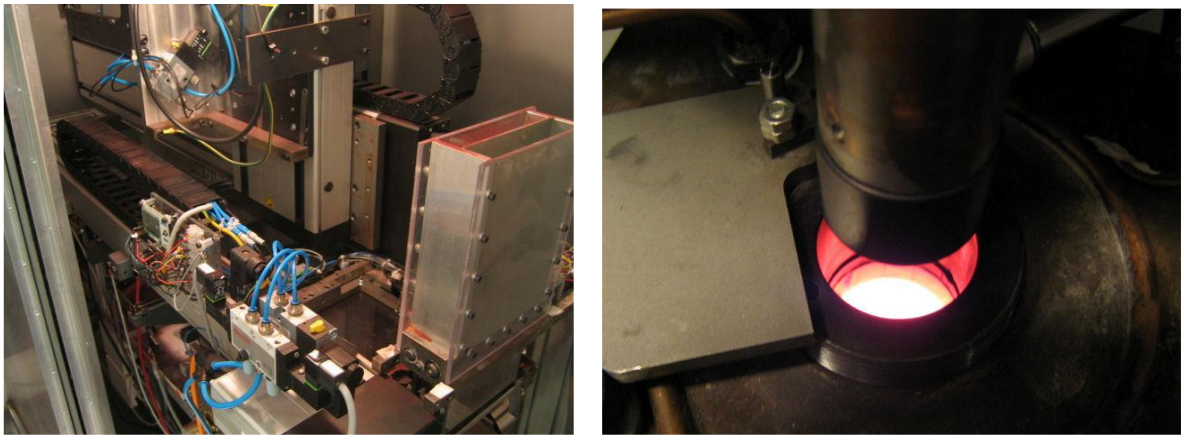

Figure 3:39: MPP test rig (left) with sintering and fusing station (right) [13]

Table 3:4: Sintef's abstract and primary from patent for the Metal Printing Process [136]

Abstract
Method and apparatus for rapid manufacturing of metal, ceramic and metal-ceramic products from building powder(s) of the relevant materials, comprising: I) at least one powder receptor (1), ii) at least one charging element (2) arranged to charge powder receptor (1), iii) at least one light source (3) arranged to illuminate powder receptor (1) with a product-adapted pattern, iv) at least one powder magazine (4) arranged to supply powder to powder receptor (1), v) at least one charging element (6) arranged to facilitate transferral of powder from powder receptor (1) to a transporting device (13), vi) a transportation device (13) arranged to receive powder (10) in a predetermined pattern from powder receptor (1) and to transport said powder to a sintering die, vii) a sintering die (18-21) arranged to receive powder layer from transporting device (13), envelope the powder layer in contact with the product being built and raise pressure and temperature in layer (17) so that the powder sinters and becomes part of the product being built.
Primary claim
Method and apparatus for rapid manufacturing of metal, ceramic and metal-ceramic products from building powder(s) of the relevant materials, comprising: I) at least one powder receptor (1), ii) at least one charging element (2) arranged to charge powder receptor (1), iii) at least one light source (3) arranged to illuminate powder receptor (1) with a product-adapted pattern, iv) at least one powder magazine (4) arranged to supply powder to powder receptor (1), v) at least one charging element (6) arranged to facilitate transferral of powder from powder receptor (1) to a transporting device (13), vi) a transportation device (13) arranged to receive powder (10) in a predetermined pattern from powder receptor (1) and to transport said powder to a sintering die, vii) a sintering die (18-21) arranged to receive powder layer from transporting device (13), envelope the powder layer in contact with the product being built and raise pressure and temperature in layer (17) so that the powder sinters and becomes part of the product being built

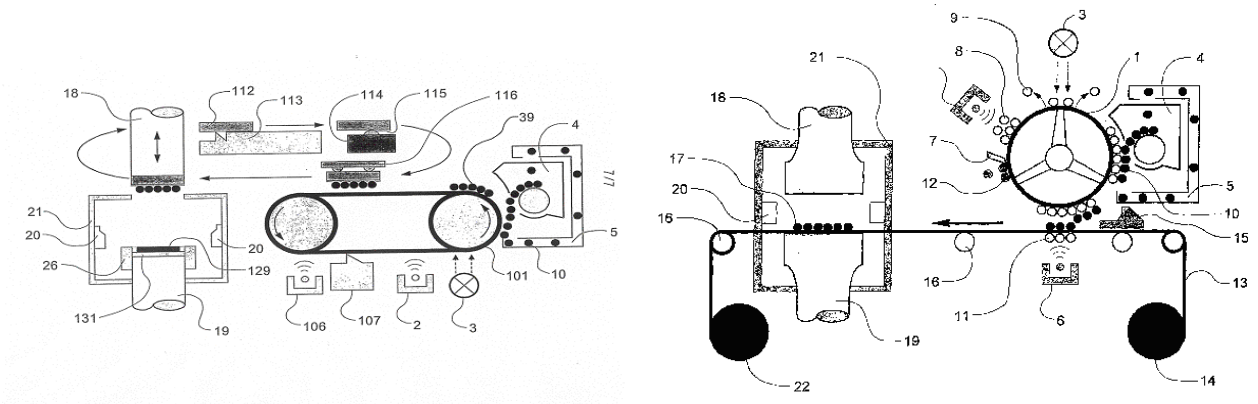

Figure 3:40: Schematics from patent application

In the MPP the metallic powder is consolidated in a furnace, above the solid state sintering temperature, to initiate immediate fusing of the particles of the build material to form the layer and also fusing of the layer being formed to the preceding layer. To form complex parts with overhanging features the MPP process requires a build and support material. To enable the build and support to be separated from one another at the end of the process one solution is to employ a build material with a lower sintering temperature than the support material. The support material remains a loose powder that can be removed at the end of the process. The researchers at Sintef explored the use of alumina powder as a support material. However, the use of non-conductive powders for a support material proved to be a significant challenge. Unlike metallic powders, which can be charged in situ, the ceramic support material is non-conductive and thus requires the use of a carrier to tribocharge with the ceramic powder. Additionally, a photoconductor is required to transfer the support material from the photoconductor to the punch, where it adheres to the inverse of the build image, forming a support.

Bovie *et al.* also explored the possibilities of functionally graded metals. Multi material deposition had been explored with iron and copper, with the copper incrementally increasing its presence as depicted in Figure 3:41.

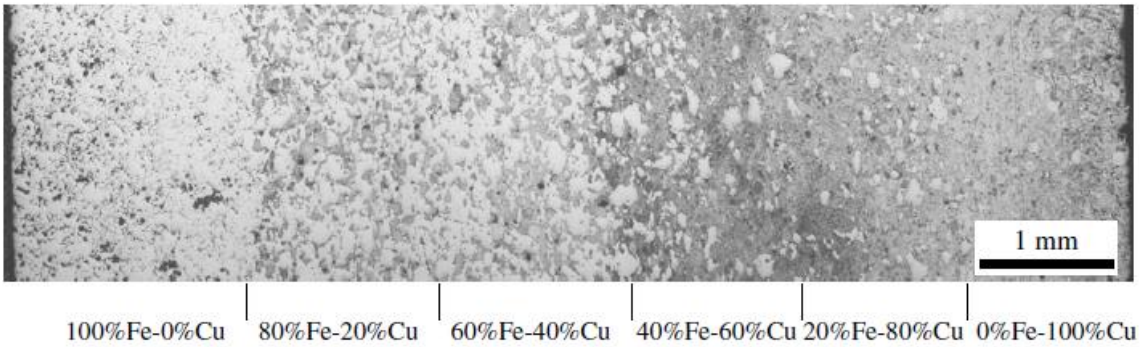

Figure 3:41: material deposition of Cu & Fe with varying alloy compositions

MPP opens up the possibility of producing alloying materials for the benefit of being able to produce functionally graded parts. However, the protracted build time for parts (several hours) results in grain growth thus reducing the mechanical properties of the part formed. In addition, the elevated temperature adds more stress to the consolidation process. Moreover, the extremely high temperatures and pressures could result in damage to the punch-efforts to resolve the issue resulted in the use of cemented carbide.

The Metal Printing Process is the only process to have explored metals and functionally graded materials for the purpose of part production. Unfortunately, due to funding issues the project was not able to progress.

3.6.8 Prof. Wimpenny & Mr Banerjee, De Montfort University (2006- 2015)

Wimpenny began to explore AM using EP by using a mono component development system but later migrated to a dual component development system[94]. The work undertaken encompassed not only the use of alternative toners for part manufacturing, but also explored support materials too[3].

PhD candidate, Soumya Banerjee, under the guidance of Professor Wimpenny, carried out the work as part of his scoping trials. Banerjee worked on a number of different areas concentrating on toner reduction, printability of the toners on a number of printers and mechanical assessment of the materials.

The extent of the research carried out by Banerjee and the results of his work are described in sections 3.6.8.1 – 3.6.8.3 and 3.6.8.5 – 3.6.8.7 This encompasses the initial scoping trials performed as well as the main trials conducted.

Banerjee's approach was initially to replicate the use of single component printer with an insulative toner, as undertaken by Cormier[2, 132]. The use of an obsolete HP LaserJet5 printer enabled printing of toner with large particle sizes due to the age of the printer.

3.6.8.1 HP Laser Jet 4 (HP-LJ4)

Trials commenced on non-magnetic single component development systems building on the work of Cormier. HDPE (FARD 3718), with a D50 of 12µm, was coated with a fumed silica flow control agent (1% by weight). The FCA was used to reduce the compaction and caking effect occurring with the HDPE powder. Fumed silica also imparts a –ve charge to the toner surface. Upon printing, it was found that the developer was not coated as would be expected from a conventional toner due to inefficient tribocharging. Furthermore, there were significant levels of toner leakage, which, over time, could damage the OPC. The HP-LJ4 is a magnetic development systems which is unsuited to the HDPE toner used in the trial [58].

3.6.8.2 Lexmark C570

Non-magnetic print engines from a Lexmark C510 printer were used to print HDPE toner with 12µm (D50) particle size[94, 137]. Banerjee began work on the Lexmark printer to see whether there was a reduction in leakage and an improvement to the charging abilities as the printer is more suited to the non-magnetic HDPE toner. A rig was built around the Lexmark C510 printer to enable a paper substrate attached to a rigid platform to be moved beneath the printer, on to which multiple layers could be applied. These layers were fused using a radiant infrared heater.

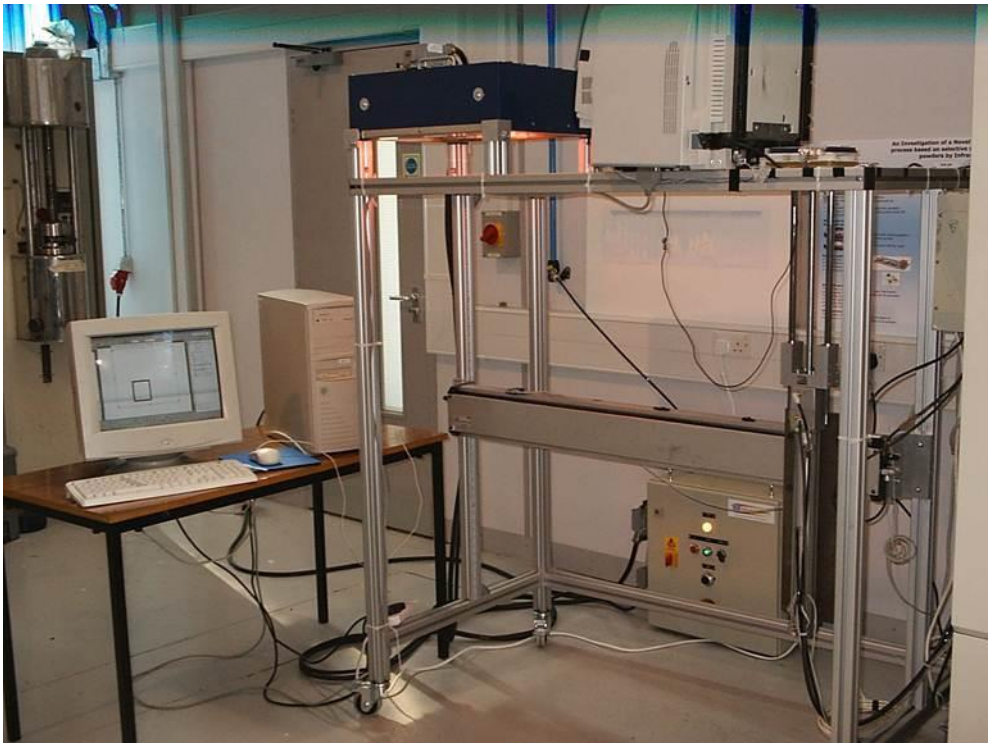

Figure 3:42: Custom built rig utilising a Lexmark C510 printer

A HDPE (FARD 3718) was coated with a FCA and also a CCA to impart a charge more favourable to the printing process. The toner was surface coated with fumed silica to resolve the issue of flow control and compaction. Varying percentages of fumed silica were used to coat the HDPE particles[4].

Table 3:5: Printing results for surface coated FARD 3718 HDPE

FARD 3718 – HDPE - 12 μm				
Sample No	**Fumed silica HDK20Tx (% by weight)**	**Conductive Agent ECTT-1 (% by weight)**	**Conductive Agent Tronox CR880 (% by weight)**	**Results**
1	0	0	0	Very thin coating on roller+ small marks on roller
2	2	0	0	Thin coating on roller+ small marks on roller
3	0.3	4	0	Thin coating on roller +small marks on roller
4	0.3	2	0	Thin coating on roller+ small marks on roller
5	0.4	1.2	0	Reasonable coating on roller +small marks on roller
6	0.4	0	1.5	Better layer and similar to sample #5

It was found that the ability to print the toner was highly reliant on the combination of FCA and CCA used. Initially it was found that negligible toner was transferred but by altering the level of FCA and CCA it was found that with 0.4% by weight of Fumed silica and 1.5% by weight of a conductive agent gave acceptable print quality (Table 3:5)

Banerjee decided to move from a toner with particles with 12µm to 8µm (D50) to enable better coating on the developer coating. The HDPE particles were coated with a CCA to enhance the conductivity of the HDPE particles and FCAs to improve fluidity. Table 3:6 summarises the results of these trials.

Table 3:6: Formulation table for control agents

FARD 3712 – HDPE - 8 µm				
Sample No	**Fumed silica HDK20Tx (% by weight)**	**Conductive agent Tronox-CR880 (% by weight)**	**Conductive agent SW- 340 (% by weight)**	**Results**
1	0.4	1.5	-	Very thin coating on developing roller
2	1.5	-	2	Better layer than sample 7
3	3	-	1	Better layer than sample 8
4	3	-	2	Best Layer

Banerjee found that by increasing the flow control agent to 3% by weight and adding a 2% by weight conductive agent, a suitable coating could be developed which was able to yield a good transfer on to the paper substrate.

Once the optimised surface coating parameters were obtained, multiple prints were taken using the Lexmark C510 printer. Tensile test images to BS ISO 37:2005 were printed to test the mechanical properties. The fuser unit was removed and 100 layers were printed and fused using an infrared heat source. However, issues with registration due to the manual process were present. The final printed part had a height of 0.5mm with an improved mechanical strength over standard toner[58].

3.6.8.3 Toner transfer methods

Wimpenny and Banerjee began transfer in a similar fashion to previous researchers, using conventional transfer (toner is attracted off the final transfer roller onto the substrate using an opposite, attractive charge). However, it was observed that the thickness of the printed layers decreases as more layers are deposited. This effect became particularly noticeable after 50 layers. This problem was also experienced by Kumar and Jones [5, 11, 49]. It was hypothesised that repulsion (where the charge on the final transfer roller is reversed at the

point where transfer is required to “throw” the toner onto the substrate) could overcome the height limitation.

Banerjee printed a number of layers, plotting the accumulated weight of toner deposited after each layer was deposited. It can be seen from Figure 3:43 that a near linear deposition rate is deposited as compared to conventional transfer. Based on these results, Wimpenny and Banerjee filed for a patent (WO 2008096105). However, subsequent trials demonstrated that repulsion only delays the detrimental effect of charge accumulation and so a more conventional tackifying approach was adopted for future trials.

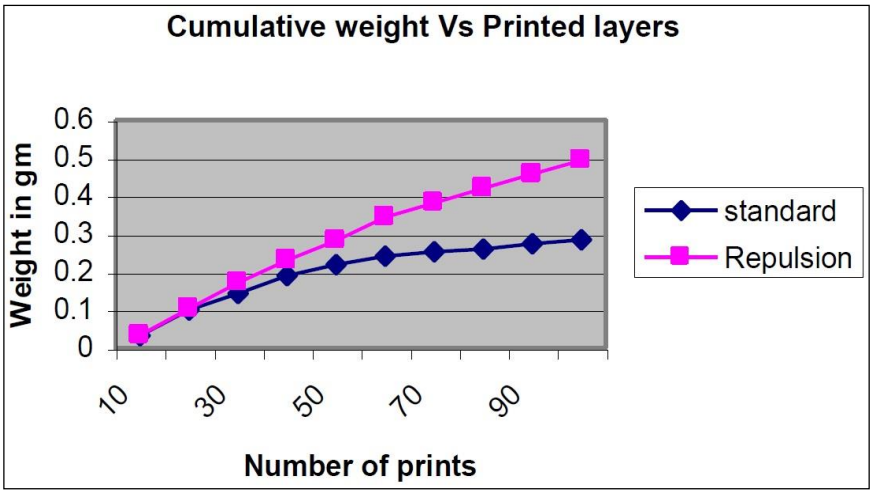

Figure 3:43: Cumulative weight Vs printed layers for standard transfer and repulsion[4]

3.6.8.4 CTG printer

Initially Wimpenny & Banerjee explored single component toners, however, they soon realised that dual component systems have more potential for industrial Additive

Manufacturing due to their inherent flexibility. Using dual component systems the carrier does a lot of the work allowing simpler polymer formulations to be used as toner.

Trials were conducted at CTG PrintTEC GmbH, Alsdorf, Germany who have developed a flexible dual component printer (CTG 900) to deposit conductive toners on the glass substrates for de-icing of automotive glazing and for depositing ceramic toners to provide decorative patterns onto ceramic tiles.

Initial trials were performed on an Electromagentic Brush Development (EMB) system. EMB, while employing electrostatic transfer, does not have a photoconductor to control the deposited area. CTG developed the EMB system to evaluate toner compositions and also as a potential coating method.

CTG demonstrated the potential of the EMB system using a thermosetting epoxy toner. The unit was modified slightly to enable fine adjustment to the height during layer build up and a part was created using the following procedure;

- A tile was heated above 150˚C and mounted on platform and allowed to cool to exactly 150˚C.
- The tile passed under final the transfer roller of EMB and the toner transferred off the transfer roller through **tackification** and **pressure**.
- The tile was placed back in the oven and heated to between 160-180˚C with the freshly deposited layer to promote cross-linking of the epoxy toner.
- The platform is lowered at five layer increments to accommodate for part growth in Z direction.
- The process is repeated until the part is produced.

The procedure detailed had enabled a part to be printed which exceeded the theoretical maximum part height modelled by Kumar [49]. To produce each layer was a lengthy process taking between 10-15 mins [5, 12]. In addition to this there was considerable physical manipulation of the part where curling would occur at the edges. Despite this, part achieved a final height in excess of 8mm (Figure 3:44).

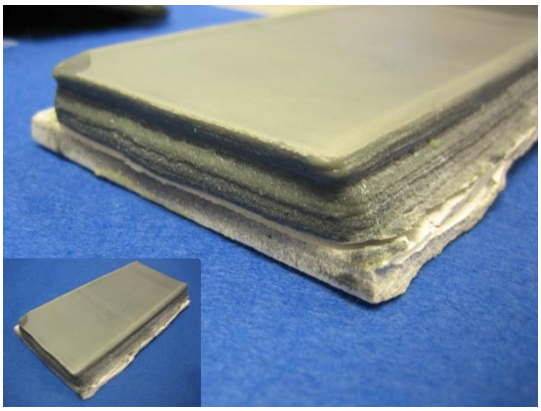

Figure 3:44: Epoxy sample produced using EMB process

Having demonstrated the potential of the EMB process Wimpenny pursued the development of a fully-fledged laser printer with an OPC (adapted CTG 900 printer) to produce parts with specific geometries – this was the Selective Laser Printer (SLP 1 rig see experimental section 3.6.8.8).

A ziggurat shape was designed as a demonstration piece. Pairing a suitable carrier with the toner, a charge of -2.83fC/10µm was achieved using a Q/d charge meter from Epping (Epping GmbH, Germany). A flat ceramic tile was used as a substrate.

Five layers were printed at a time using the CTG 900 dual component printer in a semi-automated process. The layers were consolidated by placing the substrate with the unfused layers in a convection oven for five minutes with the temperature set between 155-160˚C[5,

12]. The process was repeated at a rate of five layers at a time until a part height of >3mm was achieved as depicted in Figure 3:45. It was the results of this trial that the motion to move to a fully automated process was explored.

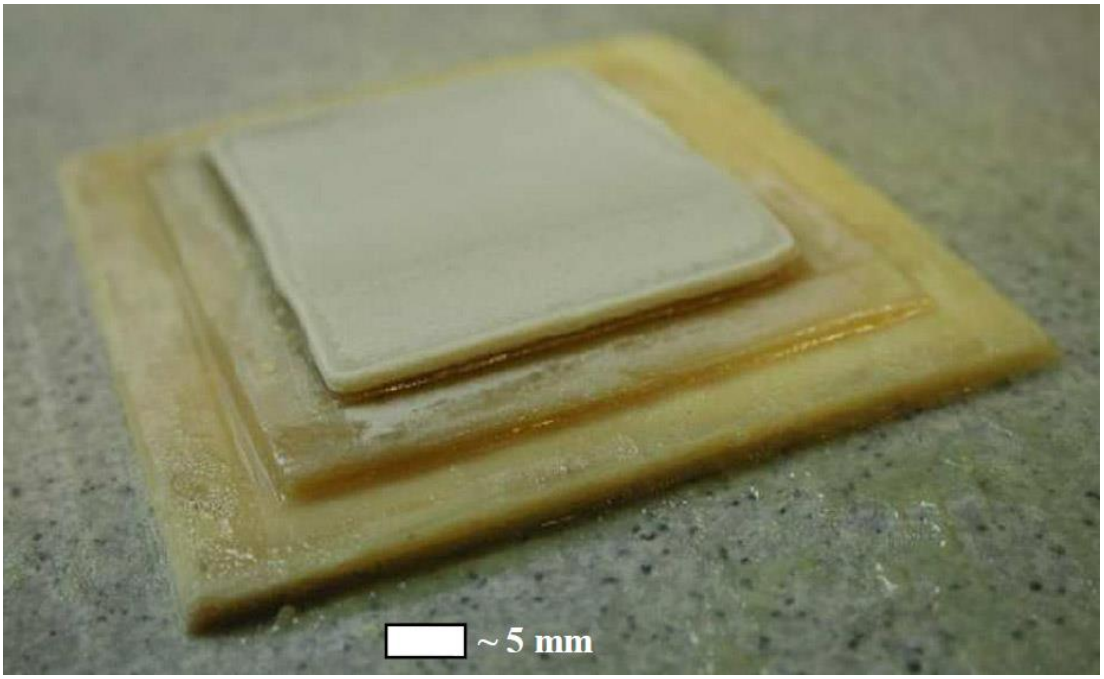

Figure 3:45: Ziggurat shape printed on SLP rig[4, 12]

3.6.8.5 Comminution and toner conversion of tough engineering polymers

Contrary to previous research, Wimpenny & Banerjee opted for tough engineering polymers, investigating HDPE, LDPE, Polystyrene and Nylon. However, later they focused the trials on Somos 201, a thermoplastic elastomer (TPE)[4, 58, 94, 137]. Somos 201, is a proprietary polymer powder which was developed by DSM for use in Selective Laser Sintering machines.

In early trials Banerjee explored a wide range of particle reduction methods. The bulk of the comminution trials were carried out using Somos powder as described in Banerjee's doctoral thesis[58]. However, many of the conference papers produced were focusing on the feasibility of tough engineering polymers such as Nylon, HDPE and PS[3, 4, 12, 58, 94, 137]. The materials sourced were off-the-shelf materials as the size required was readily available.

The decision for Wimpenny *et al*. to change to Somos was due to the inherent difficulty in managing the surface charge as well as recovery of material. Somos has dielectric and resistive properties similar to that of a standard toner[58]. The Q/d results from the scoping trials indicate that Somos is naturally more –ve than the HDPE. Moreover, Somos has a tighter charge distribution than HDPE.

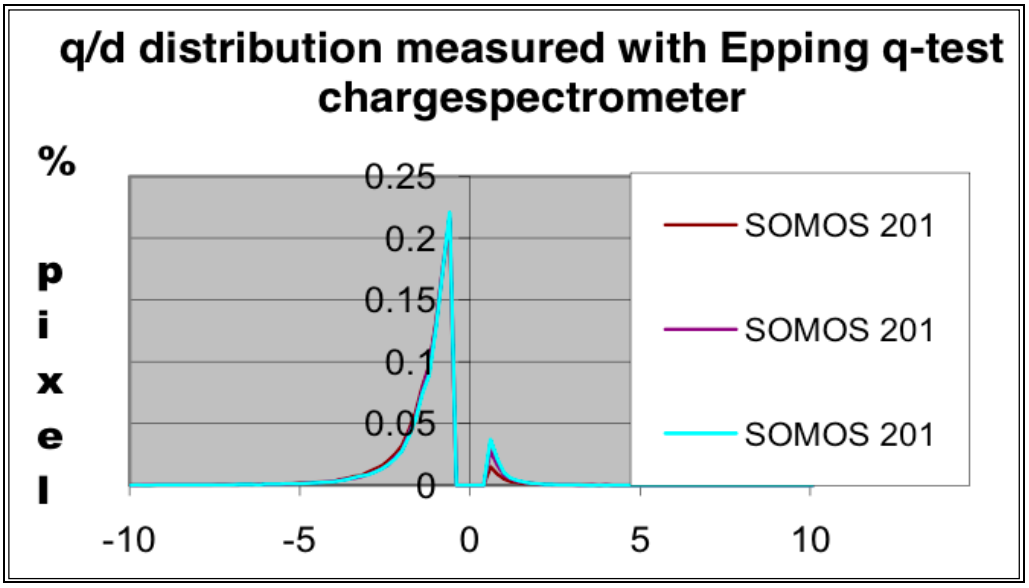

Figure 3:46: Q/d results for Somos 201[58]

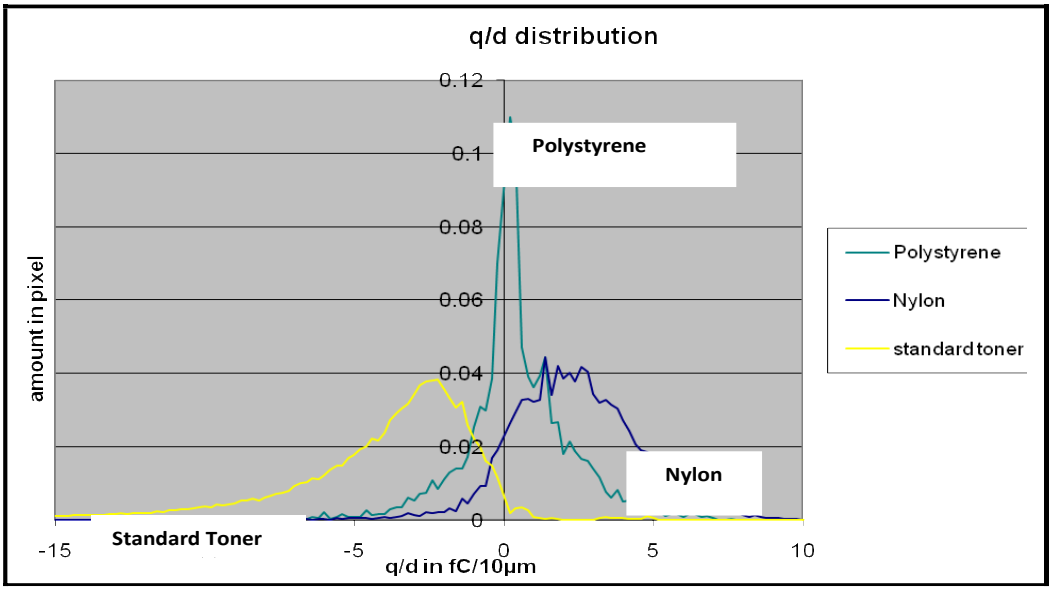

Figure 3:47: Q/m results depicting charge polarity for PS, HDPE and Nylon[58]

In order to utilise the TPE, the material (which has a D_{50} of 93µm) required sieving to recover the target material of 30µm[4].

Grinding trials were conducted in order to reduce the size of the particles to a desirable size. A planetary ball mill was initially tested but had very little effect. Further partial reduction trials were carried out on an impact mill with cryogenics. It was concluded that the efficiency was so poor that continuation was not a viable approach for this material. A fluidised jet mill with a forced vortex was eventually used to simultaneously mill and classify the material. However, it was found that only 15% of the original feedstock was reduced below 30µm. [58].

The poor results left Wimpenny & Banerjee with little option but to classify the original feedstock material. A classifier was used to collect as much of the fines produced by the attrition process. The samples were recovered with particle sizes of (D_{50}) 17, 30, 45, 60, and 100µm.

3.6.8.6 Custom-Fit

The EU FP6 funded Custom Fit project was focused on the production of customised products, individually tailored to suit the anatomy of a user. Two applications investigated were a customised motorcycle seat and motorcycle helmet – with the aim of enhancing comfort and safety. For both of these applications a flexible "rubber like" material was required. The Additive Manufacturing Research team at De Montfort University, led by David Wimpenny, explored the use of Somos 201 to produce helmet and seat components using a lattice design [138].

The Somos powder was sieved to a D_{50} of 32µm and coated with a 0.5% by weight of fumed to impart the correct charge and flow properties. A suitable carrier was paired with the Somos toner. Using an Epping Q/d meter a reading of -1.3fC/10µm to -2.6fC/10µm was measured.

Tensile test specimens were produced and printed on the SLP rig to assess the mechanical properties. A glass substrate was preheated to ~150˚C by the IR heater. When the glass reached 150˚C a print command was given. The glass substrate ran under the IR heater and passed to the printer once the temperature recorded between 130-115˚C. The large deviation in temperature is due to the manual operation of the rig. An automated process can control the temperature to between 120-115˚C[5, 12, 58].

The platform then moves to the printer where the velocity of the platform is precisely matched to that of the circumferential speed of the transfer roller to ensure that the correct image size and registration is maintained. At this point, the hot glass substrate accepts the developed image (~15µm thick) from the transfer roller using Baynum's heat and pressure approach.

The platform passes under the laser height measurement system where a digital read out is taken to determine height growth per layer. The platform is lowered by several millimetres to avoid colliding with the transfer roller on its return back to the start of the printing cycle. The platform arrives at the start position where it is raised to the correct position for printing of the next layer.

3.6.8.7 Infrared and oven sintering trials

Banerjee's main trials for his PhD study were not conducted on printed samples but on Somos powders fused in moulds to enable the fusing characteristics of the material to be observed. Tensile test samples were produced by compacting uncoated and coated toner in a mould designed to produce tensile bars to BS ISO 37: 2005. Stand-off distances (128, 178 and 228mm) and fusing times (5, 10, 20, 30, 40, 50 and 60 seconds) were used to produce samples which were then subjected to tensile testing. From the study it was found that at five seconds under the IR heater, the Young's modulus and UTS values are far greater using a stand-off distance of 128mm (Young's modulus 3.3N/mm^2 UTS 0.86N/mm^2) than using 178mm (Young's modulus 2.19N/mm^2 UTS 0.57N/mm^2) or 228mm (Young's modulus 1.81/mm^2 UTS 0.45N/mm^2). At 60 second exposure, the difference in Young's modulus for 128mm more than double that for a stand-off distance of 228mm.

Another factor assessed was the mechanical properties of different particle size (17µm and 30µm) for both coated and uncoated Somos toner. The powders were fused in the same mould but at a fixed stand-off distance of 178mm from the IR source. The results showed that the smaller toner particles were able to fuse with a better inter-particle bonding than the larger materials. This is due to the lower energy required to fuse the smaller diameter powder. Additionally, fumed silica coated samples gave significantly lower mechanical properties than the uncoated material Figure 3:48.

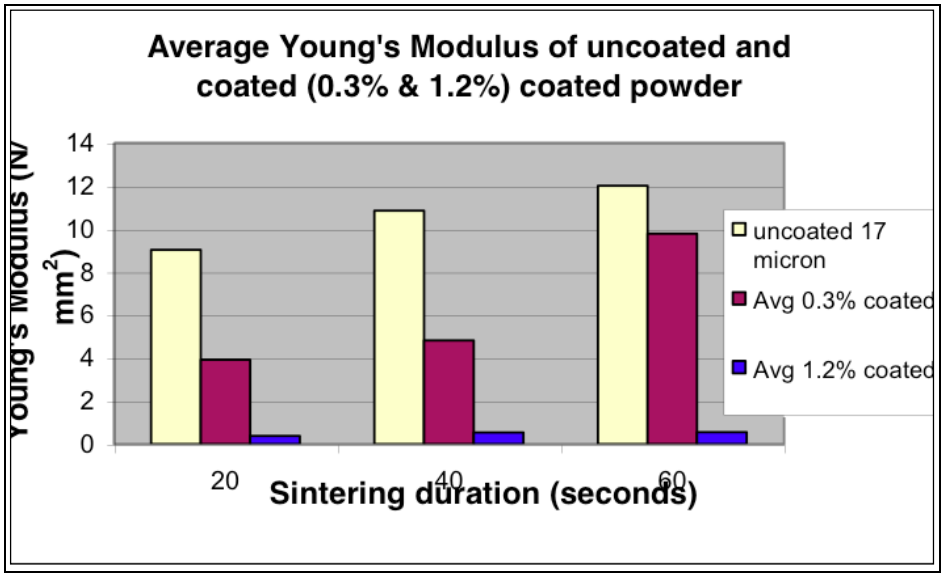

Figure 3:48: Average Young's modulus value for 17µm coated and uncoated Somos powders IR fused at 178mm stand off

From the experimental results it was deduced that a toner with a particle size of 17µm (D_{50}) , free from surface additives, yielded far superior mechanical properties. In addition, it was shown that using IR sintering, the tensile properties of the samples can match and even exceed those for parts produced by laser sintering

Summary;

In conclusion, extensive work was carried out by Wimpenny and Banerjee over a five year period.

Printing trials – acceptable deposition of fine HDPE powders was achieved using the HP LJ 4 and Lexmark C510 printer, with the latter forming the foundation of an early test rig. However, the difficulties encountered with printing HDPE prompted a move to Somos 201 based toner material using a dual component system. The transition from single

component to dual component printing was via EMB process and this also prompted a focus on final transfer via tackification through heat and pressure rather than the patented repulsion approach. With significant manipulation to reduce curling at the edges and the long intervals between fusing, a part height in excess of 8mm was built, contradicting the model outlined by Kumar[49]. Results from the EMB process heralded a SLP rig built through collaboration between industrial partners and DMU. The rig was used in a feasibility study to produce customisable inserts for helmets and seats for motorcycles.

Comminution trials - In summary, it was found that the amount of work required to reduce the thermoplastic elastomer was grossly underestimated. The comminution processes employed for toner manufacturing are more suited to brittle polymers. As a result the yield was poor. Wimpenny *et al*. decided to buy the feedstock material and to classify it to the required size. This method, while on the face appears costly, actually turned out to be the most cost effective approach of producing the fine powder required.

Main trials – The main trials in Banerjee's PhD study did not use the laser printing directly to produce the tensile parts, due to the limiting part height and poor surface finish. Instead a mould was produced and varying stand-off distances and particle sizes and coated and uncoated powders were fused. It was found that a toner with a particle size of 17µm (D_{50}) free from surface additives yielded far superior mechanical properties, however, uncoated powers are unable to pair with a carrier due to inefficient tribocharging. In addition, it was shown that using IR sintering, the mechanical properties of samples can match and even surpass those for laser sintered parts [4, 12]. An interesting finding from the work was that a fumed silica coating can inhibit the sintering process.

3.6.8.8 SLP MK1

The promising results for the CTG dual component printer paved the way to producing a near fully automated rig. The rig was an industrial collaboration between De Montfort University (Leicester, UK), CTG PrinTec GmbH, Marcam Engineering GmbH, (Bremen, Germany) and Renishaw (Plc) AMPD (formally MTT Technologies, Stone, UK) supported by a European Union Framework 6 Custom-Fit project (No 507437).

Each partner had a specific brief in developing the rig. Marcam Engineering were assigned with the development of the interface responsible for slicing the models. In addition, they were also responsible for sending single bit bitmaps at 600DPI to the CTG printers.

CTG had the task of producing an industrial dual component printer with a smaller footprint. The CTG 900 printer was based around a 900mm PC. The new printer, CTG-IC17-600 (CGT 600) was based around a 17" PC with an identical development system as the CTG 900 printer. The development of the latent image on the PC was accomplished by implementing a DAD method using a 600DPI LED array.

Renishaw AMPD with the aid of DMU were responsible with the fabrication of the rig structure and with the integration and automation of the CTG printers to the machine controller. The machine was designed with the equipment outlined in Table 3:7.

Table 3:7:List of equipment on SLP rig

Item	Designation and spec	Supplier
IR heater		
Heat sensor	ES1B Infrared thermosensor	Omron, Japan
Printer	CTG-1C17-600 (17" photoconductor 600DPI Led print head) for negative toners	CTG GmbH, Dusseldorf, Germany
Primary Z	Motor for Z height displacement	Renishaw AMPD
Non-contact height measuring device	ZS- HLDS10-2M	Omron, Japan

3.6.9 PepPer Print

Dr Stefan Guttle of Fraunhofer Institute Manufacturing Engineering and Automation in Stuttgart, Germany began developing a novel manufacturing process to deposit peptide arrays with the German Cancer research centre[15].

Peptides arrays are currently produced using a spotting process, which is carried out by robots in labs delivering a single peptide drop on to a paper like substrate. Up to 10,000 peptides can fit on a single substrate. With each peptide costing ~€5, this equates to ~ €50,000 for a full array[15].

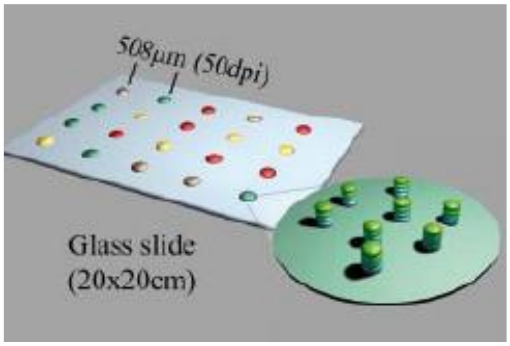

Figure 3:49: Peptide array on glass slide[15]

Using the current manufacturing process the peptide drop consists of an amino acid within an aqueous carrier. In the laser printing route the amino acid is developed into a dry toner powder which is printed onto a glass slide using a 1200dpi Oki print engine. It is noteworthy that a protein/peptide consists of ~20 amino acids and so two printers are required to complete this approach. The slide is removed and heated to 90˚C, melting the toner matrix. At this point, the amino acids are activated, thus adhering to the carrier. The toner matrix along with the charge control agents is washed away leaving behind the amino acid. The process is repeated 12-20 times, depositing over 155,000 peptides on a 200x200mm glass slide.

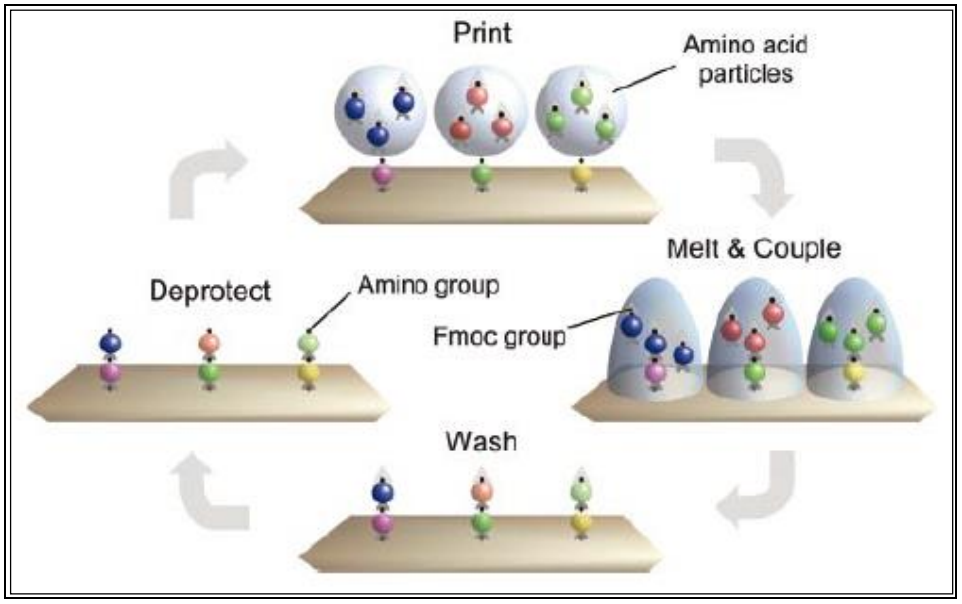

Figure 3:50: PepPer Print peptide deposition cycle[15]

Guttler et al. found that the laser printed peptides contain a denser concentration of peptides compared to current production methods. The biochips are manufactured at greater speeds and over 100 more cost effective[15]. As a result the peptides can be produced for a few cents/peptides as opposed to €5 each.

3.6.10 Jones, Warwick University/ De Montfort University (2009-2013)

The work covered by Jones is vast. However, the main body of work was related to his efforts in understanding and controlling unwanted charge accumulation during the printing and fusing process of the SLP process.

Jones' initial discovery of trapped charge came when a sample, which had been printed on the SLP rig, was removed after 18 days. It was found that the aluminium plate (acting as an electrode) was electrostatically adhered to the sample substrate. Jones reported that the force required to part the two plates was 'noticeable'. Jones concluded that the residual charge in the sample could last up to a month if untouched[5].

Using a polyester toner, Jones began printing samples with 5mm gaps. At each 5mm step an additional layer would be printed until at print 20, where 20 layers were printed (See Figure 3:51). The sample showed good transfer until around layer six, when signs of pitting began emerging. The pitting became more prominent as the layers increased and at layer 20, very little toner has actually been deposited.

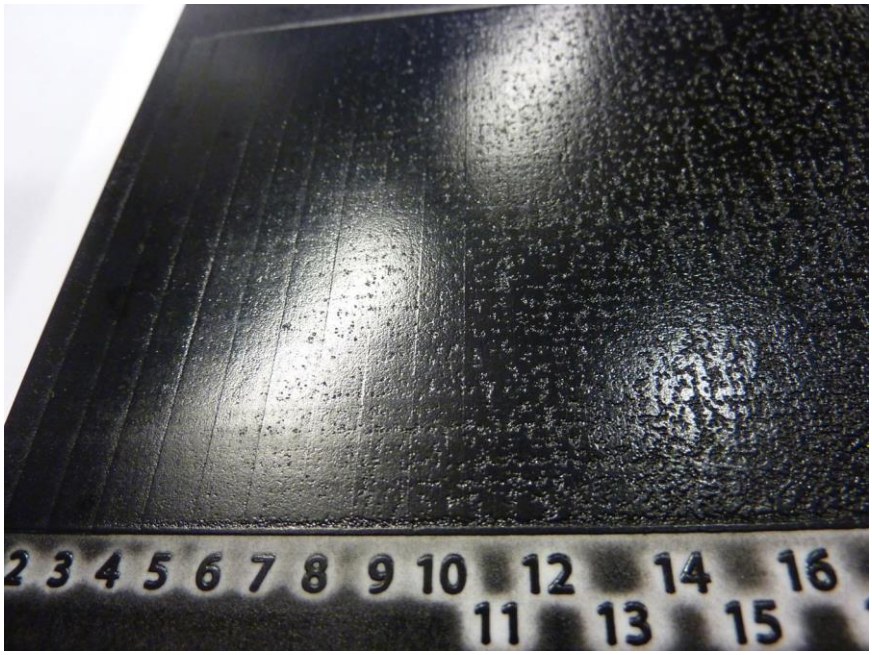

Figure 3:51: Printed black toner with increasing consecutive layer using the SLP rig[5]

Jones later looked at intentionally trapping charge by printing toner on to a film. Jones printed a polyester toner onto a polyimide film and observed the effects of trapped charge.

A small sample of the sample was cut and handled with tweezers as not to disturb the internal charge by handling. A metallic charge plate was placed 4mm above the grounded Al substrate. The small sample was placed under a metallic charge plate and a voltage of +3kV was applied via a power supply. The results (Figure 3:52) showed the sample to lift to the charge plate by the field generated. When the voltage was turned off the sample remained adhered electrostatically onto the charge plate until the polarity was inverted, in which case the sample was repelled off the charge plate and onto the metallic substrate.

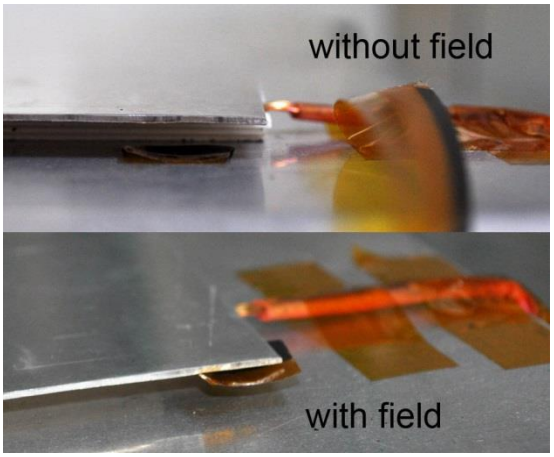

Figure 3:52: Trapped charge experiments acting with and without a field[5]

The results of the trapped charge test by using a field showed the issue that charge was present in the sample. Moreover, the previous understanding that charge is departed when fused has proven not to be the case.

Upon discovering trapped charge in the laser printed samples, Jones began to look at previously printed samples from previous CustomFIT and other projects. Samples of previously printed Somos were investigated for trapped charge. A small section of a dog bone sample was taken and placed under the 4mm gap as described above. The power supply was turned on and a field generated. The results showed part of the dog bone to lift.

What was more interesting was the sample was electrostatically attracted to the charge plate when a voltage of -3kV was applied. It was believe that the change in polarity was possibly due to the charge injection from multiple amounts of contact from the transfer roller. Another theory considered was charge migration over time causing the positive charge to migrate to the surface to balance the negative charge in the centre of the sample. Jones concluded that even after two years, the charge was still trapped inside the samples. Jones also conceded that the trapped charge can last years rather than months as initially speculated[5, 139].

Upon discovering residual charge and the large decay time, Jones concentrated his efforts in understanding how to manage and resolve the issue of charge accumulation. Jones developed a new conceptual model detailing the charge distribution for toner (Figure 3:53). The model acknowledges toners to have a non-uniform charge distribution over the surface, with some charge more concentrated than others and non-existent in certain areas of the toner surface. Furthermore, the model describes the effects during the fusing stage. It was initially thought that the charge is dissipated or neutralised once fused[5, 139, 140]. However, Jones proved that the charge is still prevalent in the fused layer. This led jones to believe charge is trapped within the sample and the charge dissipation time based on the resistive or conductive nature of the toner. Jones further explores the implications of the trapped charge in layers and the little effect charge neutralisation had on the surface due to trapped charge.

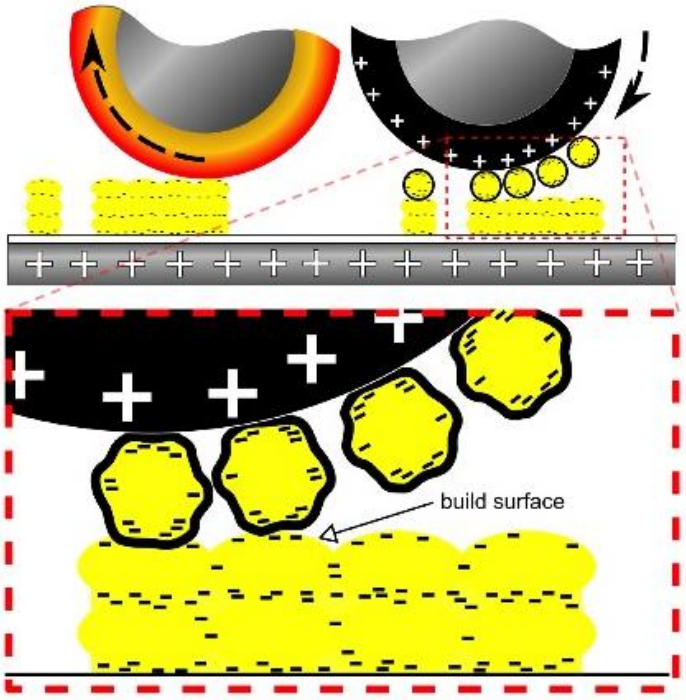

Figure 3:53: Conceptual model of charge distribution on a toner post fusing[5]

Jones concluded that it is necessary to neutralise the toner charge to avoid defects when stacking layers. Certain methods, namely the ionization fan, can have a negative impact to the part height as well as the formation of defects. Jones acknowledges several options as plausible methods of charge neutralisation, but concedes that neutralisation alone is not the answer to consistent layers. While considering the many methods, Jones recognises repulsion coupled with charge neutralisation as a method to rival tackification.

3.6.11 Arciniegas, Rochester Institute of Technology (2011-2013)

In December 2014, Arciniegas submitted a PhD thesis entitled " Towards the control of electrophotographic based 3-Dimensional printing: Image based sensing and modelling of surface defects" [141]. The study describes two areas of research; investigation of image defects and characterisation and modelling of EP for printing control, with the significant output being surface roughness. The surface roughness was to serve as a proxy for density.

The rig

The rig consists of a HP LaserJet 4700 printer with a modification to enable printing with the fuser removed. A flexible substrate is printed on to without fusing. Next, the unfused substrate is transfixed at the fusing station through an adjustable fusing roller altering the fusing pressure. The fusing roller has a similar configuration to a standard printer, containing a heat source within the core of one of the two rollers. An image of the printer and fusing station is show in Figure 3:54.

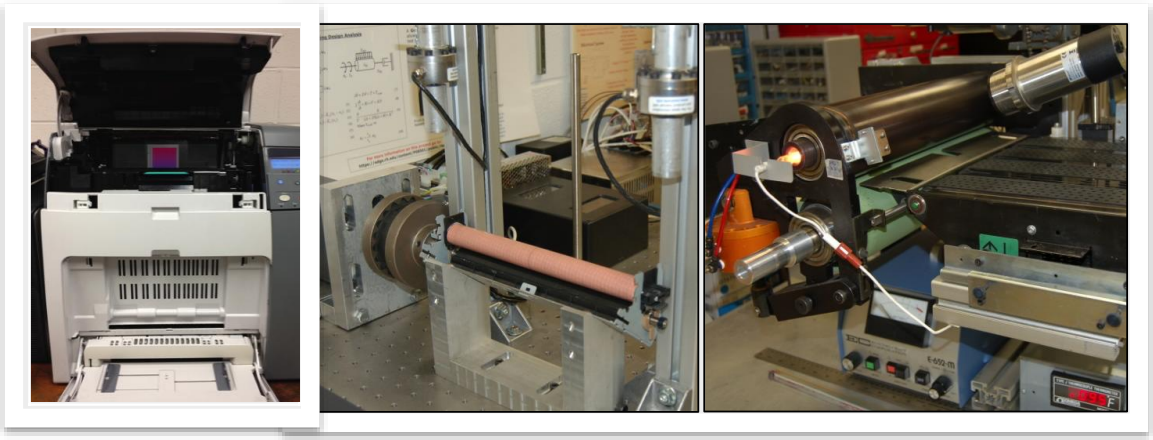

Figure 3:54: Process sequence for EP3D[141]

In 2008, Kodak donated a rig to the Chester F Carlson Centre of Imaging Science. The test bed is able to replicate the majority of laser printing steps discounting fusing and cleaning, which are manual steps. The test bed is shown in Figure 3:55.

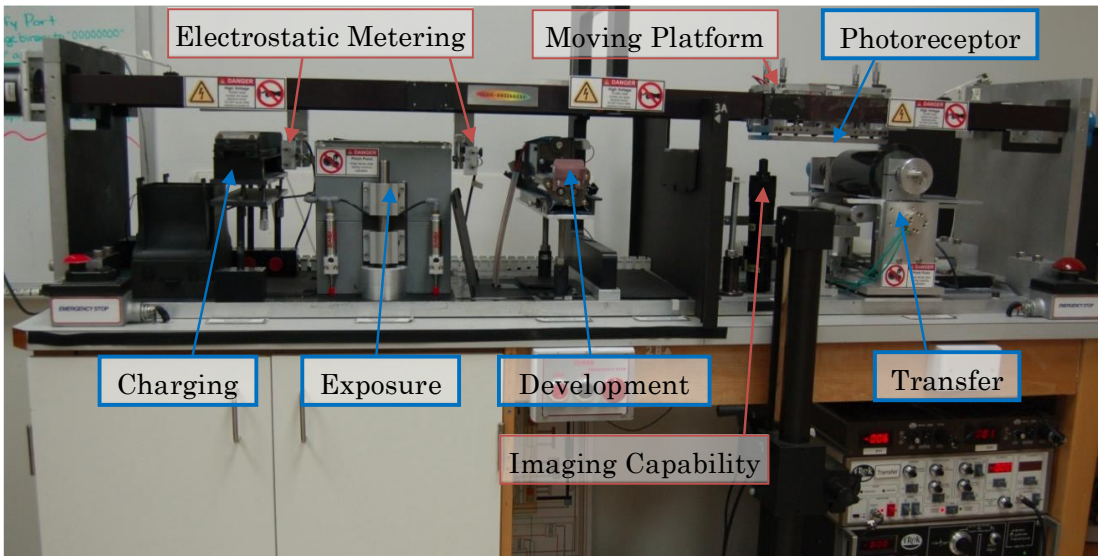

Figure 3:55: Linear test bed at Chester F Carlson centre for imaging science, Rochester Institute University[141]

Image defects and characterisation

Arciniegas initially began with characterising the surface defects. Using design of experiments (DoE), Arciniegas looked at four factors, each with two or three variables. A table of the factors and levels are shown in Table 3:8.

Table 3:8: DoE table illustrating the factors and levels[141]

Factors	Levels
A. Base Substrate	1. Paper ($4x10^{-3}$ in ≅ 0.102 mm thick, 75 g/m^2) 2. Cardboard ($9x10^{-3}$ in ≅ 0.229 mm thick, 200 g/m^2) 3. Metallic Paper ($3x10^{-3}$ in ≅ 0.076 mm thick, 109 g/m^2)
B. Number of Materials	1. Cyan Toner 2. Cyan and Magenta Toner
C. Halftoning	1. No Halftoning (100% fill) 2. Halftoning at 50% fill
D. Graded Transitions	1. No transition (constant fill) 2. 50% gradient transition applied (100% to 50% or 50% to 0% depending on the halftoning level)

Arciniegas began surface image characterisation by printing single layer prints onto a silicon coated Mylar sheet and fusing them, initially to the substrate, and then subsequent layers. This manual method was thought to circumvent height limiting. However, the process brought about new challenges. Issues of registration and excessive curling of the substrate were encountered due to multiple passes through the fusing station.

The results from the DoE highlighted half-toning, and number of materials, to have a significant statistical effect. It was also found that the substrate had very little statistical effect on the model.

Additional trials involved manually stacking 30 layers and measuring each layer at the leading and trailing edge by using a contact drag probe. Two methods of stacking were undertaken. The first, involved placing the printed layer face down (top layer of previous print or sample surface on soft roller instead of heated roller). The second process involves the fresh printed layer to be in contact with soft roller and previous layer/substrate surface in contact with heated roller). Arciniegas found the fused face down provided a lower

average surface roughness (Ra). Further trials established that reducing the transfusing speed had an improved effect on the surface roughness.

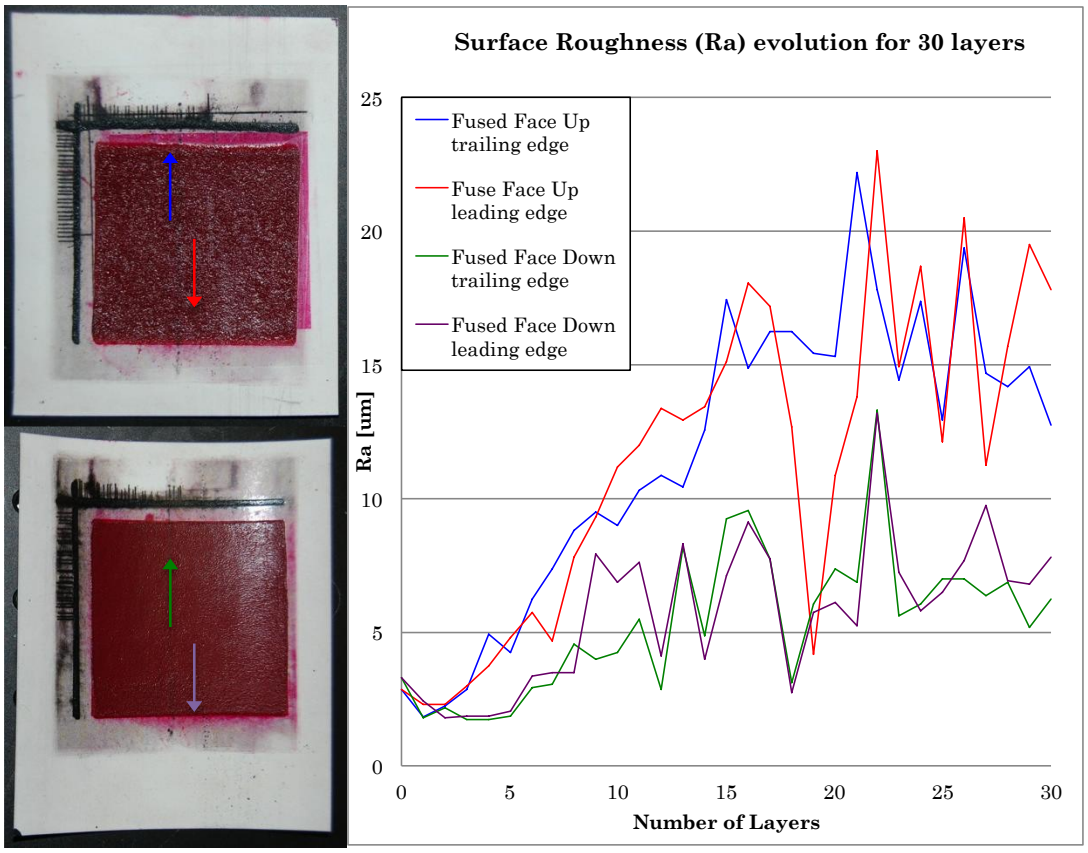

Figure 3:56: Surface roughness of 30 layer samples with corresponding graph[141]

Printing control for Electrophotographic deposition

Arciniegas modelled the electrophotographic layer deposition using Matlab to simulate the response of laying down 30 layers. The simulation provided a good approximation for the expected behaviour of the increasing layer thickness. Arciniegas found surface roughness to be dependent on the characteristic of the substrate, with a rigid substrate performing the best. This is contrary to the results from the DoE detailed above. The simulation

confirmed an increasing layer deposition could result in a growing Ra value regardless of the substrate.

Post simulation, Arciniegas carried out experiments using the rig employing two approaches; passive and feedback control. The passive approach utilised two substrates; a softer silicon coated Mylar substrate and a slightly thicker transfer belt from a HP indigo printer. The HP transfer belt, used as an intermediate substrate. Upon preheating, 100 layers were printed and transfused. Arciniegas found the layer transfer efficiency dropped as less material being deposited on to the intermediate substrate, ultimately leading to thinner layers. The deposition was measured every 10 layers and averaged 3µm/layer over the 100 layers.

The process was repeated using the silicon coated Mylar substrate and using two colours (cyan and magenta) and a single colour (magenta). The results showed the Mylar substrate to produce the greatest height of 820µm using two colours, followed by the use of a single colour, measuring 510µm. The Ra values were recorded as 37.8 µm and 32.8µm respectively for the leading edge. The HP transfer belt recorded a layer thickness of 300µm but the average surface roughness was limited to 8.4µm for the leading edge. Arciniegas concluded that the surface of the HP indigo transfer belt was facilitating a smoother surface during the transfixing stage.

Table 3:9: Measurements over 100 layers for Mylar and HP indigo substrates[141]

Intermediate Substrate	#Toner	Layer #	Height (mm)
Silicon coated Mylar	2 (CM)	100	0.82
Silicon coated Mylar	1 (M)	100	0.51
HP Indigo Belt	1 (M)	100	0.30

Using the information from the previous trials, Arciniegas simulated a feedback control whereby a layer is printed and transfused as per usual. A second step is used to 'sense' the printed region. This sends a binary signal back to the printer detailing any areas where the deposition may have been weak. A new layer is formed to compensate the previously lacking layer and is transfixed. The compensation layer is formed on the back of the information provided by the feedback, determining the deposition layer by evaluating the difference between the deposited layer and the upper limit. A simulation of this was conducted initially, with results suggesting some success.

Using Reflectance Transformation Imaging (RTI – is a process which takes pictures using multiple illuminations to visualise the image) compensation images were taken of a 100 layer sample. The results showed the surface variations to be highlighted but the generated images become more difficult as the features become less prominent. In order to circumvent this issue, a new process called GelSight was used. The process is a MIT spin off using a gel coating over the substrate and a shining a light source from three different angles. This process results in better image construction with up to 1µm resolution. The process showed great promise, as the images were able to show a detailed topology of the transfixed surface of the fused down samples, which provided the better surface roughness. This, in turn, provided a detail analysis of the surface defects potentially allowing for the control of the surface quality. It was proposed that a single layer would be printed and measured. The sample would print another layer based on the defects picked up from the GelSight images, thus filling in the defects. However, this was not carried out.

3.6.12 Stratasys – multi directional rotating OPC/transfer roller

Stratasys Inc. has expressed some interest in the use of EP for AM. Two patents were granted of the six that were applied for [14, 142], with a third granted in May 2014[143] . The process employs a method dependent on tackification for fusing. The embodiment describes the use of a bidirectional photoconductor and transfer roller for the deposition of multi materials, dependent on the rotation of the transfer roller. This move allows for the deposition of both a build and support material in one rotation.

The transfer roller is equipped with a heat source allowing for the tackification of the build and support material. A blower is described to cool the transfer roller to avoid transferring the heat to the photoconductor and thus causing potential damage. The patent also discloses the use of additional development stations to enable multiple materials to be deposited. The patent [142] makes a claim whereby 40 layers a minute can be printed, however, this claim has yet to be substantiated.

A second embodiment (Table 3:11) describes the use of a belt transfer system[142]. Moreover, a service loop is implemented to allow for different line speeds during transfer and fixing. A platen is used to receive the printed layer from the transfer belt and is pressed on to the previously printed layer.

The final embodiment describes the transfer and fusion process. The embodiment details the process to heat the both the fresh layer and the receiving layer to at least the fusion temperature by means of a non-contact radiant heater. The process is still reliant on pressure and utilises a plate press to adjoin the fresh layer to the previous layer. A transportable platform is moved to the cooling station the layer, transfixed to the previous

layer, is brought below its fusion temperature at the cooling station. At that point, the transfer medium (a belt from US patent 8488994 B2) is detached from the layer.

In summary, Stratasys' main technology relies on a bidirectional PC which allows for the integration of a build and support material, negating the need for two printers. The three patents are heavily dependent on pressure and tackification. Despite filing the patents there is no evidence that Stratasys has undertaken any work to develop and commercialise the approach.

Table 3:10: First embodiment from Stratasys for an EP based AM process

Abstract
An additive manufacturing system for printing three-dimensional part using electrophotography, the additive manufacturing system comprising a rotatable photoconductor component, first and second development stations configured to develop layers of materials on a surface of the rotatable photoconductor component While the rotatable photoconductor component rotates in opposing rotational directions, and a platen configured to operably receive the developed layers in a layer-by-layer manner to print the three-dimensional part from at least a portion of the received layers.
Primary claim
An additive manufacturing system for printing a three-dimensional part using electrophotography, the additive manufacturing system comprising: 1) a rotatable photoconductor component having a surface, and configured to rotate in a first rotational direction and a second rotational direction that is opposite of the first rotational direction; 2) a first development station configured to develop a layer of a first material on the surface of the rotatable photoconductor component while the rotatable photoconductor component rotates in the first rotational direction; 3) a second development station configured to develop a layer of a second material on the surface of the rotatable photoconductor component while the rotatable photoconductor component rotates in the second rotational direction; 4) a rotatable transfer component having a surface configured to receive the developed layers from the surface of the rotatable photoconductor component while rotating in a direction counter to the rotational direction of the rotatable photoconductor component; a platen movable along an x-axis and a z-axis and configured to receive the developed layers from the rotatable transfer component in a layer-by-layer manner to print the three-dimensional part from at least a portion of the received layers; and 5) a controller configured to selectively rotate the rotatable photoconductor component in the first and second rotational directions, to rotate the rotatable transfer component at a synchronized rate and in counter-rotation with the rotatable photoconductor component, and to move the platen at a synchronized rate with the surface of the rotatable transfer component, and to index the platen along the z-axis between layers.

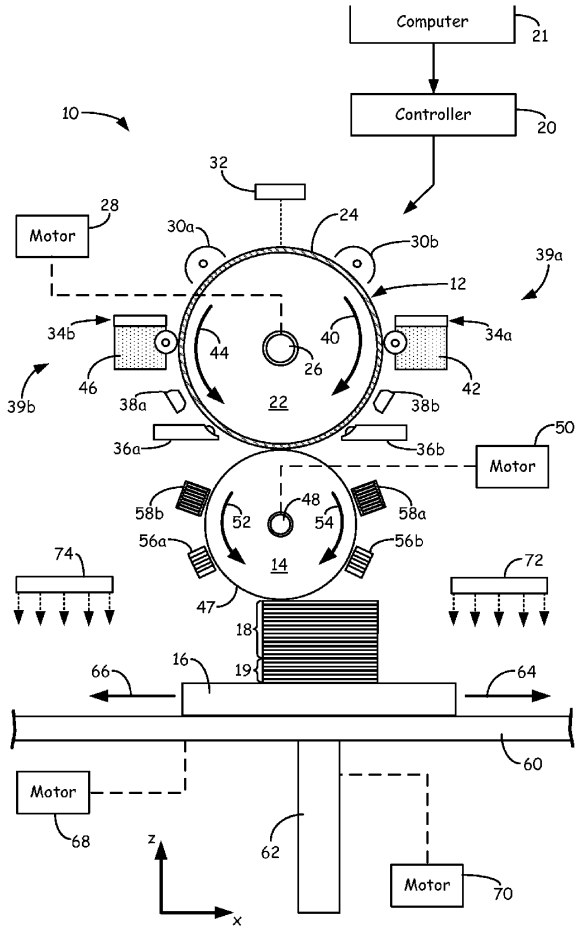

Figure 3:57: Stratasys EP based AM system

Table 3:11: Second preferred embodiment from Stratasys for an EP based AM system

Abstract
An additive manufacturing system for printing a three-dimensional part using electrophotography, the additive manufacturing system including a rotatable photoconductor component, a development station configured to develop layers of a material on a surface of the rotatable photoconductor component, a rotatable transfer medium configured to receive the developed layers from the surface of the rotatable photoconductor component, and a platen configured to receive the developed layers from the rotatable transfer medium in a layer-by-layer manner. The additive manufacturing system also includes a plurality of service loops configured to move portions of the rotatable transfer medium at different line speeds while maintaining a net rotational rate of full rotations of the rotatable transfer medium at a substantially steady state.
Primary claim
An additive manufacturing system for printing a three-dimensional part using electrophotography, the additive manufacturing system comprising: a rotatable photoconductor component having a surface; a development station configured to develop layers of a material on the surface of the rotatable photoconductor component; a rotatable transfer medium configured to receive the developed layers from the surface of the rotatable photoconductor component; a platen configured to receive the developed layers from the rotatable transfer medium in a layer-by-layer manner to print the three-dimensional part from at least a portion of the received layers from the rotatable transfer medium; and a plurality of service loops configured to move portions of the rotatable transfer medium at different line speeds while maintaining a net rotational rate of full rotations of the rotatable transfer medium at a substantially steady state.

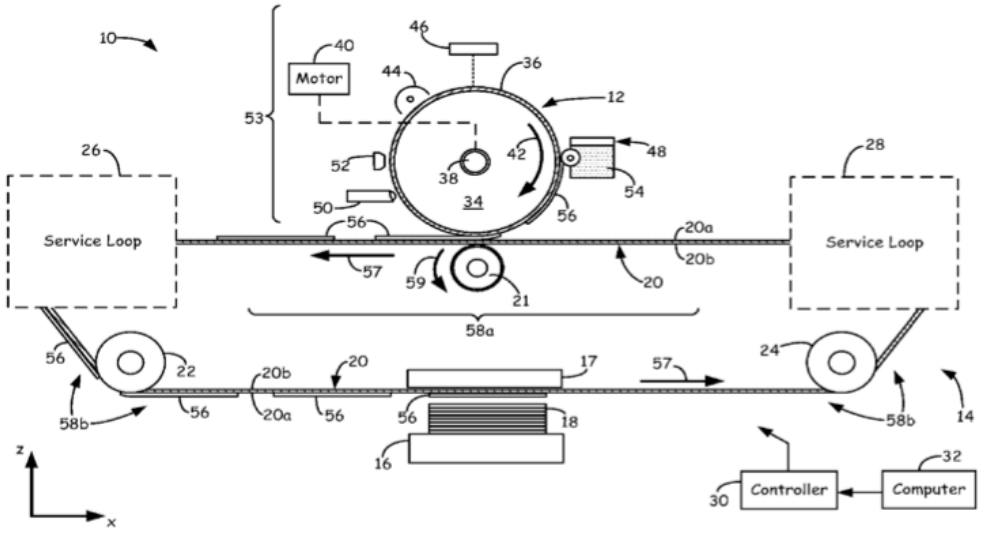

Figure 3:58: EP based AM system implementing a transfer belt system and service loops

Table 3:12: Stratasys patent: Layer transfusion with part heating for AM

Abstract
An additive manufacturing system comprising a transfer medium configured to receive the layers from a imaging engine, a heater configured to heat the layers on the transfer medium, and a layer transfusion assembly that includes a build platform, and is configured to transfuse the heated layers onto the build platform in a layer-by-layer manner to print a three-dimensional part.
Primary claim
An additive manufacturing system for printing a thermoplastic part, the additive manufacturing system comprising: an imaging engine configured to develop imaged layers of a thermoplastic-based powder having a fusion temperature; a movable build platform; a transfer medium having a transfer surface configured to sequentially receive and convey the imaged layers from the imaging engine to the build platform, and having an opposing contact surface; a heater configured to heat the imaged layers on the transfer medium to at least the fusion temperature; a heater configured to heat a previously transfused layer of a thermoplastic part being printed on the build platform to at least the fusion temperature; a heated layer transfusion element configured to transfuse a heated imaged layer conveyed by the transfer medium onto the heated previously fused layer by engaging the contact surface of the transfer medium so that the transfer medium and the heated imaged layer are pressed between the transfuse element and the build platform, and to disengage therefrom without releasing the transfer medium from the transfused layer; and a cooling unit configured to actively cool the transfused layer to below the fusion temperature while it remains on the transfer medium, so as to transfix the transfused layer before delaminating it from the transfer medium.

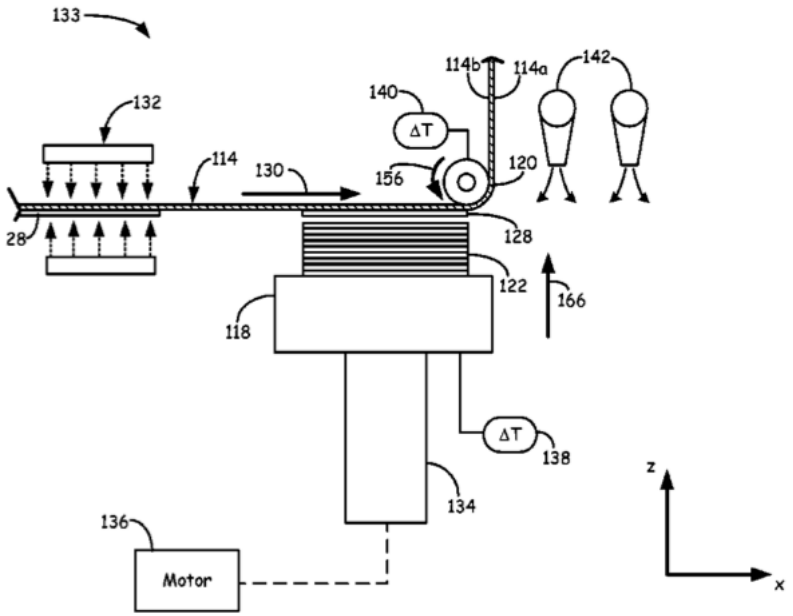

Figure 3:59: Transfer and heating process described in the embodiment by Stratasys

3.6.13 Chua & Tan, Singapore University (2012 – 2015)

A research team from Nanyang Technological University, Singapore, have also explored the use of Electrophotography for AM. Professor Chau, and Dr Tan are using electrophotography has a hybrid system. The system, dubbed Three Dimensional Xerography (3DX), utilises the traditional loose powder bed of AM, but also employs EP to deposit a binder on to the powder substrate, producing a layer, similar to the approach used by Kumar to produce ceramic parts. [144].

The research team claims that the key novelty of their approach is the binder and the manner in which it is applied to the loose powder bed. The test bed is made up of an amorphous selenium photoconductive plate, which is placed on a grounded conductive substrate. The photoconductor is charged via a charging bar between -500V to -1000V and the surface potential measured via a non-contact probe. A negative image of the cross sectional layer is placed over the photoconductor plate and a line laser is directed at the piece of paper. As the paper is a negative of the actual image to be printed the background remains charged with the remaining area discharged. The LDPE powder, a negatively charging polymer, is attracted to the discharged region of the photoconductor.

A metallic substrate with a PTFE coating is aligned above the photoconductor plate where the metallic substrate and photoconductor plate are simultaneously exposed to light. The charged areas of the photoconductor plate are discharged. Concurrently, the PTFE coated metallic substrate is subjected to a positive bias attracting the toner off the photoconductor substrate. The PTFE substrate is then transferred to the build platform and an induction heater is used to heat up the polymeric powder. When the LDPE is molten the polarity is reversed and the metallic substrate is subjected to the opposite charge (positive charge). This repels the molten polymer on to the powder bed causing

the fusion of the powders via a binder. A representation of the above description is shown in Figure 3:60.

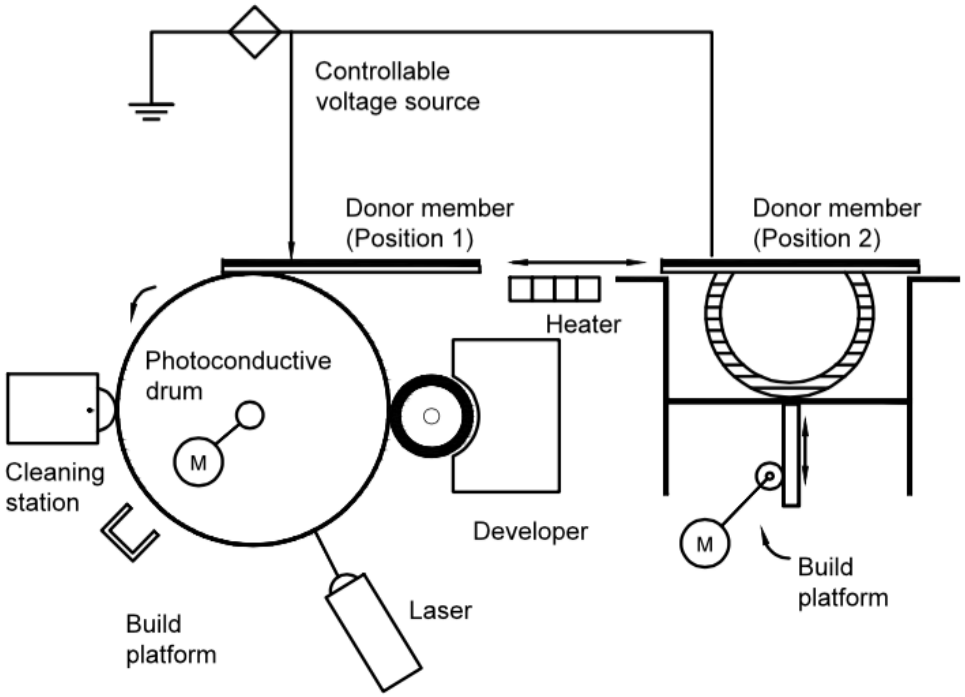

Figure 3:60: Overview of 3DX (after Chua) [144]

Tan and Chua also identified a number of possible methods for repelling the binder off the imaging member and on to the powder bed. The first method discusses the use of an additional controllable voltage source attached to the OPC. Traditionally, the photoconductor is held at ground. However, the inventers have stated by holding the voltage of the photoconductor at the same bias as the binder, the binder will be repelled at a high velocity and maintain uniformity. A use of a variable voltage source is also claimed to be advantageous by the inventers.

A second method describes the use of a donor substrate (Figure 3:61) used as a transportation device to transfer the binder material from the printer photoconductor to the powder bed. The donor transportation substrate is aligned with the powder bed and the binder is repelled onto the substrate by applying an opposing bias voltage. In this instance, the binder is heated on the donor substrate until the binder is at least partially melted.

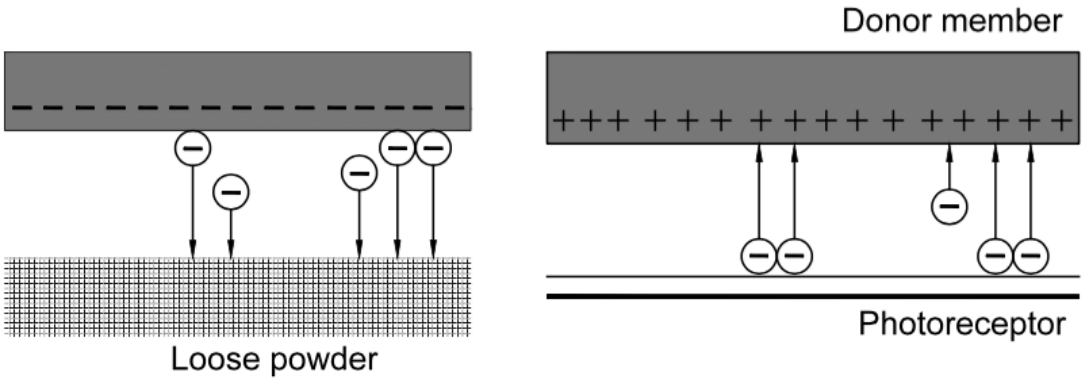

Figure 3:61: Transfer of binder from OPC (left) to the powder bed (right)(After Chua) [144]

Although Tan and Chua claim to have overcome the charge accumulation issues that inhibit toner transfer there is no evidence of samples being successfully produced using this approach and moreover, there is no evidence of any further publications. The use of repulsion is a method proposed by Wimpenny et al. Furthermore, the work appears to build on the research of Kumar and Liu and Jang [11, 145]

4 Methodology

In this chapter the aims and objects of the study are presented and contrasted with the state-of-the-art from the literature to demonstrate the novelty and contribution to science. Then, the methodology to be employed in the empirical work, are presented and justification for the proposal approach given.

From the literature study (Section 3.6) in the field of material development for electrophotography based Additive Manufacturing (AM) it is clear the majority of work has focused on the use of standard toner materials [10, 146] and moreover, the use of mechanically ground novel toner material [2, 4, 12, 137, 147]. Although this work has established the basic principles of the electrophotography based AM, the work conducted also highlights some of the key challenges which must be overcome to enable this technology to be used for the production of functional components (as shown in Table 4:1).

Table 4:1: Notable research conducted in the field of Additive Manufacturing using electrophotography

Primary researcher	Area of research	Issues highlighted and further work

Kumar	Process development –
	• Toner transfer via EP rig
	• Modelling theoretical electrostatic transfer
	• Proposed method to eliminate accumulated charge (top charging)
	Direct and indirect manufacturing via EP
	Binder deposition on substrate
		• Charge accumulation limits Z height
		• Deposition limited as height increases
		• Surface quality deterioration as height increases
		• Top charging limited response
		
		Further work
		• Liquid binders
		• New rig
		  ○ Flat PC plate
		  ○ Two image developers

Cormier	Material development • Engineering polymers for EP printing • Multi material deposition Multi-colour parts	• Engineering polymers hard to obtain in small fractions. • Height issues, opted for heat and pressure on to a separate plate to avoid charge accumulation Further work • Tough engineering polymers
Wimpenny/ Banerjee	Machine development • Development of the SLP MK1 rig Material development • Method for reducing and coating polymeric powders	• Current EP materials too brittle for AM. • Layer accumulation limits height • CCA hindrance to particle fusing Further work

		• Chemically producing toner to avoid costly milling and particle sieving • Investigate mechanical manufacturing methods to produce a more efficient method of manufacturing
Jones	Fundamental understanding of charging characteristic for AM – focused on overcoming Z-height limit. • Conceptual model detailing charge distribution • Proved charge was prevalent post fusing (trapped charge) • Methods proposed for charge management	• IR heater used in sample manufacturing has uneven heat distribution • Residual charge undermines electrostatic transfer as well as heat and pressure Further work • Expand range of polymers • Convert printer to print positive toners
Stratasys	Machine development	Only patents in the public domain
Arciniegas	Controlling EP toner deposition overcoming Z height issues • Surface defect characterisation • Development of a control strategy for toner deposition • Develop a model to compensate the toner voids	• Substrate too thin resulting in curling of layers and surface degrades as more material is deposited • Surface defect feedback control not implemented due to lack of layer registration and sensing • GelSight field of view limited to 13% of the sample (50x50mm) Further work • Explore toners with better mechanical properties • Explore more ridged substrate to avoid curling • Automate transfusing stage

From Table 4:1 it is clear that there are two primary issues limiting the successful applications of Additive Manufacturing using electrophotography; firstly, height limitation of parts due to charge accumulation. Secondly, the difficultly in producing toner from engineering polymers. These are discussed in more detail below:

1) Ability to generate parts with significant Z height due to issues of charge accumulation, which limit the toner transfer efficiency. This has been a subject of significant research [5, 11, 13, 49, 139, 141]. Although, some progress has been made, particularly in understanding the root cause of the problem and identifying the ineffective potential solutions, work is still on going in this area.

2) Provision of suitable toners based on engineering polymers. Cormier [2] used off-the-shelf engineering polymer powder as the basis of an experimental toner but the charge accumulation severely limited the printing efficiency. Work by Banerjee [4, 148] attempted to obtain toner with more favourable printing characteristics by sieving off-the-shelf thermoplastic elastomer powder to gain powder below 30µm. Unfortunately, this proved to be extremely time consuming and 85% of the original material was oversized and thus had to be discarded.

A critical issue, as identified by Banerjee, is the mechanical properties of conventional toners. Conventional toner materials are formulated from polymers that are best suited to printing of 2D images and text [4, 94] and, moreover, are brittle to ensure both rapid and efficient production by mechanical reduction. These materials present a major challenge for the deposition of multiple layers as they readily fracture through thermal stresses induced by the fusing process and lack the strength and durability for the production of engineering parts. The potential to produce toners using more appropriate materials by chemical synthesis was recognised by Banerjee (further work section)[4] but was outside the scope of his study.

Aim:

The aim of this study is to develop a toner based on an engineering polymer to be used in the SLP process with a suitable particle range and to assess the mechanical properties of parts produced using the toner developed through this route.

Objectives:

1. Review a range of engineering polymers and select the most appropriate material for further development.
2. Evaluate methods for producing the powder with the required particle size/morphology from the selected polymer.
3. Develop and test toners produced from the polymeric powder.
4. Assess the fusing characteristics of the developed toners and mechanical properties of 3D samples produced by the SLP process from the new toner material.

Novelty & Anticipated Contribution to science:

The project builds on the previous work conducted in this field [2, 4, 5, 10] to unlock the commercial potential of the SLP process by providing an efficient technique for the production of toner. The new toners will be based on a rigid engineering polymer and an integral part of the study will be to understand the relationship between processing parameters and final mechanical properties.
This study extends beyond Banerjee's work in the following key aspects;

1) Provide an efficient and cost effective route for the production of engineering thermoplastic powder for toner manufacture - Banerjee did not provide a method of generating a fine engineering powder or a cost effective method for toner manufacturing.

2) The toner employed by Banerjee was an elastomeric polymer, which fortuitously presented charging properties akin to standard toners.

3) Mechanical properties presented in Banerjee's thesis relate solely to samples prepared by fusing in moulds, rather than deposition by means of electrophotography.

A fundamental limitation of the powder production method of mechanical milling, as employed by Banerjee, which was mechanical grinding, is the efficiency of the adopted process deteriorates as the D_{50} decreases. For engineering polymers, this problem is further exasperated due to their inherent toughness.

The present study will focus on three aspects: (1) the production of fine toners by both mechanical and chemical methods (2) assessment of the printing performance and finally (3) to measure the key mechanical properties of test parts produced using the toners developed in the project.

Experimental Approach

A well-established approach for toner development and characterisation, previously employed by Banerjee, was used in this study, with some key changes highlighted below to reflect the novel nature of the trials. Four points have been expanded below to provide an overview of how the study will be conducted in order to achieve the objectives of the study;

1. Review a range of engineering polymers and select the most appropriate material for further development.

The selection of engineering polymers will be based on;

- **Mechanical properties:** Bulk material properties of common engineering polymers from the literature.
- **Ability to generate powder with a suitable characteristics for the SLP process:**

  Particle size/morphology – To enable an appropriate Q/m value and flow properties, which are compatible with the current SLP1 rig, to be achieved. Previous work by Jones and Banerjee [5, 141] has indicated particles should be in the range 20-50µm to produce an adequate layer thickness without compromising resolution or the build speed. In addition, the toner is to be broadly spherical in shape, i.e. potato shaped [149] in order to achieve a balance between flow and charging. This is explained in more detail in section 3.4.

  - *Melt Temperatures* – This will be limited by the potential thermal degradation of the photoreceptive coating on the OPC during the fusing process. A thermal limitation of 150˚C will be set on the OPC, this is explained further in section 4.1.

  - *Position in the triboelectric series* – The existing SLP1 rig (to be used in the project) requires negatively charged toners as the printers are currently set up to deposit negatively charging toners.

  - *Dielectric properties* – The candidate engineering polymers should ideally have a dielectric constant similar to a well-established negative charging toner already successfully deposited using the SLP1 printers (2.9-3.9)[150]. This is due to the close relationship the polymer has between the dielectric properties and the positioning on the triboelectric series (see Figure 4:1). With a greater dielectric constant representing a greater positive charging material.

2. Evaluate methods for producing the powder with the required particle size/morphology from the selected polymer. The techniques assessed in the study will include;

- ***Chemical synthesis*** – Developed for the efficient production of fine toners (higher resolution/thinner printed layers) based on a polymerisation process, the precipitation of powder from a polymer. A process that is rapidly replacing mechanical methods for the production of conventional toner production for printing applications.

- ***Mechanical reduction*** – A traditional technique used to produce toner material for electrophotography, albeit from relatively brittle polymer formulations, based on comminution from granules powder feedstock. Previous work by Banerjee[58] has shown has shown the grinding efficiency of a tough engineering polymer is very poor. For this reason, an advanced mechanical reduction method is proposed. The chemical synthesis method and the advanced mechanical reduction method will be compared.

- ***Particle size distribution*** – Ascertain the size and distribution of both the mechanically reduced and chemically produced powders via laser diffraction. Removal of both oversized and undersized powders is to be undertaken where necessary.

3. Develop and test toners produced from the polymeric powders – materials will be evaluated using an existing dual component printer rig (SLP1) to establish the most appropriate printing parameters based on the transfer efficiency. The key steps that will be followed are;

- ***Select a suitable carrier*** – A carrier will be paired with the polymeric powder to achieve a Q/m sufficient to promote efficient toner charging and stripping.

- ***Flow and charge properties*** – Based on the Q/m ratio for the powder generated from engineering polymers an appropriate charge control agent is to be applied to the particles and tested. A charge control agent may be used to impart the required flow properties for the material as well as govern the Q/m. A Q/m in the range of ±5 – ±25μC/g [67, 149, 151] is sought since a value greater than 25μC/g would cause great difficult in stripping the toner off the carrier. Conversely, a Q/m below 5μC/g would have poor adhesion with the carrier. This is explained further in section 4.3.

- ***Transfer voltage*** – The toner is to be transported from the developer to the substrate via the OPC and transfer roller (see Figure 7:10 for schematic layout of printer). Trials are to be conducted to identify the correct transfer voltage to enable the most efficient toner transfer.

- ***Fusing*** – Assess the fusing characteristics of the polymer using information obtained from the literature.

- ***Pressure and stand-off distance*** – Assess the effect of applied pressure stand-off distance and fusing temperature from the heat source concurrently.

4. Assessment of the fusing characteristics of the developed toners and mechanical properties of 3D samples produced by the SLP process from the new toner material.

- ***Multi layer printing*** – Undertake multi-layer deposition trials to generate samples, which will be used to measure the mechanical properties of the sintered layers.

- ***Mechanical analysis*** – Carry out an analysis of the SLP generated samples to obtain mechanical properties.

- ***Factor interactions*** – Assess the interaction between temperature, pressure and stand-off distance in order to identify the optimum interaction parameter.

4.1 Review of engineering polymers

Mechanical properties of the polymeric material are an intrinsic part of the study. Traditional toners materials are chosen primarily based on their low impact strength and low thermal fusing temperatures [37, 56, 57, 95]. Conversely, Additive Manufacturing (AM) applications often require a polymer that is able to withstand high temperatures and possess good impact, tensile and elongation properties. This notion has been echoed by many researchers [2, 4, 5, 94]. In addition, the candidate polymer must have the ability to be transferred via a biased electrostatic field.

Particle size is paramount in laser printing. Previous research [4, 5] has indicated toners, for the SLP process, are to be in the size range between 20-50µm to allow for a greater build up layer thickness, while preserving the resolution of the printed layer. Morphology also plays an integral role in both the flow and charging capabilities of the toner particles.

Mechanically milled toners are known to have favourable charging characteristics due to their multiple contact points as a result of the irregularity from the reduction technique [37, 76], albeit at a detriment to the flow properties of the toner. As a result, the toner is required to be surface coated with a flow control agent. Chemically produced toners suffer far less with flow issues, although, due to their high circularity factor, they experience inadequate charging. To ensure appropriate charging between the toner and a select carrier, the toner should be manufactured using a chemical production method capable of producing potato shaped or non-spherical toner. Employing a mechanically milled process, the toner should be coated with an appropriate flow control agent.

The melt temperature of the polymer is also crucial to part production. A material should be tough but not possess too high a melt temperature. The deposited material is fused by melting, using a radiant infrared (IR) heater. Damage can occur to the OPC with prolonged contact with materials above 180˚C [152]. For this reason the melt temperate of the polymer should be below 150˚C to preserve the OPC.

The SLP1 printers utilise negatively charging toners. As such, the materials are to be based on negatively charging materials. This is to be carried out by consulting a triboelectric series. The candidate material should ideally be placed mid range on the negative scale of the triboelectric series to allow for the surface charge to be manipulated to increase or decrease the negative charge with the carrier should the need arise. Ideally, the candidate material should have dielectric properties close to a standard negatively charging toner. Scharfe [42] has demonstrated that the dielectric properties have a close relationship to the location of the material on the triboelectric series (see Figure 4:1) with a higher dielectric constant of the polymer representing a greater tendency to charge positive. This is further exaggerated with the influence of humidity producing a more conductive surface. This is discussed in more detail Section 3.3.3.

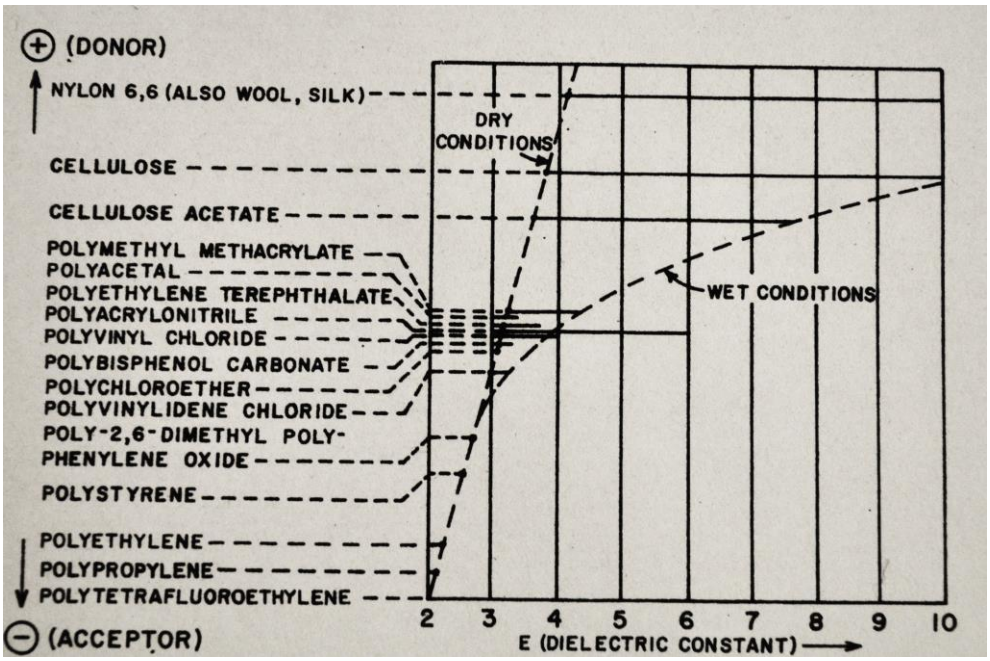

Figure 4:1: Triboelectric series with dielectric constants[42]

4.2 Evaluation of powders

After a suitable material, which satisfies the aforementioned criteria, has been selected the issue of powder production must be considered. Table 4:2 shows the contrasting properties between standard laser printing toners and toners required for AM toners.

Table 4:2: Conventional toner versus Additive Manufacturing

Properties	Conventional toner	AM toner
Mechanical properties	Brittle	Tough
Size	5-20µm	20-50µm
Temperature	>60˚C	<100˚C

A number of chemical production methods are presented in the literature survey. From the methods available, Evaporative Limited Coalescence (ELC) will be employed in the

study. Evaporative Limited Coalescence was selected due to its ability to convert any polymer that can be dissolved in a solvent.

Toner manufacturing via chemical production requires a greater investment of both capital and research compared to mechanical milling. It has taken a while for industry to adopt the chemical route. The process is generally applied to the production of high volume toner products. One of the key drivers for the take up of the technology is the increase in print resolution, typically to 1200-2400 dpi, which requires finer toner particles that can be produced more efficiently by chemical rather than mechanical (comminution) methods – even advanced methods based on cryogenic milling [107].

In the study, the ELC process will be compared with mechanical methods of particle reduction to assess the efficiency between each process. Mechanical grinding trials will be conducted in both an ambient and cryogenic environment (low temperatures have been shown to significantly aid particle reduction[107, 110, 111, 114, 153]).

While both methods will invariably produce different particle size distributions (PSD), each will be assessed via a diffraction method employed by the toner manufacturing industry[4, 5, 56, 93]. After a PSA has been conducted, the toners will be classified, where necessary. Ideally, toner would be a fixed size rather than cover a size range. However, to produce a toner in a single size is impractical on a commercial level. Alternatively, the toner would require a very tight size distribution allowing the Q/m to be better managed. The scatter plot (Figure 3:16) shown in Section 3.3.7: Toner size (pg 38) demonstrates how change in the particle size can affect the Q/m.

In the interest of producing a commercially viable engineering based toner, the SLP1 rig will employ a toner with a particle range between 20-50µm. This will also allow the toner size range to strike a balance between resolution and layer build up [5, 58] as using a standard toner with its thin layers would severely limit the speed of SLP process.

In order to achieve this, the toner will be screened to remove the fines (undersized) and oversized particles. Oversized particles can cause abrasions to the surface of the OPC causing subsequent prints to suffer in quality. Undersized toners can suffer from hot offset [5, 154] (caused by heating the toner and it back transferring on to the fuser roller and OPC). For the reasons outlined above, particles greater than 50µm and below 20µm are to be removed to avoid damage to the printer components.

4.3 Toner development and print optimisation

The powder flow and charge characteristics are important factors for performance. Generally, mechanically milled toners require a flow control agent (FCA) to reduce the friction between particles[149]. A Q/m is conducted prior to the addition of the flow control agent due to the FCA also imparting a charge. A Q/m is carried out to assess the charge magnitude with the chosen carrier. A number of carriers will be trialled with the carrier selected based on the charge magnitude and percentage of toner being able to charge to the magnitude. A Q/m range between -5 to -25µC/g will be used as suggested by the literature [42, 67, 149, 151] as increasing the Q/m would require greater field strength at each transfer stage. A reduced Q/m would lead to a weak bond between the carrier and toner and the transfer efficiency would drop.

When the correct Q/m has been achieved, the toner concentration is to be found. The carrier surface is required to be encapsulated with as much toner as possible. Incorrect toner concentration can lead to problems during the printing phase. For instance, a carrier with a low toner concentration will reduce the amount of toner that is brought to the OPC. This lack of toner will invariably result in a lower density print, which in the case for AM parts, leads to either a thinner cross section or a lower density in regions of the printed cross section. A developer with a high toner concentration will cause dusting, leading to printer damage and poor printing output[149, 152]. As such, the correct concentration is crucial in maintaining a fully functional printer and preserving

the layer thickness. The toner is to be added in concentrations from 5% (by weight) upward and tribocharged in a manner describe by the literature[5, 152] as successfully employed by Banerjee. The developer is observed under an optical microscope with an appropriate contrasting substrate to determine the ideal toner concentration. A carrier with a high toner concentration will show loose powder on the substrate as well as the carrier fully covered. See Figure 6:13 in Section 6.2.1: Carrier pairing and printer voltage settings (page 175) for details.

After obtaining the correct Q/m and toner concentration, the voltage to allow for the successful and efficient transfer of toner from the developer unit to the transfer roller is required. The AM toner will require a specific voltage, due to the manufacturing process, surface additives and material type. As the AM toners are completely new, voltages from an established toner should be used from previous research[5]. This will form the basis and the toner transfer voltage can be adjusted at every subsequent station thereafter.

Fusing trials will be required to consolidate the layer. Analytical methods, such as differential scanning calorimetry (DSC) will be employed to obtain a precise melting temperature of the polymeric toner. Carrying out an on rig experiment will confirm whether the results corroborate will the results from the DSC.

Pressure is thought to be intrinsic in creating a fully consolidated structure using an AM based electrophotographic system[2, 4, 8, 9, 12, 14, 49, 94, 141, 155]. A pressure reading of the standard applied load is to be found, this will form the initial pressure. Pressure sensors will be used to set up the initial pressure and record real time pressure exerted during the printing process.

The stand-off distance will be set according to a well-established approach employed by Banerjee and Jones [4, 5]. An IR unit is to be placed above the substrate in a customised housing. The IR housing has predrilled locations, which allow for the height of the IR unit

to be adjusted manually. As the height of the IR unit is dependent on the distance from the substrate, the pressure is to be set preceding the height adjustments.

4.4 Assessment of the fusing characteristics

Supported by information from the literature, the melting point of the material, empirical fusing trials using the SLP1 rig will be conducted. A detailed design of experiments is presented in Chapter 5. A three factor with three levels, full factorial design will be employed to observe the interaction between the key parameters;

1. Temperature,
2. Pressure
3. Stand-off distance.

- **Temperature** – The temperature is to be adjusted to below the maximum allowable temperature of the OPC. For this reason, when the fusing temperature has been found, the temperature shall have a deviation of 10˚C between each level and shall be at a safe temperature below the degradation temperature of the OPC (180˚C). Due to the envisaged prolonged contact of the OPC the maximum temperature will not exceed 150˚C

- **Pressure** – The initial pressure is to be found using the paper test as described in Section 5.3.7. Once the standard pressure has been found, load increments of 2N will be increased between each level. The 2N increase has been selected to avoid damaging the transfer roller and printer, as advised by the machine manufacturer.
  As the load is applied, by setting the platform at a raised level prior to the printing trials, damage to the transfer roller can occur in the form of leaving an impression, indentation or even incisions on the transfer roller. The increase distance can, in turn, lead to a reduced amount of toner transfer.

- **Stand-off distance** – The stand-off distance will be set using the approach developed by Banerjee[4]. An infrared (IR) heater will be positioned at a known distance from the platform by setting the IR heater in one of the three pre-determined positions.

4.5 Mechanical property assessment

Jones [5] has shown the SLP rig to print five layers consistently without adverse effects to the layer deposition rate and integrity. A sample comprising of five layers will be printed, with three samples per experiment, to provide sufficient data whilst enabling the limited experimental toner available to be preserved for all the test parameters of interest to be evaluated.

The samples will be printed to cover the entire surface of the substrate to ensure transfer issues are properly evaluated, as well as enabling removal of the sample from the substrate without damaging it. Due to the limited thickness of the samples DMA will be employed to assess the mechanical properties. In addition to the assessment of the physical and mechanical properties, interaction between the factors will also be evaluated. Determination of the statistical significance as well as the correlation between the factors will be assessed.

5 Experimental

This chapter describes the details of the experiments conducted. The chapter has been split into the following sections to reflect the key activities;

- Material selection
- Toner Manufacturing
    - Mechanical methods
    - Chemical methods
    - Summary of the two techniques

The chapter will converge to outline further experiments in which both chemical and mechanical toners will follow the same set of experiments;

- Printer set-up and material optimisation
- Printing
- Mechanical analysis
- Chemical analysis

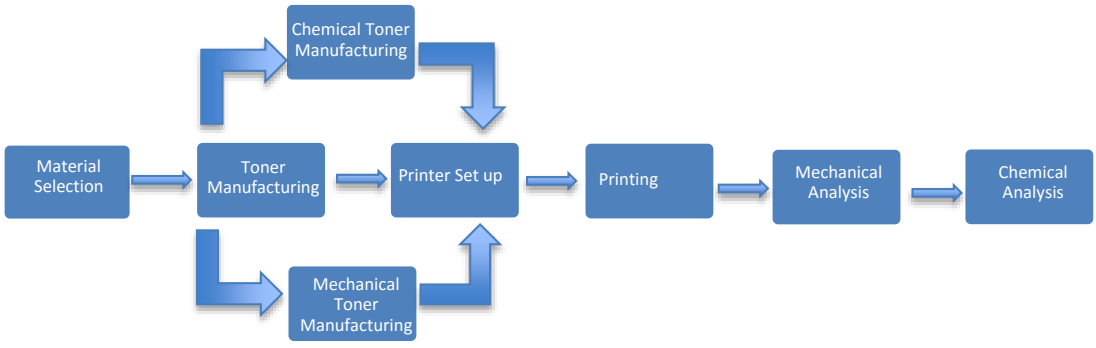

Figure 5:1: Flow diagram of experimental procedure

5.1 Material selection

In addition to selecting an engineering polymer with suitable mechanical properties, the material selected should also have the desired characteristics for production of a toner (this is explained and justified in Section 4.1: Review of engineering polymers).

The requirements are summarised below;

- Polymer initially in a coarse powder form with a negative charge
- Capable of generating powder with a particle fraction between 20-50µm
- An engineering polymer with a melt temperature below 200˚C
- An engineering polymer that is comparable or exceeds the mechanical properties of traditional SLS and/or FDM parts.

Tribocharging: Polymers in a powder form are not particularly common. The reason stems from the low demand of the polymer powder, which does not warrant the additional comminution steps or chemical production techniques to produce a finer powder. Due to this reason, only a small number of polymers could be sought and tested. A list is compiled of the possible polymers (negatively charging) for use as a toner based on the triboelectric series is given in Table 5:1.

Table 5:1: List of polymers with their respective properties

Material supplier & designation		Supply form (D_{50} in µm)	T_m/*T_g (˚C)	Tensile modulus (MPa)	Dielectric Constant
PEEK	Ketaspire KT 880FT	36	343	3700	3.3
	Vicote 702	50	343	3700	
PES	2020 SR Micro	50	225	-	3.5
PTFE	Algoflon L101-1	3.5	332	44	2.0-2.1
PAI	Torlon AL-30	100	250	-	3.9
	Torlon AL-50	50	250	-	
	Torlon 4000TF	50	250	146	
ABS	Magnum 8391	420	*99	2340	2-3.5
	Polylac PA-757	380	*101	36.2	

Melting point: A number of potential toner materials were rejected due to their high melting point, see Table 5:1. Based on this analysis it is clear that acrylonitrile butadiene styrene (ABS) is the most suitable material for the trials, highlighted in yellow.

5.2 Toner manufacturing

Toner manufacturing using chemical and mechanical methods was explored. This section will describe the procedure used for the trials.

5.2.1 Chemical Manufacturing of Toner

5.2.1.1 Polymerisation of Styrene

A starting point for the polymerisation trials begins with polystyrene due to its long history of synthesis. In addition, polystyrene allows a wide range of techniques that can be applied for successful synthesis of micron sized powders. Moreover, polystyrene is an established material used in Laser Sintering applications as well as an established toner material. Furthermore, polystyrene, a constituent of ABS, will be used as a stepping stone towards the production of ABS toner, enabling the difficulty of conducting the polymerisation process to be gauged.

A chemical polymerisation test rig was designed based on information from the literature [7, 156]. The components used to assemble the test rig are listed below;

- Clifton HP1-1D hot plate (Nickel-Electro LTD, UK) with an accuracy of ±0.5°C.
- PT100 closed loop temperature control probe.
- Glass 5 pot reaction vessel.
- PTFE stirring rod and mixing blade.
- Glass condenser to cool the exhaust vapour.
- Variable speed mechanical mixing device.

- Nitrogen gas feed to purge the atmosphere.

A silicone oil bath (containing two litres of PSF-2cSt silicone oil) was placed on top of the hot plate and the PT100 probe placed in the silicone oil bath to regulate the temperature via the hotplate, to between 80-85°C. The reaction vessel was assembled with the condenser and stirring rod (connected to the mixing device). The nitrogen gas feed was connected to the reaction vessel to provide an inert atmosphere during the polymerisation process. The speed of the mixing device was set to ensure homogeneity of the phases and produce the desired particle size. An image of the experimental rig is shown in Figure 5:2.

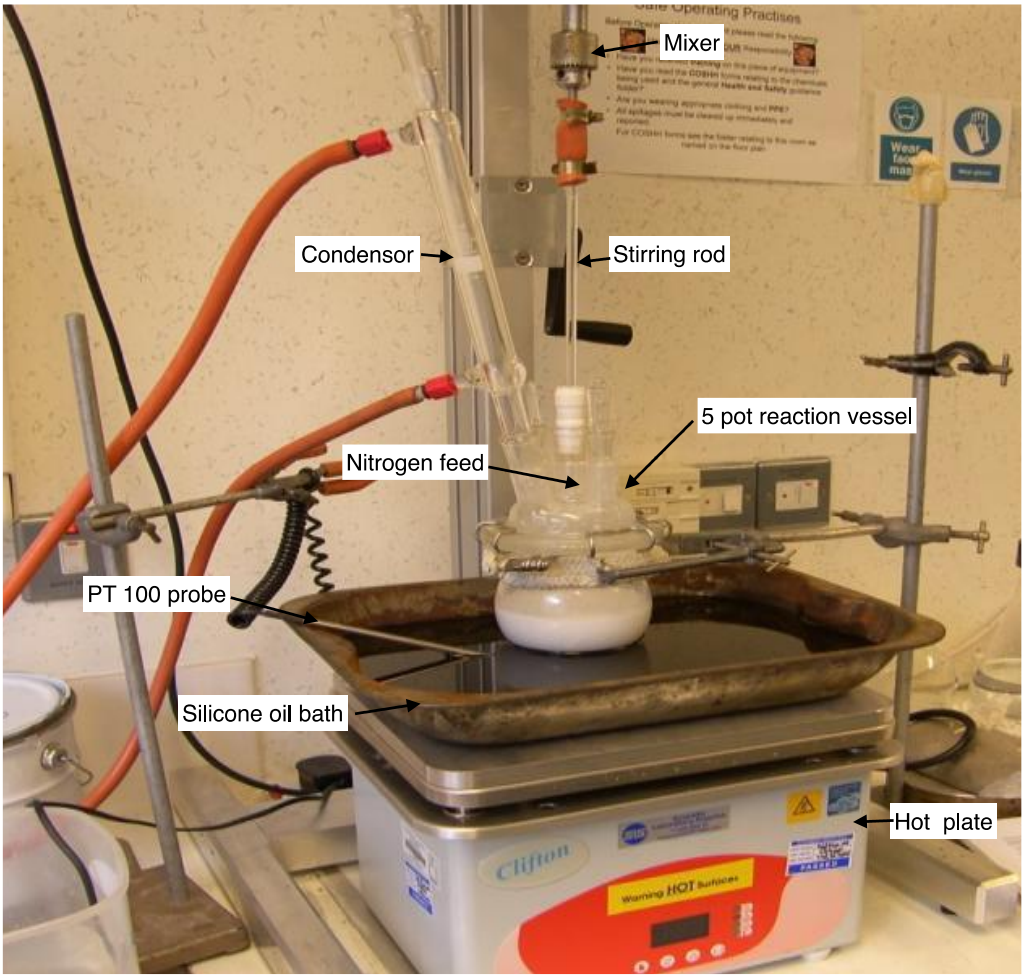

Figure 5:2: Layout of apparatus for the polymerisation of styrene

Table 5:2: Table displaying materials and equipment

Item	Designation	Supplier / other information
Styrene monomer	Reagent Plus, (Containing 4-tert-butylcatechol inhibitor)	Sigma Aldrich, Missouri, USA
Initiator	Benzoyl peroxide	Sigma Aldrich, Missouri, USA
Surfactant	Evo-bond PVA	Evo-stick, St Denis, France
Alumina filter bed	4-10µm alumina	
Filter paper	Whatman Grade 1 qualitative filtration paper	Sigma Aldrich, Missouri, USA
Precision balance	Ohaus Voyager Pro 613CN balance	Ohaus, New Jersey, USA.
Vacuum pump	Welch 25225C-02 (rotary vacuum pump)	Gardner Denver, Illinois, USA
Convection oven	Genlab, Mino/18	Gernlab Ltd, Cheshire, UK
Electron microscope	Zeiss Evo HD15	Carl Zeiss Ltd, Cambridge, UK
Particle size analyser	Cilas 990 0.2-500µm size analyser	Cilas, Orleans, France

Dispersion Phase: The styrene monomer was filtered through an alumina (100-200µm) powder bed suspended over a filter paper to remove the 4-tert-butylcatechol inhibitor[56]. The monomer was then weighed using a precision balance. The initiator was added at the quantity specified in Table 5:3 and dissolved in the purified styrene monomer. The details of the materials and equipment used are shown in Table 5:2.

Continuous phase: The continuous phase was produced from distilled water and a surfactant – both were carefully weighed using the precision balance based on an existing formulation[156] (see Table 5:3). The distilled water was heated via the hot plate. A small amount of the heated water was added to the PVA to accelerate the diffusion process, creating a fully dissolved solution. The dissolved solution was added to the remaining heated water in the reaction vessel to create the continuous phase.

The weights for the dispersion and continuous phase are added as shown in Table 5:3 and are referenced in g/mol.

Table 5:3: Polymerisation Experiment 1 recipe

Phase	Weight (g/mol)
Dispersion Phase	
Styrene Benzoyl Peroxide (BPO)	0.214 0.45×10^{-3}
Continuous Phase	
Distilled water PVA	13.87 22.7^{-3}

Polymerisation: The dispersion phase was added to the continuous phase in the reaction vessel and homogenised using a paddle stirrer, rotating at 4400RPM for 10 minutes, whilst being continuously heated to initiate polymerisation. Once both the phases were homogeneous, the mixture was left to polymerise for 12 hours with no further agitation.

Powder recovery: When the polymerisation processes was complete, the recovery of the precipitate was undertaken. The precipitate, along with the continuous phase was poured into a funnel lined with one layer of filter paper. A slight vacuum was applied to the outlet of the funnel, via a trap, for 1-2 minutes until the solution had been completely expelled and there was no further solution being drawn into the trap. The precipitate was placed in a convection oven for six hours at 30˚C. The precipitate was observed under an electron microscope to assess particle size and morphology. The results are reported in section 6.1.

The procedure described above was repeated for two further polymerisation experiments, PE2 and PE3, and is described below.

PE2: The Polymerisation experiment was repeated, however, the weight of the initiator was doubled to $0.9x10^{-3}$g/mol and the mixing speed was reduced to 1500RPM (as shown in Table 5:4) as the literature indicates that by increasing the initiator a finer powder be synthesised, without the need to increase the mixing speed[156].

Table 5:4: Polymerisation experiment 2 recipe

Phase	Weight (g/mol)
Dispersion Phase	
Styrene Benzoyl Peroxide (BPO)	0.214 0.9×10^{-3}
Continuous Phase	
Distilled water PVA	13.87 22.7×10^{-3}

PE3: A final polymerisation experiment (PE3) was carried out. Using the original recipe from PE1, the weight of the surfactant and initiator are doubled to 0.9×10^{-3} and 22.7×10^{-3} g/mol, respectively, from the original recipe in Table 5:3. All remaining components were kept the same as PE1. The mixing speed was set to 1700 RPM to homogenise the two phases. The changes to the composition and mixing conditions stem from the recommendations made from the literature, where the increase in mixing speed, can assist in yielding a finer particle size[156].

Table 5:5: Polymerisation experiment 3 recipe

Phase	Weight (g/mol)
Dispersion Phase	
Styrene Benzoyl Peroxide (BPO)	0.428 0.9×10^{-3}
Continuous Phase	
Distilled water PVA	13.87 45.4×10^{-3}

5.2.1.2 Chemical production of ABS

A scoping trial was undertaken to manufacture 35µm (D_{50}) particles using ELC. Firstly, 30g of ABS (Dow Magnum 8391, Dow Chemicals, MI, US) powder with D_{50} of 420µm was dissolved in ethyl acetate at 18% by weight.

The emulsion was combined with an aqueous phase consisting of silicon buffers and carnauba wax stabilisers. Using a proprietary "shape solution" procedure, particles can be produced to the desired shape and size [124]. This method reduces the risk of particle agglomeration during evaporation of the solvent to leave the precipitated particles. The precipitate is filtered and then washed and dried to remove the buffers and stabilisers. There is no evidence that the ELC process has ever been used to produce such large toners and this is particularly novel in the context of an Additive Manufacturing application.

In order to study the morphology and the particle size, an analysis was performed using a Coulter MultiSizer 2 (Beckman Coulter, California, USA) and Scanning Electron Microscope (SEM).

Once the appropriate process parameters, required to produce powder in the desired particle size range, were established they were used to produce a large trial batch of material (4.5kg). Due to novelty of generating ABS toners using the ELC route and the significant commercial potential arising from this development, the parameters used to produce the chemically produced ABS toner cannot be shared. However, the methodology for developing the parameters is described in Section 3.4.2.3: Evaporative Limited Coalescence.

5.2.2 Mechanical Milling of the Toner

This section will aim to explain the methods undertake to convert a large polymeric particle into a fine particle to the size as outlined in section 4.

5.2.2.1 Ambient grinding of ABS polymer

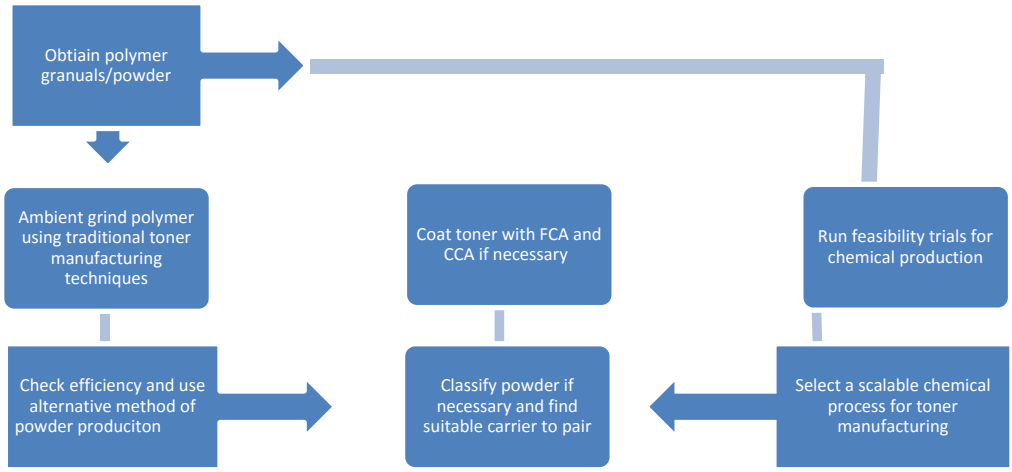

Figure 5:3: Flow chart for the production of fine polymeric powders and toner manufacturing

Based on the results of previous work [58] it was decided to utilise specialised industrialised mechanical milling methods to produce the powder for the trials. Ten kilograms of coarse (D_{50} of 420µm) ABS powder (DOW Magnum 8391, Dow Chemicals, MI, US) was supplied to Hosokawa Micron Ltd. (Runcorn, UK). Although the company has significant experience in the production of polymeric powder from coarse feedstock it had not successfully produced fine powders (below 50µm) using tough engineering polymers before.

The coarse ABS powder was reduced to a D_{50} of 35µm using an impact mill (Hosokawa Micron LTD, UK) fitted with a 50 ATP classifier with a 100µm gap for screening the material. One kg of the ABS powder was processed at ambient temperature for one hour

in the impact milling machine, rotating at 18,000 RPM. The grinding efficiency was analysed using a particle size analyser (Malvern Mastersizer 2000, Malvern Instruments Ltd, UK). The particle size distribution (PSD) of the Magnum 8391 ABS material was assessed before and after impact milling.

5.2.2.2 Cryogenic grinding of ABS polymer

In addition to mechanical milling trials at room temperature cryogenic milling trials were also performed at Hosokawa and Fraunhofer UMSICHT.

5.2.2.2.1 Hosokawa

One kg of ABS powder (Polylac PA-757, Chi Mei Corporation, Taiwan) with an initial D_{50} of 380µm was used. The same milling equipment and procedure was employed, as the ambient trials (described in Section 5.2.2.1) but the powder was cooled in liquid nitrogen for 20 minutes prior to the milling operation. In addition, liquid nitrogen was poured in to the mill at the beginning of the comminution cycle. The nitrogen cooled polymer was milled for a period of one hour.

5.2.2.2.2 Fraunhoffer

Final comminution trials were carried out by Fraunhofer UMSICHT using liquid nitrogen as the cryogenic medium. The machine setup at Fraunhofer consists of a two-phase cooling system, as explained in the literature review (section 3.4.1). Ten kilograms of ABS powder (DOW Magnum 8391) feedstock was cooled for 20 minutes prior to grinding and then fed in to the grinding chamber. A Gotic DSM 250 rotating pin mill chamber with a constant cooled air jet supply was used with a 100µm gap for screening the reduced material. The material was classified into <100µm and >100µm with a particle size

distribution carried out for the powders below 100µm using a Malvern Mastersizer 2000.

5.3 Print set up and optimisation

5.3.1 Carrier pairing

Using a triboelectric charge analyser from Torrey Pines Research (TEC 3 Tribo tester, Torrey Pines Research, New York, USA) the charge over mass (Q/m) was tested against three carriers to obtain the optimum Q/m. The carriers were received from Powdertech Inc. (Powdertech International Corp. Kentucky, USA). Each carrier has a polymer coating imparting a positive or negative charge, depending on the toner being paired. Table 5:6 below shows the carrier identity and its respective polymer coating. In the interest of confidentiality, the exact polymer coating has been kept anonymous, however, a brief description of the polymer has been divulged.

Table 5:6: Polymer coatings on carrier

Carrier Identity	Polymer shell
C1	Silicone
C2	Acrylic
C3	Fluoropolymer

Three carriers were selected with three different surface coatings suitable for charging with each of the toners. A sample of the developer was produced by weighing 45g of carrier to 5g of toner using a precision balance to make a 50g sample with a 10% by weight concentration of toner. The developer was placed in a glass jar and tumbled in a Wheaton bottle roller (Wheaton, New Jersey, USA) at 45 RPM for 15 minutes until the developer was homogenised. This process was repeated for all three carriers in order to

find the most efficient Q/m between the carrier and toner for both the chemical and mechanical toners.

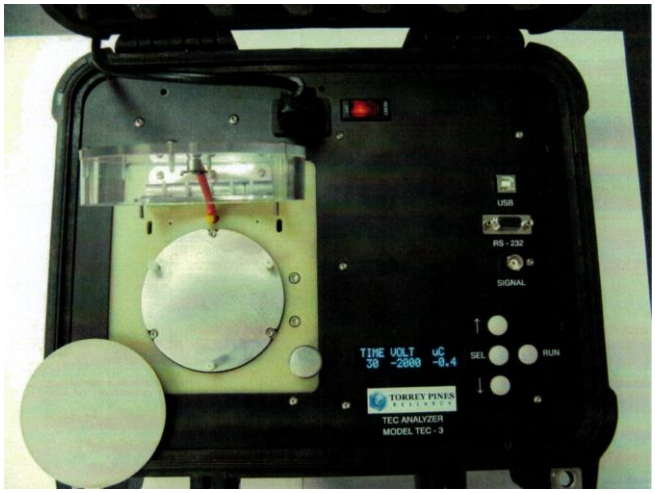

Figure 5:4: TEC-3 charge analyser from Torrey Pines Research

Using a TEC -3 triboelectric charge analyser, a Q/m was conducted for the two ABS toners. The carrier was selected based on the toner exhibiting the most efficient Q/m range and percentage of the toner within the range (see Section 3.3.2)

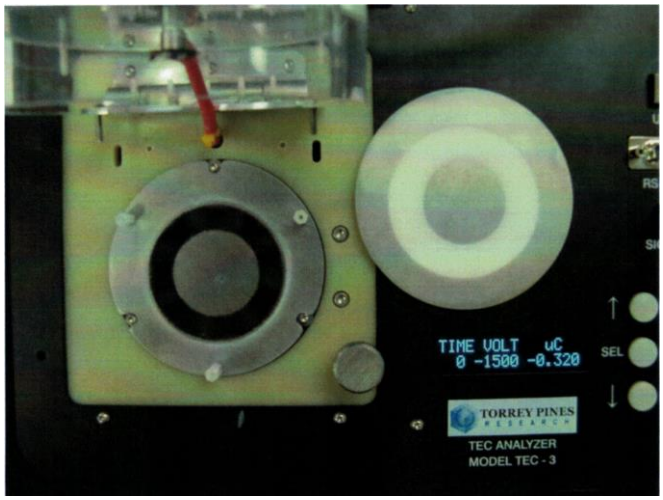

Figure 5:5: Magnetic plate with black ring (left) and charge plate with white ring (right)

The lower plate is weighed and the balance zeroed. The precise amount of the developer, as specified above, is placed on the lower plate. The upper plate (left of Figure 5:5) is weighed, noted and placed on the three insulating spacers on the lower plate. Once the two plates are aligned and in position the lid is closed and 2000V (polarity dependant on toner being tested) is applied across the plates. The rotating multi-pole magnets cause the developer to be agitated, while the induced field detaches the toner from the carrier and onto the charge (upper) plate. The process is continued for 60 seconds. The experiment is stopped and the charge reading in µC measured by the unit is recorded.

The upper charge plate is removed and weighed to establish the amount of toner transferred by subtracting the weight of the original plate. The charge per unit mass or Q/m is derived using Equation 7.

$$Q/m = \frac{C}{T_{up}} \qquad \text{Equation 7}$$

Where:

C is the charge recorded on the display

T_{up} is the weight of the toner on the upper plate (discounting the weight of the plate)

5.3.2 Developer ratio and mass

Once a suitable carrier was selected an experiment was conducted to determine the appropriate carrier to toner ratio. Developer (toner + carrier) samples were produced with toner concentrations of 5, 6, 7, 8, 9, 10 and 12% by weight. Ten grams of each sample was carefully measured with a precision balance and placed in a glass bottle, which was placed on a bottle for 15 minutes to homogenise and create a charge

between the fine powder and carrier. Using a Leica DM750 light Microscope (Wetzlar, Germany), the charge magnitude was assessed visually by observing the attraction between the carrier and toner and residual toner on the contrasting surface of the substrate. The amount of toner electrically charged with the carrier is dictated by the attractive force between the toner and carrier and the concentration of toner to carrier. A well charged developer will show a carrier surface completely covered with toner and little to no toner on the contrasting substrate.

Once the ideal toner to carrier concentration was achieved the toner to carrier ratio was used to produce 1.6kg of developer. The developer was placed on the bottle roller for 15 minutes at 45 RPM to tribocharge the carrier and toner.

When the developer showed a homogenised colour, denoting a sufficient charge, the developer was placed inside the reservoir of the developer unit and sealed shut. The doctor blade gap was measured using a feeler gauge and increased to accommodate the larger particle size for the experimental developer. The magnetic roller was turned to produce the brush, or coating, on the magnetic roller. Once an acceptable brush (continuous, dense and even coating) was achieved the developer unit was placed back in the SLP unit.

5.3.3 Differential Scanning Calorimetry of toner

A differential scanning calorimetry (DSC) was conducted to ascertain the T_g for the mechanical and chemical toners. Using a Mettler AT261 balance (Mettler-Toledo Inc., Ohio, USA) the toner was weighed (see Table 5:7) and placed into aluminium pans and sealed by crimping. The pans were placed in a Perker Elmer Jade DSC machine (Perker Elmer Inc., Massachusetts, USA). Prior to being placed in the machine, the pans were pierced to avoid bursting during the heating cycles. The DSC was run at three ramp rates; 10˚C/min, 20˚C/min and 30˚C/min from 25˚C to 250˚C and back to 25˚C. Once the

experiments were complete, the software was used to calculate the T_g from the curves. The DSC would provide a definitive answer to the T_g of the material. The results are to be used during the printing of the toner.

Table 5:7 : Weights of pans corresponding to DSC ramp rates

DSC ramp temp (˚C)	10˚C/min	20˚C/min	30˚C/min
DMU130725RB (Chemical toner)	3.87g	3.25g	3.96g
DMU130625RC (Mechanical toner)	7.18g	8.65g	8.65g

5.3.4 Surface additives

The toner was sent to Zorbrist Engineering (Neuenhof, Switzerland) to select an appropriate surface additive to improve the flow of the cryogenically ground material. HDK 2000/4 silica from Wacker (Munich, Germany) was added at 0.3% by weight to the mechanically milled toner and shear mixed for five minutes.

5.3.5 Machine equipment

The SLP rig was developed with support from the EU framework 6 Custom fit project (No: 507437). The rig was a collaborative activity between Renishaw AMPD PLC (formally MTT Technologies), De Montfort University, UK, Marcam, GmbH (owned by Materialise), and CTG PrinTEC GmbH. Since then, the research into toner development has been a collaboration with Renishaw AMPD PLC, Renishaw PLC and De Montfort University with funding provided from The UK Technology Strategy Board under the SPRINT project (project number: 100735; TP number: TP14IHVM/611IBD219A). A photograph and a schematic diagram of the rig, showing the primary and secondary platforms along with the relevant sections at which the platform stops, can be seen in Figure 5:6 and Figure 5:7 respectively.

Figure 5:6: SLP rig

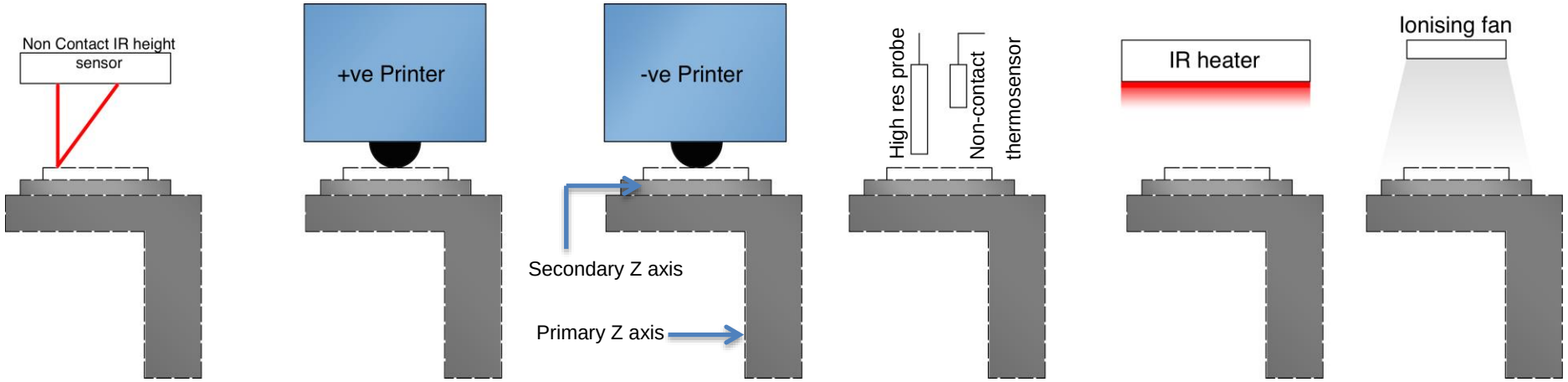

Figure 5:7: SLP rig schematic and the platform with the primary and secondary Z axis

The heart of the process are the printers from CTG PrinTEC. The printers were originally built to deposit negatively charging toners. One printer was converted to enable printing positive toners due to the developments encountered during the project. Additionally, this opened up the flexibility to using any polymer on the triboelectric series. The printers were based on a larger CTG900 printer (900mm photoconductor). De Montfort commissioned two CTG-1C17-600 printers with a 413.8mm (17”) photoconductor.

Marcam developed the interface responsible for producing 1-bit uncompressed bitmaps at 600DPI resolution to the CTG printers.

Renishaw responsibilities rested on the fabrication of the rig. The primary Z platform is transported on a 6 meter ball screw driven along the X-axis. The primary Z platform would make the coarse movements along the Z axis. Additionally, a secondary Z platform was fitted to the primary Z platform to allow for 10µm incremental movements allowing for more control during the pressure set up (see Figure 5:7).

Incorporated into the secondary Z platform was a set (three off) pressure sensors. The platform was fitted with a unidirectional gimbal design to allow the platform to be adjusted to provide full contact with the transfer roller of the printer. Under the gimbal were located three 500N load cells to measure the real time applied load. The output from the load cells was converted using the digitiser and RS323 cable. Freeware data logger software from Mantracourt Electronics Ltd was used to record the data readings.

Table 5:8: On rig equipment

Item	Designation and spec	Supplier
Ionising fan	KS21H	Killstat, UK
IR heater		
Heat sensor	ES1B Infrared thermosensor	Omron, Japan
Probe	6000B- 5C high resolution probe	Trek Inc, NY, USA
Electrostatic volt meter	347-3-H-CE Voltmeter	Trek Inc, NY, USA
Printer	CTG-1C17-600 (17" photoconductor 600DPI Led print head) for negative toners	CTG GmbH, Dusseldorf, Germany
	CTG-1C17-600 (17" photoconductor 600DPI Led print head) for positive toners	CTG GmbH, Dusseldorf, Germany
Non-contact height measuring	ZS- HLDS10-2M	Omron, Japan
Pressure sensors	CDFM3 500N load cells	Applied Measurments Ltd, Aldermaster, UK
Load cell digitiser and housing	RS323 DSC	Applied Measurments Ltd, Aldermaster, UK
RS323 to USB cable	USB-RS232-WE-1800-BT	EasySYNC, Glasgow, Scotland
Software	Freeware data logging software	Mantracourt Electronics Ltd, Exeter, UK
Primary Z	Motor with 1mm resolution displacement	Renishaw AMPD
Secondary Z	Motor with 10µm resolution displacement	Renishaw AMPD

A circular recess 94mm in diameter and 1.75mm deep was machined into a Macor machinable glass ceramic sheet (150x150x12mm). A further channel, measuring 10mm wide by 0.5mm deep, was also cut into the ceramic to accommodate a brass electrode to charge an aluminium plate (charge plate). An aluminium plate 93mm in diameter by 1mm thick was cut to act as the charge plate. A ceramic substrate with a PTFE coating

on one face was placed on top of the charge plate to form the charge plate assembly. The charge plate assembly was placed into the recess in the ceramic plate and in contact with the electrode as shown in Figure 5:8.

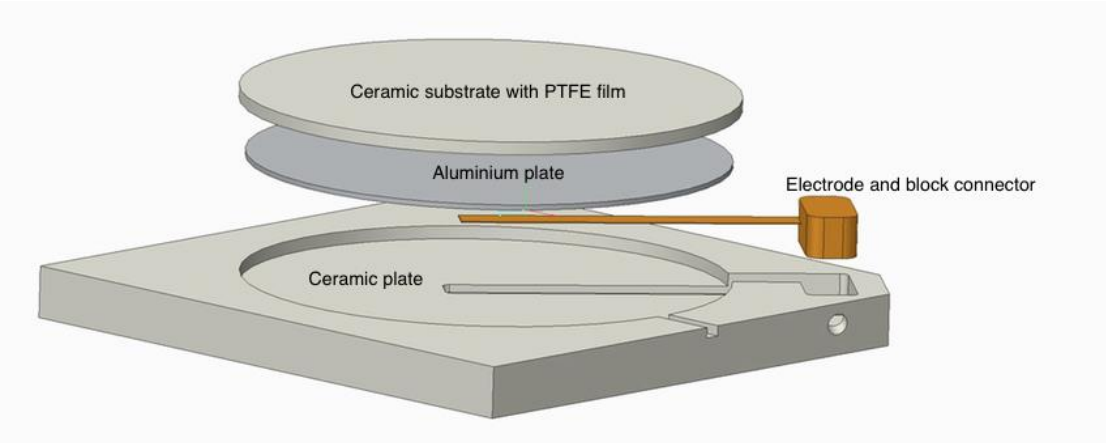

Figure 5:8: Charge plate assembly with ceramic plate

A power supply with a high voltage (HV) cable was used to ensure no breakdown of the sheath would occur during operation. The HV cable was attached to the block connector situated in the ceramic holder using a banana connector to accommodate ejection and insertion during the printing process without damaging the ceramic plate. The voltage was set to +2500V DC to attract the toner off the transfer roller. Using an electrostatic voltmeter with a high-resolution probe, the surface charge was measured throughout the printing operation.

Table 5:9: List of equipment and materials

Item	Designation	Suppler
Substrate with PTFE film	ADS96R Alumina tile (Ø93.8mmX1mm)	Coorstek, Colorado, USA
CHARGE PLATE ASSEMBLY		
Ceramic plate	Macor machineable ceramic	Corning Inc, NY, USA
Charge plate	Aluminium plate Ø93mmx1mm	DMU
Brass charge electrode	Brass sheet 8mmx5mmx0.1mm	DMU
Connector block	Brass block ceramic holder 8mmx6mm	DMU
Electrostatic voltmeter	347-3- H-CE Electrostatic voltmeter	Trek Inc, NY, USA
Power supply	477-304 high voltage switchable power supply	Brandenburg, Dudley, UK

5.3.6 Printer voltage setting

Using voltage settings established for an existing epoxy toner (Atotech XA 066, Atotec Deutchland GmbH, Berlin, Germany) as the starting point for the trials, tests were conducted to assess the efficiency of transfer for the newly developed ABS toner materials. Table 5:10 depicts the initial voltages applied to the different sections, which can be adjusted to improve the efficiency of transfer.

Table 5:10: Voltage settings for epoxy toner

Printer position	Voltage (V)
Developer bias	300
OPC corona charge	-6000
OPC surface charge	-720
Transfer roller	475

Each of the voltages were fine-tuned by observing the toner transfer at each stage based on a visual assessment of the density until a dense layer was transferred from the OPC to the substrate.

5.3.7 SLP unit set-up

Setting the correct contact pressure is critical – too low and insufficient transfer and poor part density can occur and too high and it can damage the transfer roller. The procedure used to set the pressure is described below.

The platform was brought to the transfer roller by moving to the 'Printer 1' position. At this position the transfer roller is a set distance from the absolute datum ensuring the platform position will always be consistent. Once the platform has reached the transfer roller a 75GSM sheet of paper is placed between the transfer roller and substrate and the platform is raised until there is a small gap (~1mm) between the paper and the transfer roller. Using the secondary Z drive, the gap is reduced in 10µm increments until the paper is gripped slightly by the transfer roller. At this point the pressure exerted on the secondary Z platform by the transfer roller is recorded. Once this setup procedure has been completed the pressure to be used in the subsequent trials has been established. Further trials need not use the method described above (known as the pull test). Instead, the secondary Z can be driven up and a sheet of paper placed on top to continue with the correct gap and the pressure set according to the digital pressure sensors.

5.3.7.1 Heat profile

The output of the infrared radiant heaters must be set to give the required fusing of the deposited layers. To do this the procedure below was used;

Calibration of the ES1B controller;

First, the ceramic substrate with a PTFE coating is placed on the mini Z plate with the temperature of the ceramic substrate monitored. The ceramic substrate is heated under the infrared heater for 30 seconds. The platform was sent to the infrared thermosensor

(ES1B, Omron, Japan) located on the machine and the reading shown compared to a true value from the hand held thermometer (N85FR, Precision Gold, UK) and the value on the ES1B modified to ensure that the required set temperature is achieved (see Figure 5:9).

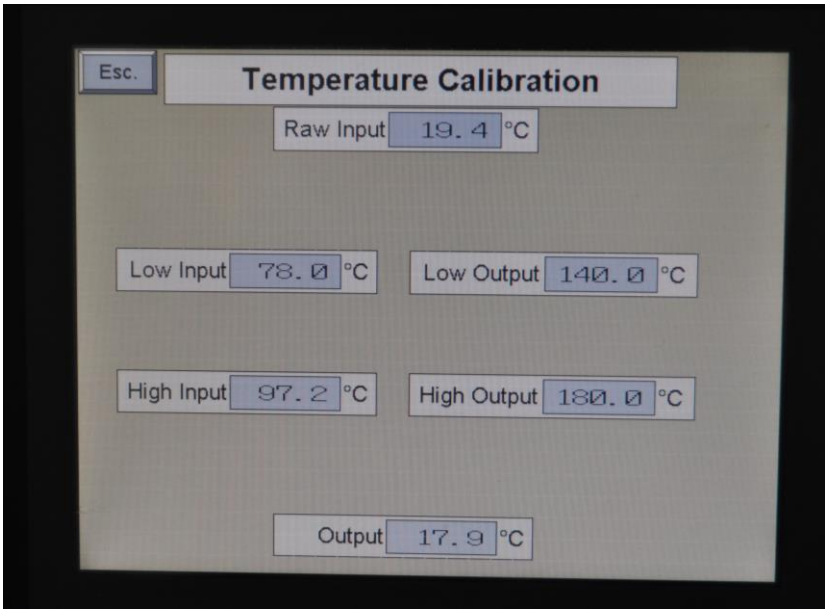

Figure 5:9: On board temperature calibration setting adjustment

5.3.7.2 Temperature set up:

The starting point for fusing the deposited toner is 101˚C, established from the results from the DSC trials (Section 7.4.4). A medium wave IR heater (Flare FSMw, Infrared Systems, UK) was used as a heat source at the standard 105mm stand-off distance (established in earlier work). The settings to control the temperature of the substrate were set to an upper limit of 103.5 and a lower limit of 98.5˚C 9 (on the ES1B, control unit – see Figure 5:9)

5.3.7.3 Print trials to observe fusing

The DSC determined the temperature required to initiate melting of the toner. However, the precise temperature used on the rig is influenced by a number of factors including the pressure applied. Using a starting pressure of 6N with a stand off distance of 105mm from the substrate. A ceramic substrate was placed on the mini Z with the voltage supply on and a print command given. The fusing performance was assessed visually by examining the printed sample for damage during the printing process and the ability to lift the printed sample off the ceramic substrate without breaking. If the layer was inadequately fused, the temperature was increased by 10˚C until the sample was fused using the fixed load and stand off settings.

5.4 Printing

Parameters

A set of factors and levels (see Table 5:11) are placed in a statistical package, JMP (SAS, North Carolina, USA) and design of experiment (DoE) is produced. The values found in Table 5:11 are derived from the results of the experiments conducted in 7.4.5 & 7.4.6. The stand off distance was found using a well established approach employed by both Jones and Banerjee [5, 58].

Table 5:11: Parameters and levels for a 3^3 DoE Matrix

Factors	Level 1	Level 2	Level 3
Temperature (˚C)	130	140	150
Load (N)	6	8	10
Stand-off (mm)	105	135	75

A 3^3 experimental matrix was constructed adopting the classical approach. The software has a random generator assigning the experiments. Each experiment was completed in a random order, as dictated by the software.

Printing procedure;

The charge plate assembly was removed from the platform and weighed, including the ceramic substrate. The charge plate was placed back on to the mini Z and the HV cable connected to provide the voltage source. Prior to printing the height of the platform was adjusted to apply the correct pressure. The height of the platform was adjusted as described in section 5.3.1.

The platform was sent to the home position where it sits beneath an ionising fan prior to the print cycle. The HV supply was turned on and +2500V was applied to the aluminium plate charging the surface of the ceramic substrate.

Both printers were turned on and initialised, charging the developer. A file was selected and a print command given. At this point the pressure sensing software was set to zero to record real-time pressure.

The platform moves at a speed of 5m/min and the infrared heater turns on as the printer approaches close proximity of it. The platform passes under the infrared heater and travels to the thermosensor where the temperature of the substrate surface is measured. In addition, the high-resolution probe was set up 3mm above the substrate to measure the surface charge. A reading from the high resolution probe was taken from the digital read out on the electroscope. If the surface temperature is too low the platform will return to the start position and the cycle will be repeated until the desired temperature is achieved. Once the appropriate temperature is reached, the platform

progresses to Printer 1. Here, the toner, in the form of the selected image, will be deposited onto the transfer roller for the substrate to accept via heat and pressure, as well as the electrostatic field derived from the HV supply. The platform will progress past Printer 2, which is raised to avoid contacting the transfer roller with the platform, and make its way to the height measuring system to complete the cycle. It should be noted that the height measurement was not used for the experiment due to a technical fault, though the automated process dictates the platform to travel the entire length of the machine.

Upon returning to the start the HV supply is turned off and the pressure reading software is stopped. The entire charge assembly with the substrate is measured and the reading is logged along with the pressure sensor readings. The assembly is placed back on to the secondary Z drive and the next layer is deposited. This process is repeated for the experimental matrix using a full factorial design of experiments.

5.5 Mechanical analysis

5.5.1 Dynamic Mechanical Analysis

A mechanical analysis of the material is required to determine the physical properties of the samples relative to factors. A dynamic mechanical analysis (DMA) of the material was carried out. The thin discs were removed from the Teflon coated ceramic substrate and samples were cut to a geometry of 45mm x 10mm.

The samples were placed in a Mettler Toledo (formally, Triton Technologies Ltd, Grantham, UK) Tritec 2000 DMA. The DMA machine was orientated in the horizontal position and calibrated using the in-process software. Using a torque screwdriver with a 0.5Nm torque setting, the samples were fixed in a dual cantilever clamp. The temperature of the experiment was set to a constant 30˚C by placing on the thermal chamber lid. The frequency was set to 1Hz. The height of the sample was measured

using a Mitutoyo vernier calliper (Mitutoyo CD-15CP, Kanagawa, Japan) at three points, an average was taken. The average height was recorded and input into the DMA software to obtain a reading for the modulus value. The modulus value measurements were placed in an excel spread sheet and analysed.

5.6 Chemical analysis

5.6.1 Energy Dispersion X-ray (EDX) and Scanning Electron Microscope (SEM) sample preparation

The samples were cut into a 5mm x 5mm sections and placed on the spectroscopy pads. For energy dispersive X-ray samples (EDX) a carbon pad is used and for scanning electron microscope samples (SEM) samples, a standard pad is used. Prior to placing the samples on the pads, the pads are placed on an aluminium stub to enable the sample to be held in the crucible to manipulate the orientation as well as the field of view. The SEM is a Zeiss Evo HD15 Electron Microscope fitted with an 80mm^2 Oxford instrument X-Max EDX detector (Oxford Instruments Plc, Abingdon, UK). An image of the SEM with the EDX detector is illustrated in Figure 5:10.

Figure 5:10: SEM machine coupled with EDX detector

5.6.2 Fourier Transform Infrared Spectroscopy

A Bruker Alpha 1 (Bruker Corp., Massachusetts, USA) Fourier transform infrared (FT-IR) spectroscopy was employed as a tool to observe the difference between mechanically milled (DMU130625RC) and the chemically produced (DMU130725RB) toners. Using a spatula, toner DMU130625RC is placed on the detector (see Figure 5:11 for detector) above the infrared light source. The quantities need not be measured, so long as the detector had complete coverage of the material to be analysed.

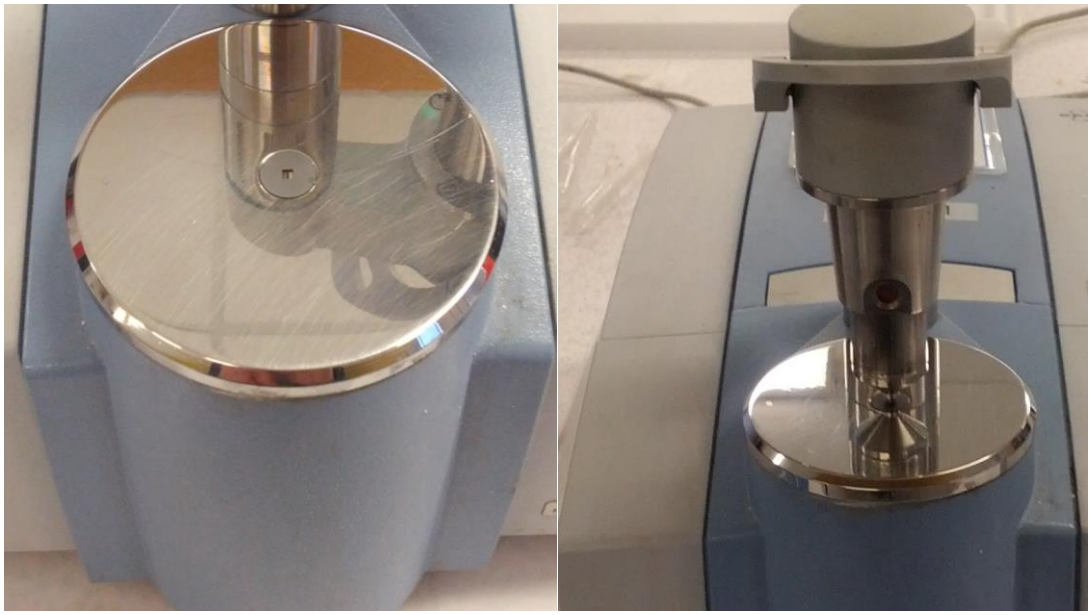

Figure 5:11: Detector in centre of plate (left) Cover placed over detector during analysis (right)

The lever is pushed down securing the powder and allowing the infrared laser to progress with the analysis. The process is repeated for toner DMU130725RB.

6 Chemically Produced Toner

6.1 Polymerisation of Styrene

A styrene monomer was synthesised to yield a multi chain polymer, polystyrene. The findings from the experiments are discussed below.

6.1.1 Polymerisation Experiment 1

A particle size analysis (PSA) of the synthesised toner was carried out to establish the size and fraction of the powder in Polymerisation Experiment 1 (PE1). Figure 6:1 displays the particle size distribution (PSD). Polymerisation Experiment 1 generated a sample with a wide PSD (ranging from 0.2µm to <500µm microns). Due to the limitations of the PSA, particles greater than 500µm cannot be registered.

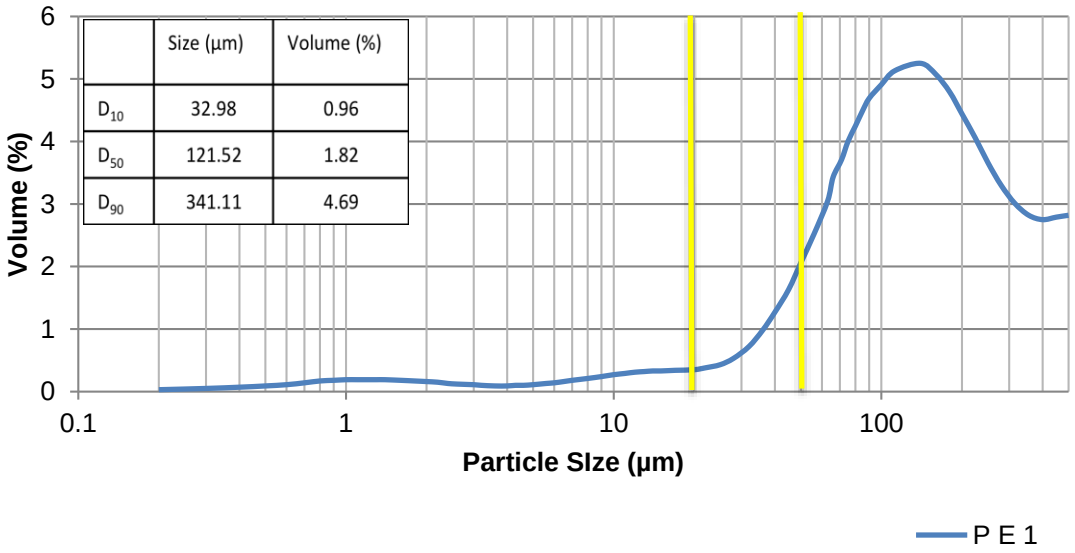

Figure 6:1: Particle size distribution for PE1 polystyrene synthesis

The D_{50} (median of the sample) from PE1 measured 121µm. The D_{90} and D_{10} measured 341µm and 33µm respectively. For the Selective Laser Printing (SLP) of polymeric toners the acceptable size distribution is 20-50µm. The yellow lines shown on the graph details the amount of material produced within the required range from the PE1 experiment.

The morphology of the PE1 sample was characterised using an electron microscope. An SEM micrograph (Figure 6:2) shows the sample to be predominantly spherical in shape, although the presence of irregular shaped particles was evident within the sample. Furthermore, some of the fine powders had coalesced forming an agglomerated particle or satellites to the larger particles, denoted by the orange circle.

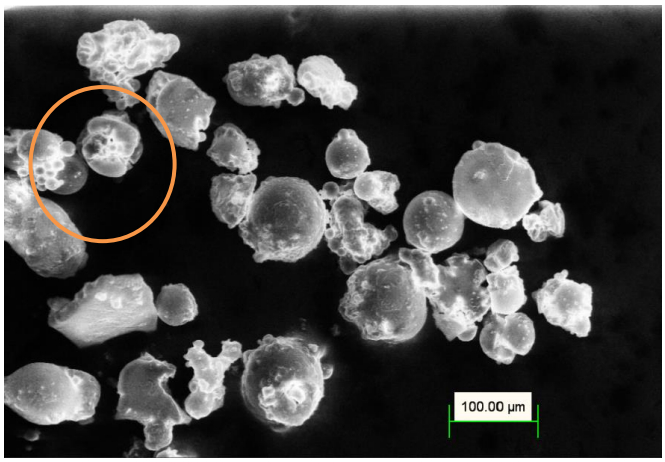

Figure 6:2: SEM of PE1

The agglomeration is thought to be attributed to insufficient agitation during the homogenising phase and the lack of an appropriate amount of stabilising agent in the continuous phase[156, 157]. The process was able to produce 8.75g of synthesised styrene from 22.51g of monomer and initiator, of which, only 10% of the toner was within the target range of 35µm (D_{50}). The process of polymerisation should have yielded a powder with a tighter distribution and greater yield. However, based on the literature the size of the particle should be controllable[117, 119, 156, 158–160]. By

increasing the amount of the initiator it should be possible to reduce the size of the particles and also narrow the distribution.

6.1.2 Polymerisation Experiment 2

The size of the particles synthesised in PE1 were far greater than the required 20-50µm range. Therefore, to synthesise finer particles with a tighter distribution the amount of initiator was increased.

There was a significant reduction in size of the synthesised toner. The D_{90} measured 233µm with a 2.98% volume of the sample compared with the results of the previous experiment (PE1). Moreover, the D_{50} was reduced to 89.89µm with a 5.43% volume. The D_{10} measured 19.96µm with a 0.35% volume of the sample. The mass of the synthesised styrene weighed 12.88g. The conversion rate was recorded as 56.68% showing a huge increase in the output of the toner. However, the total yield of powder within the correct particle range was 12.24%. This is an increase from PE1, although substantially low considering the output mass. A PDS of PE2 is shown in Figure 6:3.

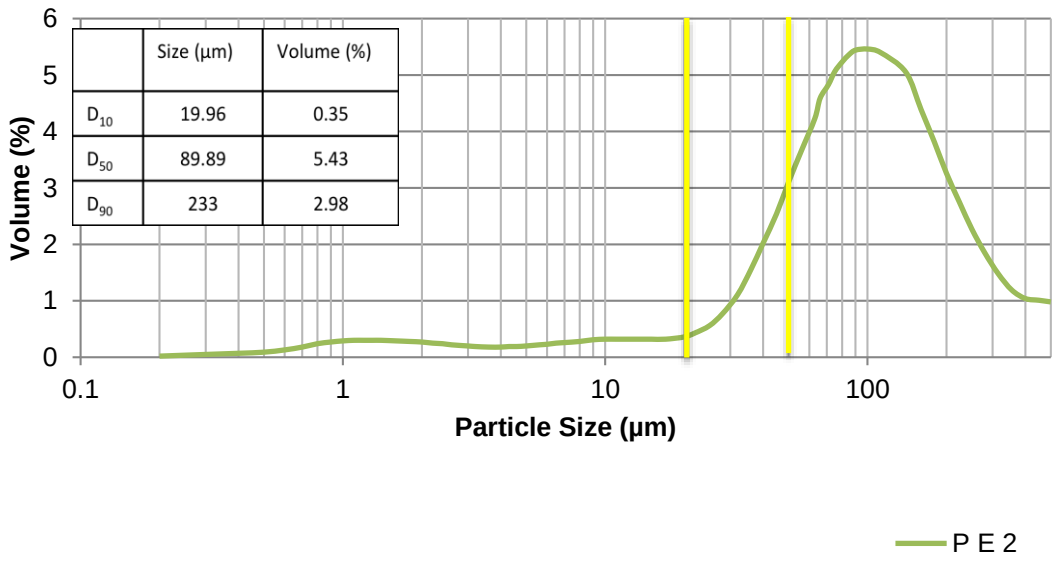

Figure 6:3: PSD of PE2 polystyrene synthesis

The resulting particle morphology of the PE2 (Figure 6:4) shows a large reduction in irregularity. Comparing PE2 micrograph (Figure 6:4) with that of PE1 (Figure 6:2) the micrograph of PE2 shown in Figure 6:4 is more refined and spherical in shape, with a narrower size distribution. This is attributed to the improved mixing speed and the increase in the initiator as suggested by the literature[156, 161, 162].

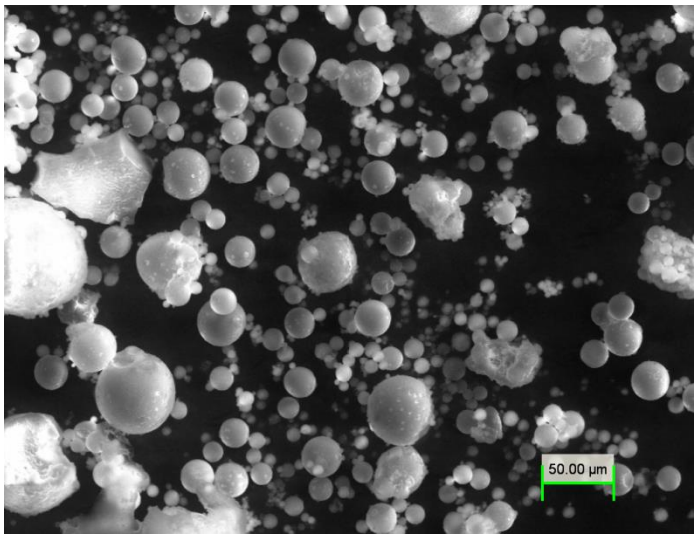

Figure 6:4: SEM of PE2

Although an improvement from the previous experiment (PE1) the yield was still too low to make chemical production an economically viable method of toner manufacturing. Literature [156, 161, 162] suggests the increase in initiator can have a positive effect on both the control of the size and the distribution. Polymerisation Experiment 2 clearly demonstrated that by increasing the initiator concentration finer particles with a tighter distribution can be synthesised.

A comparison between PE1 and PE2 is presented below. It can be seen (Figure 6:5) that an increase in the initiator concentration combined with a reduced mixing speed results in smaller particles with a narrower PSD of the polystyrene powder. PE2 also yields 3.86% more powder within the required range. Moreover, particles greater than 500µm were reduced in volume from 2.58% to 0.98%. The increase in initiator assisted in a

greater yield due to a greater conversion of the monomer. The higher concentration of initiator allows for more of the initiator to form chains with the monomer while the thermal decomposition rate remains constant, thus allowing for more of the monomer to be converted in to a polymer[117]. The experimental results are in keeping with the literature, which indicates the increase in initiator can lead to a greater yield and more controllable size.

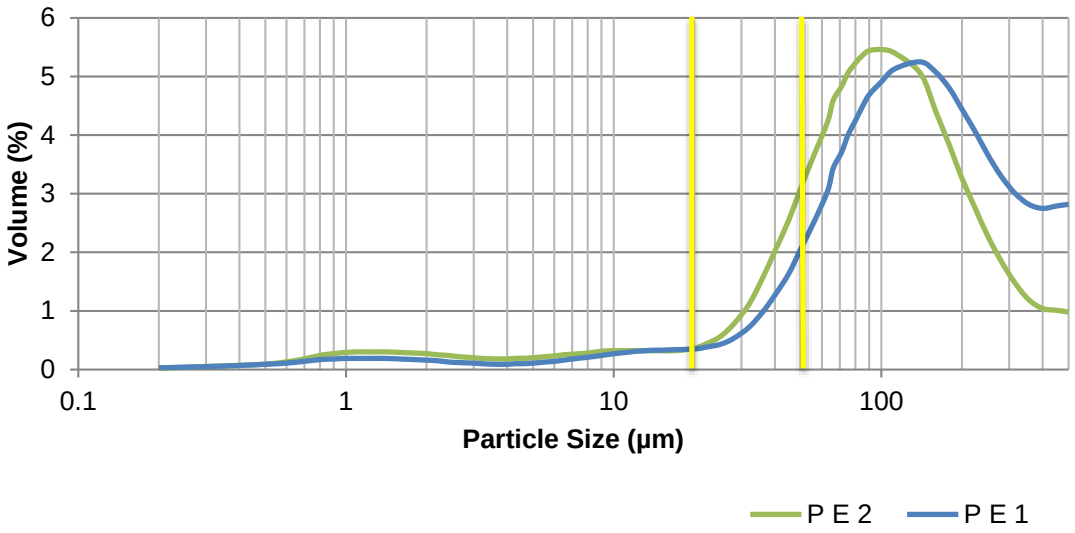

Figure 6:5: comparison of PSD for PE1 and PE2

6.1.3 Polymerisation Experiment 3

A third experiment, Polymerisation Experiment 3 (PE3), was conducted by increasing the quantities of both the stabiliser (PVA) and the initiator (Benzoyl peroxide). Compared to PE1, these ingredients were doubled.

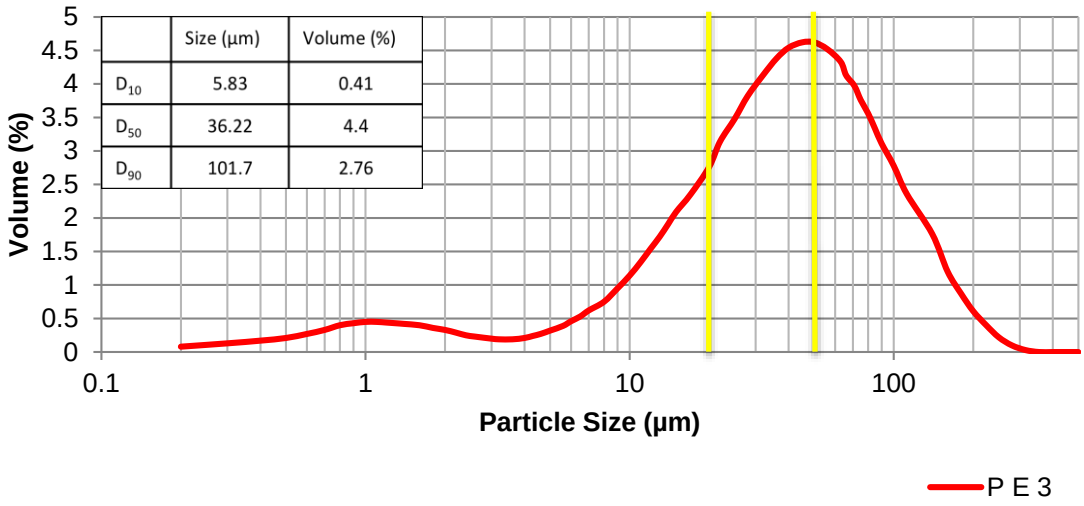

Figure 6:6: PSD of PE3 synthesised styrene

The results of the PSD in Figure 6:6 indicate a reduction in particle size and a tighter distribution as compared to the previous experiments (PE1 and PE2). The D_{50} for PE3 was recorded as 36.22µm at 4.4% in volume. The D_{10} measured 5.83µm with a volume of 0.41% and D_{90} measured 101.7µm with a 2.76%. This is a significant drop in particle size and size distribution from the previous polymerisation experiments (PE1 and PE2). The conversion rate shows 45.016g of initiator and monomer created 8.12g of fine styrene polymer. Though the conversion rate is lower than of PE2, it was observed that a small amount the material was baked on to the inside of the glasswear, which could account for a reduction in the mass. The overall reduction in particle size and a tighter distribution was expected, based on the information in the literature[156, 161, 162]. The experiment was able to demonstrate a larger quantity of the material within the required particle range (20-50µm). Moreover, particles greater than 315µm were completely eliminated.

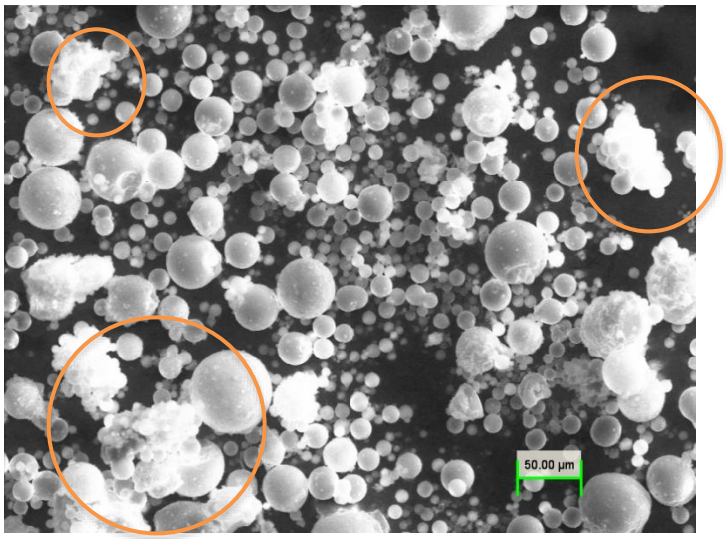

Figure 6:7: SEM micrograph of PE3

An SEM micrograph (Figure 6:7) shows the particles to be mostly spherical with very little sign of irregularity. The micrograph does, however, exhibit areas of agglomeration of fine powder (see orange circles). The yield from PE3 was recorded as 35.49%, the largest recorded yield of the three experiments. Based on the output of the measured toner the conversion rate of the experiment was calculated to be 18.08%. This is due to the increase in concentration of both the stabilising agent and the initiator. The results were as expected due to the increase in the initiator allowing a greater conversion of the monomer and the PVA allowing the homogenised phases to not coalesce.

This initial feasibility study was conducted to synthesise polystyrene with a target particle size ranging 20-50µm. The first experiment did not produce sufficient toner in the required size range with the particles generally oversized the D_{50} measured 121.52µm. However, with each successive experiment, the particle size was reduced. Moreover, polymerisation of styrene has been able to produce fine powders with a narrower particle distribution mostly spherical in shape.

Figure 6:8 exemplifies the collective results of the polymerisation experiments graphically. It can be seen that an increase in the initiator concentration resulted in a

strong reduction in particle size, particularly at the tail end along with an increased volume within the desired range.

2.21

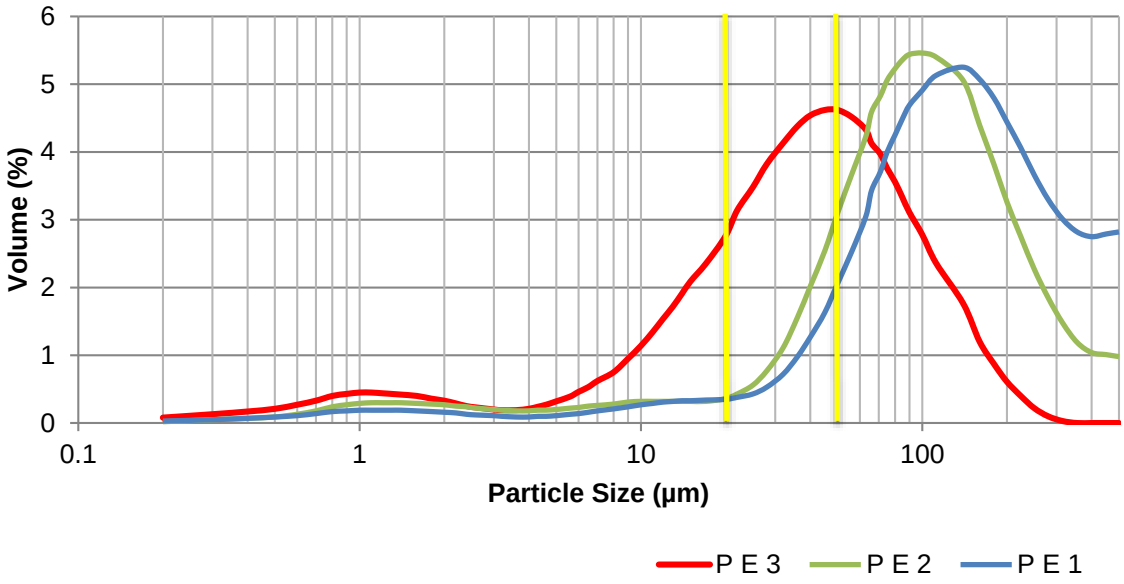

Figure 6:8: PSD of PE1, PE2 and PE3

By increasing both the initiator and the stabiliser, the PSD curve for PE3 was able to totally eliminate particles greater than 500µm. Moreover, the distribution was tightened and an increased yield within the target range (20-50µm) was produced.

The results from the three experiments are shown in Table 6:1. Based on the yield of PE3, it can be stated that 100g of the initiator and monomer can produce 6.39g of styrene toner.

Table 6:1: PSA and yield of PE1, PE2 and PE3 of synthesised styrene

Experiment	D_{10} (µm)	D_{50} (µm)	D_{90} (µm)	Conversion Rate (%)	Yield (%)	Yield (g)
PE1	33	121	314	38.88	8.38	0.73
PE2	20	90	233	56.68	12.24	1.58
PE3	6	36	101	18.03	35.49	2.88

Although the economics of the yield is still an issue that needs to be addressed, the experiments have demonstrated that chemically synthesised polymeric powders, with a 20-50µm range, can be produced. The literature also suggests that the process can be up-scaled[56, 117, 120]. The polymerisation process can be finely tuned and adapted to produce the necessary yield. While the results are promising, the use of styrene as a toner [3, 4, 12, 37, 42, 56, 57, 91, 94, 95, 97, 148, 163, 164] is well documented in Electrophotography. Also, the original scope requires an engineering polymer with a melt temperature greater than that of styrene and with enhanced mechanical properties. As styrene is one of the constituents in Acrylonitrile Butadiene Styrene (ABS), a commonly used engineering polymer, it provides a good indication of the challenges of polymer synthesis of ABS. Indeed, given the difficulties encountered in generating acceptable powder from polystyrene using suspension polymerisation from a monomer, it was concluded that the use of this approach for ABS (producing a copolymer on to which a third polymer is grafted on to) would be impractical for commercial toner production.

6.2 Chemically produced ABS toner

Based on the results of the trial to produce toner by polymerisation of styrene, an alternative polymerisation process, Evaporative Limited Coalescence (ELC), was used to produce ABS toner using the same material as employed for the comminution trials, Magnum 8391. As the ELC process is predominately used in the manufacturing of fine toner between 2-20µm, a number of experiments were carried out at lab scale to increase the size of the particles to the target range (20-50µm).

Figure 6:9 illustrates five experiments completed with a PSA to assess the size and the volume percentage of toner produced.

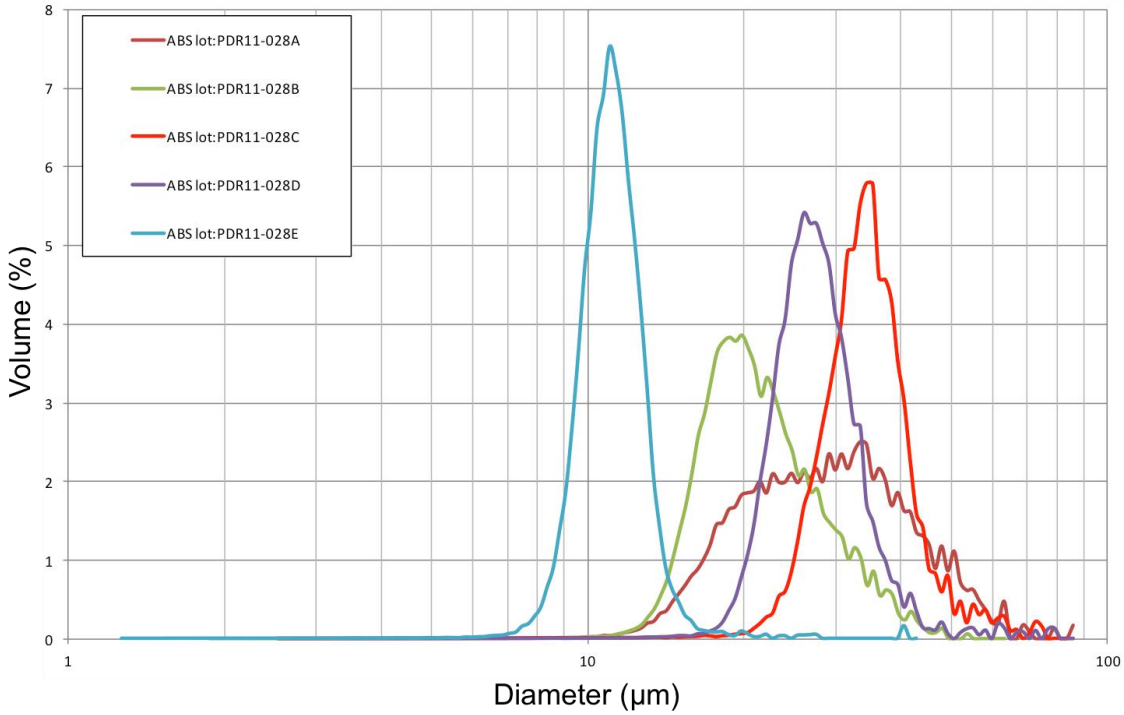

Figure 6:9: Volume distribution of ABS toner prepared via chemical process

The graph (Figure 6:9) illustrates a tight distribution, expected from a chemically produced toner. The peaks of each of the experiments are shown to vary, but as the experiments progressed (ABS 1-5) the distribution narrowed and there was an increase in the quantity of toner produced. Experiment ABS 5 was undertaken to demonstrate the ability of the ELC process in creating fine polymeric toners.

Table 6:2: PSD from chemically produced toner

	D10	D50	D90
ABS 1	17.74	28.72	46.38
ABS 2	15.97	20.8	31
ABS 3	27.14	34.32	43.28
ABS 4	22.09	27.27	35.1
ABS 5	9.04	11.12	13.14

Table 6:2 displays the particle size distribution for each of the five experiments carried out via ELC. It is clear from the table and Figure 6:9, that the most suitable experiment to upscale to pilot production is ABS 3. The D_{50} is shown to be very close to the target size of 35µm with a very narrow distribution of 16.14µm between the D_{10} and D_{90}. Overall, the majority of the particles are within the 20-50µm target size.

An SEM micrograph (Figure 6:10) shows the shape of the particles produced using the ELC process. It is evident that the ELC process is able to produce particles that are consistent in size and shape. The toner has been produced with a rough surface and non-spherical, potato shape. The rough surface is able to provide more contact points to improve charging conditions with the carrier[5, 37], although not to the extent of mechanically milled toners.

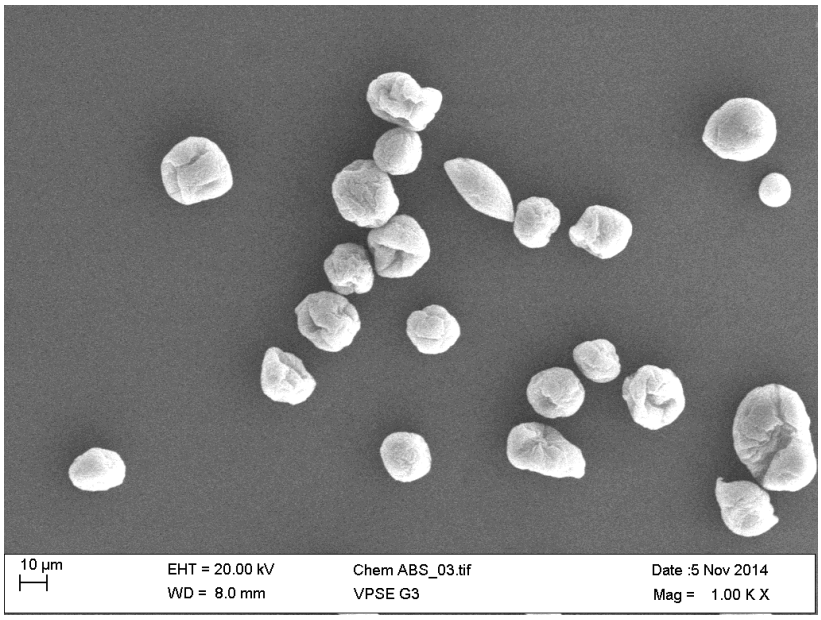

Figure 6:10: SEM micrograph of ABS toner produced via chemical process

From the initial trials, the ELC process was modified in an effort to produce a tighter distribution toner. Based on the ABS 3 experiment, the process was fine tuned and adjusted at multiple steps within the system to accommodate the 35µm (D_{50}) particle size. The PSD is shown in Figure 6:11. The figure shows the D_{50} particle size to be 26µm with the D_{10} measuring 20µm and D_{90} measuring 33µm.

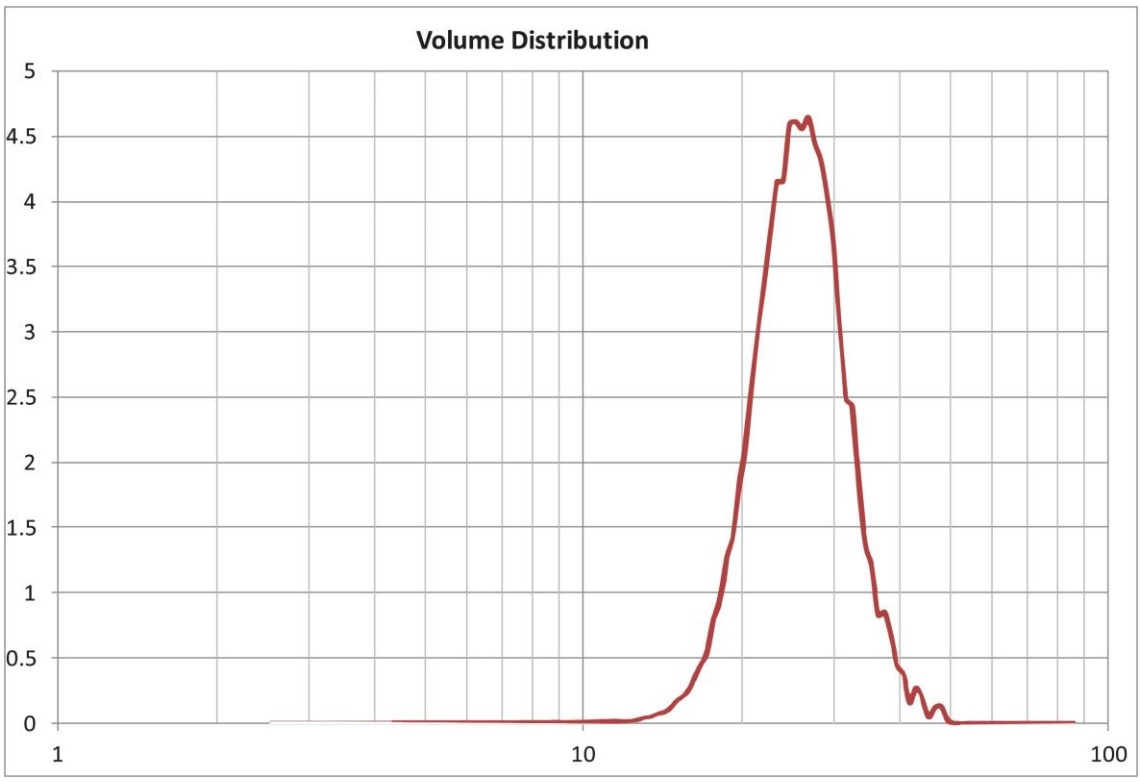

Figure 6:11: Particle size distribution of chemically produced ABS via the ELC process based on ABS 3

A PSD displaying the size from 10µm to 60µm with a standard scale along the X-axis is shown in Figure 6:12. The figure shows the size of the particles with a sharp rise in volume from approximately 12µm, retaining the tight distribution until it reaches the volume peak at approximately 28µm. After the peak, the quantity of toner reduces gradually with increasing particle size, ending at approximately 53µm. The ELC process generated toner as expected, however, it was assumed that the distribution towards the tail end would have followed a similar trend as ABS 5, as shown in Figure 6:9. Unfortunately, as ELC is ideally suited to 2-20µm toners, empirically adjusting the process has caused the tail end (large particle size) of the volume distribution curve to be much broader.

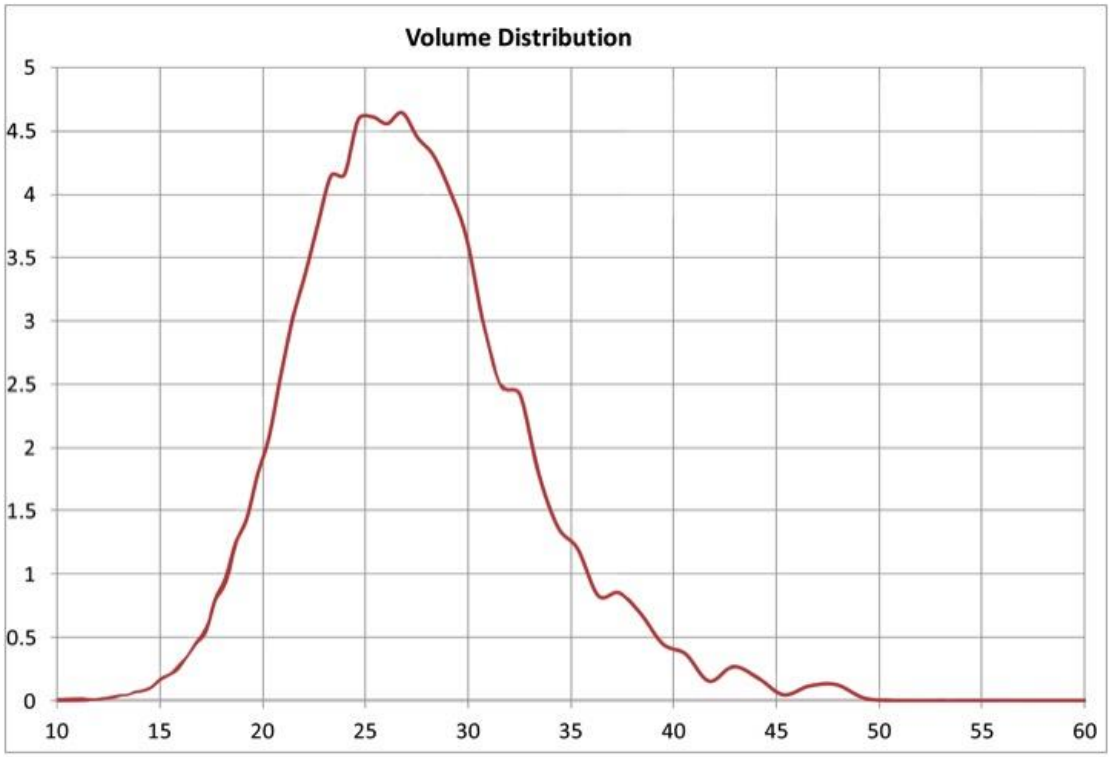

Figure 6:12: Particle size distribution of chemically produced ABS toner showing the distribution between 10µm to 60µm

The ELC process is intended for the production of fine polymeric toners up to 20µm in size, and capable of producing an extremely tight distribution. Additive Manufacturing requires a larger toner, up to 50µm to give a balance of resolution and layer thickness. The ELC process has demonstrated the flexibility in producing toners with larger sizes than the process is intended for. The distribution is wider than for standard toners, however, the AM toner was within the required distribution. Further development trials in the future will focus on optimising the particle size distribution.

6.2.1 Carrier pairing and printer voltage settings

The results from the tribocharging between carriers C1, C2 and C3 for toner DMU130729RB are shown in Table 6:3.

Table 6:3: Tribocharging results between carrier and toner at given voltages

Powder	Carrier	Applied Voltage			
		-2kV		+2kV	
		Q/m	Powder ratio	Q/m	Powder ratio
DMU130729RB (Chem)	C1	-1.5	70.00%	8.7	92.00%
	C2	-2.2	49.20%	1.2	68.40%
	C3	-11.8	4.40%	45.5	84.40%

DMU130729RB toner was charged with three carriers. Literature has suggested that a Q/m range between 2µC/g–25µC/g [151] is adequate to provide a suitable electrostatic adhesion between the carrier and toner. Studying the charge with a -2kV voltage, it can be seen from Table 6:3 that the charge is not within the range permitted to provide an adequate adhesion to the carrier. Where the Q/m ratio is at an acceptable level, the percentage of the toner charging with the carrier (powder ratio) is too low to be of any use. The same test was conducted using a positive 2kV voltage to observe its performance. It was found that toner DMU130729RB was able to charge with two carriers. The powder ratios for both carriers with the toner were above 80%, bar one, which measured below 70%. Carrier C1 has a charge of 8.7µC/g with 92% of the toner charging. The charge ratio is within the range indicated from the literature. In addition, the powder ratio was very favourable. Carrier C2 was able to produce a charge of 1.2µC/g with a 68.4% charge ratio. The charge was well below the lower limit range, moreover, the powder ratio was considerably lower than when paired with carrier C1. Toner DMU130729RB was able to produce a Q/m of 45.5 µC/g when tribocharged with carrier C3. A powder ratio of 84.4% was also recorded. The powder ratio was still not as

efficient as carrier C1, however, the main reason for dismissing the carrier was due to the excessive adhesion force between the toner and carrier. Acting on the results above, it is clear that carrier C1 is able to provide an acceptable electrostatic adhesion and powder ratio.

It is noted that the toner produced by the chemical process has a surprising positive charge, which was not expected as the toner was initially selected based on its ability to charge negatively. Despite extensive investigations the reason for the polarity change is still unknown, but the most likely cause for the shift in polarity is due to the chemicals and additives used during the ELC process. It is plausible that the material has a residual additive either internal or external to the material. A number of chemical analytical methods have been explored in order to ascertain the change in charge. This is discussed in the Analysis of Chemically Produce Toner section.

In the interest of future-proofing the SLP rig and providing additional flexibility, one of the two printers was converted to enable printing of positive toners. This work has already been discussed in the methodology chapter (Section 4). This approach will provide greater flexibility to the process and increase the range of material, which can be processed using it.

In order to print the toner, the carrier and toner must be added at a specific concentration to enable appropriate tribocharging. If a low concentration of toner is charged with the carrier an insufficient quantity of toner will be offered to the OPC. Should the toner concentration be too high, dusting can occur which can cause the OPC to be scratched. Additionally, an increase in heat can cause the dusting to fuse on to the OPC rendering its photosensitive layer redundant. Each concentration was tribocharged and observed under a digital microscope, as shown in the figure below.

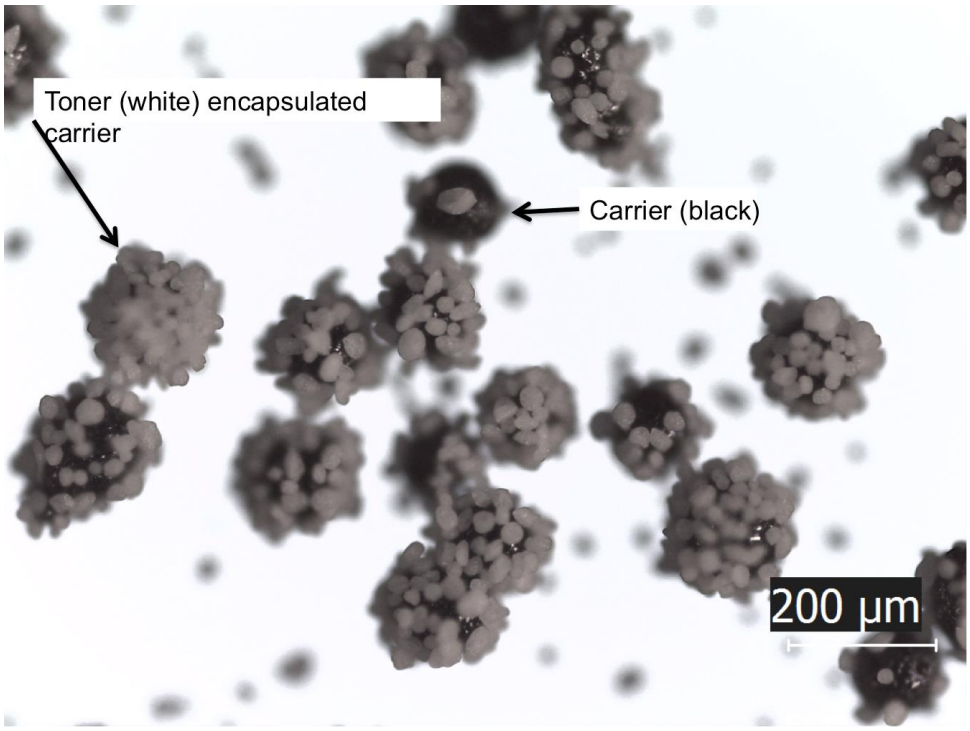

Figure 6:13: Micrograph of chemically produced ABS toner DMU130729RB charged with carrier C1 at 8:92 ratio respectively

DMU130729RB was found to favour a toner concentration of 8% by weight. A micrograph of the toner charging with the carrier is shown in Figure 6:13. In addition to imparting the required charge, the level of toner gave appropriate surface coating (full coverage of the carrier particles with negligible shedding of toner). The carrier is clearly covered with toner with little free space left on the surface. Moreover, there is very little toner on the background, although the charge was created with vigorous shaking between the carrier and toner. In the developer unit the material would be mixed with far less vigour during the printer cycle start up.

Toner DMU130729RB was mixed with the carrier C1 at a ratio of 8:92 by weight, toner to carrier. A total of 1600g was weighed, mixed and fed in to the printer developer unit. The rollers were turned manually to coat the magnetic roller and create the brush. The developer unit was placed in the printer and the printer turned on to charge the toner

to the carrier in a standard charging cycle. This would give a clear indication whether the toner had charged correctly.

The developer unit was removed from the printer and examined. Figure 6:14 shows the poor adhesion between the toner and carrier. The developer was black in colour, rather than a grey, indicating the carrier to be only partially covered by toner, since the black of the carrier and the white of the toner would produce a grey brush. This, coupled with the excessive dusting, suggests that the toner requires additional surface additives in order to achieve the correct charging characteristics.

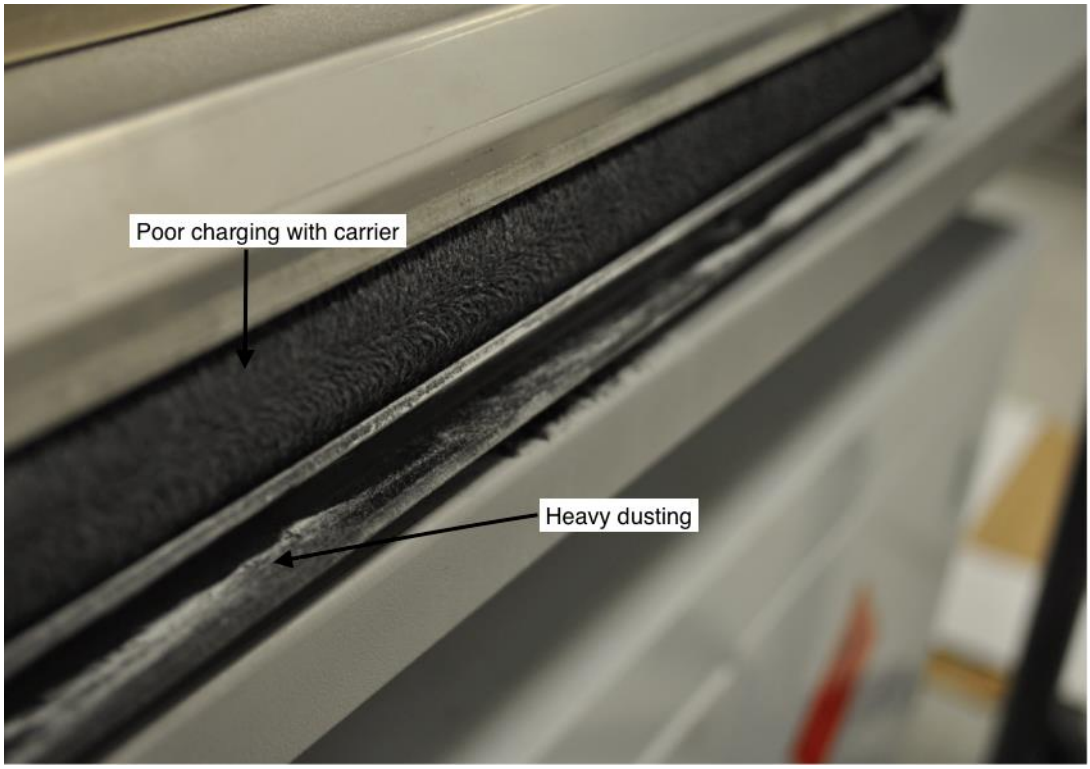

Figure 6:14: Developer unit with toner DMU130729RB charged with carrier at a ratio of 8:92

The toner concentration with the carrier for DMU130729RB was found to be an acceptable figure (8% by weight). However, when printing trials were performed problems manifested. The lack of CCAs on the surface of the toner produced insufficient tribocharging between the toner and carrier, resulting in premature separation between

the two. To exploit the positive charge toner would require a complete change to the current printer, which was beyond the resources available to undertake this study. However, it has been recommended that this should form the basis of a future study (see Further Work). Charging is an issue that affects chemically produced toners more so than mechanically milled toners. This is usually countered by the inclusion of CCAs during the chemical synthesis process with the addition of surface additives post synthesis. Additionally, an upgrade to the printer is required to counter the poor cleaning of the OPC, an issue commonly associated with chemically produced toners[165].

Most chemical methods of toner manufacturing require the use of monomers and a polymerisation process[7, 91, 97]. In theory, the ELC process is able to produce a toner from any polymer that can be dissolved in a solvent. This gives the ELC process a distinct advantage over other chemical methods of toner manufacturing, opening up a huge area of research for high performance engineering polymers. Previous work from Banerjee[4, 58] has shown common engineering polymers such as HDPE and thermoplastic elastomers are difficult to grind from pellets or stock size. Wilczek *et al.* [107] have also shown to achieve fine grinding of polymers from their stock size, a significant cost is apportioned to the use of cryogenics, with a figure of 40% not uncommon. The ELC process is able to fill the gap between mechanical milling and chemical production by dispersing the coarse polymer powder into a solvent and producing a fine, regular shaped toner. This negates the need for monomer, requiring less capital investments.

7 Mechanical Toner Development

Due to the difficulty in generating a suitable toner to print by chemical means it was decided to pursue a mechanical toner route with a view that a mechanically milled ABS toner can be produced with a negative charge. The section discusses the results from this means of producing a toner and the traditional method once employed to produce larger sized particles by both ambient and cryogenic grinding (comminution).

7.1 Reduction of ABS at ambient temperature

The PSD of the Magnum 8391 ABS pre ground pellets were recorded prior to, and after comminution, using a Malvern particle size analyser. A PSD of the Magnum ABS is shown in Figure 7:1. The D_{50} of the feedstock ABS measured 420µm. The D_{10} measured 215µm and the D_{90} measured 861µm.

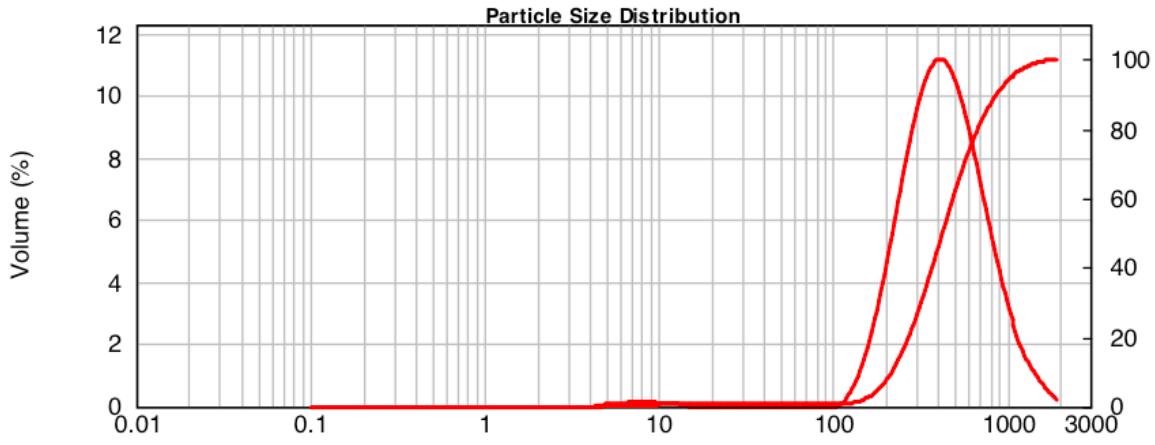

Figure 7:1: PSD of pre ground Magnum 8391 ABS

The feedstock material was fed into the milling machine and milled as per the parameters outlined in Section 5.2.2. The results from the grinding trials are shown in Figure 7:2.

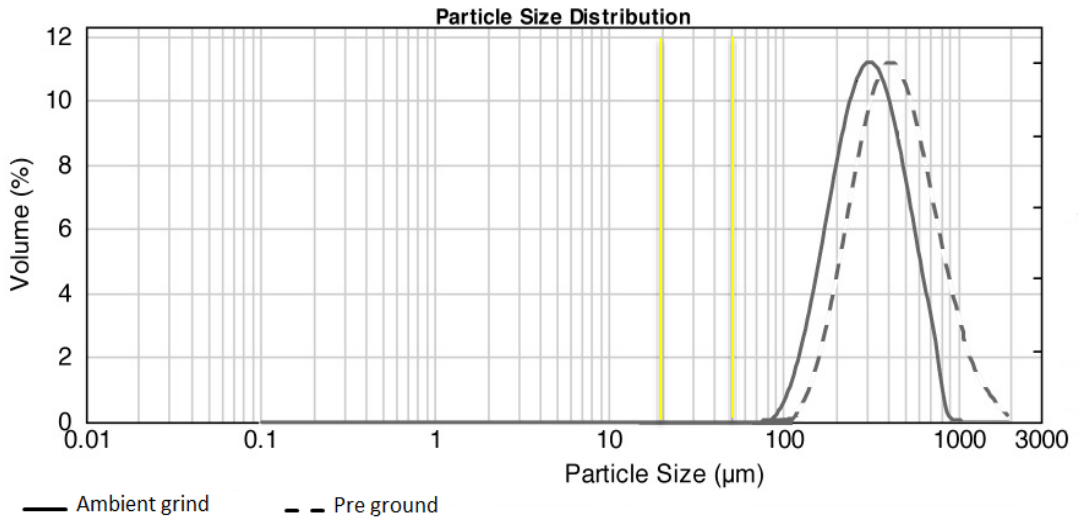

Figure 7:2: PSD of pre ground and milled (ambient) Magnum 8391 ABS

The results from the ambient grinding trials (Figure 7:2) to begin with show encouraging signs. The particle size of the D_{90} was reduced to 549µm from 861µm, a 44% reduction from the original feedstock. However the D_{50} was reduced by 33% from 420µm to 302µm. The D_{10} measured 163µm, resulting in a 52µm reduction or 28% reduction. It is clear that ambient grinding is better suited to larger ABS particles. This is due to the inherently tough nature of the material.

7.2 Reduction of ABS using Cryogenics

The Polylac PA-757 ABS coarse polymer powder was cooled in liquid nitrogen and fed in to the mill. In addition, liquid nitrogen was poured intermittently into the mill during the reduction cycle. The PA-757 ABS was trialled due to its lower mechanical properties compared to Magnum 8391 (see Table 5:1 in section 5.1).

The results from the PSA (Figure 7:3) show that while the D_{50} was reduced from 380µm to 223µm, the particles were incapable of being ground down to the desired target size of 20-50µm, again, because of the inherent tough nature of the ABS polymer. The D_{10}

measured 88µm, a difference of only 46µm from the original feedstock. Though the D_{90} was significantly reduced from 942µm to 424µm, the target particle size was not achieved in any viable quantity. It is clear from the results that despite using cryogenic milling and an ABS powder with lower mechanical properties, the impact mill at Hosokawa was unable to reduce the ABS in to a suitable size. This could possibly be due to the material not being cooled enough, although it is likely that the impact mill used was not efficient enough to reduce the particles down to the degree required. An alternative process such as air jet milling could have proved to provide a much more efficient process.

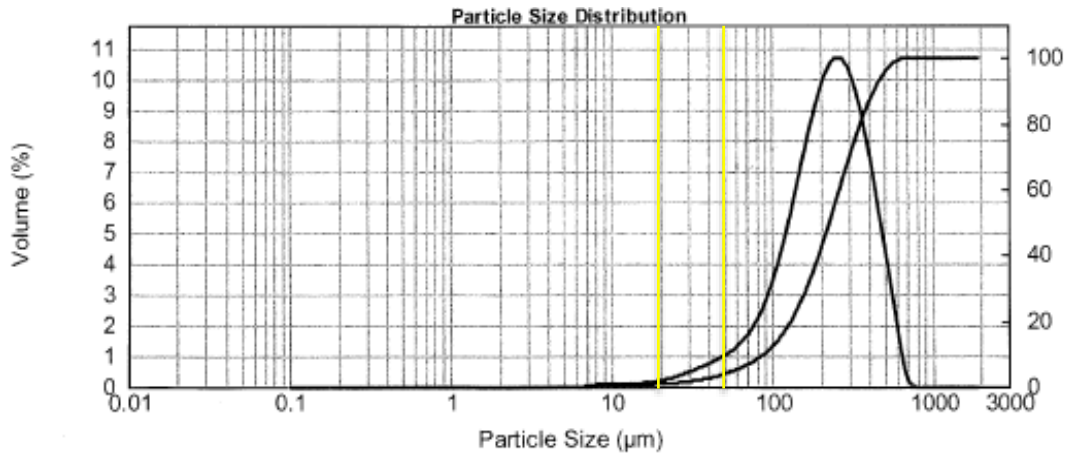

Figure 7:3: Particle size analysis of Polylac PA-757

Following on from the ambient grinding trials at Hosokawa Micron, the Magnum 8391 ABS polymer was sent to the Fraunhofer UMSICHT, Germany, to determine whether a more efficient grinding process is achievable. A 10kg bag of ABS powder was sent for cryogenic comminution trials. The material was cooled and milled as described in Section 5.2.2.2.2. A PSD of the milled material was carried out. The results (Figure 7:4) showed a significant reduction in the PSD from the original feedstock.

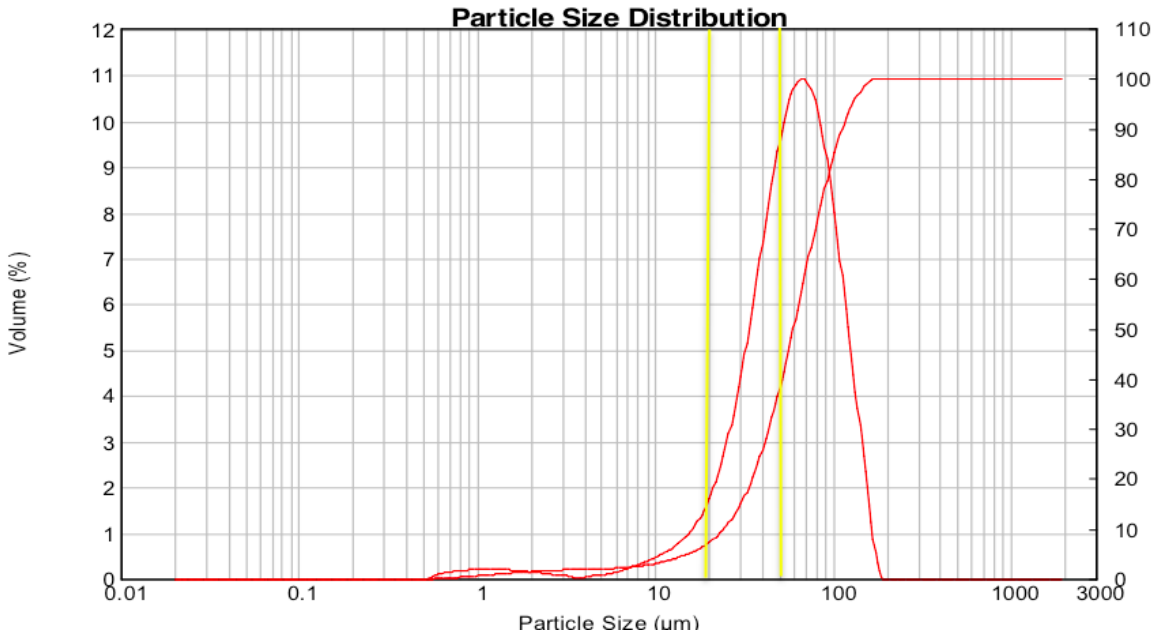

Figure 7:4: PSD of ABS Magnum 8391 after cryogenic grinding in Germany

From the PSD in Figure 7:4, it can be seen that the tail has a peak measurement of 112µm (D_{90}), down from 861µm. The D_{10} has a particle size of 24µm from 215µm and the D_{50} measures 59.9µm from 420µm. Figure 7:4 indicates 42.74% of the powder was within the 20-50µm range. A graphical representation of both the feedstock material and the cryogenically ground material from Fraunhofer is depicted in Figure 7:5. The graph shows that there has been a major shift in PSD from the original feedstock material.

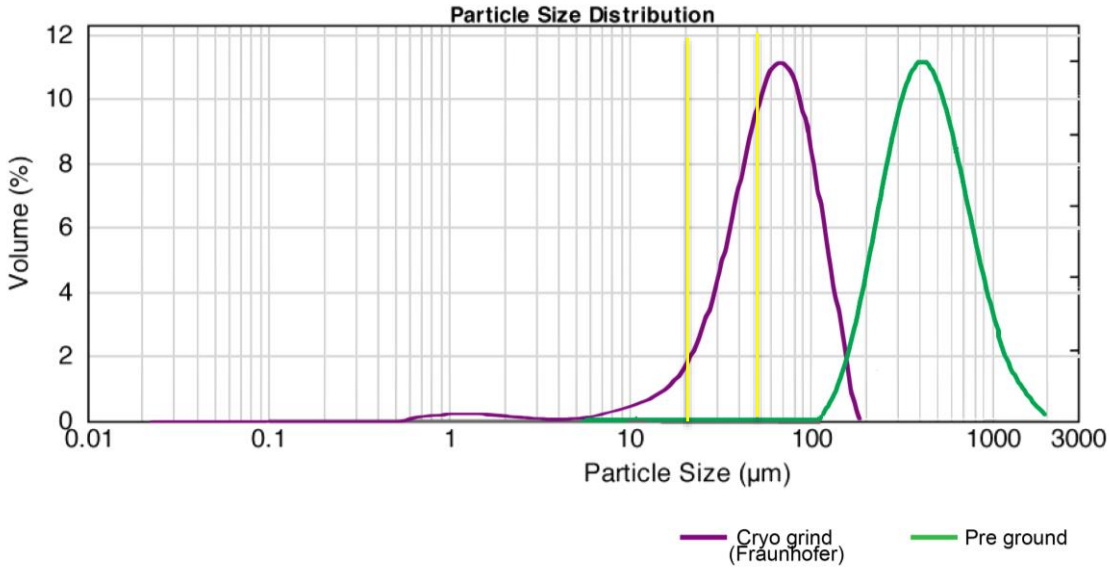

Figure 7:5: Graph to compare feedstock material and cryogenic grinding trials undertaken at Fraunhofer

The trials conducted by Fraunhofer have proven to demonstrate a higher efficiency of comminution than that at Hosokawa. The comminution process has greatly reduced the particle size. Moreover, the process by Fraunhofer was able to achieve the required size in a greater quantity than the trials conducted at Hosokawa, thus, making the Fraunhofer comminution process a viable option for future toner developments. The table below (Table 7:1) illustrates the efficiency between each of the cryogenic grinding approaches.

Table 7:1: Comparison of cryogenic comminution trails

Particle size	Original (µm)	Hosokawa (µm)	Fraunhofer (µm)
D_{10}	215	163	26
D_{50}	420	302	60
D_{90}	861	549	112

It can be seen from Table 7:1 there is only a limited reduction in particle size between the original feedstock material during the cryogenic comminution trials conducted at

Hosokawa. The reduction in particle size was as expected, with the larger particles exhibiting the greatest reduction, a trend that has been had been echoed by a number of researchers [102–104, 109, 166]. However, it is evident the resultant yield, of which only 3.13% is in the desired particle size, was too low to use. The trials conducted by the Fraunhofer group however, have shown their novel process has a far greater effect on reducing the PSD.

It is noteworthy that whilst both Hosokawa and Fraunhofer UMSICHT are experts in their field of comminution, neither had any experience in comminution of ABS polymers to such a degree. Hosokawa, due to production requirements and budgetary limitation were unable to perform a comprehensive study which could have improved the results whereas Fraunhofer UMSICHT, who are a research laboratory were able to perform more exhaustive tests.

This could well have been a contributing factor to the poor particle reduction at Hosokawa. In addition, the trials conducted by the Fraunhofer group have used a novel approach by cooling the material to sub-zero temperatures for a defined time and also continuously maintaining the sub-zero temperature by the addition of significant quantities of liquid nitrogen during the process.

Comparing the output from Banerjee [4] for the thermoplastic elastomer (TPE) Somos, the results showed that the required size was not produced in a viable quantity (20µm). The comminution trials adopted by Banerjee was able to convert 24.6% of 12g which was recovered from the 1kg of the TPE material using an air jet mill as described in Section 3.6.8. However, this was highly inefficient and it was considered more efficient to classify the stock Somos than it was to undertake comminution trials.

7.3 Summary of the toner development trials

The aim of the toner development trials for both the chemically produced and mechanically milled toner was to establish the effectiveness of each process.

Previous work by Banerjee [167] has shown the mechanical milling process to have very little impact on particle reduction. To summarise the grinding trials, Banerjee began with one kilo of PBT powder with a PSD of 126µm (D_{50}). Of the one kilo of powder, only 12g were recovered through the incorporated sieves during air jet milling, of which 24.6% was within the particle range required. This gives an insight into the poor grinding efficiency associated with engineering polymers.

The table below shows the grinding efficiency for both the mechanically milled and chemically produced ABS toners. Work conducted by Banerjee is also included to provide a comparison.

Table 7:2: Summary table comparing previous work with current methods of particle reduction for ABS

Particle size	Banerjee (µm)	Hosokawa (µm)		UMSICHT (µm)	ELC (µm)
		Ambient	Cryo		
D_{10}	12.2	163	88.25	26	20
D_{50}	26.4	302	223.07	60	26
D_{90}	52.6	549	424.24	112	33
Efficiency	0.028%	0%	3.23%	42.74%	98.6%

The results from Table 7:2 show the progressive nature of the grinding trials. The trials conducted by Banerjee demonstrate the poor conversion rate of the grinding process due to the inherent properties of polybutylene terephthalate (PBT). The trials resulted in only being able to convert 0.028% of the material within the 20-50µm range.

Continuing from Banerjee's work, the grinding trials at Hosokawa progressed with the introduction of a liquid nitrogen cryogen to aid particle reduction. This enabled a 3.23% yield in material in the required size range, however the return is not enough to warrant continuing with the process. Final grinding trials were undertaken by UMSICHT. Using the novel grinding method demonstrated a significant improvement over the previous methods. A yield of over 42% was recovered, highlighting a possible method for mechanical particle reduction.

Final trials were undertaken by chemical means. Chemical production has been used in the toner industry for some time and is now the preferred method of producing fine particles. An ELC process was employed to chemically produce a powder that was centred round 35µm (D_{50}). The results shown in Table 7:2 highlights the ELC process to be extremely efficient in producing toner within the 20-50µm range, moreover, the ELC process is able to produce a toner with a predefined shape allowing for better flow or charging properties.

While the grinding trials were not all conducted using the same material, it does provide an insight in to the difficulty and complexity in reducing a tough engineering material in to fine powders for the purpose of a toner. The results also highlight the rationale behind why the toner industry is heavily invested in chemical production techniques over traditional mechanical methods for fine toner production.

All trials from hereon in will focus exclusively on Magnum 8391 ABS powder, either as a chemical toner (DMU 130729RB) or a mechanically milled toner (DMU130625RC).

7.4 Printing parameters

7.4.1 Flow control additives

Mechanically milled toners suffer from agglomeration and packing under their own weight due to the irregular shaped particles. To decrease the friction and promote flow a flow control agent (HDK 2000/4) from Wacker was shear mixed with the polymer at 3% and the flow was assessed in process by the fluidity of the formed vortex.

7.4.2 Toner conversion and print optimisation

The results from the tribocharging between DMU130625RC toner and carriers C1, C2 and C3 and toner are shown in are shown in Table 7:3.

Table 7:3: Tribocharging results between carrier and toner at given voltages for toner DMU130625RC

Powder	Carrier	Applied Voltage			
		2kV		-2kV	
		Q/m	Powder ratio	Q/m	Powder ratio
DMU130625RC (Mech)	C1	0	0.00%	-6	85.60%
	C2	0	0.00%	-8.5	88.00%
	C3	0	0.00%	-1.5	39.60%

Toner DMU130625RC was unable to measure a Q/m with the +2kV voltage supply with any of the carriers, which was as expected due to the field producing an attractive force. The same trial was repeated with a –ve 2kV voltage supply. Carrier C1 demonstrated a charge of -6 µC/g from the experiment. It was found that 85.6% of the toner was able to charge with the carrier. DMU130625RC toner was able convey a charge of -8.5µC/g with carrier C2 with a powder ratio of 88%. Carrier C3 recorded a charge of -1.5 µC/g with a 39.6% powder ratio. Carrier C1, though had a Q/m within the range and a good charging ratio, was not selected due to the increased powder ratio and Q/m recorded with carrier C2. C3 was dismissed on the grounds of the weak adhesion force (-1.5 µC/g)

and poor charge ratio. The higher charge and powder ratio made carrier C2 the ideal candidate to commence printing trials with.

Similar to DMU130729RB toner, a toner to carrier loading must be found to give the optimum surface coating. A number of toner concentrations were made up from 5 to 12%. Each concentration was mixed and observed under a digital microscope as shown in the figure below. The correct toner concentration for DMU130625RC toner was found to be 8% toner to 92% carrier (by weight) as it demonstrated an appropriate compatibility with carrier C2 and minimal dusting. A micrograph of the image shows the toner and carrier loading (Figure 7:6). It can be seen that the carrier is totally covered with toner with very little toner on the background.

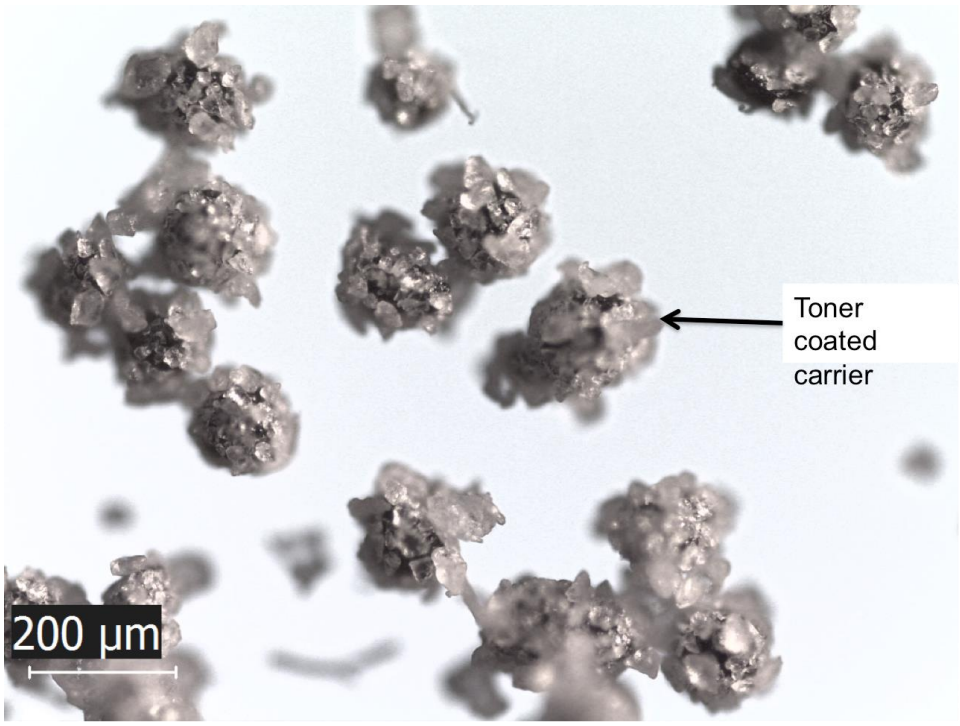

Figure 7:6: Micrograph of mechanically ground ABS toner DMU130625RC charged with carrier C2 at 8:92 ratio respectively (400X mag)

The results have shown the mechanically milled DMU130625RC toner to charge with the carrier at -2kV voltage. This is in line with the expectations as the toner is situated in the negative spectrum of the triboelectric series. In addition, the Q/m between the

chosen carrier and toner was able to demonstrate a value within the limit discussed the literature[151] and with an adequate ratio.

7.4.3 Printer voltage optimisation

DMU130625RC toner was mixed with the carrier at a ratio of 8:92 producing 1600g. The developer mix was homogenised and fed in to the printer developer unit. The rollers were turned manually to coat the magnetic roller giving an indication as to the level of charging. An additional amount of toner was placed in the reservoir, and added once the toner was shown to be at a low level. The image shown in Figure 7-8 illustrates a light brush and poor coverage across the roller due to the larger diameter carrier beads and reduced doctor blade gap. The set up shown in Figure 7-8 has a doctor blade gap intended for carrier beads with an 80µm diameter. Owing to the increased size of the carrier beads, (from 80µm to 120µm), the magnetic roller was unable to be coated adequately.

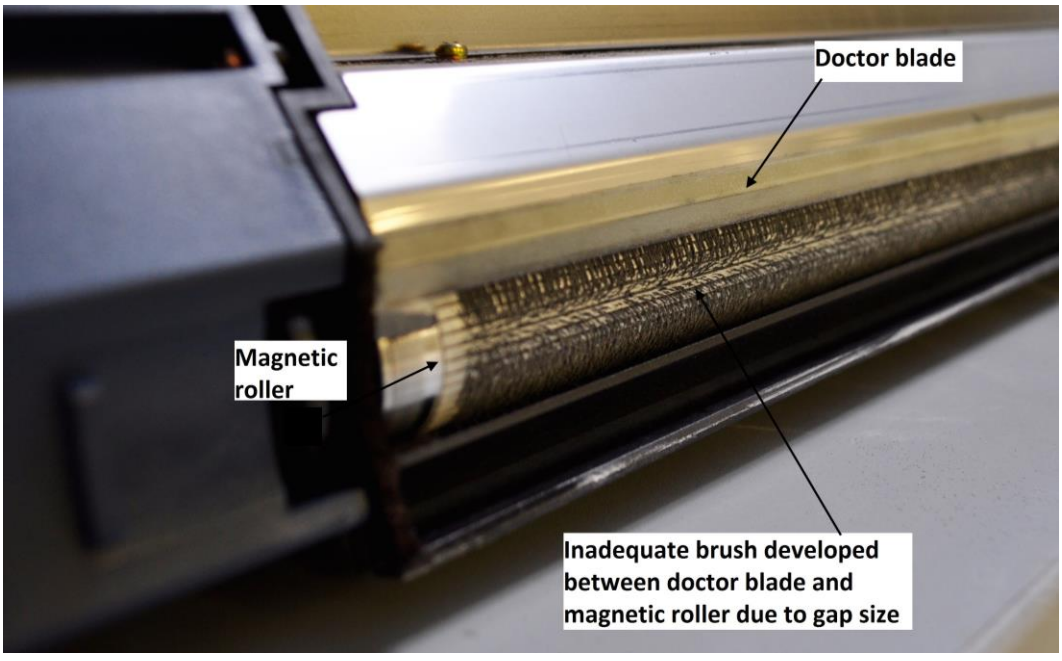

Figure 7:7: Developer unit with poor magnetic roller coverage due to insufficient doctor blade gap

The distance between the doctor blade and the magnetic roller was increased by 400µm to account for the larger carrier being used. The increase in the doctor blade gap led to a uniform and complete coverage of the magnetic roller as seen in Figure 7:8. It can also be seen that the brush is grey and homogeneous in colour with very little dusting. This denotes a good, stable charge with the carrier.

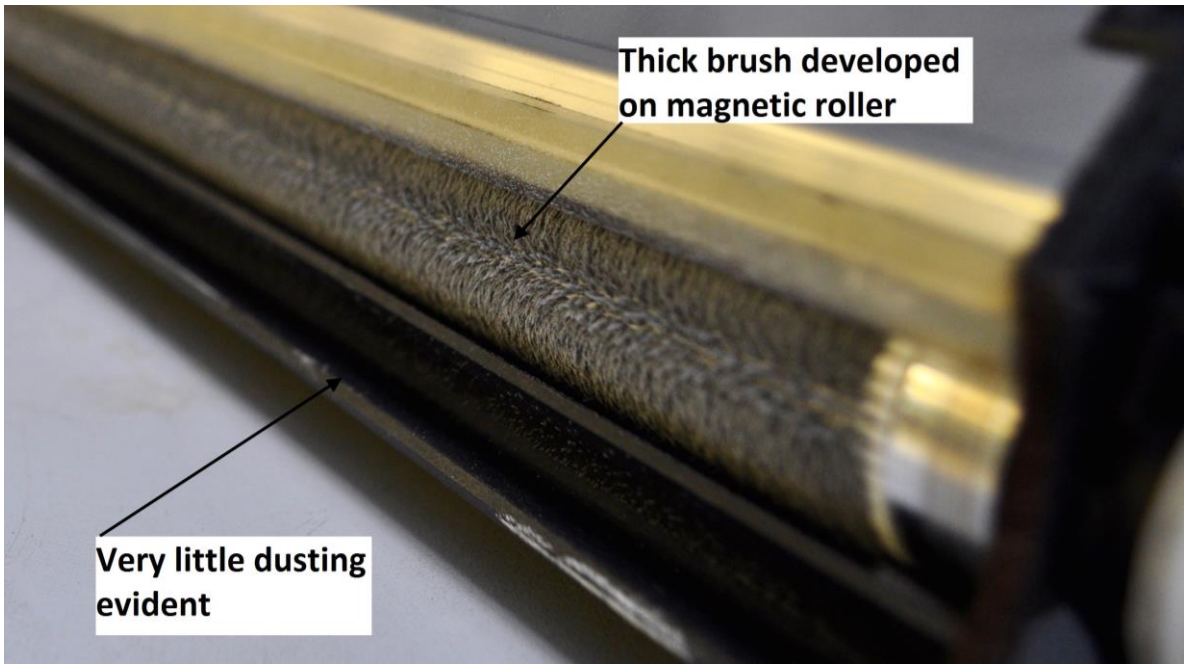

Figure 7:8: Developer unit with complete coverage of magnetic roller and uniform distribution due to increased distance from the doctor blade

With the doctor blade settings increased to give an improved coating, the voltage settings required adjusting for efficient toner transfer. Voltage settings using an established toner [5] (epoxy toner) formed the basis for the DMU130625RC toner (see Table 7:4). A test print was taken but transfer from the OPC to the transfer roller was interrupted to enable the quality of the print to be assessed visually. From Figure 7:9, it is clear the voltage settings for the epoxy, an established toner, was unable to coat the OPC with the required density. This was understandable as the Q/m differ between the two materials resulting in a different voltage to strip the toner off the carrier. It can be

concluded that as there is very little toner on the OPC Figure 7:9, the epoxy toner has a lower Q/m than DMU130625RC toner.

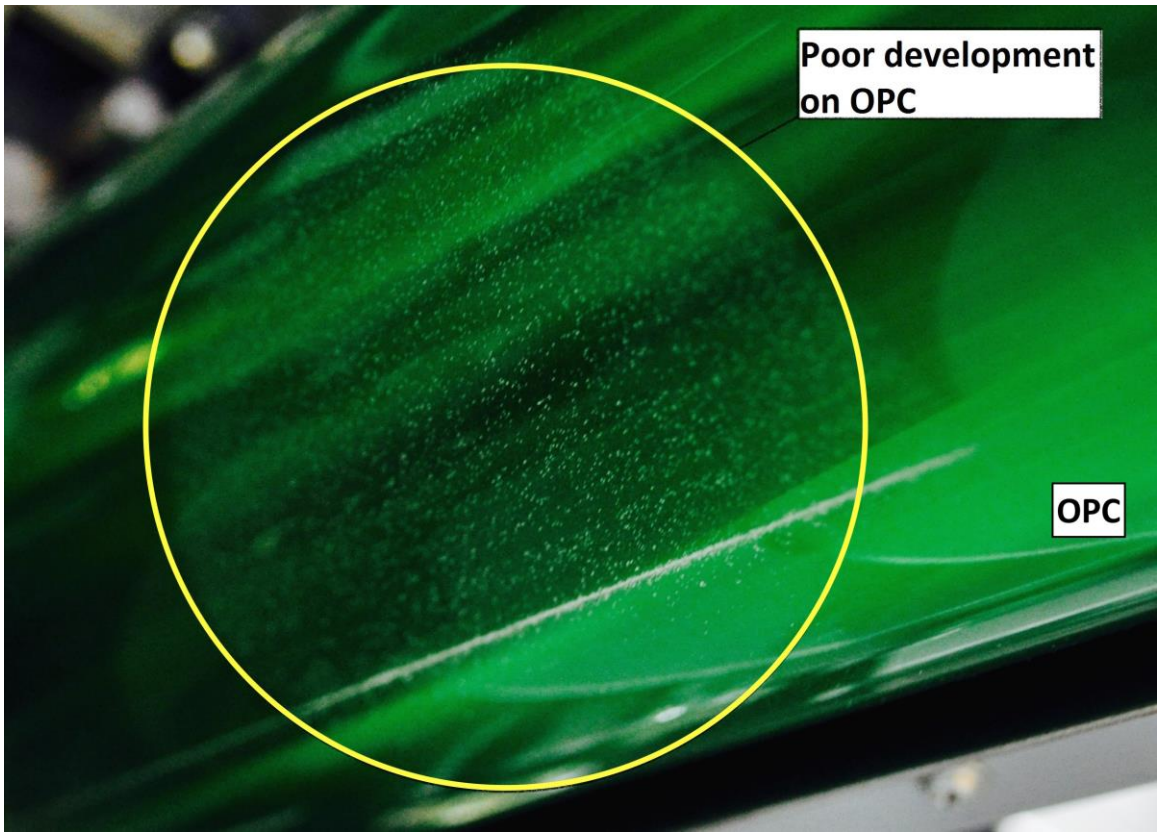

Figure 7:9: Poor toner development on OPC

The voltage settings for DMU130625RC toner are based on an established Atotech epoxy toner by Jones[5] (see Table 7:4). The initial print resulted in a poorly coated OPC. The voltages at each station were adjusted to provide an efficient transfer of DMU130625RC toner from the developer unit to the OPC. The voltage settings for the Atotech epoxy and DMU130625RC toner are show in Table 7:4.

Table 7:4: Voltage settings for epoxy toner and DMU130625RC toner

	Developer bias	OPC Charge	OPC surface charge	OPC core	Transfer corona	Transfer roller
Epoxy (initial settings)	-1313	-6000	-1622	~-900	5700	-425
ABS (developed settings)	-400	-6000	-720	0	0	400

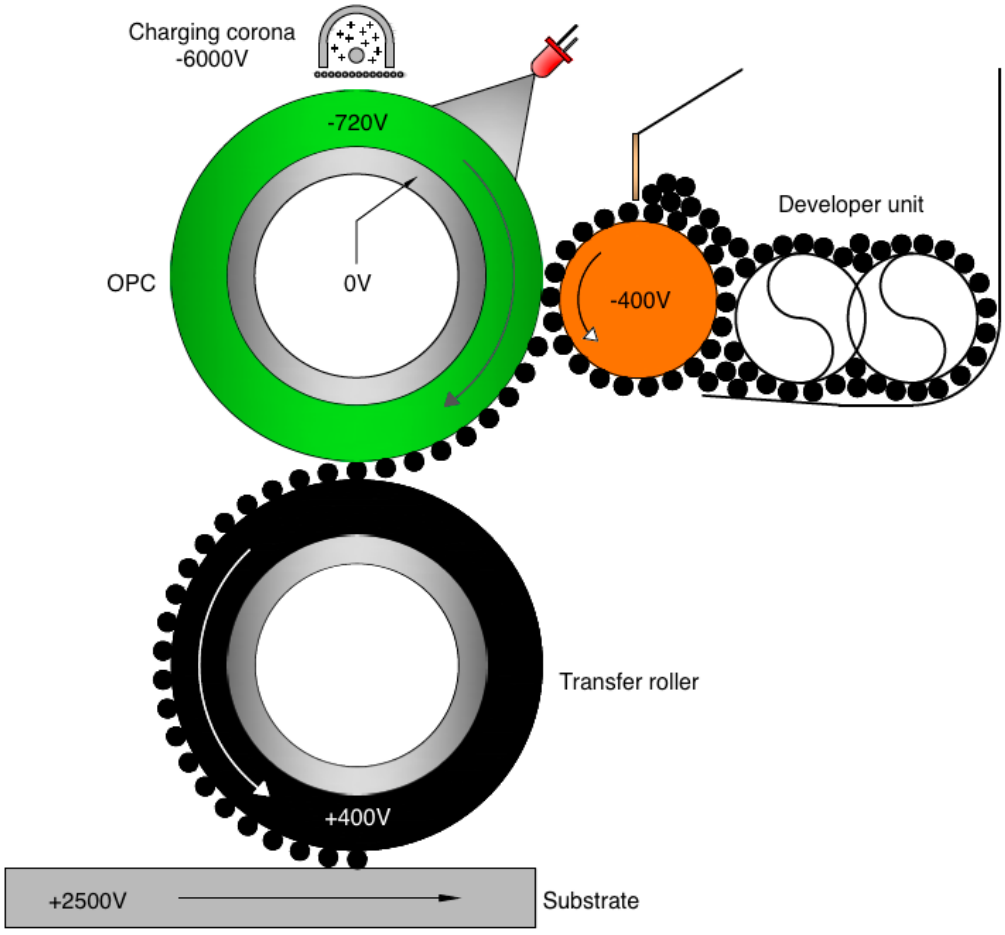

Figure 7:10: Schematic with the efficient voltages at each position of toner transfer (after Jones)[5]

Once the voltage was optimised for the OPC, the same optimisation was carried out for the transfer roller. The transfer roller is the final step, which transfers the toner to the substrate with pressure. Figure 7:11 depicts a transfer roller with a dense coating on the surface transferred from the OPC via electrostatic transfer. The schematic shows in

detail, the voltages at each station to provide the most effective electrostatic transfer of toner from the developer unit to the transfer roller.

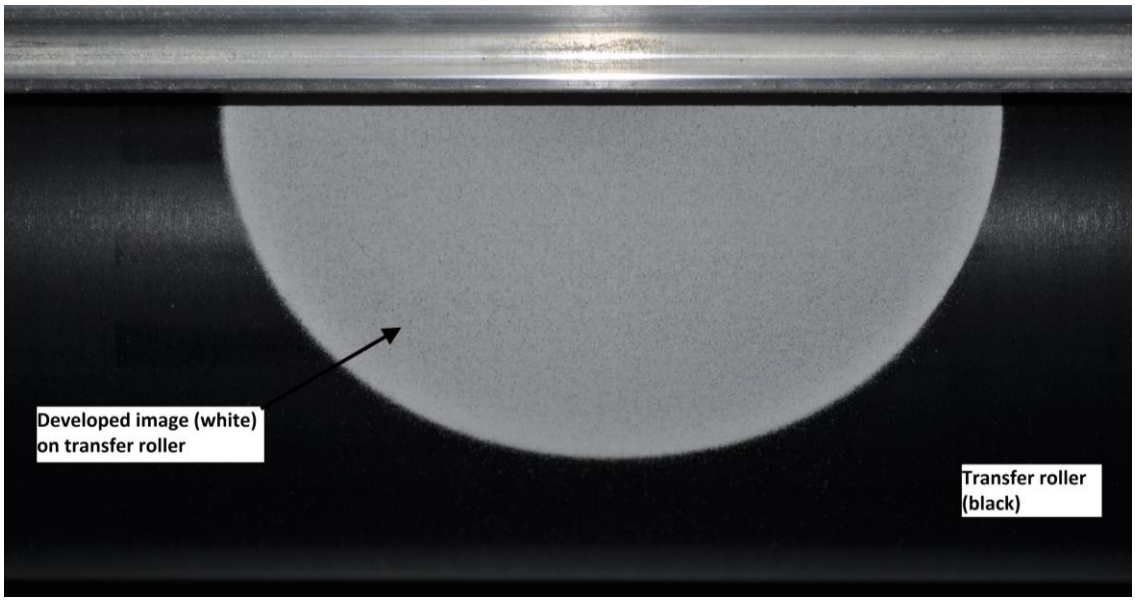

Figure 7:11: Dense layer (white) transferred from OPC on to transfer roller (black) via electrostatic deposition

7.4.4 Differential Scanning Calorimetry of ABS

A differential scanning calorimetry (DSC) was carried out from 23˚C and heated to 250˚C at ramp rates of 10˚C, 20˚C and 30˚C min^{-1} to obtain the T_g for the DMU130625RC toner. The results are depicted in Table 7:5.

Table 7:5: Tg results of DMU130625RC via DSC analysis

Ramp rate	DMU130625RC (˚C)
10˚C/min	97.16
20˚C/min	99.01
30˚C/min	103.22

An increase in T_g was seen as the ramp rate was increased. It was seen that at ramp rates of 10˚C/min a T_g of 97.16 was recorded. A ramp rate of 20˚C/min resulted in a 97.01˚C

while at 30˚C/min the T_g was 103.22. A graphical representation of the DSC results is shown in Figure 7:12

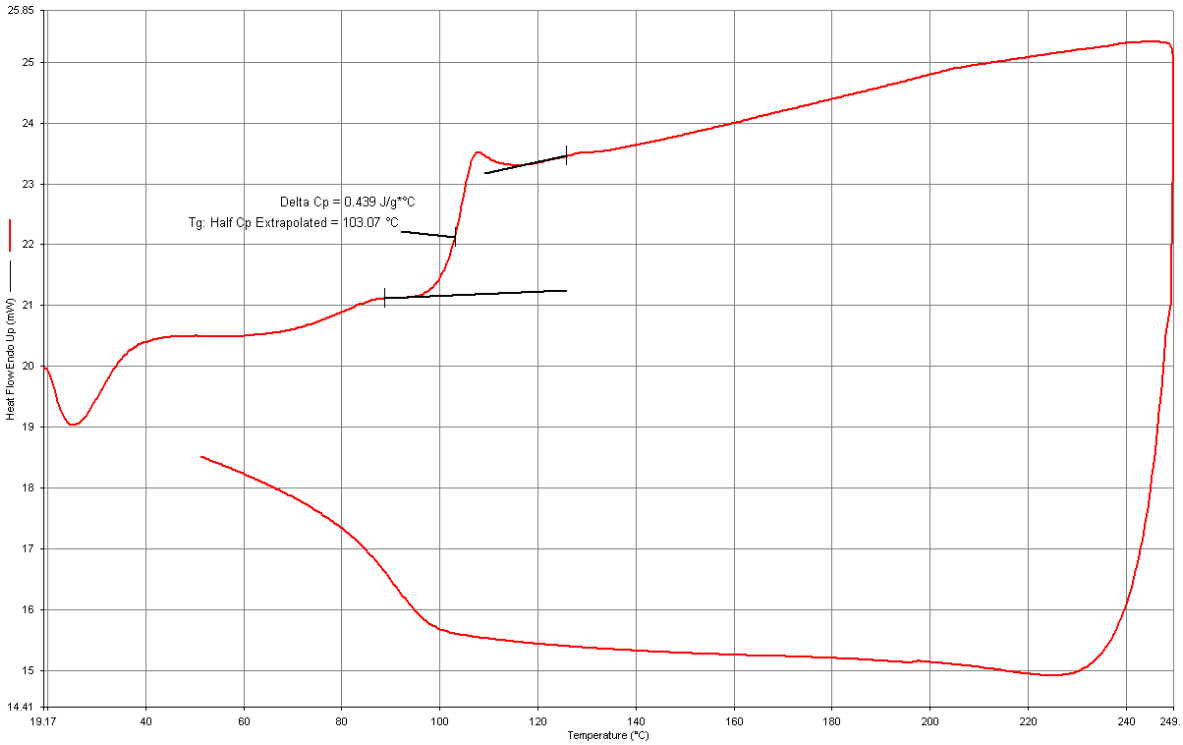

Figure 7:12: T_g of mechanically produced DMU130625RC ABS toner using DSC at 30˚C min^{-1} ramp rate

The results indicate that as the ramp rate is increased the T_g is also increased. However, from literature[168], it is suggested that the increased ramp rate provides a more accurate T_g. The largest ramp rate used was 30˚C giving a T_g of 103˚C for the mechanically milled toners. This was also echoed for the chemically produced toner. For this reason, a temperature of 103˚C was chosen as an initial fusing temperature for the ABS toner.

The DSC is shown to provide a value for the T_g, which differs from the manufacturer's method (Vicat softening point), due to the variation in the manner in which the temperatures are obtained. The T_g has a wide window and as such, can occupy a multitude of temperatures. Moreover, the process of finding the T_g via the software is based on the author's interpretation of the results. The results are unable to be compared with the manufacturer's data sheet due to displaying a Vicat softening

temperature against the experimental T_g. However, the results coincide with a generic ABS from literature [169, 170].

7.4.5 Manual method of determining T_g

In order to substantiate the results of the DSC, the DMU130625RC toner was printed on the SLP 1 rig. A visual assessment is undertaken to look for adhesion between the particles as evidence of fusion. For example, a change in colour with a greater transparency would indicate a greater degree of fusing as the material is in a phase transition. It was found that the temperature from the DSC was insufficient to fuse the DMU130625RC toner particles together. A sample was produced with five layers with a fusing temperature of 103˚C, although, the toner did not exhibit a suitable inter-particle bonding. Rather, the layer formed was lightly fused and crumbled back in to powder upon physical contact.

It is thought that the initial surface temperature of the substrate and subsequent layers were not hot enough to counter the temperature decline during the movement from the heating to the transfer stage. In addition, the ambient temperature of the laboratory may have caused the substrate temperature to further cool, not allowing for the transferred toner to be completely fused during the deposition stage. In order to alleviate the poor fusing in the layers, the fusing temperatures were sought empirically. A temperature range from 110˚C to 130˚C was tested in increments of 5˚C.

At a fusing temperature of 110˚C, the five layers did not fully consolidate. A loosely bonded skin was formed which broke on contact. The temperature was increased to 115˚C to observe whether the temperature rise was sufficient to fully sinter the layers (see Figure 7:13).

Figure 7:13: Fused ABS at 115˚C (5 layers)

From Figure 7:13 it is evident that at 115˚C the temperature was still too low to fuse the layers resulting in failure of the sample during printing. The experiment was repeated to examine the fusing efficiency at 120˚C. The results showed that even at 120˚C, the sintering temperature was inadequate in fusing the layers effectively, although there was an improvement on 115˚C. At 125˚C the sample displayed signs of further improvement with a stronger bond (see Figure 7:14), although the samples were still fragile.

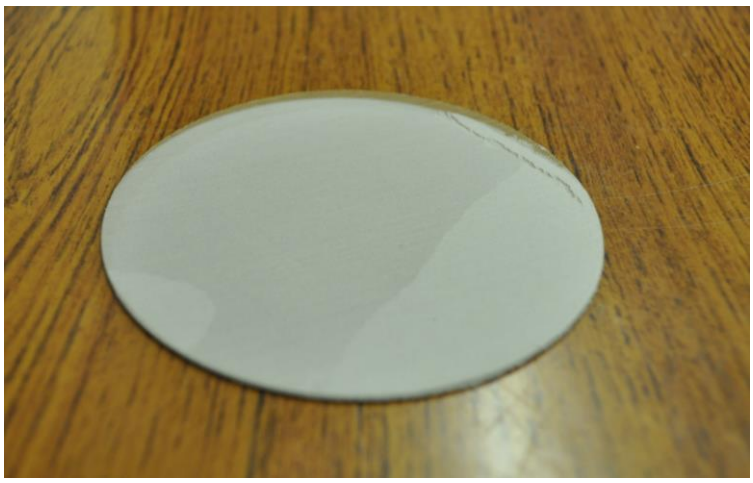

Figure 7:14: Fused ABS at 125˚C (5 layers)

The experiment was repeated at 130˚C to find the fusing temperature for the mechanical toner. Five layers were printed and assessed visually and physically.

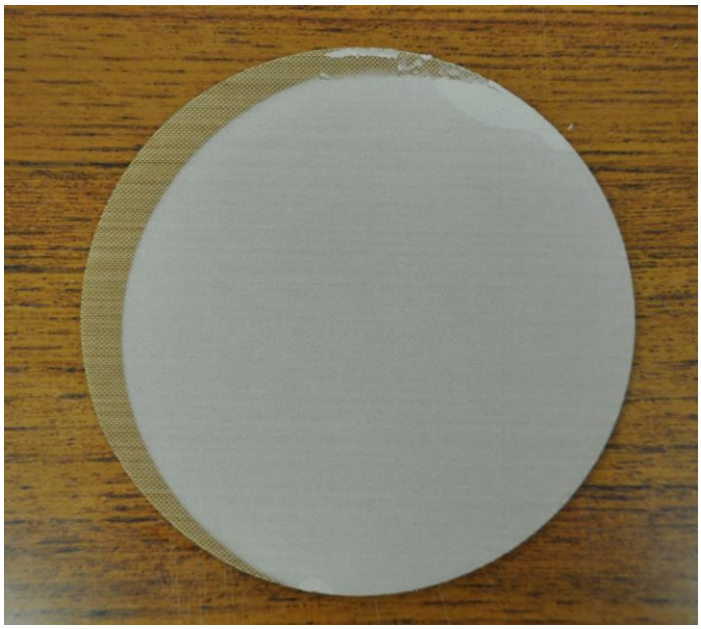

Figure 7:15: Fused ABS at 130˚C (5 layers)

It is shown in Figure 7:15 that the sample is adequately fused as the sample was removed off the substrate without breaking and there is no evidence of any slipping from the transfer roller. The sample is shown to be a fused and the layers consolidated and free from delamination on handling.

Table 7:6: Fusing temperature with corresponding results

Fusing Temp (˚C)	Level of fusing
103	Powder form, no visible fusing
110	Poor fusing, sample broke on contact
115	Light fusing, sample broke on contact
120	Improvement on 115˚C, but cannot be handled
125	Good fusing, however, very fragile
130	Well sintered and handled without breaking

The results from the DSC trials results corroborate with the literature[169, 171], however, the temperature required to achieve a contiguous fused layer was significantly (27˚C) higher than that expected. This could be attributed to the following reasons;

1) Incorrect temperature measurement – The thermosensor has been calibrated in accordance with the method described by Jones [5]. Therefore, this is unlikely.

2) Surface coating – The surface coating on the ABS toner is known to suppress inter-particle fusing as described by Banerjee[4]. In addition, the DSC results were undertaken using uncoated ABS due to concerns over damaging the equipment.

3) It is known from the literature[122, 169, 171, 172] that amorphous materials such as ABS do not have a sharply defined melting point, but rather, have a wider softening range. These materials are viscous and coalescence of particles freely occurs in the presence of heat and pressure[27, 173].

The temperature settings have shown with standard pressure, an adequate fusing regime can be found (Table 7:6).

7.4.6 Determination of Load

The results of the pressure tests were carried out by driving up the secondary Z platform against the transfer roller of the printer. By placing an A4 sheet of paper between the transfer roller and ceramic substrate an impression of the nip region was taken, allowing the contact region to be accurately measured.

Figure 7:16: Substrate with nip region vertically across the substrate

The nip region is highlighted as a straight line running across the substrate as illustrated in Figure 7:16. The area across the width of the region is measured by the length and width of the line.

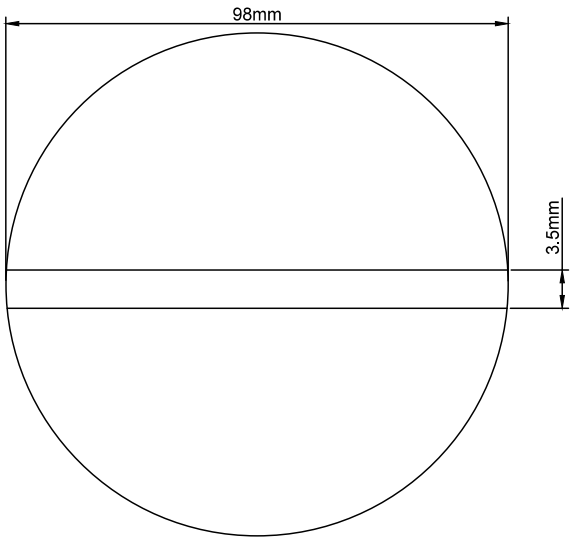

Figure 7:17: Schematic of ceramic substrate with nip region dimension

The pressure was calculated using the following equation;

$$P = \frac{\mathrm{F}}{\mathrm{A}}$$ Equation 8

Where;

F = Exerted force measured by the pressure sensors (N)

A= Length multiplied by the width of the contact region (mm^2)

P= Pressure reading (Pa)

Measuring the contact region to be 3.5mm with and 93mm across the substrate, the contact area was calculated to be 325.5mm^2. The applied force generated from the paper test was measured to be 6N, resulting in 18.433kPA as the standard pressure. Table 7:7 displays the load and pressure equivalent with a 3.5mm nip region

Table 7:7: Load and pressure equivalent

Load (N)	Pressure (kPa)
6	18.433
8	24.577
10	30.722

From the pressure reading, it was noted that the paper test represented a 6N force (20.8kPa). For future reference, load will be stated rather than pressure as a direct value from the load cells, as the contact area will change making a pressure value very difficult to calculate.

7.5 Electrophotographic printing of ABS

The results of the experimental work outlined in this section focus on the influence of three factors; (1) Fusing temperature, (2) Fusing load and (3) Stand-off distance. As described in the methodology chapter (Section 4) the printed discs were produced and analysed for their physical and mechanical properties. The sample numbers were derived from the Design of Experiment software (JMP). Outlining the three parameters a number was assigned to each level as shown in Table 7:8.

Table 7:8: Parameter and levels

	Level		
	1	2	3
Temperature	130	140	150
Load	6	8	10
Stand off	105	135	75

Using the DoE software, the parameters and levels were entered in to the software and the experiments were generated. A table of the corresponding sample number and their respective parameters are shown in Table 7:9.

Table 7:9: Sample No. with respective parameters

Sample No/DoE No		Temp (˚C)	Load (N)	Stand off (mm)
1	332	150	10	135
2	331	150	10	105
3	333	150	10	75
4	322	150	8	135
5	321	150	8	105
6	323	150	8	75
7	312	150	6	135
8	311	150	6	105
9	313	150	6	75
10	232	140	10	135
11	231	140	10	105
12	233	140	10	75
13	222	140	8	135
14	221	140	8	105
15	223	140	8	75
16	212	140	6	135
17	211	140	6	105
18	213	140	6	75
19	132	130	10	135
20	131	130	10	105
21	133	130	10	75
22	122	130	8	105
23	121	130	8	75
24	123	130	8	135
25	112	130	6	75
26	111	130	6	105
27	113	130	6	135

The graphs constructed below display the error bars from the standard deviation. The error bars were calculated using the following equation.

$$\sqrt{\frac{\sum(x-\bar{x})}{(n-1)}}$$

Equation 9

7.5.1 Height

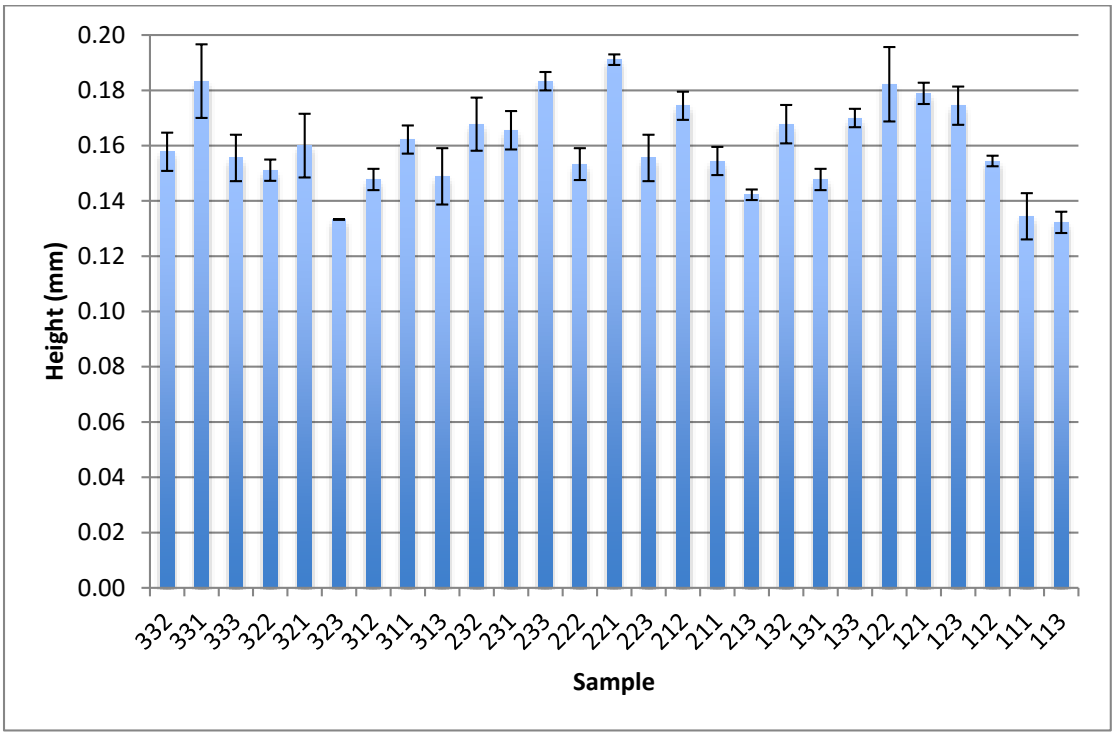

Figure 7:18: Height of samples with error bars

Figure 7:18 shows the height of 27 samples produced using five printed layers varies 60µm between the maximum and the minimum values. The maximum height of the samples was 190 µm and the minimum height recorded was 130 µm. This suggests an average layer thickness of 38µm for the maximum height and 26µm for the minimum height sample. The most frequent height readings were 0.13mm and 0.17mm with an average height of 0.175mm achieved over the entire 27 samples. The error bars on the graph displays a good correlation between the samples. However, at sample no 331 and 122, the standard deviation is increased with a standard deviation of 20µm for the samples. The sample with the greatest height was achieved by using a temperature of 140˚C, a load of 8N and a stand-off distance of 105mm.

Contrary to the expected nominal 50µm layers, the measured layers range between 130µm to 190µm. The most likely explanation to the discrepancy is due to the poor

consolidation of the material through insufficient heating and applied pressure. In light of the higher than expected sample height, it would be expected that the mechanical properties would be significantly less compared to the bulk properties of the ABS material. This is discussed further in the chapter. In addition to poor consolidation of the material, any surface anomalies caused by localised balling (semi fused particles) will lead to an increase in the measured thickness value. Again, this is discussed further in Section 7.5.3.

Using a two sigma limit, a control chart is formed as shown in Figure 7:19. It is clear that samples 323, 332, 111 and 113 are out of the control limits. A regression analysis was carried out using Design of Experiments software. The analysis highlighted temperature as a significant factor with a P value of 0.0907 (a P value of less than 0.1 is considered significant). The R^2 value of the model was 0.629, which describes the model as not statistically significant. A value of 1 or closer is shown to have a perfect fit.

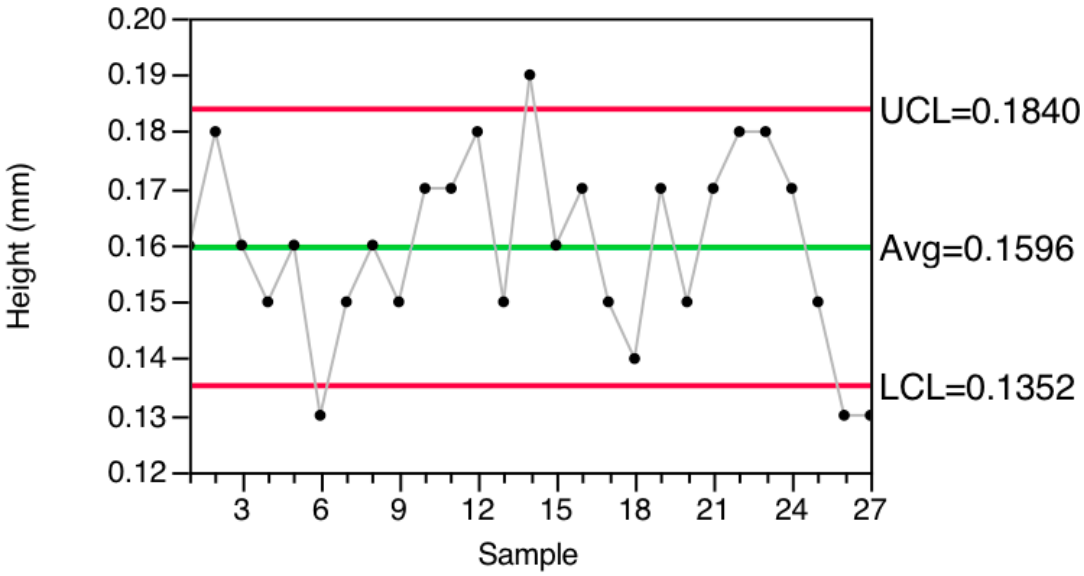

Figure 7:19: Control chart for height with two-sigma deviation

7.5.2 Mass

The mass of the samples against the respective samples is shown in Figure 7:24. The graph represents the average mass of the samples and the standard deviation represented by the error bars. The mass varies from 37mg to 57mg, with 46mg as the average mass of the sample.

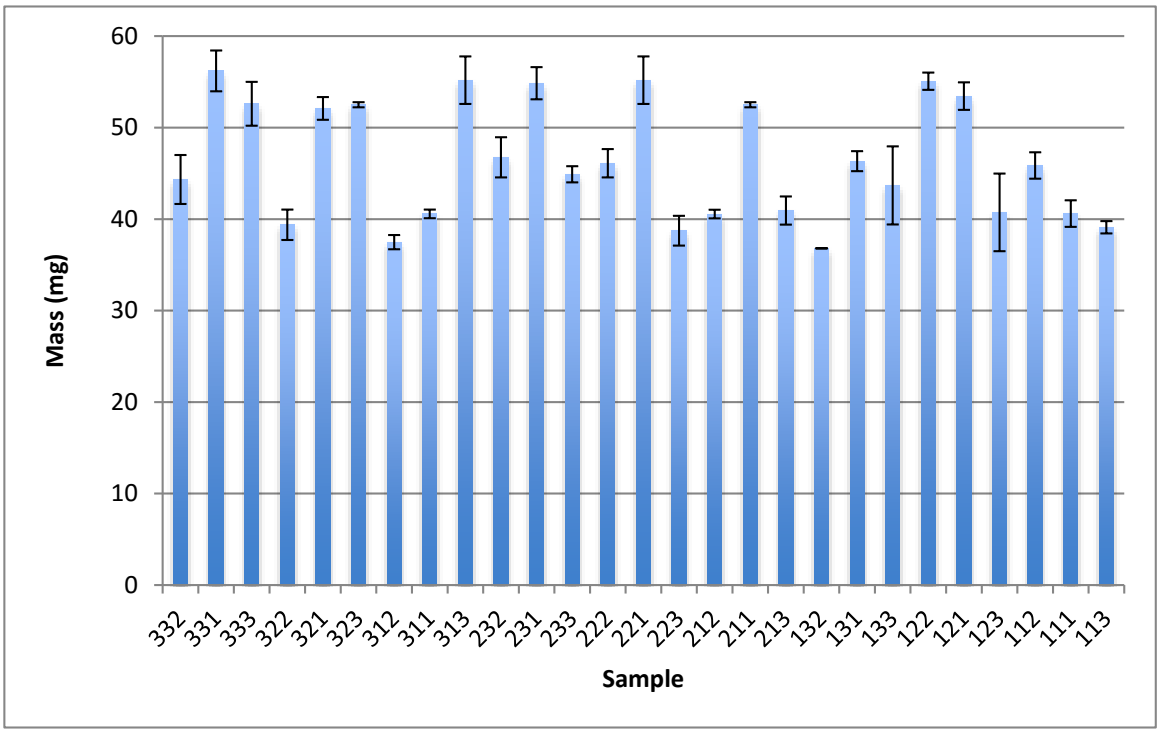

Figure 7:20: Mass vs sample

Comparing Figure 7:18 and Figure 7:20, a trend can be seen. At sample 331, the mass recorded its highest value at 56mg. Comparing the height of sample 331, it is clear that the height achieved was 0.18mm. The maximum of 0.19mm was obtained by sample 221, with the corresponding mass at 55mg (second highest value). The lowest height, sample 323 and sample 113, recorded a mass of 52mg and 39mg respectively. This is still above the lowest value of 37mg recorded by sample 312 and 132, with a height of 0.13mm. The mass of the samples did not produce a direct comparison with the height, however, for the majority, a trend can be seen to show that as the height increases, the

mass is also increased. The mostly likely cause for a breakdown in the link between part height and mass is a change in the density of the sample – this is studied in Section 7.5.3.

Further analysis of the results was carried out via a control chart. Using the standard deviation, an upper control limit (UCL) and lower control limit (LCL) was set (see Figure 7:21) using JMP statistical software.

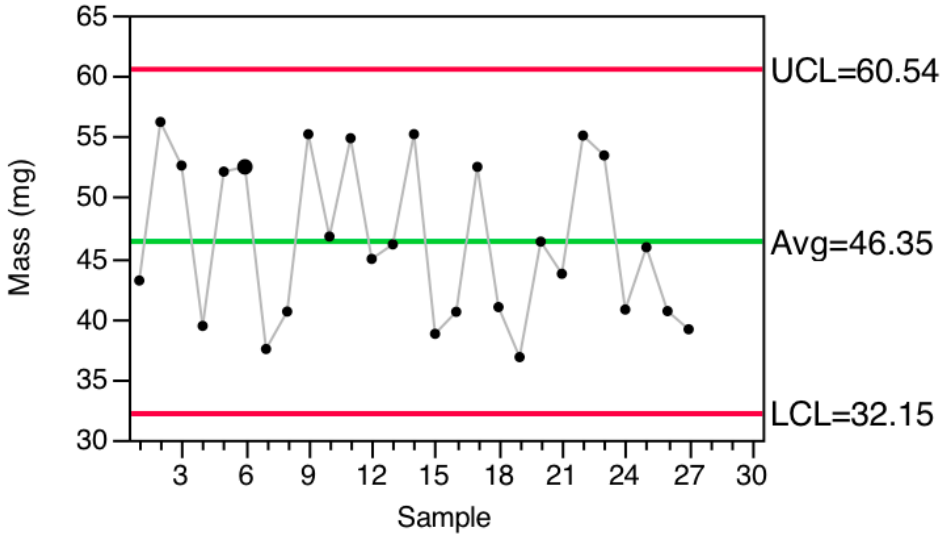

Figure 7:21: Control chart depicting samples outside the UCL and LCL using standard deviation

Figure 7-23 shows that while the samples are within the predefined control limit, the deviation is still relatively large as very few samples are close to the average (46.35mg). Variability charts can be seen in Figure 7-23a-c. Again, very little can be initially deduced from the samples, as the results show no clear trend between the parameters and the resultant mass. However, the stand-off distance has shown to have a high impact on obtaining a greater mass. The recorded mass nearly always obtained a peak value (compared to the other stand-off distances) when the stand-off distance was set to 105mm regardless of the applied load or temperature. This trend runs true for the majority of the samples with only 3 of the 27 samples recording a lower mass at a 105mm stand off from the IR heater.

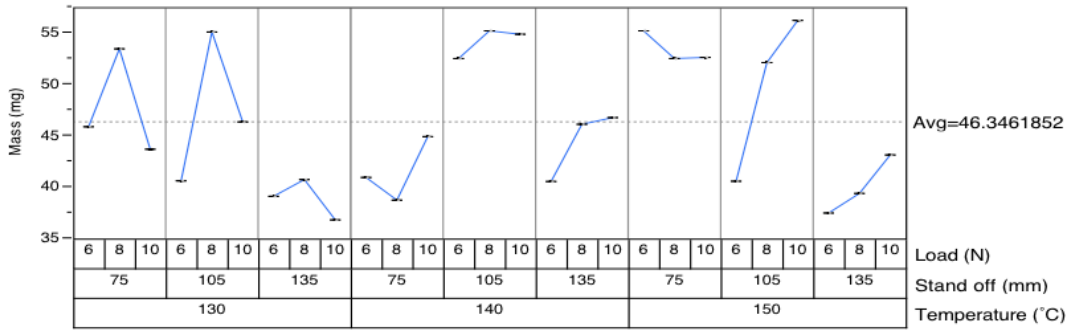

a

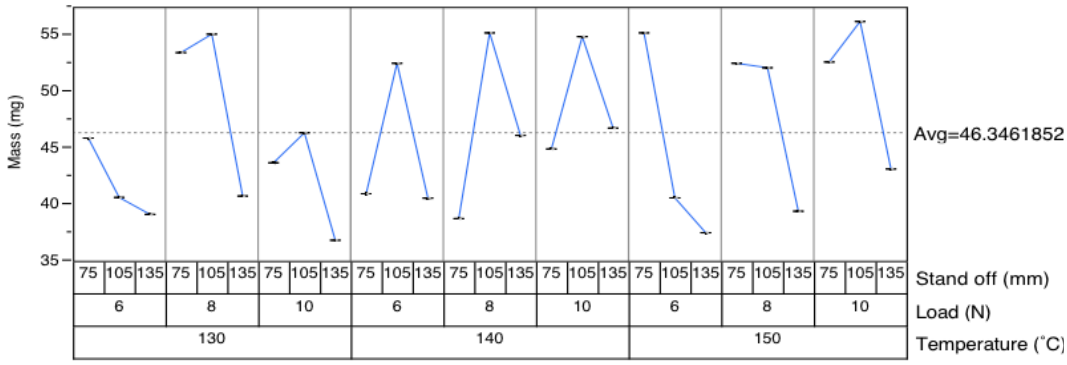

b

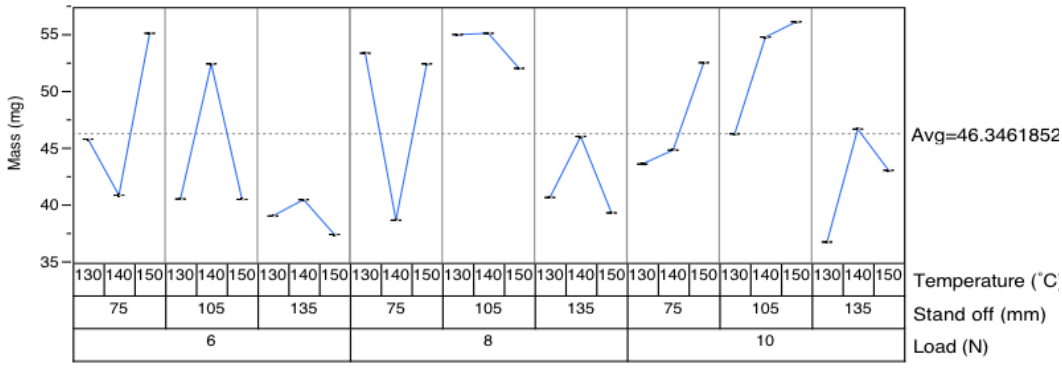

c

Figure 7:22: Variability chart for load (a), stand off (b) and temperature (c) against mass of the sample

A low degree of heat and pressure coupled with a soft transfer roller are the likely cause of the anomalies seen the in the date presented. The top surface of the sample (see Figure 7:26, pg 215) shows an adequately fused layer with the exception of partially

fused clusters of balled toner particles. The partially fused particles could potentially be the larger particles, which required a greater amount of heat and pressure to enable a flat and consolidated surface to be formed. Moreover, the protruding toner particles could also account for the inaccuracies in the height measurement in the samples. Each deposited layer is previously heated to ensure a tacky surface on to which the transfer roller can deposit a fresh layer of toner. If the IR radiation is not able to sufficiently heat the larger particles, they are less likely to deform under pressure resulting in poor consolidation, porosity and uneven surfaces with large peaks. The next layer will further exaggerate the defects.

A regression analysis of the results was undertaken to quantify the impact of the factors. The load recorded a P value of high statistical significance (0.0002) with interactions between temperature and load providing a significant effect (P value = 0.0171) and also temperature and stand-off (P value =0.0522). The stand-off distance alone, was shown to have a P value of 0.1462, which suggest statistically, stand-off distance has very little bearing on the mass of the sample contradicting earlier results from Figure 7:22a-c. However, the regression analysis and the results from Figure 7:22a-c suggest the interaction with the stand-off distance is of significance. While the regression model does not provide firm statistical evidence to link the correlation with the variation model due to the confidence level of the model (77%), a relationship can be established.

Another factor to consider is the effect of surface charge against the mass. Charge accumulation is well known to have a detrimental effect on toner deposition [2, 5, 10, 11, 13, 126, 139]. The accumulation of a repulsive surface charge has a negative effect on toner deposition, which ultimately can influence the sample density, height and the mechanical properties.

The surface charge on the deposited layer of the sample was measured using the high-resolution probe and electrostatic voltmeter. The graph indicates that the surface voltage decreases as mass of the sample increases.

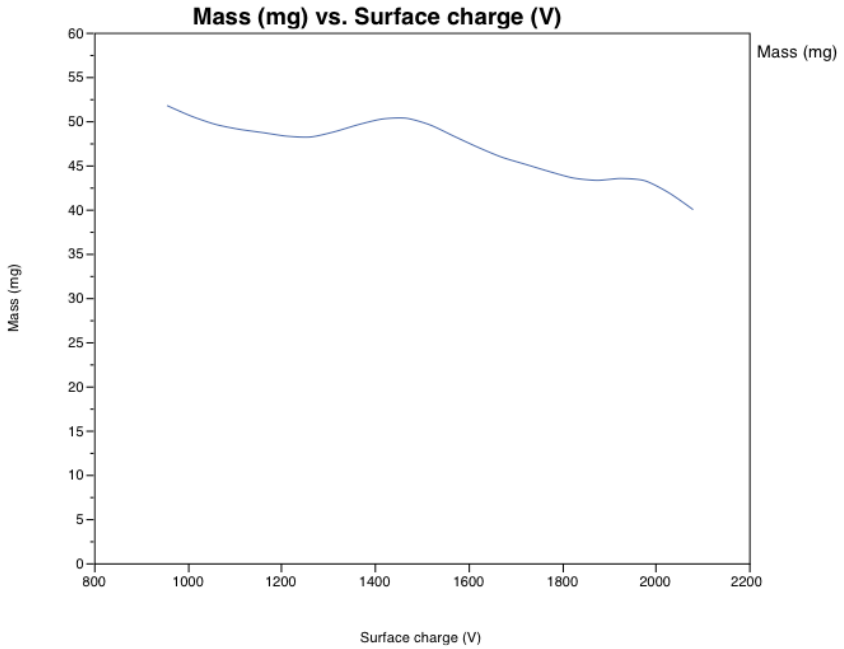

Figure 7:23: Mass vs surface charge

Figure 7:23 indicates a correlation between the mass of the samples and the surface charge recorded at the final layer. It can be seen that when the surface charge is at 1000V, the mass is not at its peak. A downward trend is seen until approximately 1250V, where the mass is increased, although not above the peak seen at ~950V. The graph continues the trend of mass decay as the surface charge increases, with a slight increase at 1900V before the mass continues downwards. The general trend of the graph demonstrates a decline in the toner deposited as the surface charge increases. This is in agreement with the literature [2, 5, 49, 76, 139, 144, 167], however, since the sample is believed to be inadequately consolidated, the sample height is artificially inflated, reducing the field strength further.

7.5.3 Density

The density can be measured by its apparent or bulk properties. The apparent density is defined as "the weight in air of a unit volume of a material" and is used to determine the density of powders. ASTM defines the bulk density as "*the weight per unit volume of a material including voids inherent in the material as tested*"[174] and is used for moulded parts. In the case of the SLP samples, the density will be compared to the bulk properties, since the samples have been sintered.

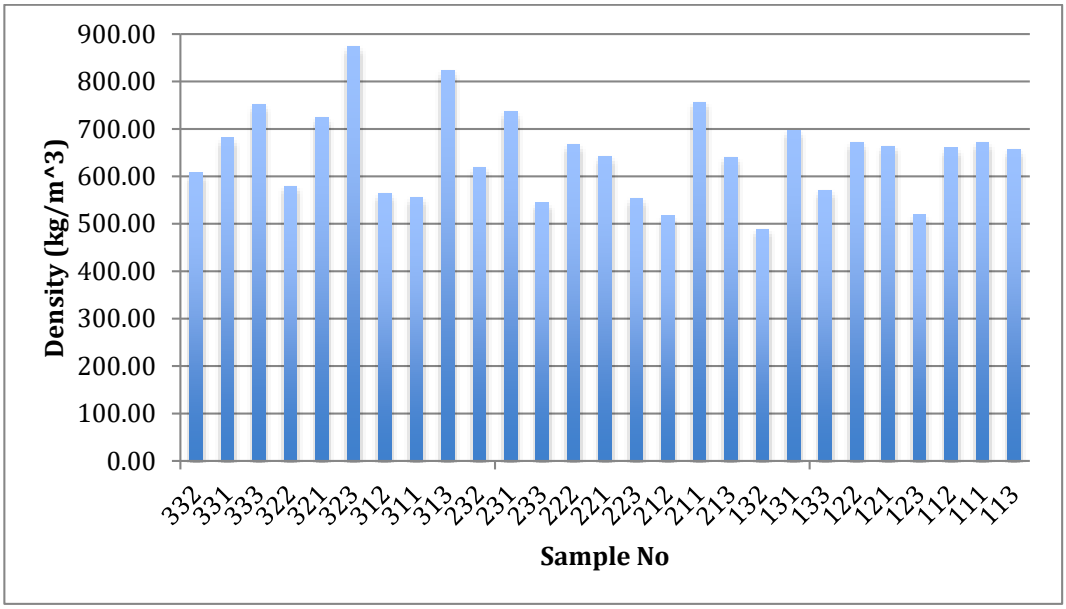

Figure 7:24: Density Vs Sample

The densities of the samples (see Figure 7:24) range from 487.59kg/m^3 to 874.94kg/m^3. When compared to the bulk density of ABS (1050kg/m^3) the samples demonstrate densities ranging from 49%–83%. This indicates that the samples suffer from high levels of porosity (typically between 17% and 51%). Processes such as Selective Laser Sintering claim density of 80 to 100% of the bulk density of the polymer can be achieved [28, 29, 175].

SEM micrographs were taken of the samples to assess the nature of the fused samples and the porosity present. From sample 132 (Figure 7:25) it is clear that significant porosity exists within the sample and this extends through multiple layers. Particle bonding is present, with areas displaying signs of necking. However, the porosity and large gaps between particles could imply there is insufficient toner deposition or lack of heat and/or pressure.

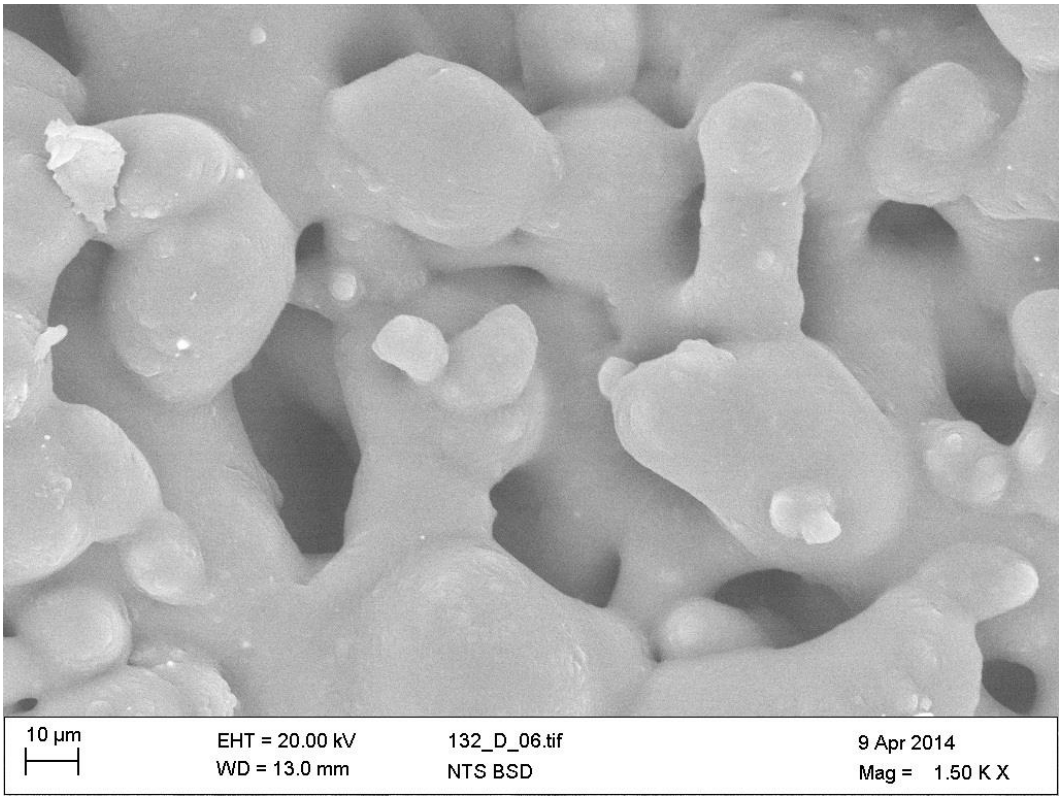

Figure 7:25: SEM micrograph of inter particle bonding of a layer and porosity (DoE 132)

Comparison of the samples with the greatest and least density was also undertaken; Samples No. 312 (Figure 7:25) and 323 (Figure 7:26). Sample No. 323 has a density of 842.22 kg/m^3, contrasting sample 312 with a density of 487kg/m^3. An SEM micrograph shows the surface of sample 323 (Figure 7:26) and highlights the inter-particle bonding at the surface of the sample. It is clear that its surface exhibits very little porosity. However, there is clear evidence of larger particles and agglomerates present in the micrograph indicating insufficient heat and/or lack of pressure to fuse the particles to

produce a smooth surface. An additional hypothesis, which could explain the poor surface texture, is the transfer roller, deforms preventing a smooth flat surface from being produced. Although the surface appears to be fully fused overall the sample has a density of 83% against the bulk polymer.

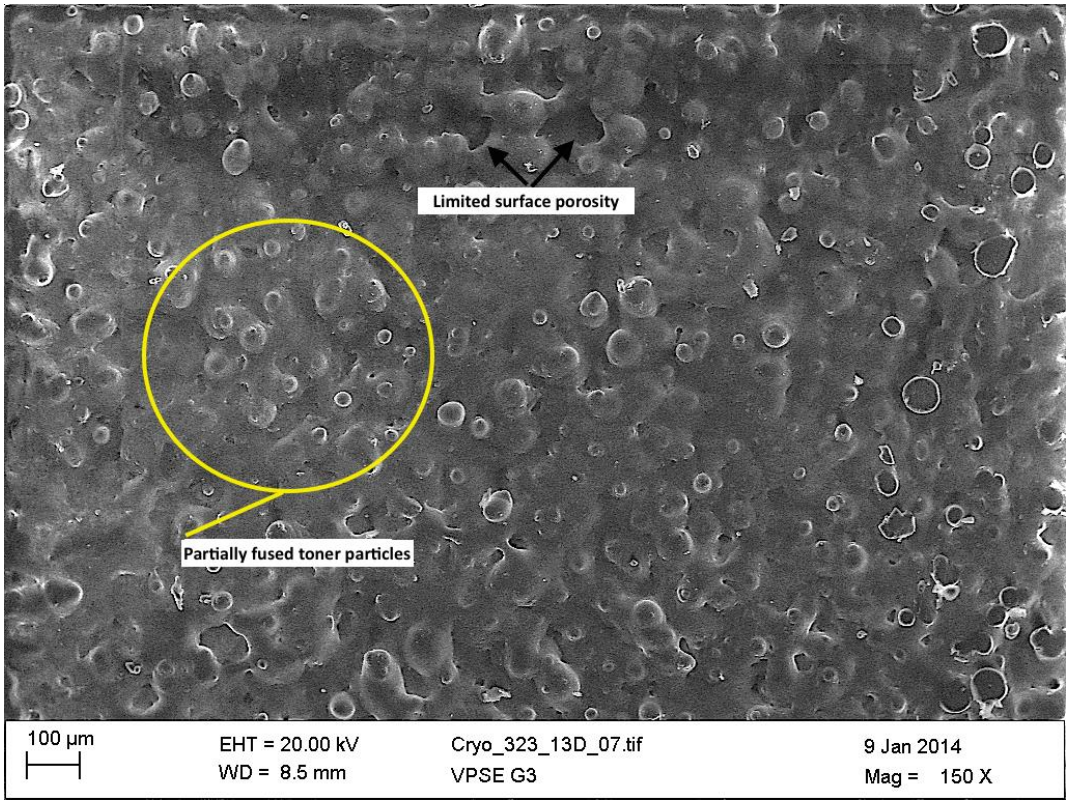

Figure 7:26: SEM micrograph for sample 323 displaying inter-particle bonding

An SEM profile of sample 132 is shown in Figure 7:27. The micrograph also demonstrates inter-lamina bonding occurs, but again, a lack of heat and/or pressure results in poorly consolidated layers. The weak inter-particle bonding may also be attributed to the viscoelastic properties of the polymer itself. It can be seen that the applied load was insufficient to consolidate the powder even at temperatures up to 150˚C. To overcome the viscoelasticity of the material, it is necessary for the temperature and/or the pressure to be increased [117, 118]. Unfortunately, the current architecture of the rig does not allow for the increase due to the temperature limitation on the OPC and the

maximum allowable pressure on the transfer roller. However, by segregating the heating and pressure phase from the transfer phase a greater temperature and pressure can be applied, which could potentially lead to improved consolidated layer. Additional methods to overcome the restrictions the current rig has with respect to heat and pressure can be found in the Further Work Chapter.

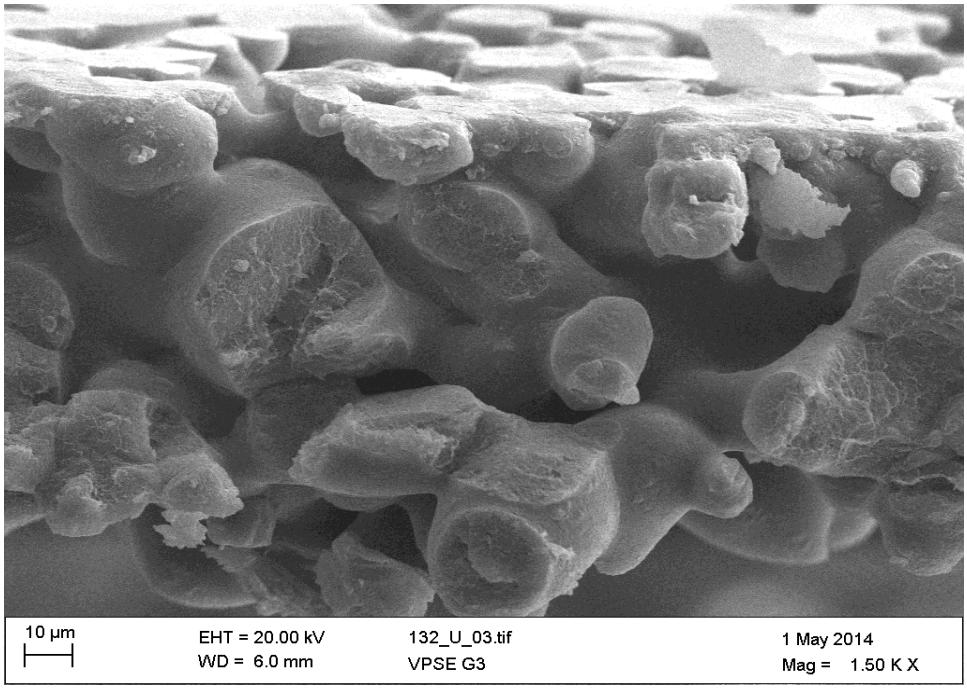

Figure 7:27: Cross section of multilayer prints of sample 132 with a high degree of porosity

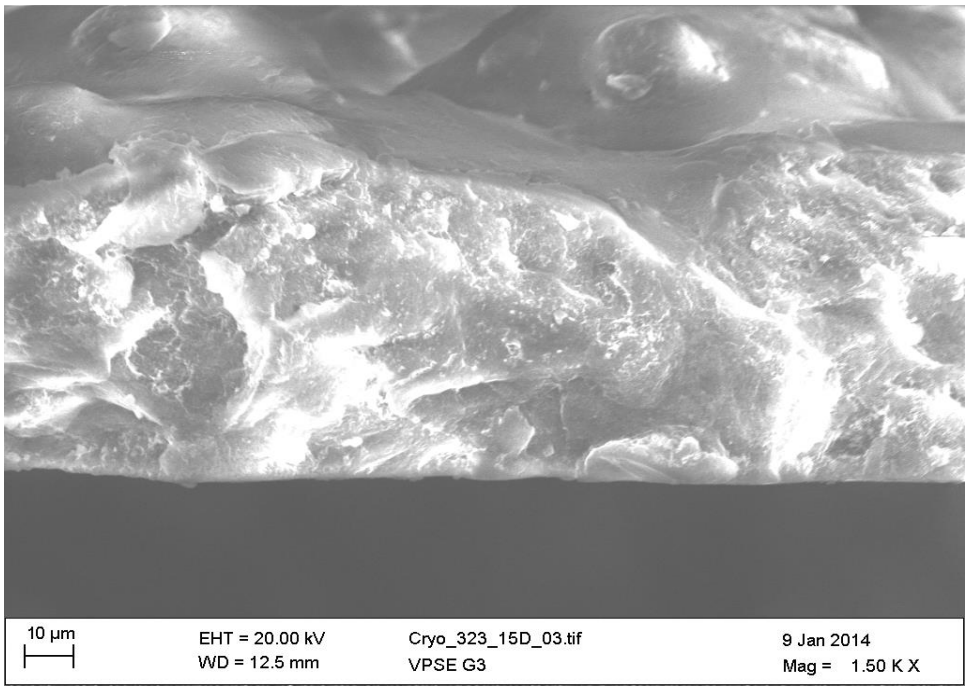

Figure 7:28: Cross section of multilayer prints of sample 323 with low visible porosity

A cross section of sample 132 and 323 is shown in Figure 7:27 and Figure 7:28, respectively. The micrograph illustrates a significant increase in density in sample 323 (Figure 7:28) compared to the sample 132 (Figure 7:27). However, the cross section still highlights areas of light porosities within the sample, this is further exemplified in Figure 7:29. It is clear that the majority of the particles are fused to the previous layers, although the sample exhibits poor inter-lamina bonding. The layer formation shows the particles to have contoured around the previous layer rather than forming a distinct homogenous layer. This suggests that the temperature was too low to enable particles to fully fuse and consolidate. Moreover, the partially disassociated layers will invariably contribute to delamination and inferior mechanical properties, a phenomenon that is well documented in the FDM (Fused Deposition Modelling) process [172, 176].

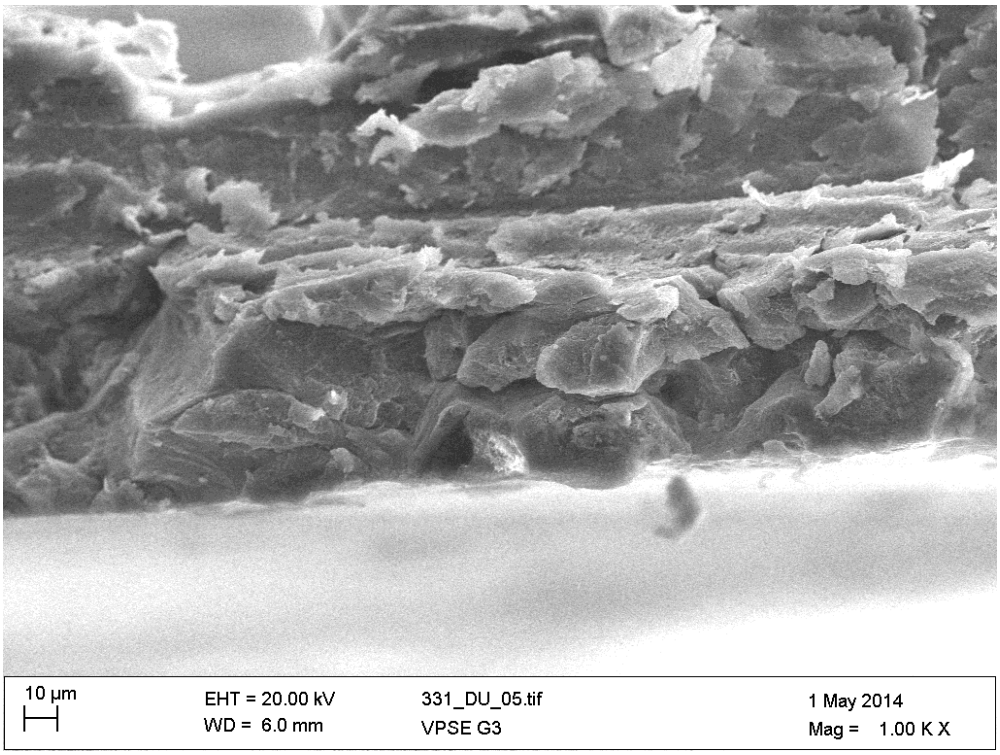

Figure 7:29: Cross section of sample 331 at 1000x

Using a control chart (Figure 7:30), the samples were assessed with a two-sigma deviation from the mean to assess the outliers of the samples. It was found that sample 323 was outside the control limit.

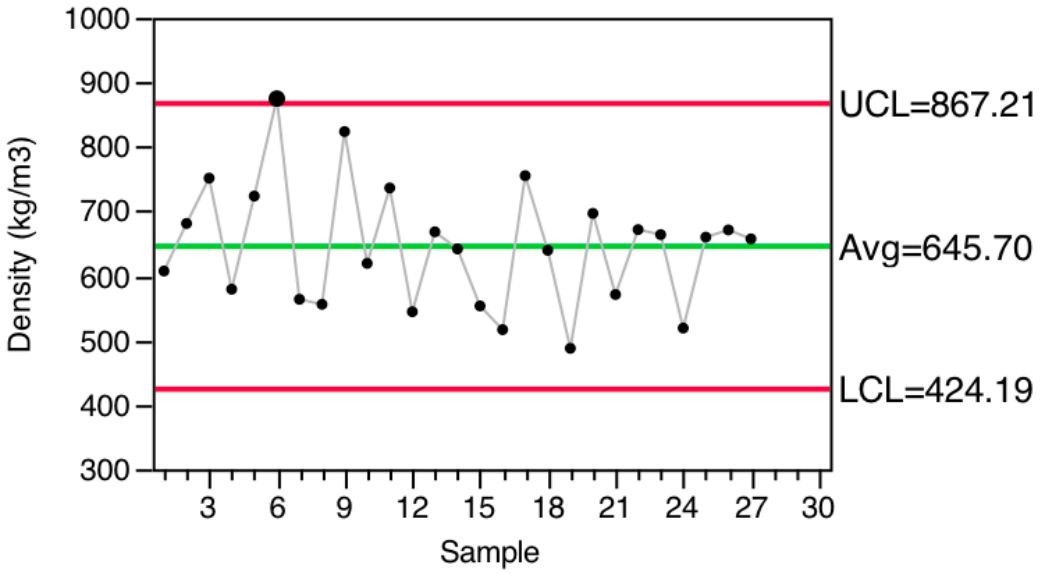

Figure 7:30: Control chart with a two-sigma approach for density

Using the information from the control chart sample No. 323 (sample 6 in Figure 7:30) was omitted from the results to reduce the error in the graph. A mass vs density graph was constructed to understand the relationship, this is shown in Figure 7:31.

Although, it can be seen from Figure 7:31, the graph does largely represent a linear relationship. Due to the varying thickness of the samples, the geometry is inconsistent, deviating from an expected linear relationship between the mass and density. The graph begins at linear trend, however, at approximately 550kg/m^3, there is a slight deviation - one potential explanation could be due to the measuring process. Owing to the fragile nature of the samples, it was difficult to measure and thus control the geometry precisely, leading to potential anomalies.

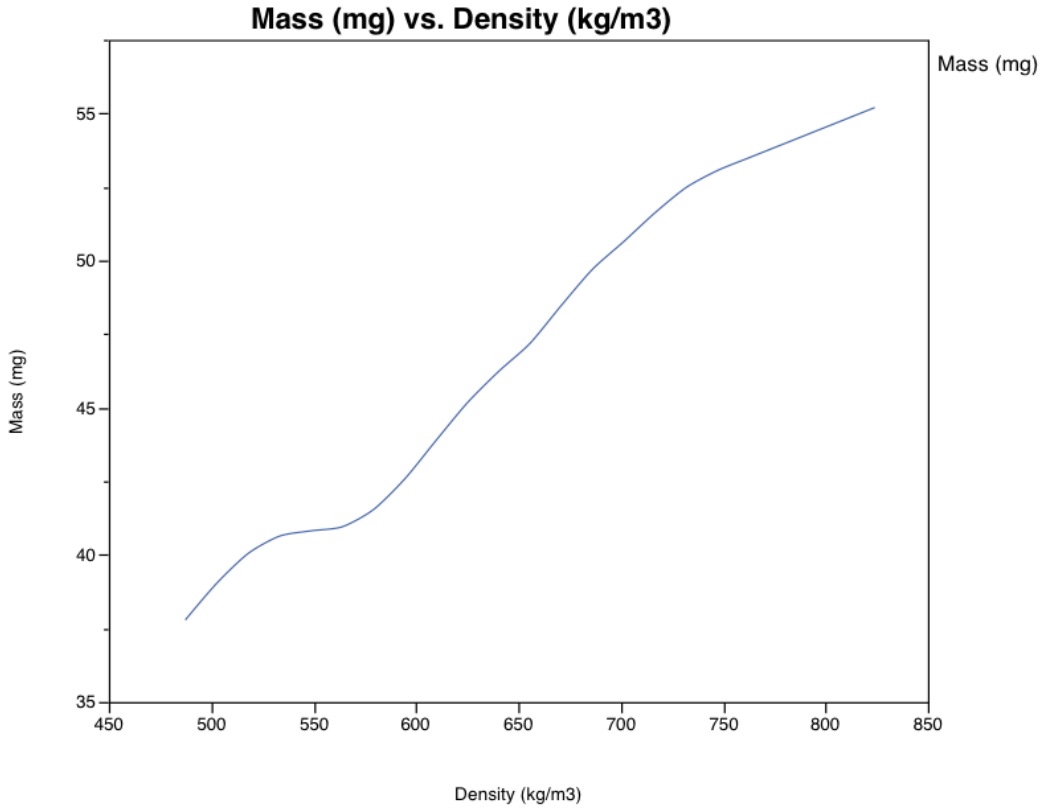

Figure 7:31: Mass Vs Density

The relatively low density of the samples compared with the bulk polymer demonstrates the challenge of fusing the ABS powder which, due to its amorphous nature, does not readily fuse unless significant pressure is applied [173, 175, 177, 178].

It is clear from graphs Figure 7:30 and Figure 7:31 that the densities of the samples have a large variation; this is further exemplified in the SEM micrographs (Figure 7:25, Figure 7:26, Figure 7:27, Figure 7:28 and Figure 7:29). The density of the samples are shown to be inconsistent, possibly due to the way the layer is consolidated as a result of the mechanism by which it is deposited. The top surface of the previously deposited layer is subjected to preheating to enable tackification at a temperature between 130-150˚C. The next layer is deposited on top of it; this is likely to lead to greater consolidation at the bottom of every deposited layer and lower deformation of the particles resulting in poor consolidation in the middle of each layer from the lack of heat penetrating the

particles from below or the reduction in temperature from the IR heaters to the printer. Unfortunately, there is not enough evidence to support this theory.

In addition, the nature of the heating method employed could have potentially led to localised temperature variations, which can result in varying densities across the consolidated layer. It has been reported by Jones [5] that the Infrared radiant heater produces heat spots, which provide localised heating regions. Given the poor results, this could lend an explanation to the poor density of the samples.

7.5.4 Tensile modulus

Each sample, with its three repetitions, was placed in a Dynamic Mechanical Analysis (DMA) machine in order to derive the tensile modulus. The results are shown in Figure 7:32. The error is calculated from the statistical mean using the standard deviation equation as mentioned in the Experimental Chapter (Section 5). It can be seen that the tensile modulus varies considerably over the sample set. The maximum tensile modulus attained (Sample 113) was 3600MPa, which is 36% higher than the quoted modulus for the bulk polymer (2300MPa). However, this maximum value is significantly higher than the modulus value for the other samples tested. This is in complete disagreement with the density results and SEM micrographs, pointing to an irregularity within the measurement.

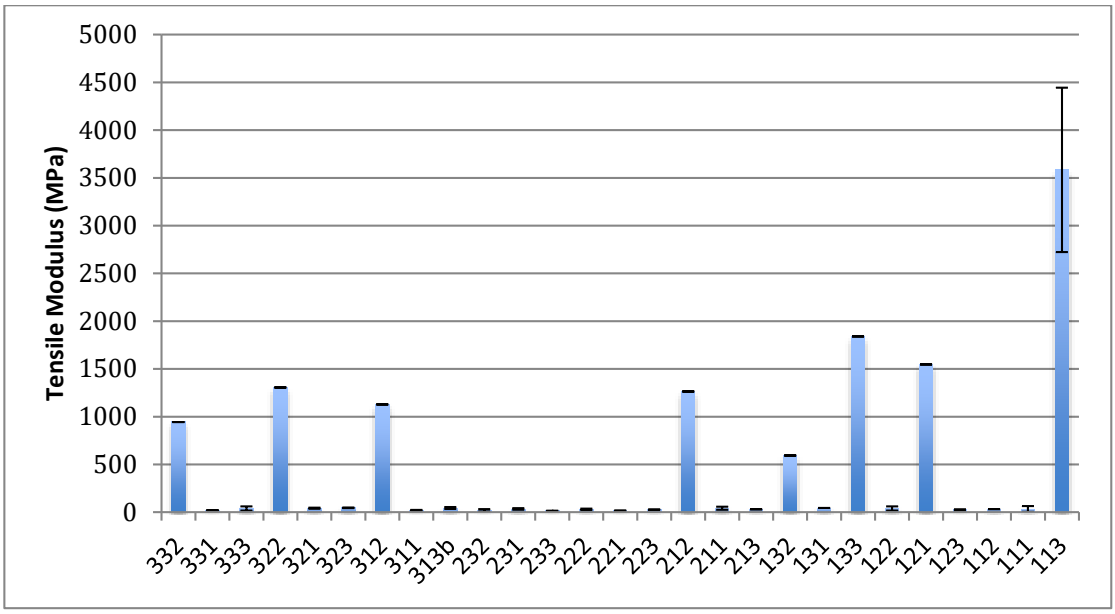

Figure 7:32: Tensile modulus Vs samples for lower modulus values

Figure 7:32 highlights the majority of the samples were unable to obtain a modulus anywhere near the manufacturers quoted value. The tensile modulus was compared against the densities from Figure 7:24, with the results showed no clear relationship. This was not as expected as the increase in heat and pressure should have yielded a greater density, thus, greater tensile modulus. A second graph was constructed to illustrate the modulus values for the remaining sample set.

Figure 7:33 illustrates the remaining samples with a value too low to see in the previous graph (Figure 7:32). The samples show values ranging from 14MPa to 46MPa. For the purpose of illustration, the samples able to record a value greater than 100MPa have been greyed out.

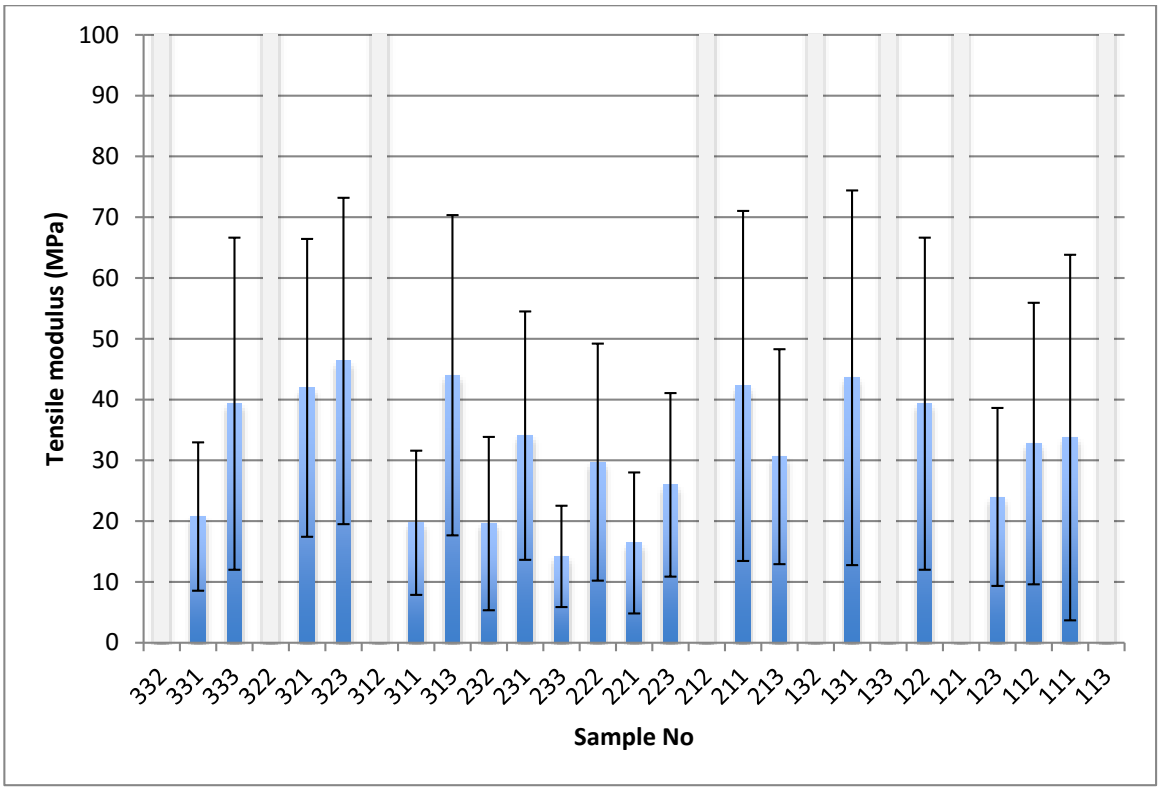

Figure 7:33: Tensile modulus values for sample range

It is clear that the samples suffer from large deviations, even at low modulus values. In addition, the error bars exhibit large deviations in a few samples, with sample 111 displaying the biggest deviation in the graph (Figure 7:33). The friable nature of the samples makes them sensitive to damage during sample preparation and handling (particularly loading in to test equipment). This damage could account for the large errors in the sample and the low overall modulus values in the test. From studying the data in Figure 7:32 and Figure 7:33, it is hard to establish a relationship between the parameters and resultant modulus. Due to the poor findings, the results for the tensile modulus were not analysed further.

The lower than expected density and tensile modulus, as well as the high levels of porosity, was a disappointing result. Samples of Somos 201 prepared by Jones [140] using the SLP 1 rig give tensile properties which were far higher (particularly elongation to failure) than those samples produced by conventional Selective Laser Sintering and

approaching the values for moulded polymer samples. Unfortunately, it was not possible to emulate these results with ABS toner used in this study. There are a number of potential reasons for this, however it is the nature of the ABS polymer, which is likely to be the significant cause. ABS, is an amorphous polymer which has a wide softening range, rather than at sharp melting point, as seen in crystalline/semi-crystalline materials such as nylon. It has been reported [27, 173, 177–180] that the undefined melt point of the ABS material has a detrimental effect on the mechanical properties of the parts due to the difficulty in consolidating the powder – this is also substantiated by the poor density of the samples produced.

The work conducted by Banerjee highlighted issues, which could be playing a role in the current study. Banerjee found the surface coating to inhibit inter-particle bonding[58]. Though the SEM micrographs seen in Figure 7:25,Figure 7:26,Figure 7:27 and Figure 7:28 have shown the varying degrees of bonding, the surface coating could well have compounded particle bonding issue with the amorphous phase porosity.

Summary of mechanical properties;

The predicted height of the sample was 50µm, however, the height was considerably greater ranging between 130µm to 190µm. The larger than expected sample height and deviation is suggested to be down to two factors. The first is limited to the amount of heat and pressure being applied to the deposited layer, reducing the ability to fully consolidate the layer. This lack of heat and pressure presents a second problem, as the ABS toner is unable to overcome the inherent viscoelastic properties, limiting the deformation, allowing the particles to return back to shape. This causes particles to sit as lumps of partially fused balls on the surface. The partially fused particles result in inaccuracies when measuring the height, artificially increasing the height of the samples.

The mass of the samples varied with a similar trend to the height. A statistical analysis of the samples has been shown to favour stand-off distance, particularly 105mm. However, a regression analysis showed load to be of high significance and an interaction between the temperature and pressure was also shown to be of statistical significance. A mass V's surface charge graph (Figure 7:23) shows the mass to increase as the surface charge decreases; this was in line with the literature.

The sample density ranged between 49-83%, with the SEM micrographs supporting the measured values. The SEM micrographs were also found to show surface balling as a result of the unfused larger particles requiring greater heat and pressure. A mass V's density graph follows a linear trend but due to the lack of heat and pressure, the graph is not completely linear. The poor density in the samples is likely to be attributed to the lack of heat and pressure. In addition, the IR unit used has been shown to emit a non-uniform heat distribution.

The low modulus values obtained by DMA demonstrated the need for a better means of testing the fragile samples. The issues with mounting the samples have shown huge disparities between each sample set, but also the deviation from sample to sample, represented by the error bars. Due to the large error in the samples, they were not analysed. A method to remedy the issue of the fragile samples can be based on additional heat and pressure. As the current rig architecture is not set up to accommodate the additional heat and pressure required to produce a fully consolidated layer, the Further Work Section details steps towards producing a fully consolidated layers.

Banerjee conducted work using an IR heat source, produced bulk sintered samples using Somos powder (Polybutylene terephthalate, purpose made for Selective Laser Sintering[138]). The manufacturer quoted a tensile modulus of 15.5MPa[138]. The semi-crystalline material with a sharp melting point, produced samples with changes to the

tensile moduli depending on whether the particles were coated or uncoated. Banerjee found uncoated samples of 17µm Somos powder to exhibit a tensile modulus of 9MPa (41.93% off the manufacturers quoted value) and a tensile modulus of only 4MPa (74.2% off manufacturers quoted value) for surface coated samples placed in a mould. Moreover, Jones conducted experiments using the SLP rig and Somos. Jones discovered, that the material properties surpassed the manufacturers quoted data and leaned towards more traditional bulk properties associated with Polybutylene terephthalate (PBT) with the addition of pressure[140]. It can be hypothesised that the semi crystalline nature of the Somos material favoured the SLP process, and with the implementation of pressure, responded well with mechanical properties surpassing the manufacturers quoted figures.

It is indicated from the results that the ABS toner requires higher levels of pressure and potential higher temperatures to be applied to achieve acceptable fusing on the particles. Unfortunately, with the current printer architecture, this is not feasible to increase the temperature and pressure further.

8 Analysis of Chemically Produced Toner

8.1 Energy Dispersive X-ray

Energy dispersive X-ray (EDX) was employed to analyse the difference between the two Magnum 8391 toners; DMU130729RB (chemical) toner and DMU130625RC (mechanical) toner using a mapping technique. The results are discussed below.

8.1.1 Pre-ground ABS

Energy dispersive X-ray (EDX) was used to try and determine the difference between the chemically produce toner (DMU130729RB) and the mechanically milled toner (DMU130625RC). Initial EDX trials were to be conducted using the virgin base material directly from the supplier (Magnum 8391). This would serve as a benchmark when comparing both toners (DMU130625RC and DMU130729RB).

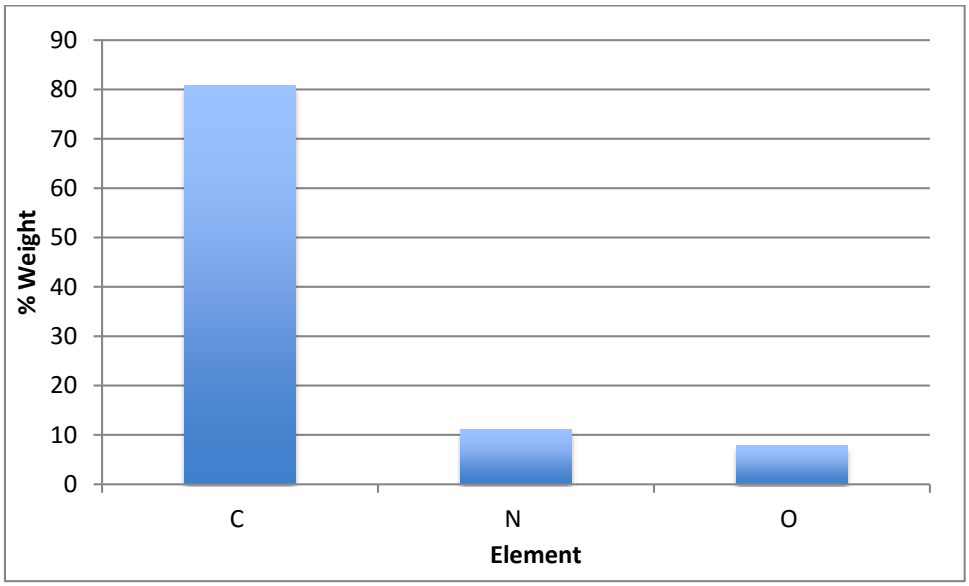

Figure 8:1: Graph displaying elements by weight for virgin ABS powder

Table 8:1: Percentage weight of elements found in virgin Magnum ABS

Element	Weight %
C	80.88
N	11.16
O	7.96

8.1.2 DMU130625RC

A chemical analysis was undertaken by means of energy dispersive X-ray (EDX) to confirm the composition of the mechanically milled ABS toner. The EDX trials were of uncoated mechanically milled ABS (DMU130625RC).

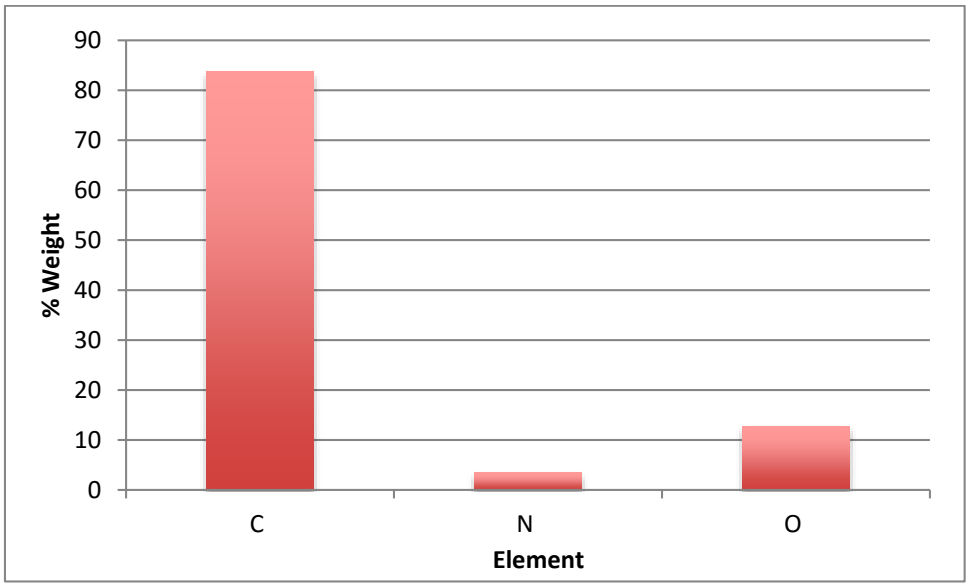

Figure 8:2: EDX quantitative results with percentage weights of each of the elements found in sample DMU130625RC

From Figure 8:2 becomes obvious that the most abundant element is carbon. The next most abundant element was found to be oxygen and finally, nitrogen. Table 8:2 illustrates the weight percentage elements making up the toner. It is clear that almost 84% of the toner is made up of carbon with 3.42% of the toner made up of oxygen. Nitrogen accounts for the remaining 12.77% of the toner.

Table 8:2: Elements identified by EDX for toner DMU130625RC

Element	Weight %
C	83.81
N	3.42
O	12.77

Comparing the DMU130625RC results against the virgin ABS it can be seen there is a very strong correlation between the results. The carbon and oxygen have almost 4% variation from the virgin ABS. However the nitrogen is significantly less in the mechanically milled toner. The reason for the reduced amount of nitrogen is not fully understood and requires additional analysis to understand the effects cryogenic milling has on the virgin powder.

8.1.3 DMU130729RB

The same analysis was conducted for DMU130729RB (chemically produced) toner to observe the difference in chemical composition between the two processes. It was anticipated that any foreign elements making up the toner would be picked up in the spectroscopy.

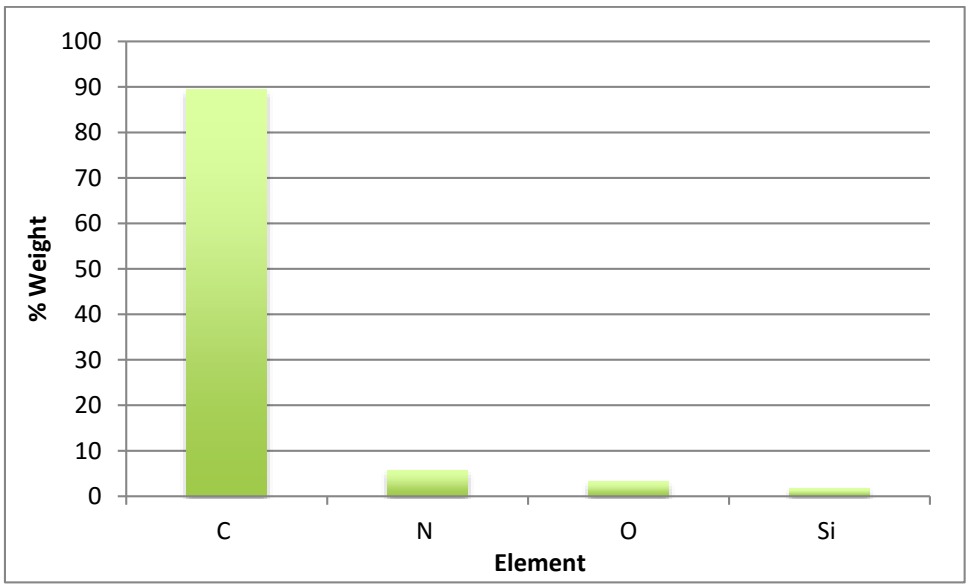

Figure 8:3: EDX quantitative results with percentage weights of elements found in sample DMU130729RB toner

Figure 8:3 illustrates DMU130729RB toner with the chemical elements present on the surface of the sample. Nitrogen is present in the sample making up 3.17%. Interestingly, Oxygen now represents a greater percentage of the toner surface. This could possibly be due to surface oxidation, however, this is not definitive. In the chemically produced toner, there is now the inclusion of silicon identified through EDX. As toner DMU130729RB has not had any surface coating the silicon is suspected to have originated from the manufacturing process. Silicon was originally used as a buffer to avoid coalescing of the particles. The post processing washes the silicon away before packaging. It is possible during the washing stage that some residual silicon is left of the surface. A graph demonstrating the elements present against all three of the ABS materials is exemplified in Figure 8:4.

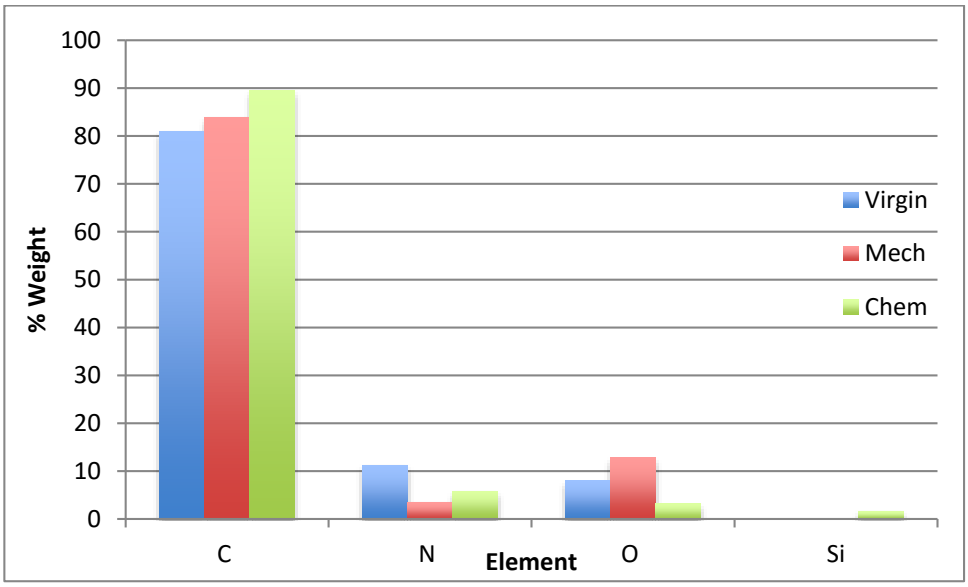

Figure 8:4: Graph identifying the elements present in toner DMU130729RB by EDX

Table 8:3: Table depicting the weight % and atomic % of DMU130729RB toner

Element	Weight%		
C	80.88	83.81	89.44
N	11.16	3.42	5.74
O	7.96	12.77	3.17
Si	0	0	1.65

The weight percentage of each of the elements present within the particles is shown in Table 8:3. It can be seen that carbon makes up 89.44% of the total weight of the particle followed by nitrogen with 5.74% and oxygen contributing 3.17%. An interesting observation is carbon has a greater presence in the chemically produced toner. Another interesting finding is that silicon is present in DMU130729RB, making up 1.65% by weight. Both the virgin ABS and DMU130625RC toner have no evidence of silicon present during the EDX scan. The identification of silicon is important as it has brought to light an element that was previously unseen in the previous EDX experiments. It is unclear how the carbon has become so prominent in the chemically produced toner. Moreover, how the silicon was found in the EDX spectroscopy. It is plausible that during the washing stage of the ELC process, the silicon (used as a buffer during chemical production) was incorporated into the material. However, it is unclear whether the silicon has bonded with any of the other elements causing the change in polarity. Another explanation that lends itself is improper washing of the toner after production. It is possible that the silicon is the residual surface coating left over from the ELC process during the washing stage. Further investigation is required to understand the rationale behind the shift in polarity between the two toners.

8.2 Fourier Transform Infrared Spectroscopy (FT-IR)

An FT-IR Spectroscopy was undertaken to determine the change in polarity between DMU130625RC toner and DMU130729RB toner. Atoms in the molecules are excited with the movements reacting to the IR in a manner typical of the element and chemical bonding. Each atom vibrated at a distinct frequency based on the strength (absorbance units) of the bond, as well as the length of the bond[181, 182]. The results of the spectroscopy between the two toners and the virgin material (Magnum 8391) are shown in Figure 8:5, Figure 8:6 and Figure 8:7.

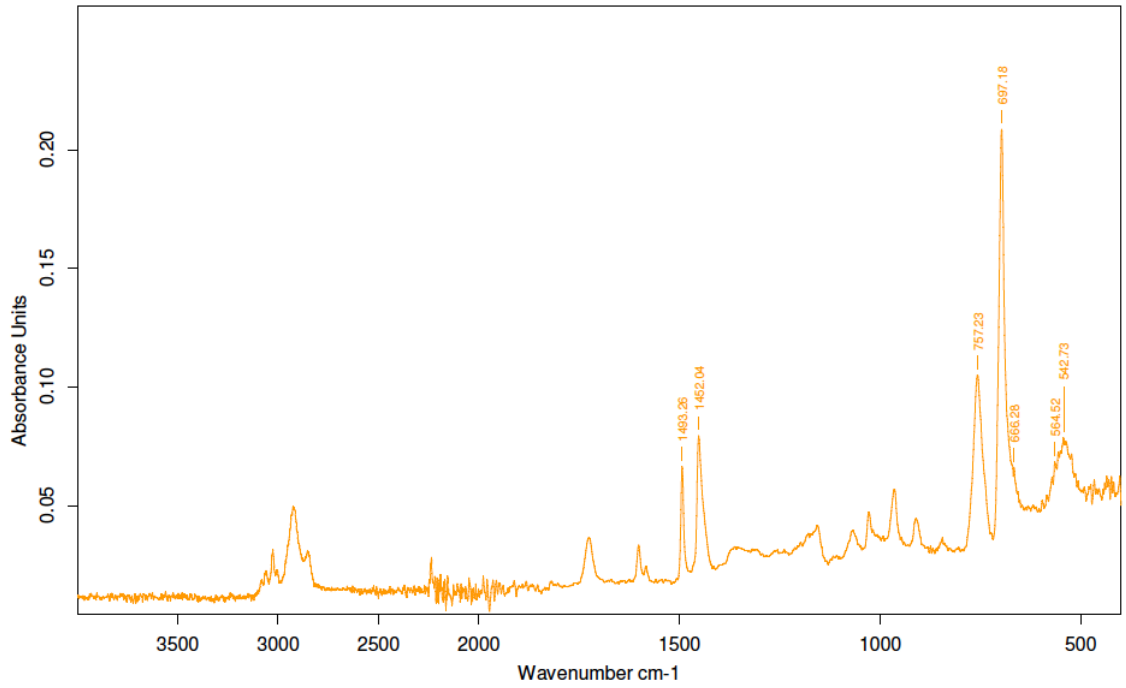

Figure 8:5: FT-IR spectrum of Magnum 8391 ABS (unprocessed)

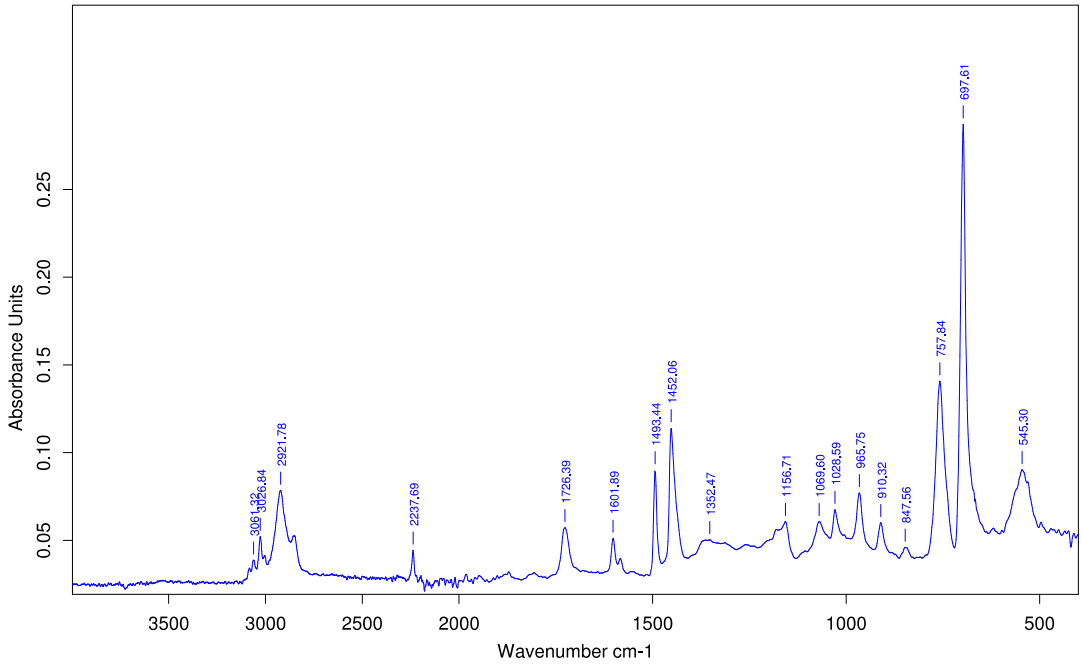

Figure 8:6: FT-IR spectrum for DMU130625RC (mechanically milled) toner

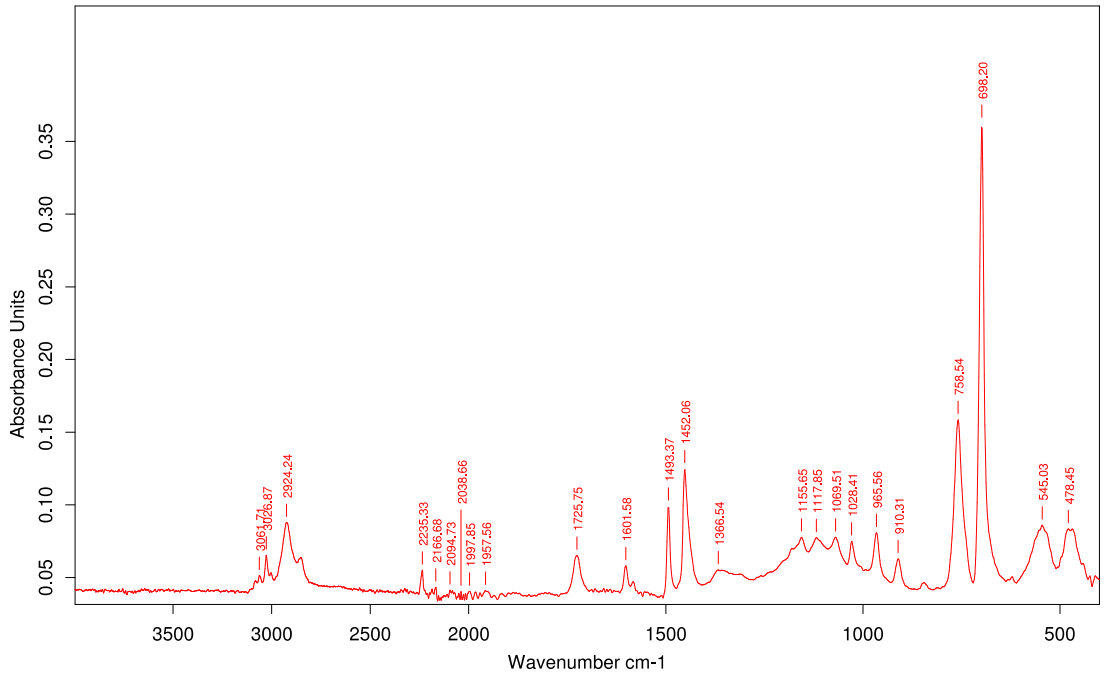

Figure 8:7: FT-IR spectrum for DMU130729RB (chemically produced) toner

On comparison, there is very little difference between the graphs Figure 8:5, Figure 8:6 and Figure 8:7) with the transmittance aligning and wavenumbers being very similar to each other. When super imposing the graphs in Figure 8:6 and Figure 8:7 it becomes apparent the graphs have a subtle difference. The peaks are shown to be exactly at the same wavenumber and the transmittance intensity is almost identical, see Figure 8:8.

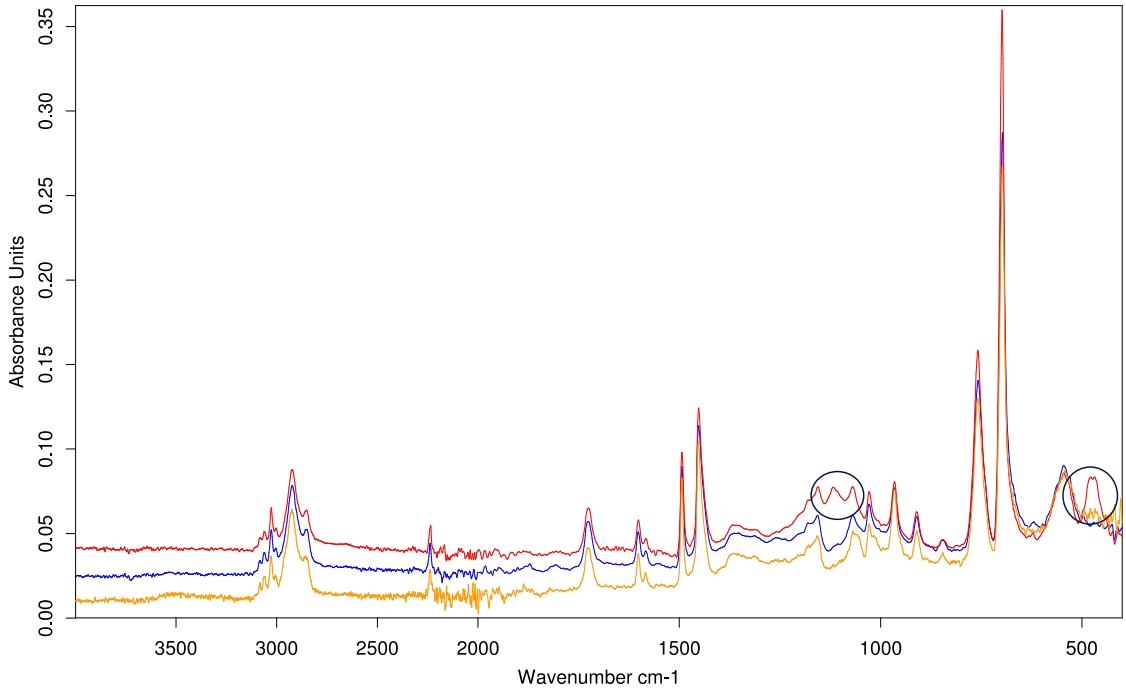

Figure 8:8 Super imposing raw Magnum (orange), mechanical (blue) and chemical (red) ABS after FT-IR with the irregularities circled in black

The differences are highlighted by the circles around the two peaks at 1116.01cm^{-1} and 476.62cm^{-1} in Figure 8:8. Studying the chemical structure of ABS in Figure 8:9 and relating it to the correlation table (Figure 8:10) for infrared spectroscopy, indicates the overall vibrations at the corresponding peaks at the wavenumbers are typical of ABS. However, at 1116.01cm^{-1} and 476.62cm^{-1} (the fingerprint region) the peaks for DMU130729RB (chemical toner) are altered from what is typically seen of ABS. At 1116.01cm^{-1} the DMU130729RB toner (red line) was shown to have a carbon-to-carbon (single bond) skeletal vibration. The skeletal vibration spans from 1300cm^{-1}–500cm^{-1}, which covers multiple peaks that are expected. At 476.62cm^{-1} the anomaly was detected as a ring in and out of plane bending with a variable bond at 476.62cm^{-1}. This suggests an issue in the benzene ring of the styrene component of the DMU130729RB toner. From Figure 8:8 it can be seen that DMU130625RC toner has identical wavenumbers to the unprocessed ABS Magnum 8391 suggesting that there is no change to the material by mechanical milling.

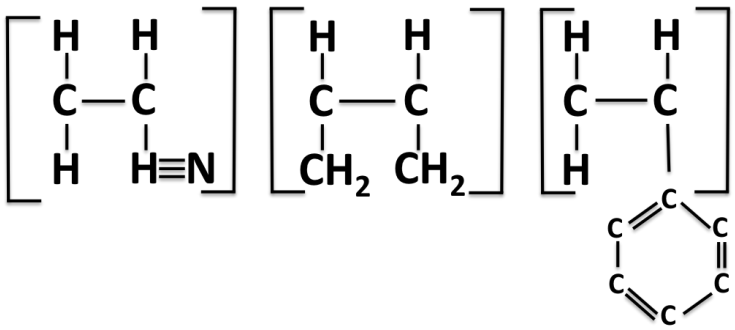

Figure 8:9: Chemical structure of ABS

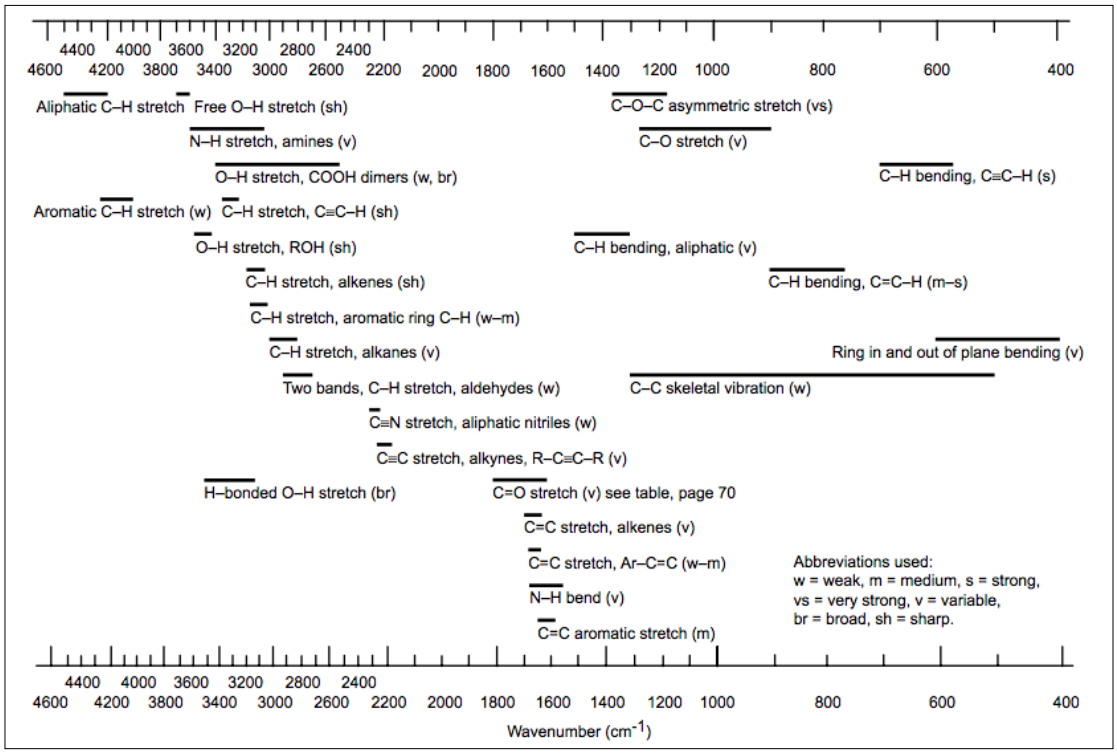

Figure 8:10: FT-IR correlation table [181]

From the EDX trials it was hypothesised that the discovery of silicone in DMU130729RB toner may still have been present in the sample attributing to the change in polarity of the ABS powder. Unfortunately, as the silicon is unknown, no FT-IR experiment was carried out, instead, FT-IR spectrums from the literature were compared.

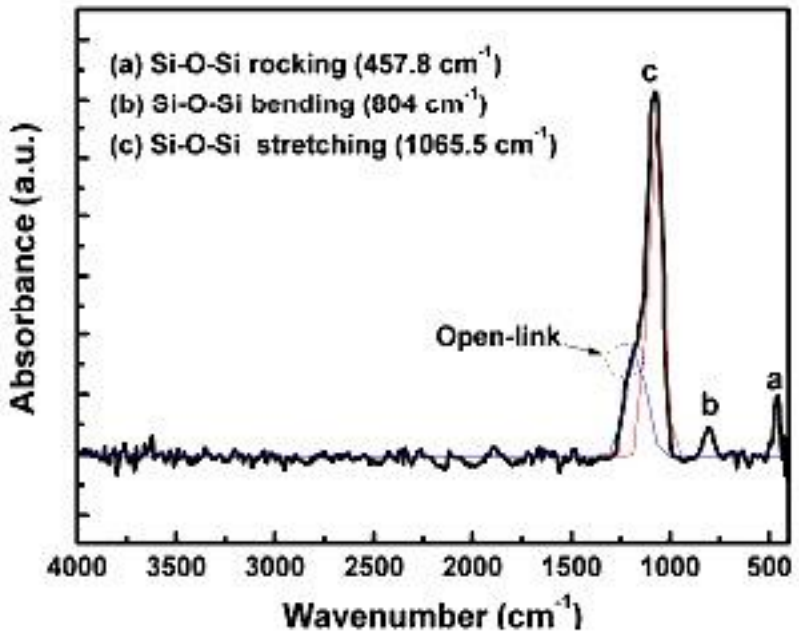

Figure 8:11: FT-IR spectrum of SiO_2 film[183]

Figure 8:11 shows the absorbance spectrum of a silicon dioxide sample. It can be seen that points (a) 457.8cm^{-1} & (c) 1065.5cm^{-1} highlighted in Figure 8:11, corresponds with the anomalies at 476.62cm^{-1} and at 1116.01cm^{-1} in Figure 8:8.

The two wavenumbers where the anomalies were identified at 1116.01cm^{-1} and 476.62cm^{-1}, are partially within the fingerprint region spanning from 1450 cm^{-1}-500 cm^{-1} [181, 182]. This region is notoriously difficult to gauge the purporting vibration, thus making it challenging to identify the component[182, 184]. However, work by Wang[183] and by Scopel [185] suggested by the absorbance peaks of the FT-IR for silicon dioxide may be present although this cannot be definitively proven without further investigation.

The results from the EDX trials have highlighted silicone to be present in DMU130729RB toner. The results from the FT-IR have indicated DMU130729RB toner to have inconsistent results compared to the virgin ABS and DMU130625RC toner. The literature

has indicated silicone to be present, however, additional experiments are required to confirm the exact material included in DMU130729RB toner.

9 Conclusion and Further work

CHEMICAL PRODUCTION

Styrene

- The study has demonstrated that chemical synthesis is a viable technique for the production of a fine polymeric powder with a tight particle size distribution suitable to act as a toner for the SLP process.

- It was found that by changing the recipe, the size of the particle and the distribution could be tailored to match the specific requirements of the SLP process.

- Conversion rates of the synthesised styrene vary depending on the recipe used. It was found that PE1 had a conversion rate of 38.88% from the monomer and initiator of which 8.38% was within the target size. Polymerisation experiment 2 was found to have a conversion rate of 56.65% from 23.19g of monomer and initiator and a yield of 12.24% of the styrene toner within 20-50µm. PE3 had a conversion rate of 18.08% from 45.48g of monomer and initiator producing 35.49% of the styrene with a particle size between 20-50µm. The poor conversion rate of PE3 was due to the fine powder baking to the glasswear.

ABS

- It was found that the Evaporative Limited Coalescence (ELC) process, although utilised heavily in the production of fine toners, is able to produce larger sized toner particles, potentially suitable for use in an electrophotography based Additive Manufacturing process.

- The ELC process was found to produce non-spherical regular shaped particles, which allows for better charging with the carrier than spherical toners.

- Adjusting the process parameters for the ELC process, in order to generate larger size particles, also results in a significant broadening in the particle size distribution in the D_{50} to D_{90} range.

- It was possible to pair a carrier to the DMU130729RB toner. However, due to the ELC process, the charge was not as concentrated as expected, resulting in inadequate long term adhesion between the carrier and toner.

- It was found that the ELC process is a highly efficient process for converting ABS into a toner with a conversion rate of 98.6% for the ABS polymer at the 20-50µm fraction size.

- It was found that the toner produced by ELC means converted a naturally negatively charging toner to a positively charging toner. This is an interesting feature and identifying the cause could lead to alternate charge deposition, which may enable parts with greater height to be produced.

MECHANICAL GRINDING TRIALS

- From the grinding trials it was found that the Magnum 8391 ABS was impossible to efficiently air jet mill under ambient conditions to the required 20-50µm. This is based on a feed rate rate of 1kg/hr.

- It was found that cryogenic grinding of Polylac PA-757 via air jet milling (based on cooling times of 20 minutes with small additions of liquid nitrogen during the comminution processing) was unsuccessful. A grinding time of one hour for 1kg of original feedstock produced 3.88% of the toner within the required toner size.

- Based on the trials conducted at Fraunhofer UMSICHT, it was found that cryogenic pin milling for Magnum ABS gives a significantly improved yield when grinding to achieve a particle size of <100µm based on a starting size of 1200µm (D_{97}). The grinding process has a conversion rate of 66% based on a 10kg throughput. It was found that 58.33% was within the target size.

- Based on previous research it was found the trials conducted at Fraunhofer UMSICHT had greater particle reduction efficiency for fractions between 20-50µm.

- The grinding efficiency of the trials is shown in Table 9:1, it can be seen that the most efficient method of producing toner in the 20-50µm range is the chemical process (ELC) having achieved an efficiency of 98.6%.

Table 9:1: Efficiency of the trials conducted by mechanical grinding and chemical manufacturing

Particle size	Hosokawa (µm)		UMSICHT (µm)	ELC (µm)
	Ambient	Cryo		
D_{10}	163	88.25	26	20
D_{50}	302	223.07	60	26
D_{90}	549	424.24	112	33
Efficiency	0%	3.23%	42.74%	98.6%

PRINTING PARAMETERS

- Carriers based on the charging properties from the literature were found to have a Q/m and charge ratio suitable for the SLP process. DMU130625RC toner had a Q/m of 8.5µm with carrier C2 and an 88% charging ratio. DMU130729RB was found to have an 8.7µC/g with a 92% charge ratio when charged with carrier C1. A toner loading test showed the most effective toner to carrier loading was 8:92 by weight for both toners.

- It was found that by increasing the doctor blade gap, the larger carrier particle could be facilitated and a thicker brush can be developed, resulting in a greater layer density.

- DMU130729RB was found not to charge adequately with the carrier in the developer unit. It was found that the reduced roughness in the surface area was the cause. A CCA was required with an additional upgrade to the printer to remedy the cause. Due to time and budgetary limitations, this was not pursued.

- A set of voltages have been identified which enable the efficient transfer of ABS toner from the developer unit to the substrate. It was found that a developer bias of -400V with an OPC charge of -600V, and OPC surface charge of -720V and a transfer roller charge of +400V was able to develop an image on to the OPC and transfer roller and are suitable for printing DMU130625RC toner.

FUSING TEMP

- Through DSC it was found that a ramp rate of 30˚C/min gave the most consistent T_g reading for both the chemical and mechanical ABS toner.

- A temperature of 103˚C was found to be the glass transition (T_g) temperature for DMU130625RC toner with a particle fraction size between 20-50µm.
- It was found that at the T_g defined by the DSC, DMU130625RC toner was unable to fuse adequately. The optimal fusing temperature can only be found by conducting in-process sintering trials to produce a consolidated layer.

- Fusing trials confirmed that the temperature required to fuse the ABS toner, DMU130625RC, is 130˚C as compared to a T_g as defined by DSC, of 103˚C.

PRINTER SETTINGS AND OPTIMISATION

- It was found that integration of load cells with data acquisition software provides a repeatable method for setting the initial force between the transfer roller and substrate on the SLP rig. Moreover, using this approach it is possible for real time pressure readings to be taken during the fusing process conducted on the SLP 1 rig.

- A set of voltages allowing for the efficient transfer of the DMU130625RC toner and are shown in Table 9:2.

Table 9:2: Printer voltage set up to enable efficient transfer of DMU130625RC toner

Developer bias	OPC Charge	OPC surface charge	OPC core	Transfer corona	Transfer roller
-400	-6000	-720	0	0	400

PRINTING ABS

- It is found that single and multilayer printing of ABS toner DMU130625RC is achievable using the SLP1 rig.

- High levels of porosity were found in the samples in spite of the load applied during toner transfer. Unfortunately, the pressure was also not high enough to overcome the viscoelastic nature of the amorphous ABS polymer.

CHEMICAL ANALYSIS

EDX

- It was found that DMU130729RB (chemically produced by ELC method) ABS toner found traces of silicon, which were not present in the original material or the mechanically milled toner.

- It is concluded that EDX alone is insufficient to reliably determine the cause in polarity shift between toner DMU130625RC and toner DMU130729RB.

FTIR

- Subtle changes in the wavelength were found between DMU130625RC and DMU130729RB. Two additional peaks were identified at 1116.01cm^{-1} and at 476.62cm^{-1} respectively for DMU130729RB. It was found that the peaks resided in the fingerprint region of the infrared spectrum of the FTIR.

- It has been concluded that FT-IR is not a suitable method to outright identify the perpetrating component(s) responsible for the change in charge polarity of toner DMU130729RB. However, when coupled with EDX, the results can give a good indication.

FURTHER WORK

The further work has been split into sections to enable additional work to be carried with the rig in its current state or with small or major modifications.

Current rig set-up

- It has been demonstrated in the study that the current heat and pressure regime is inadequate to consolidate the layer sufficiently to produce a fully dense part using ABS. The current configuration of the printer does not allow the temperature to be increased further, to a point where the ABS reaches a viscous state. To overcome this problem a high temperature OPC could be employed in future work. The application of additional pressure during transfer may also help to densify the samples produced. Unfortunately, this will require changes to the structure of the equipment. By affixing the printer to the rigid frame of the rig more pressure can be exerted to the platform.

- The literature review has recognised the need for a better development system to produce a thicker layer on the transfer substrate. The literature review has also shown conductive magnetic brush to produce a denser homogeneous layer. A revision to the carrier should be considered, especially if a chemically produce toner is to be employed.

Minor modifications

- In order to print DMU130729RB (chemically produced) toner it was found that the cleaning blade would need to be upgraded. By upgrading the cleaning blade (as well as coating the DMU130729RB toner), the chemically produced toner can be printed. By making these modifications it may be possible to achieve higher density samples.

Major modifications

- An alternative approach requires a substantial revision of the machine. In order to overcome potential damage to the OPC from heat arising from fusing, it is proposed that printing and heating, as well as the pressure steps are segregated. Moreover, the changes described below could enable the size of the machine to be significantly reduced thus improving the potential for practical commercialisation of the process. The current platform can be replaced with a transfer belt, which can be produced from a high temperature material with a low coefficient of friction. The transfer belt can enable the printed layer to be transferred to a separate heating and pressure station where the layer can be subjected to sufficient heating and pressure to ensure full densification of the layer. The OPC is not in the vicinity of the heat source thus protecting it from damage. Pressure can be applied via a stamp press or similar on to the transfer belt and transferred to a substrate of choice. A transfer belt such as PTFE or similar would be the ideal candidate for a transfer belt.

Height limitations

- Charge accumulation is a common issue that has yet to be overcome. Without overcoming this, the system is reliant on excessive heat and pressure. Isopropanol alcohol (IPA) is known to be used as a cleaning agent for substrates prone to static charge accumulation [186, 187], for this reason it is suggested during post fusing that the surface is wiped with IPA to neutralise the charge.

- It was noted that DMU130729RB measured a positive charge rather than a negative charge. In addition to upgrading the cleaning blades of the printer (to enable positive toner printing), a second printer suitable for depositing negative toner can be added. This combination of printers will enable alternative negative and positive toner layers to be deposited, which in principle could overcome the

issues of charge accumulation. This is would represent a major development for the industry enabling parts of unlimited Z height to be produced.

- Jones [5] has shown that corona charging has a stronger effect than an ionising fan which was used prior the layer transfer, showering the substrate with positive ions, to make the surface more receptive to toner transfer. Trials should be performed to assess the efficacy of this approach.

- The study has shown that ABS requires temperatures significantly above the T_g to achieve fusing. However, polycarbonate, another polymer with a relatively high T_g has a lower melt temperature and narrow melting range. Thus enabling the polycarbonate to undergo viscous flow that could potentially be used to produce dense layers.

Reference

1 Urbach, J.C., Fisli, T.S., Starkweather, G.K.: Laser scanning for electronic printing. Proceedings of the IEEE. 70, pp. 597–618 (1982).

2 Cormier, D., Taylor, J., Unnanon, K., Kulkarni, P., West, H.: Experiments In Layered Electro-Photographic Printing. Solid Freeform Fabrication Symposium. pp. 267–274. , Texas (2000).

3 Banerjee, S., Wimpenny, D.I.: Laser printing of soluble toners for Rapid Manufacturing. The 2nd Conference on Additive Technologies. , Ptuji, Slovenia (2008).

4 Banerjee, S.: Development of a novel toner for an electrophotography based Additive Manufacturing process, PhD., De Montfort University, (2010).

5 Jones, J.: Investigation of a Laser Printing Based Additive Manufacturing Technique, Unpublished PhD., Warwick University, (2013).

6 Robert E. Nuuja, Potini, S.: Laser vs LED Featuring Xerox Hi-Q LED Technology Conventional [Online] Xerox Corp. Available from http://www.office.xerox. com/latest/XOGWP-15.pdf., [Accessed: 12/07/14] (2009).

7 Ribes, C., Bautista, Y., Sanz, V.: Preparation of Chemically Prepared Tonners (CPT) by Polymerisation for Ceramic Decoration. NIP27 & International Conference on Digital Printing Technologies and Digital Fabrication 2011. Minnesota, USA. pp. 425–428. (2011).

8 Bynum, D.K.: Automated manufacturing system using thin sections, US Patent 5,088,047 (1992).

9 Grenda, E.P.: Apparatus of fabricating 3 Dimensional objects be means of electrophotography, ionography or a similar process, US Patent 6,206,672 (2001).

10 Kumar, A. V, Dutta, A.: Layered manufacturing by electrophotographic printing. 29th Design Automation Conference, Parts A and B., Chicago, Illinois. pp. 205–211. (2003).

11 Kumar, A. V., Dutta, A., Fay, J.E.: Electrophotographic printing of part and binder powders. Rapid Prototyping Journal. 10, pp. 7–13 (2004).

12 Wimpenny, D.I., Banerjee, S., Jones, J.B.: Laser printed elastomeric parts and their properties. Solid Freeform Fabrication. Austin Texas (2009).

13 K. Bovie C Vander Eijk, R.K.: Material issues of the Metal Printing Process, MPP, Solid Freeform Fabrication., Austin Texas (2006).

14 Hanson, W.J., Sanders, R.J., Bacus, M.W., Chillscyzn, S.A.: Electrophotography-based Additive Manufacturing System with Transfer-medium Service Loops, US Patent 20130077997,(2013).

15 Guttler, S., Groning, M., Willems, P., Biesinger, B., Breitling, F., Bischoff, R., Stadler, V., Felgenhauer, T., Leibe, K., Fernandez, S., Cancer, G.: An efficient manufacturing process for highly complex biochips using laser printing technique. NIP24 & International Conference on Digital Printing Technologies and Digital Fabrication 2008. pp. 471–475 (2008).

16 Hermann, D.S., Larson, R., Ab, S.T.: Selective Mask Sintering for Rapid Production of Parts , Implemented by Digital Printing of Optical Toner Masks. NIP24 & International Conference on Digital Printing Technologies and Digital Fabrication 2008. pp. 885–889 (2008).

17 Pomerantz, I., Cohen-Sabban, J., Bieber, A., Kamir, J., Katz, M., Nagler, M.: Three dimensional modelling apparatus, US Patent 4961154, (1990).

18 Wholers, T.: The Wohlers Report 2010: Additive Manufacturing state of the industry: Annual worldwide progress report. Wohlers Associates, Fort Colins. pp.6-29 (2010).

19 Chua, C., Leong, K., Lim, C.: Rapid Prototyping: Principles and Applications. World Scientific Publishing Co. Pte, Ltd, Singapore, pp. 43-51 (2010).

20 Crump, S.S.: Apparatus and method for creating three-dimensional objects, US Patent 5121329, (1992).

21 Agarwala, M.K., Jamalabad, V.R., Langrana, N.A., Safari, A., Whalen, P.J., Danforth, S.C.: Structural quality of parts processed by fused deposition. Rapid Prototyping Journal. 2, pp. 4–19 (1996).

22 Weeren, R. van, Agarwala, M., Jamalabad, V.R., Bandyophadyay, A., R.Vaidyanathan, Langrana, N., Safari, A., Whalen, P., Danforth, S., Ballard, C.: Quality of Parts Processed by Fused Deposition. Solid Freeform Fabrication 1995. Austin, Texas (1995).

23 Wendel, B., Rietzel, D., Kühnlein, F., Feulner, R., Hülder, G., Schmachtenberg, E.: Additive Processing of Polymers. Macromolecular Materials Engineering. 293, pp. 799–809 (2008).

24 Sun, Q., Rizvi, G.M., Bellehumeur, C.T., Gu, P.: Effect of processing conditions on the bonding quality of FDM polymer filaments. Rapid Prototyping Journal. 14, pp. 72–80 (2008).

25 Ahn, S.-H., Montero, M., Odell, D., Roundy, S., Wright, P.K.: Anisotropic material properties of fused deposition modeling ABS. Rapid Prototyping Journal. 8, pp. 248–257 (2002).

26 Bellini, A., Güçeri, S.: Mechanical characterization of parts fabricated using fused deposition modeling. Rapid Prototyping Journal. 9, pp. 252–264 (2003).

27 Goodridge, R.D., Tuck, C.J., Hague, R.J.M.: Laser sintering of polyamides and other polymers. Progress in Material Science. 57, pp. 229–267 (2012).

28 Amado-Becker, A., Ramos-Grez, J., Yañez, M.J., Vargas, Y., Gaete, L.: Elastic tensor stiffness coefficients for SLS Nylon 12 under different degrees of densification as measured by ultrasonic technique. Rapid Prototyping Journal. 14, pp. 260–270 (2008).

29 Caulfield, B., McHugh, P.E., Lohfeld, S.: Dependence of mechanical properties of polyamide components on build parameters in the SLS process. J. Mater. Process. Technol. 182, pp. 477–488 (2007).

30 Carlson, C.F.: Electro Photography, US Patent 2,221,776 (1942).

31 Owen, D.: Copies in seconds: How a lone inventor and an unknown company created the biggest breakthrough since the Gutenberg. Simon & Schuster, New York, pp. 22-48, (2004).

32 Wise, E.N.: Development of electrophotographic images. US patent 2,618,552, (1952).

33 Bixby, W.E., Ullrich, O.A.J.: Method for the production of a xerographic plate, US Patent 2,753,278,(1956).

34 Xerox Corporation: Company History. [Online] Available from http://www.xerox.co.uk/about-xerox/history-timeline/1950-decade/engb.html. [Accessed: 23/03/12], (1999).

35 Starkweather, G.K., Calid, S.: Flying spot scanner with runout correction, US Patent 4,040,096, (1977).

36 IBM: History, [Online] IBM, Avaliable from http://www-03.ibm.com/ibm/history/history/year_1976.html, [Accessed 29/11/14]

37 Schein, L.B.: Electrophotography and development physics. Springer (1988).

38 Duke, C.B., Noolandi, J., Thieret, T.: The surface science of xerography. Surface Science. 500, pp. 1005–1023 (2002).

39 Lee, M.H., Ayala, J.E., Grant, B.D., Imaino, W., Jaffe, a., Latta, M.R., Rice, S.L.: Technology Trends in Electrophotography. IBM Journal of Research and Development. 28, pp. 241–251 (1984).

40 Law, K.-Y.: Organic Photoconductive Materials: Recent trends and developments. Chemistry Review. 93, 3. pp. 449-486. (1993).

41 Schaffert, R: Method and apparatus for printing electrically, US Patent 2576047, (1951).

42 Scharfe, M.: Electrophotography principles and optimisation. Research studies press Ltd, Letchworth, pp. 62, (1984).

43 Hirakawa, H.; Murata, Y., Mechanism of contact charging photoconductor and insulator with DC-biased conductive roller, Industry Applications Conference, 1995. Thirtieth IAS Annual Meeting, IAS '95., Conference Record of the 1995 IEEE , vol.2, pp.1539,1542. (1995).

44 Loutfy, R.O., Hor, a.-M., Hsiao, C.-K., Baranyi, G., Kazmaier, P.: Organic photoconductive materials. Pure Applied Chemistry. 60, pp. 1047–1054 (1988).

45 Whitfield, R.., Richmond, H.., Johnson, T..: Overview of ozone human exposure and health risk analyses used in the U.S. EPA’s review of the ozone air quality standard. Journal of Environmental Studies and Science. 72, pp. 483–516 (1998).

46 Heal, M.R., Heaviside, C., Doherty, R.M., Vieno, M., Stevenson, D.S., Vardoulakis, S.: Health burdens of surface ozone in the UK for a range of future scenarios. Environment International. 61, pp. 36–44 (2013).

47 Singh, B.P., Kumar, A., Singh, D., Punia, M., Kumar, K., Jain, V.K.: An assessment of ozone levels, UV radiation and their occupational health hazard estimation during photocopying operation. Journal of Hazardous Materials. 275, pp. 55–62 (2014).

48 Lee, C.-W., Dai, Y.-T., Chien, C.-H., Hsu, D.-J.: Characteristics and health impacts of volatile organic compounds in photocopy centres. Environmental Resolution. 100, pp. 139–49 (2006).

49 Kumar, A. V, Dutta, A.: Investigation of an electrophotography based rapid prototyping technology. Rapid Prototyping. 9, pp. 95–103 (2003).

50 www.answers.com: Xerography: Laser and LED printers, http://www.answers.com/topic/xerography, [Accessed: 14/04/13], (1998).

51 Morita, K., Ikeda, Y., Tanaka, Y.: Organic Photoconductors for Printers. Fuji Electron. Rev. 53, pp. 52–57 (2011).

52 Nakamura, Y.: Material Technology for Organic Photoconductors. Fuji Electron. Rev. 53, pp. 48–51 (2011).

53 Thourson, T.L.: Xerographic Development Processes : A Review, IEEE Transaction on electron devices , 19, pp. 495-511,(1972).

54 Electrophotographic toner and development process using chemically prepared toner, US Patent 7016632, (2006).

55 Schein, L.B.: Recent advances in our understanding of toner charging. Journal of Electrostatics. 46, pp. 29–36 (1999).

56 Chudasama, R.A., Jones, J. B. and Wimpenny, D. I. Synthesis of an Electrophotographic Toner for Additive Manufacturing **in** Annuals of DAAAM for 2012 & Proceedings of the 23rd International DAAAM Symposium. Editor Branko Katalinic, Published by DAAAM International, Vienna, Austria. pp 0001 - 0004. (2012).

57 U, J.H., Yanagida, N., Tamura, M.: Toner prepared by the direct polymerization method in comparison with the pulverization method. Colloids and Surfaces A: Physicochemical and Engineering Aspects, pp. 215–220 (1999).

58 Banerjee, S.: Development of a Novel Toner for Electrophotography based Additive Manufacturing Process, PhD., De Montfort University, (2011).

59 Hirakawa, H., Murata, Y.: Generation of Fine Dry Toner and it's Charging Characteristics. IEEE Industry Applications Conference. San Diego, CA . pp. 2026–2030. (1996).

60 Whitney, J.G.: Toner charge and environmental interactions with toner adhesion. Presented at NIP 27 & International Conference on Digital Fabrication 2011, (2011).

61 Al-Rubaiey, H.: Toner Transfer and Fusing in Electrophotography, Graphic Arts, 39, pp. 1–28 (2010).

62 Mizes, H., Ott, M., Eklund, E., Hays, D.: Small particle adhesion: measurement and control. Colloids Surfaces A Physicochemistry. Eng. Asp. 165, pp. 11–23 (2000).

63 Takeuchi, M.: Adhesion forces of charged particles. Chemical Engineering Science. 61, pp. 2279–2289 (2006).

64 Rimai, D.S., Quesnel, D.J., DeMejo, L.P., Regan, M.: Toner to Photoconductor Adhesion. Journal of Imaging Science and Technology. 2, pp. 197-186, (2001).

65 Feng, J.Q., Hays, D.A.: Relative importance of electrostatic forces on powder particles. Powder Technology., pp. 65–75 (2003).

66 Owens, D.K.: Adhesives: Measuring Stickiness - Natural Products, *Chemecology* Vol. 22. pp. 23-29. (1993).

67 Schein, L.B.: Electrophotography. In: J.Chang, A. Kelly, J.C. (ed.) Handbook of Electrostatic Processes, Mercel Dekker Inc., New York, pp. 321–349, (1995).

68 Pai, D.M., Springett, B.E., Corporation, X., York, N.: Physics of electrophotography. Review of Modern Physics. 65, pp. 163–215 (1993).

69 Walton, O.R.: Review of Adhesion Fundamentals for Micron-Scale Particles. KONA Powder Part. J. 26, pp. 129–141 (2008).

70 Béguin, L., Vernier, A., Chicireanu, R., Lahaye, T., Browaeys, A.: Direct Measurement of the van der Waals Interaction between Two Rydberg Atoms. Physics Review Letter. 110, pp. 201-262 (2013).

71 James, Q.N.G., Hays, D.A.N.A.: Electric field detachment of a uniformly charged dielectric sphere on a dielectric coated electrode. IEEE Industry Applications Conference. 6, 1883–1890 (1996).

72 Schein, L.B.: Recent Progress and Continuing Puzzles in Electrostatics. Applied Physics. 316, 1572–1573 (2007).

73 Rimai, D.S., Weiss, D.S., Cristina de Jesus, M., Quesnel, D.J.: Electrophotography as a means of microfabrication: the role of electrodynamic and electrostatic forces. Comptes Rendus Chimie. 9, pp. 3–12 (2006).

74 Anderson, J.H.: The effect of additives on the tribocharging of electrophotographic toners. Journal of Electrostatics. 37, pp. 197–209 (1996).

75 Shinjo, Y., Nishizawa, H., Tsunemi, K., Saitoh, M., Corporation, T.: Study of Tribo-Charging Characteristics between Toner and Carrier. NIP 13 & International Conference on Digital Printing Technologies and Digital Fabrication 13, pp. 123–127 (1997).

76 Schein, L.B., W.S.Czarnecki, Christensen, B., Mu, T., Galliford, G.: Experimental Verification of the Proximity Theory of Toner Adhesion. Journal of Imaging Science and Technology. 48, pp. 417–425 (2004).

77 Rimai, D.S., Alexandrovich, P., Quesnel, D.J.: Effects of submicrometer particulate silica addenda on the adhesion of micrometer-size particles to a polyester-composite substrate. Journal of Adhesion. 79, pp. 1041–1066 (2003).

78 ASTM, F1425-06: Standard Test Method for Determining the Tribocharge of Two-Component Developer Materials. ASTM International. West Conshohocken, PA (2011).

79 Nomura, T., Satoh, T., Masuda, H.: The environment humidity effect on the tribo-charge of powder. powder Technol. 135-136, 43–49 (2003).

80 Anderson, J.H.: Humidity dependence of tribocharging of electrophotographic carriers coated with poly(vinylidene fluoride)-poly(methyl methacrylate) blends. Journal of Electrostatics. 63, pp. 59–67 (2005).

81 Matsusaka, S., Masuda, H.: Electrostatics of particles. Advanced Powder Technology. 14, pp. 143–166 (2003).

82 Noll, C.G.: Electrostatic Charge Elimination Techniques. In: Chang, J.S., Kelly, A.., and Crowley, J.M. (eds.) Handbook of Electrostatic Processes.. Mercel Dekker Inc., New York. pp. 733–749. (1995).

83 HP: Material safety data sheet. [Online] Available from: www.hp.com/hpinfo/globalcitizenship/.../us/lj_92274a_us_eng_v6.pdf. [Accessed 19/02/14](2013).

84 Ricoh: Material Safety Data Sheet. [Online] Available from: http://www.ricoh-usa.com/products/brochures/CL7000.pdf. [Accessed 19/12/13] (2003).

85 Xerox: Replenisher- Black / Cyan / Magenta / Yellow Trade Name : Xerox 700 Digital Color Press , Xerox 700i Digital Color Replenisher- Black / Cyan / Magenta / Yellow. [Online] Available from: http://www.xerox.com/download/ehs/msds/P-7010.en-us.pdf. [Accessed 28/09/12] (2012).

86 Xerox: Phaser® 6250 Color Laser Printer data sheet. [Online] Available from: http://www.office.xerox.com/userdoc/P6250/6250_Web/pdfs/msds.pdf. [Accessed 11/11/13]. (2003).

87 Lexmark: Materials safety data sheet. [Online] Available from: http://www.lexmark.com/pdf/msds/en/laser_color/1361210.pdf. [Accessed 22/10/2014] (2003).

88 HP: Material safety data sheet. [Online] Available from: http://www.hp.com/hpinfo/globalcitizenship/environment/productdata/pdf/elmd052.pdf. [Accessed 03/02/15]. (2011).

89 Michel, E., Baur, R., Macholdt, H.T.: Charge stabilizers: properties and applications. Journal of Electrostatics. pp. 51-52, 91–96 (2001).

90 Fujifilm: Charge Control Agents. [Online] Available from: http://www.fujifilmimagingcolorants.com/ep_charge.html. [Accessed: 03/08/2011]. (2006).

91 Julien, P., Gruber, R.: Dry Toner Technology. In: Diamond, A., Weiss, D. (eds.) Handbook of Imaging Materials. Second Edition.. Mercel Dekker Inc., New York. pp. 173-192 (1995).

92 Horiba Scientific: A Guidebook To Particle Size Analysis. [Online] Available from: https://www.horiba.com/fileadmin/uploads/Scientific/Documents/PSA/PSA_Guidebook.pdf. [Accessed: 20/09/2014]. (2014).

93 Habermann, R., Zobrist, B.: Investigations in the Influence of rounded Toner Particles on the Image Quality Parameters. NIP26 & International Conference on Digital Printing Technologies and Digital Fabrication 2010. 26, pp. 208–212 (2010).

94 Banerjee, S., Wimpenny, D.I.: Laser Printing of Polymeric Materials. Solid Freeform Fabrication. Austin, Texas. (2006).

95 Ahmadi, a, Williamson, B. Theis, T. Powers, S..: Life-cycle inventory of toner produced for xerographic processes. J. Clean. Prod. 11, pp. 573–582 (2003).

96 Ricoh: Ricoh adds new toner production lines at Tohok [Press release]. Available from: http://ricoh.com/release/2012/. [Accessed: 16/03/14]. (2012).

97 O'Rourke, J., AuClair, C., Renault, J., Malabadi, H., Kmlecik-Lawrynowlcz, G.: Xerox Technology: EA (Emulsion Aggregation) Toner [White paper]. [Online] Available from: http://www.office.xerox.com/latest/SUPWP-01U.pdf. [Accessed 29/04/2014]. (2013).

98 Galliford, G., Particle shape of toners and the advantage of using chemical toner manufacturing methods. [Online] Available from: http://www.gallifordconsulting.com/Particle%20Shape%20of%20Toners.pdf. [Accessed 18/03/2014]. (2005).

99 Asua, J. m.: Emulsion Polymersization: From Fundamental Mechanisms to Precess Development. Polym. Sci. Part A Polymer Chemistry. 42, pp. 17 (2003).

100 De Castro, C.L., Mitchell, B.S.: The use of polymeric milling media in the reduction of contamination during mechanical attrition. Journal of Material Research. 17, pp. 2997–2999 (2011).

101 Liang, S.B., Hu, D.P., Zhu, C., Yu, a. B.: Production of Fine Polymer Powder under Cryogenic Conditions. Chemical Engineering Technology. 25, pp. 401–405 (2002).

102 Molina-Boisseau, S., Le Bolay, N.: Fine grinding of polymers in a vibrated bead mill. Powder Technol. 105, pp. 321–327 (1999).

103 Verheezen, J.J. a M., van der Voort Maarschalk, K., Faassen, F., Vromans, H.: Milling of agglomerates in an impact mill. International Journal of Pharmaceutics. 278, pp. 165–72 (2004).

104 Mishra, B.., Thornton, C.: Impact breakage of particle agglomerates. International Journal of Mineral Processing. 61, pp. 225–239 (2001).

105 Bajal, J.K.: Grinding the tough plastics at cryogenic temperatures. Plastic Design Process. 1. 25–29 (1977).

106 Schmidt, J., Plata, M., Tröger, S., Peukert, W.: Production of polymer particles below 5µm by wet grinding. Powder Technology. 228, pp. 84–90 (2012).

107 Wilczek, M., Bertling, J., Hintemann, D.: Optimised technologies for cryogenic grinding. International Journal of Mineral Processing. 74, pp. 425–434 (2004).

108 Nakahura, Y., Butswada, N.: Direct measurement of toner size particles. IEEE: Industry Applications Society Annual Meeting. pp. 2239–2242 (1989).

109 Wennerstrum, S., Kendrick, T., Tomaka, J., Cain, J.: Size reduction solutions for hard-to-reduce materials. Powder Bulk Engineering. pp. 1–5 (2002).

110 Jonna, S., Lyons, J.: Processing and properties of cryogenically milled post-consumer mixed plastic waste. Polym. Test. 24, pp. 428–434 (2005).

111 Krejčová, A., Pouzar, M., Černohorský, T., Pešková, K.: The cryogenic grinding as the important homogenization step in analysis of inconsistent food samples. Food Chem. 109,pp. 848–854 (2008).

112 Paul, S., Chattopadhyay, a. B.: Effects of cryogenic cooling by liquid nitrogen jet on forces, temperature and surface residual stresses in grinding steels. Cryogenics (Guildf). 35, pp. 515–523 (1995).

113 Yano, O., Yamaoka, H.: Cryogenic properties of polymers. Prog. Polym. Sci. 20, pp. 585–613 (1995).

114 Yildiz, Y., Nalbant, M.: A review of cryogenic cooling in machining processes. Int. J. Mach. Tools Manuf. 48, pp. 947–964 (2008).

115 Yamaoka, H., Miyata, K., Yano, O.: Cryogenic properties of engineering plastic films. Cryogenics (Guildf). 35, pp. 787–789 (1995).

116 Li, C.H., Lu, B.H., Ding, Y.C., Al, M.: Innovative Technology Investigation into Cryogenic Cooling Green Grinding using Liquid Nitrogen Jet. Management and Service Science. pp. 1–4 (2009).

117 Odian, G.: Principles of polymerization. John Wiley & Sons, Inc., New Jersey, pp. 464-470. (2004).

118 Painter, P., Coleman, M.: Fundamentals of Polymer Science; An Introductory Text. Technomic Publications, Lancaster, Pennsylvania, pp.27-52. (1994).

119 Seymour, R.., Carraher, C.. J.: Polymer Chemistry: An Introduciton. Mercell Dekker Inc., Florida, USA , pp. 294-310. (1996).

120 Balakrishnan, T., Ford, W.T.: Particle size control in suspension copolymerization of styrene, chloromethylstyrene, and divinylbenzene. J. Appl. Polym. Sci. 27, 133–138 (1982).

121 Sperling, L.H.: Introduction to physical polymer science. John Wiley & Sons, Inc., New York, pp. 9-14. (1986).

122 Rosato, D.V.: Rosato's Plastics Encyclopaedia and Dictionary. Hanser Gardner Publications, Munich, pp. 347. (1993).

123 Wikipedia: Emulsion Polymersation. [Online] Available from: http://en.wikipedia.org/wiki/Emulsion_polymerization. [Accessed: 28/04/2013]. (2006).

124 Santilli, D., Webster: Method for the preparation of electrostatographic toner of controlled shape by evaporative limited coalescence, US Patent 5,238,159 (1994).

125 Comizzoli RB, Lozier GS, R. DA: Electrophotography A Review. IEEE. 60, 4.,348-349. (1972).

126 Gundlach, R.W.: Apparatus for developing a powder image on a xerographic plate, US Patent 2,777,418, (1957).

127 Hoshino, Y.: Conductivity Mechanism in Magnetic Brush Developer. Japanese Journal of Applied physics. 19, pp. 2413–2416 (1980).

128 Kumar, A. V: Electrophotographic Solid Freeform Fabrication. Masters Thesis. University of Florida, Gainesville, Florida (1999).

129 Fay, E.J.J.: electrostatic analysis of and improvements to electrophotographic solid freeform fabrication, Masters Thesis, University of Florida, Gainesville, Florida. (2003).

130 Kumar, A. V, Dutta, A.: Electrophotographic layered manufacturing. Journal of Manufacturing Science and Engineering. 126, pp. 571–576 (2004).

131 Manjooran, N.J., Kumar, A., Sigmund, W.M.: Development of a liquid toner for electro-photographic solid freeform fabrication. Journal of European Ceramic Society. 26, pp. 2459–2465 (2006).

132 Cormier, D., Engineering, I., Carolina, N.: An Investigation of Selective Coloring with 3-D Laser Printing. 4, Journal of Manufacturing Processes, pp. 148-152 (2002).

133 Larson, R.: Method and device for manufacturing three-dimensional bodies. US Patent 6,531,086. (2003).

134 Sintermask: Additive Manufacturing with Selective Mask Sintering flash black : cut through.(2009).

135 Benning, M.J., Dalgarno, K.W.: The conceptualisation of a novel electrophotographic Rapid Prototyping system. (1998).

136 Bakkelund, J., Karlsen, R.: Method and apparatus for rapid manufacturing of metal, ceramic and metal-ceramic products. WO 2004037469A1. (2004).

137 Banerjee, S., Wimpenny, D.I.: Rapid Manufacturing of thermoplastic parts by Laser Printing. 2007 International Conference on Polymers and Moulds Innovations. , Ghent, Belgium (2007).

138 3D systems: Material Safety Data Sheet. [Online] Available from; http://www.3dsystems.com/products/datafiles/vanguard/datasheets/RZ_Somos_uk.pdf. [Accessed 14/06/2013]. (2011).

139 Jones, J.B., Gibbons, G.J., Wimpenny, D.: The Influence of Residual Toner Charge on 3D Laser Printed Objects. NIP 28 and International Conference on Digital Fabrication 2012. Quebec, Canada. pp. 327–331. (2012).

140 Jones, J., Wimpenny, D.I., Gibbons, G.J., Sutcliff, C.: Additive manufacturing by electrophotography: Challenges and successes. International Conference on Digital Fabrication 2010. Austin, Texas. pp.549–553. (2010).

141 Arciniegas, A.: Towards the control of electrophotographic based 3-Dimensional printing: Image based sensing and modelling of surface defects. PhD. Rochester University. (2014).

142 Hanson, W.J., Sanders, R.J., Bacus, M.W., Chillscyzn, S.A.: Electrophotography-based additive manufacturing system with reciprocating operation. US Patent 20130077997. (2013).

143 Chillscyzn, I.S.A., Comb, J.W., Hanson, W.J., Sanders, J.R., Fe, S., Us, C.A., Bacus, M.W.: Layer transfusion with part heating for Additive Manufacturing. WO2013044047, (2014).

144 Tan, Y., Chua, C.: An Additive Manufacturing method based on xerography. Innovative Developments in Virtual and Physical Prototyping. CRC Press. pp. 603–607. (2011).

145 Liu, J.H., Jang, B.Z.: Layer manufacturing using electrostatic imaging and lamination. US Patent 6,376,148. (2002).

146 Kumar, A. V, Zhang, H.: Electrophotographic powder deposition for freeform fabrication. 10th Solid Freeform Fabrication Symposium , Austin, Texas (1999).

147 Jones, J.B., Wimpenny, D.I., Gibbons, J.G.: Additive Manufacturing under pressure. Rapid Prototyping Journal. pp. 89-97(2013).

148 Banerjee, S., Wimpenny, D.I.: Feasibility study of Laser Printing of Thermoplastic materials for Rapid Prototyping. ICMR07 conference (2007).

149 Zobrist, B.: Technical Discussion: Charging and toner issues, (2012).

150 Jones, J., Gibbons, G., Wimpenny, D.: Transfer Methods toward Additive Manufacturing by Electrophotography. NIP17: International Conference on Digital Fabrication 2001. 1, pp. 180–184 (2001).

151 Springette, B.E.: A Brief Introduction To Electrophotography. In: Diamond, A.S. and Weiss, D.S. (eds.) Handbook of imaging materials. CRC Press, New York pp. 154–156. (2002).

152 Schoenberger, A.: Technical Discussion: Printer voltages and carrier pairing. (2013).

153 Paul, S.: A Study of Effects of Cryo-cooling. International Journal of Machine Tools Manufacture. 35, pp. 109–117 (1995).

154 Thompson, D., Tyagi, D.: Tutorial T14: Fusing Technologies and Toner Materials Relationships. NIP 24: 24th International Conference on Digital Printing Technologies. , Pittsburgh, Pennsylvania (2008).

155 Eijk, C. van der, Mugaas, T., Karlsen, R., Skjevdal, R., Boivie, K., Åsebø, O.: Metal Printing Process: A Rapid Manufacturing Process Based on Xerography using Metal Powders. Material Science and Technology. 3, pp. 3–9 (2005).

156 Sandler, S.R., Karo, W., Bonesteel, J., Pearce, E.M.: Polymer synthesis and characterization, A laboratory manual. Academic Press, California (1998).

157 Richards, J.R., Congalidis, J.P.: Measurement and control of polymerization reactors. Comput. Chem. Eng. 30, pp. 1447–1463 (2006).

158 Speikamp Hans-Dieter, H., Kuhnel, A., Bretschneider, J.: Process for controlling the partical size in the preparation of expandable styrene polymers by suspension polymerisation. US Patent 5,189,069. (1991).

159 Crowley, T.J., Meadows, E.S., Kostoulas, E., Doyle III, F.J.: Control of particle size distribution described by a population balance model of semibatch emulsion polymerization. Journal of Process Control. 10, pp. 419–432 (2000).

160 Thickett, S.C., Gilbert, R.G.: Emulsion polymerization: State of the art in kinetics and mechanisms. Polymer (Guildf). 48, pp. 6965–6991 (2007).

161 Kim, O.H., Lee, K., Kim, K., Lee, B.H., Choe, S.: Effect of PVA in dispersion polymerization of MMA. Polymer (Guildf). 47, pp. 1953–1959 (2006).

162 Sudol M. S. El Aasser and S. Shen, E.D.: Control of particle size in dispersion polymerization of methyl methacrylate. Journal of Polymer Science. A. Polymer Chem. 31, pp. 1393-1402 (1993).

163 Kim, S., Huh, M., Yoon, N.: Dry Toner Technology PVA Chemical Toner, Yeungnam University, 16/05/2000. Available from: http://www.docstoc.com/ docs/137804135/Dry-Toner-Technology-PVA-Chemical-Toner-Samsoo-Kim. (2000).

164 Kiatkamjornwong, S., Pomsanam, P.: Synthesis and Characterization of Styrenic-Based Polymerized Toner and Its Composite for Electrophotographic Printing. Journal of Applied Polymer Science. 89, pp.238–248 (2003).

165 Aoki, T.: Chemical Toner Technology and the Future. NIP19: International Conference on Digital Fabrication 2003. New Orleans, LA. pp. 2–4. (2003).

166 Senna, M.: More Chemistry for Finer Particle Technology. Chemical Engineering Research and Design. 76, pp. 767-774. (1998).

167 Gabbot, P.: A Practical Introduction to Differential Scanning Calorimetry. In: Gabbot, P. (ed.) Principles and Applications of Thermal Analysis. Blackwell Publishing, Oxford. pp. 17–40. (2008).

168 Basdekis, C.H.: ABS Plastics. Rehold Publishing Corporation, New York. pp. 23-26. (1964).

169 Stratasys: Characterisation of material properties [White paper:]. [Online] Available from: http://www.stratasys.com/resources/white-papers. [Accessed 22/11/14]. (2011).

170 Stratasys: Mech. Data Sheet: ABS-M30 ABS-M30. [Online] Available from: http://usglobalimages.stratasys.com/Main/Secure/Material%20Specs%20MS/Fortus-Material-Specs/MaterialSS-FDM-ABSM30-03-15-EN-Web.pdf. [Accessed 11/03/14]. (2013).

171 Rodríguez, J.F., Thomas, J.P., Renaud, J.E.: Mechanical behavior of acrylonitrile butadiene styrene (ABS) fused deposition materials. Experimental investigation. Rapid Prototyping Journal. 7, pp. 148–158 (2001).

172 Kruth, J., Levy, G., Schindel, R., Craeghs, T., Yasa, E.: Consolidation of Polymer Powders by Selective Laser Sintering. International Conference on Polymer Mould Innovation. pp. 15–30 (2008).

173 ASTM D883-12: Standard Terminology Relating to Plastics. ASTM International, West Conshohocken, PA (2012).

174 Tontowi, A.E., Childs, T.H.C.: Density prediction of crystalline polymer sintered parts at various powder bed temperatures. Rapid Prototyping Journal. 7, pp. 180–186 (2009).

175 Zein, I., Hutmacher, D.W., Tan, K.C., Teoh, S.H.: Fused deposition modeling of novel scaffold architectures for tissue engineering applications. Biomaterials. 23, pp. 1169–1185 (2002).

176 Kruth, J.P., Wang, X., Laoui, T., Froyen, L.: Lasers and materials in selective laser sintering. Assembly Automation. 23, pp. 357–371 (2003).

177 Nelson, J., Vail, N.K., Sun, M.M., Barlow, J.W.: Post-Processing of Selective Laser Sintered Polycarbonate Parts. Annual International Solid Freeform Fabrication Symposium. , Austin, Texas (1991).

178 Pham, D.T., Dimov, S., Lacan, F.: Selective laser sintering : applications and technological capabilities. Journal of Engineering Manufacture. 213, pp. 435–449.

179 Williams, J.D., Deckard, C.R.: Advances in modeling the effects of selected parameters on the SLS process. Rapid Prototyping. Journal. 4, pp. 90–100 (1998).

180 Everett, D.R.: Infrared Spectroscopy. The Chemical Educator: Modern Chemical Techniques. Royal Society of Chemistry. pp. 62–91 (1998).

181 Shriver, D., P.W.Atkins: Inorganic Chemistry. Oxford University Press, Oxford. pp. 223-247. (2010).

182 Wang, N.-F., Kuo, T.-W., Tsai, Y.-Z., Lin, S.-X., Hung, P.-K., Lin, C.-L., Houng, M.-P.: Porous SiO_2/MgF_2 broadband antireflection coatings for superstrate-type silicon-based tandem cells. Optics Express. 20, pp. 7445-7452. (2012).

183 Banwell, C., McCash, E.: Infrared Spectroscopy. In: Fundamentals of molecular spectroscopy, Fourth Edition. McGraw-Hill, Berkshire. pp. 55-100. (1994).

184 Scopel, WL;, F., MCA;, A., MI: Local order structure of a-SiOxNy : H grown by PECVD. Brazilian Journal of Physics. 32, pp. 366–368 (2002).

185 Ohmi, T., Sudoh, S., Mishima, H.: Static charge removal with IPA solution. IEEE Transaction on Semiconductor Manufacturing. 7, pp. 440–446 (1994).

186 Smallwood, J.: Technical Discussion: Neutralisation Techniques for Electrostatics, (2013).

Appendix